NASA/TM—2012-217409

Large-Scale Weibull Analysis of H–451 Nuclear-Grade Graphite Specimen Rupture Data

Noel N. Nemeth
Glenn Research Center, Cleveland, Ohio

Andrew Walker
Wright State University, Dayton, Ohio

Eric H. Baker
Connecticut Reserve Technologies, Gates Mills, Ohio

Pappu L. Murthy
Glenn Research Center, Cleveland, Ohio

Robert L. Bratton
U.S. Department of Energy, Idaho National Laboratory, Idaho Falls, Idaho

October 2012

NASA STI Program . . . in Profile

Since its founding, NASA has been dedicated to the advancement of aeronautics and space science. The NASA Scientific and Technical Information (STI) program plays a key part in helping NASA maintain this important role.

The NASA STI Program operates under the auspices of the Agency Chief Information Officer. It collects, organizes, provides for archiving, and disseminates NASA's STI. The NASA STI program provides access to the NASA Aeronautics and Space Database and its public interface, the NASA Technical Reports Server, thus providing one of the largest collections of aeronautical and space science STI in the world. Results are published in both non-NASA channels and by NASA in the NASA STI Report Series, which includes the following report types:

- TECHNICAL PUBLICATION. Reports of completed research or a major significant phase of research that present the results of NASA programs and include extensive data or theoretical analysis. Includes compilations of significant scientific and technical data and information deemed to be of continuing reference value. NASA counterpart of peer-reviewed formal professional papers but has less stringent limitations on manuscript length and extent of graphic presentations.

- TECHNICAL MEMORANDUM. Scientific and technical findings that are preliminary or of specialized interest, e.g., quick release reports, working papers, and bibliographies that contain minimal annotation. Does not contain extensive analysis.

- CONTRACTOR REPORT. Scientific and technical findings by NASA-sponsored contractors and grantees.

- CONFERENCE PUBLICATION. Collected papers from scientific and technical conferences, symposia, seminars, or other meetings sponsored or cosponsored by NASA.

- SPECIAL PUBLICATION. Scientific, technical, or historical information from NASA programs, projects, and missions, often concerned with subjects having substantial public interest.

- TECHNICAL TRANSLATION. English-language translations of foreign scientific and technical material pertinent to NASA's mission.

Specialized services also include creating custom thesauri, building customized databases, organizing and publishing research results.

For more information about the NASA STI program, see the following:

- Access the NASA STI program home page at *http://www.sti.nasa.gov*

- E-mail your question to *help@sti.nasa.gov*

- Fax your question to the NASA STI Information Desk at 443–757–5803

- Phone the NASA STI Information Desk at 443–757–5802

- Write to:
  STI Information Desk
  NASA Center for AeroSpace Information
  7115 Standard Drive
  Hanover, MD 21076–1320

NASA/TM—2012-217409

Large-Scale Weibull Analysis of H–451 Nuclear-Grade Graphite Specimen Rupture Data

Noel N. Nemeth
Glenn Research Center, Cleveland, Ohio

Andrew Walker
Wright State University, Dayton, Ohio

Eric H. Baker
Connecticut Reserve Technologies, Gates Mills, Ohio

Pappu L. Murthy
Glenn Research Center, Cleveland, Ohio

Robert L. Bratton
U.S. Department of Energy, Idaho National Laboratory, Idaho Falls, Idaho

National Aeronautics and
Space Administration

Glenn Research Center
Cleveland, Ohio 44135

October 2012

Acknowledgments

The authors gratefully acknowledge the efforts of Erin Nemeth in the reconstruction of the specimen fracture stresses from the original 1976 report of Price. This included learning optical character recognition (OCR) software, manual input where OCR failed, and painstaking cross checking of the results.

Level of Review: This material has been technically reviewed by technical management.

Available from

NASA Center for Aerospace Information
7115 Standard Drive
Hanover, MD 21076–1320

National Technical Information Service
5301 Shawnee Road
Alexandria, VA 22312

Available electronically at http://www.sti.nasa.gov

Large-Scale Weibull Analysis of H–451 Nuclear-Grade Graphite Specimen Rupture Data

Noel N. Nemeth
National Aeronautics and Space Administration
Glenn Research Center
Cleveland, Ohio 44135

Andrew Walker
Wright State University
Dayton, Ohio 45435

Eric H. Baker
Connecticut Reserve Technologies
Gates Mills, Ohio 44040

Pappu L. Murthy
National Aeronautics and Space Administration
Glenn Research Center
Cleveland, Ohio 44135

Robert L. Bratton
U.S. Department of Energy
Idaho National Laboratory
Idaho Falls, Idaho 83415

Summary

A Weibull analysis was performed of the strength distribution and size effects for 2000 specimens of H–451 nuclear-grade graphite. The data, generated elsewhere, measured the tensile and four-point-flexure room-temperature rupture strength of specimens excised from a single extruded graphite log. Strength variation versus specimen location, size, and orientation relative to the parent body were compared. In our study, data were progressively and extensively pooled into larger data sets to discriminate overall trends from local variations. Weibull modulus (strength scatter) was predominantly constant throughout the log, but significant local variations in average strength were clearly evident. Specimens with an axial orientation relative to the extrusion direction were stronger than specimens with a radial orientation. Radial specimens behaved closer to a two-parameter Weibull distribution, whereas axial specimens followed a three-parameter distribution. The possibility that this difference was due to a compressive residual stress that affected the Weibull threshold parameter was investigated. Alternatively, a Monte-Carlo simulation was used to demonstrate that a similar behavior, which could be easily confused with a three-parameter Weibull or another distribution, also results from the local average strength variation. This alternative distribution was asymptotically two-parameter Weibull in behavior. The effect of the two different sizes of tensile specimens was much smaller than that predicted from Weibull analysis, possibly because of grain size effects. The size effect between the tensile and four-point-flexure specimens was more consistent with Weibull predictions. The Weibull modulus was similar for the two sizes of tensile specimens but was higher for the four-point-flexure specimens. A simplified nonlinear finite element analysis of the flexure specimens that examined the effect of changing effective volume with load could account for only a small portion of this discrepancy. Overall, the Weibull distribution described the behavior of the pooled data very well. However, the issue regarding size effect remained. This exercise illustrated that a conservative approach using a two-parameter Weibull distribution is best for designing

graphite components with low probability of failure for the in-core structures in the proposed Generation IV (Gen IV) high-temperature gas-cooled nuclear reactors. This exercise also demonstrated the continuing need to better understand the mechanisms driving stochastic strength response. Extensive appendixes are provided with this report to show all aspects of the rupture data and analytical results.

1.0 Introduction

There is a renewed interest in nuclear energy because nuclear power plants generate zero greenhouse gas emissions, ample fuel ore is available, and the mining of nuclear fuel ore has a lower environmental profile in comparison to the mining of fossil fuels such as coal. Next-generation nuclear reactor designs call for gas cooling and the use of nuclear-grade (i.e., low-impurity-level) graphite for the fuel element and moderator (see Fig. 1). At present, 10 countries, including the United States, have agreed to cooperate in developing the fourth-generation nuclear energy system (Generation IV International Forum (2010)). The Generation IV (Gen IV) system is expected to come into service in 2030.

In the United States, the U.S. Department of Energy is conducting Gen IV research to develop the Very High Temperature Reactor design concept for the Next Generation Nuclear Plant (NGNP) Project (Idaho National Laboratory et al. (2005)). The application of heat is essential to nearly all basic material and commodity manufacturing processes, and heating processes account for about 17 percent of all industrial energy use (U.S. Department of Energy (2008)). The design for the NGNP graphite-moderated reactor will address this by employing either a prismatic graphite-block-type core or a pebble-bed core to generate electricity and produce process heat in a highly efficient manner. This will reduce the need to burn fossil fuels to produce process heat and thereby reduce green-house emissions. The NGNP will have a projected service life of 30 to 60 years and be designed to ensure that passive-decay heat is removed without fuel damage or radioactive material releases during accidents.

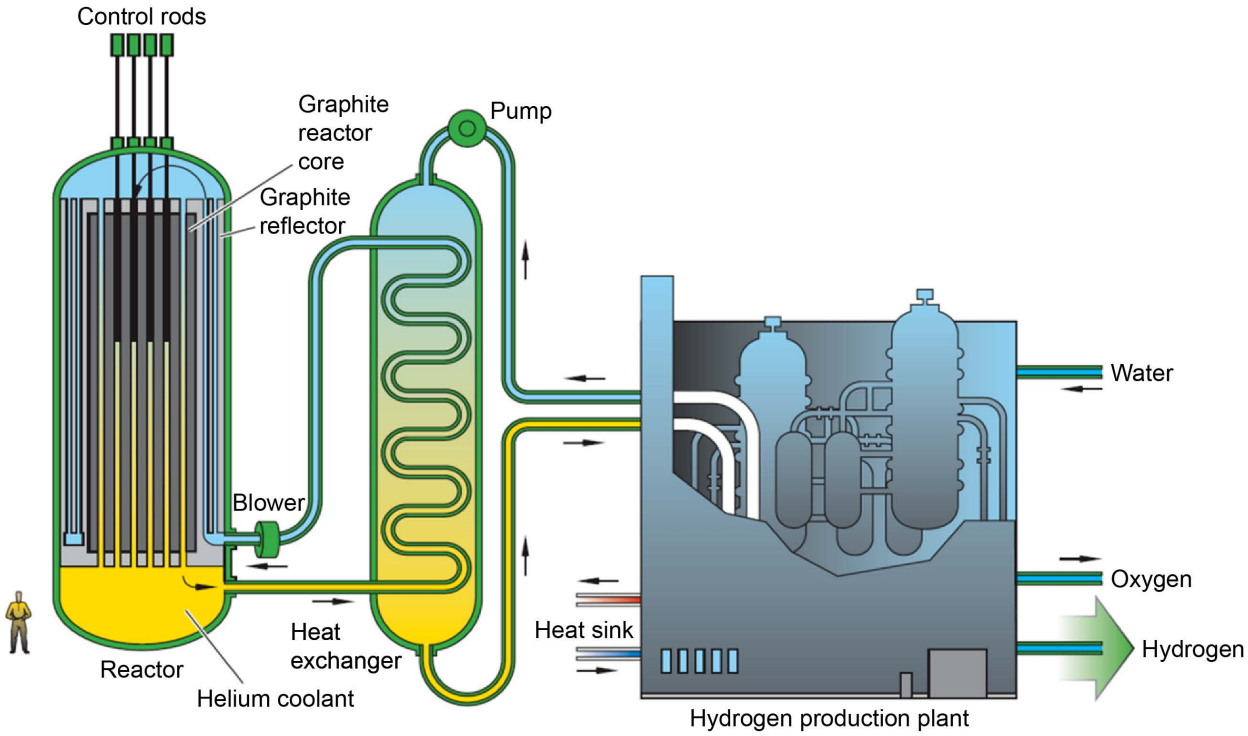

Figure 1.—Generation IV very-high-temperature gas-cooled reactor using graphite for neutron reflection and moderation within the reactor core. Reproduced from U.S. DOE Nuclear Energy Research Advisory Committee and Generation IV International Forum (2002).

The development of dependable design and material characterization methods for the graphite structures used in the reactor are important to the NGNP Project because large amounts of graphite (up to thousands of tons) would be required for the reactor core and because the individual graphite bricks that surround the nuclear fuel may experience significant loads. Of particular concern is the potential for crack formation and even rupture in individual blocks. Therefore, failure theories—and/or effective design strategies that can predict and mitigate failure from fracture—are needed.

In Great Britain, graphite-moderated gas-cooled reactors have been used successfully for decades. In the United States, the first, and only, high-temperature gas-cooled nuclear reactor put into commercial service was the Fort St. Vrain (FSV) power station built near the town of Platteville in Colorado. The station became operational in late 1976 and had a power output of 330 MW (Bramblett et al. (1981)). The facility, however, experienced many recurring problems requiring extended shutdowns. Other problems included the jamming of a control rod and the leakage of water into the reactor core. As a result, the plant became too costly to operate and was closed in 1989 (Pinner (2012). FSV was a helium-cooled, graphite-moderated reactor of a prismatic design. Nuclear-grade H–451 near-isotropic graphite from Great Lakes Carbon Corporation was used for the fuel element and moderator material. An H–451 graphite fuel block from FSV is shown in Figure 2.

An important characteristic of graphite is that its strength is stochastic—an individual specimen can show a large random fluctuation in strength from a population mean. Graphite can also have a nonlinear stress-strain response, and this behavior can be different in tension than in compression. This is a result of the distributed damage that accumulates with increasing load within the material prior to rupture. This behavior can be described as quasi-brittle or ductile-like. In contrast, classically brittle materials, such as ceramics and glasses, fail abruptly without prior damage accumulation, although they similarly display large scatter in strength. In addition, although graphite fracture behavior is essentially independent of temperature, exposure to radiation will affect this response. Further information regarding graphite fracture behavior and statistical models of fracture relevant to graphite can be found in the review article Nemeth and Bratton (2010) and in the more detailed version of this article (Nemeth and Bratton (2011)).

Probability distributions can describe the strength variability of graphite, but is one type of distribution more appropriate to use than another? Often distributions such as normal (gaussian), log-normal, or Weibull can fit experimental data nearly equally well within the range typically sampled between 1 and 99 percent probability of failure. Deviations from one distribution to another only become

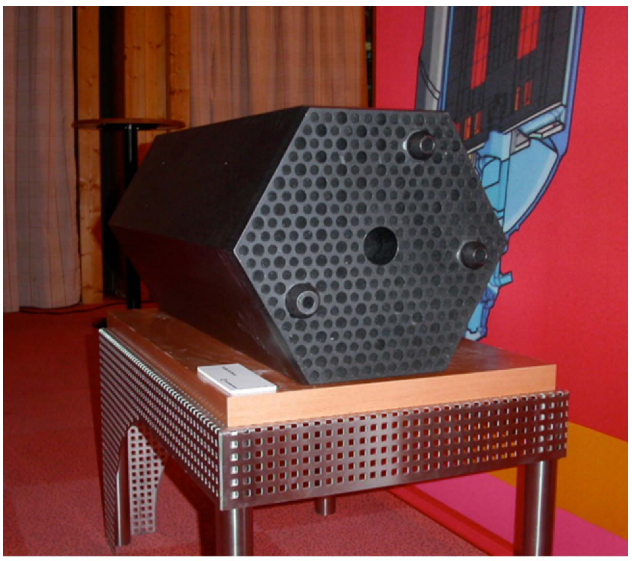

Figure 2.—Prismatic graphite fuel element from Fort St. Vrain high-temperature gas-cooled reactor; see Pinner (2010).

apparent in the tails of the distribution (i.e., at very high or very low probabilities of failure). However, obtaining experimental data at low probabilities of failure (the lower tail of the distribution and the region of highest interest) requires prohibitively large numbers of specimens. Danzer et al. (2008) indicates that several thousand experimental tests may be required to properly discern a difference between a normal and a Weibull distribution. Hence, it is difficult or impractical to determine a best distribution based solely on fit to data. From a design perspective, the conservatism (or nonconservatism) of one distribution relative to another distribution can be an important discriminator because these distributions extrapolate differently at the lower tail where confirmatory data typically do not exist. In this regard, the use of the two-parameter Weibull distribution can be justified because of its conservatism in comparison to other distributions (e.g., see Liu (1997) and Nemeth and Bratton (2010, 2011)). In this report we attempt to demonstrate some of these issues using a relatively large data set of H–451 specimen rupture data that were previously reported in Price (1976).

For FSV, an extensive materials characterization program was required to certify the H–451 material for use in the reactor. Part of this program was the strength testing work reported by Price (1976). Price rupture tested over 2000 cylindrical-shaped specimens that had been excised from a large cylindrical-shaped billet (or "log"). Price used tensile specimens of two different sizes and four-point-flexure specimens of one size. The original intent of the study was to examine the statistical strength distribution, the strength variation versus specimen orientation and location within the log, and the effect of specimen size and stress gradient on strength (size effect). Since 1976 there have been significant refinements in the art of tensile and flexure testing, but there have been very few published studies (for either brittle materials like ceramics and glasses or for graphite) on data sets as large as those used by Price. That fact alone makes the Price data still useful for study and demonstration, particularly with regard to the Weibull modulus (the strength scatter parameter), which is difficult to measure accurately unless a large number of specimens are available (with the exception of inferring Weibull modulus from size-effect studies, but this is not a direct measure of this parameter).

In this report, the fracture data from Price (1976) were reexamined. The objective of this new effort was to present the original data as Weibull plots (instead of the normal distribution plots of the original Price report) and to pool the data (using the WeibPar program from Connecticut Reserve Technologies (2009)) into progressively larger sets to better ascertain the overall stochastic distribution trends with greater statistical confidence. The CARES/Life program (Nemeth et al. (2003)) was also used to investigate the size-effect relationship between the tensile specimens and the four-point-flexure specimens. This exercise also was performed to demonstrate analytical procedures that can be used to help certify newer grades of graphite for the proposed Gen IV high-temperature, gas-cooled nuclear reactors.

Appendixes A to F show all the data that were generated for this report. Appendix A contains tables and figures of individual slab data that compare slabs 1 to 4 for a particular specimen type, location within the slab, and orientation. Appendix B contains tables and figures of pooled data for slabs 1 to 4 that compare the strength distributions versus location within the slab and orientation for large tensile, small tensile, and flexure specimens. Appendix C contains tables and figures of pooled data for slabs 1 to 4 that compare the effects of location within the slab and orientation. Appendix D contains tables and figures of large superpooled data sets that compare the strength distribution of large tensile, small tensile, and flexure specimens. Appendix E contains tables and figures of the large superpooled data sets for the small and large tensile specimens only, and Appendix F compares the mean, standard deviation, and Weibull parameters for the individual slab data with the values reported by Price. Appendix G defines the symbols used in this report.

2.0 Price Report: Background and Summary

Price (1976) conducted more than 2000 ambient temperature tensile and four-point-flexure rupture tests on specimens from one log of extruded near-isotropic petroleum-coke-based nuclear graphite (Great Lakes Carbon Corporation grade H–451). The purpose of the investigation was to explore the statistical

distributions of tensile and flexural strengths within a graphite log. Factors that were explored included the (1) systematic variation of strength with orientation relative to the extrusion direction and location within the log, (2) dependence of strength on specimen size, and (3) relationship between flexural strength and tensile strength.

All specimens were taken from the same log of Great Lakes Carbon Corporation H–451 graphite. Four 127-mm- (5-in.-) deep slabs were cut transverse to the axis. Two slabs (1 and 4) were located within 25 mm (1 in.) of the two ends of the log, and two slabs (2 and 3) were located adjacent to the midlength plane of the log. The locations of the slabs are shaded in Figure 3. Each slab was cut into an edge section (the annular cross section in Fig. 4) and a center section (the circular cross section in Fig. 5) on a radius of 108 mm (4.25 in.).

Cylindrical test specimens were core drilled in the axial and radial orientations from the central zone and the edge zone of each slab, according to the plan shown in Figures 4 and 5. Large tensile specimens, right cylinders 12.8 mm (0.505 in.) in diameter by 76 mm (3 in.) long; small tensile specimens, 6.4 mm (0.25 in.) in diameter by 23 mm (0.9 in.) long; and flexure specimens, 6.4 mm (0.25 in.) in diameter by 51 mm (2 in.) long, were machined from the cores. Identification of the specimens was retained throughout. This sampling plan gave approximately equal numbers of the three types of specimens, with each type spread uniformly over the sampling zone.

The tensile specimens were joined between aluminum end pieces with epoxy cement, using V-block jigs to ensure axial alignment. Then the specimens were tested to failure in an Instron tensile testing machine that used roller-link chains to apply the load to the specimen end pieces. Stress-strain curves were measured on four representative 12.8-mm-diameter specimens out of each batch using a 51-mm (2-in.) gauge-length extensometer. On the remainder of the specimens, only the failure load was measured.

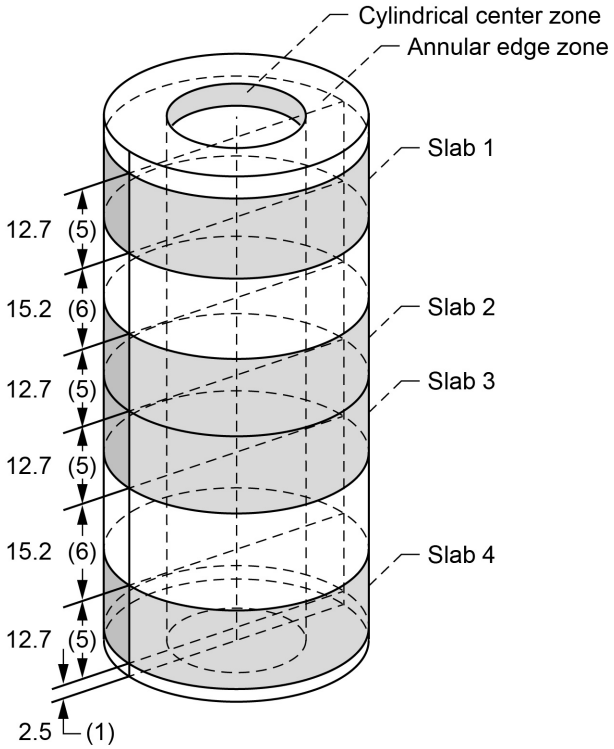

Figure 3.—Locations of slabs (shaded) for statistical strength testing in log 5651–90 of H–451 graphite. All dimensions in inches. Figure not drawn to scale. Copyright General Atomic; adapted from Price (1976).

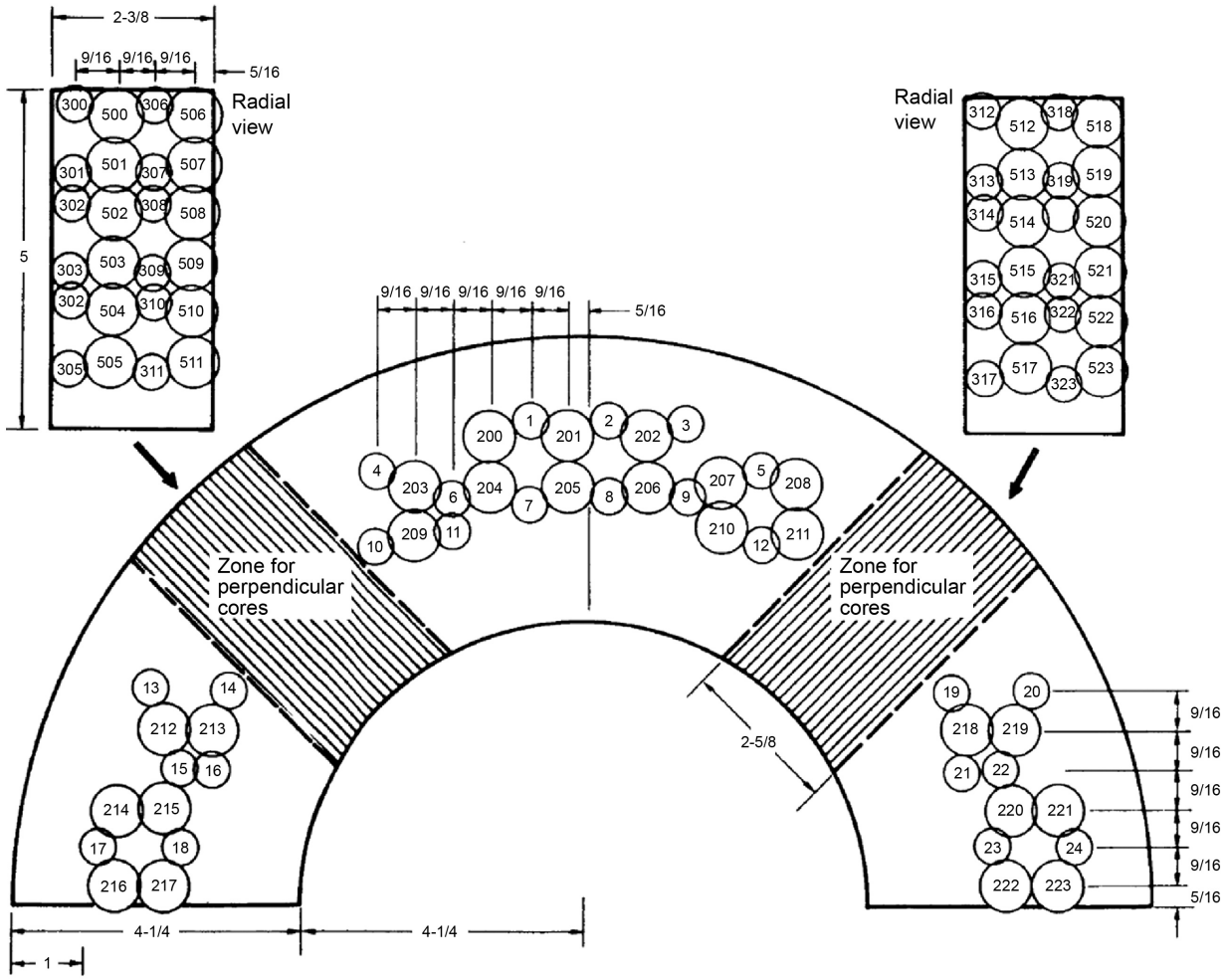

Figure 4.—Coring plan for edge of slabs. All dimensions in inches. Copyright General Atomic; reproduced from Price (1976).

The flexure specimens were tested in four-point-flexure with the loading points equally spaced 12.7 mm (0.5 in.) apart. The modulus of rupture (MOR) was calculated from the failure load using simple beam theory. Because of non-linear-elastic behavior, the MOR overestimated the outer fiber stress at failure and a correction was applied. Price used the following approximation for the stress-strain curve (Woolley (1965)):

$$\sigma = E\varepsilon_o\left[1-\exp\left(-\frac{\varepsilon}{\varepsilon_o}\right)\right] \tag{1}$$

where σ is the stress, E is the slope of the stress-strain curve at zero strain, ε is the strain, and ε_o is a constant for a given type of graphite which characterizes the curvature of the stress-strain curve. Price used Equation (1) in place of Hooke's Law to calculate the relationship between flexure moment and outer fiber strain in a beam. He obtained the following relationship between the MOR (flexure strength calculated assuming elastic behavior) and the true outer fiber strain at fracture ε_f for a cylindrical beam:

$$\mathrm{MOR} = E\varepsilon_f\left[1-0.34\left(\frac{\varepsilon_f}{\varepsilon_o}\right)+8.33\times10^{-2}\left(\frac{\varepsilon_f}{\varepsilon_o}\right)^2-1.62\times10^{-2}\left(\frac{\varepsilon_f}{\varepsilon_o}\right)^3+2.60\times10^{-3}\left(\frac{\varepsilon_f}{\varepsilon_o}\right)^4\right] \tag{2}$$

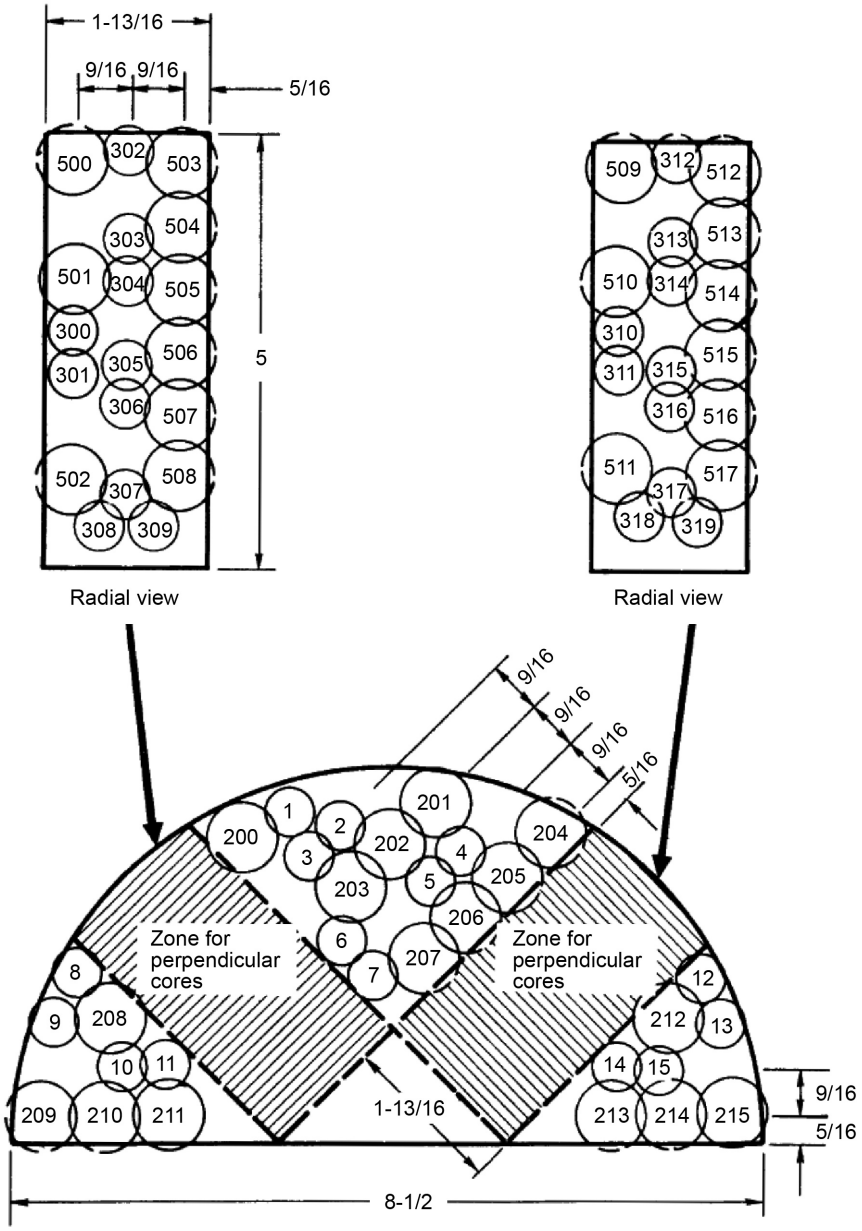

Figure 5.—Coring plan for center of slabs. All dimensions are in inches. Copyright General Atomic; reproduced from Price (1976).

Correction factors were applied to convert the conventionally calculated MOR to the true outer fiber stress at fracture for graphite with $\varepsilon_o = 0.004$ as shown in Figure 6. This value of ε_o is an average obtained from stress-strain curves on both axial and radial specimens.

Henceforth in this report, "axial" refers to the axial orientation of specimens and "radial" refers to the radial orientation of specimens that were excised from the parent graphite log. Also, "center" and "edge" refer to the center location and edge location, respectively, of specimens excised from the log. Price found the following: The mean strengths showed systematic dependence on orientation and location. Axial specimens were an average of 19 percent stronger than radial specimens when tested in tension. In flexure, axial specimens were an average of 13 percent stronger than radial specimens. Edge specimens were an average of 16 percent stronger than center specimens when they were tested in tension, and were

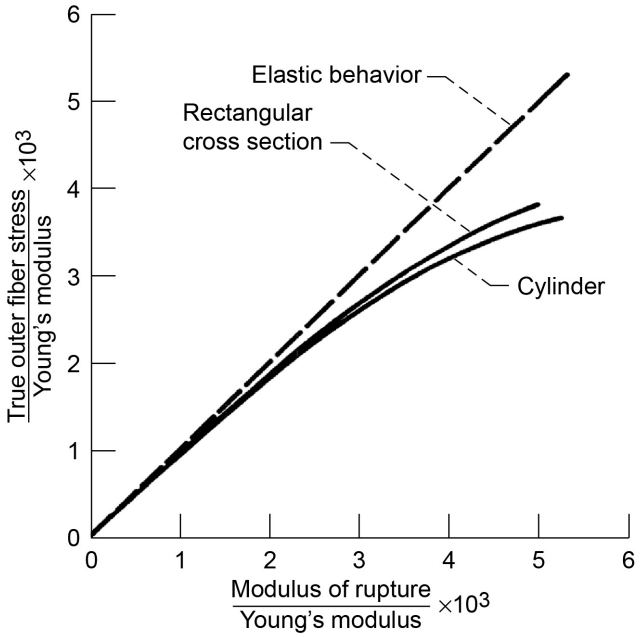

Figure 6.—Correction factors for flexure-test H–451 graphite data to allow for nonlinear stress-strain relationship, assuming that $\sigma = E\varepsilon_o[1 - \exp(\varepsilon/\varepsilon_o)]$, where σ is stress, E is the slope of the stress-strain curve at zero strain, ε is strain, and ε_o is a constant. Copyright General Atomic; reproduced from Price (1976).

7 percent stronger when they were tested in flexure. There were additional local fluctuations in strength that, in some cases, corresponded to local variations in density. The coefficient of variation (COV) for axial tensile strengths from the same zone in the parent log averaged 11.2 percent, compared with 14.7 percent for radial tensile strengths. For flexure strengths, the COV was lower than for tensile strengths, averaging 7.9 percent for the axial specimens and 9.0 percent for the radial specimens. Price did not investigate the nature of the strength anisotropy versus the specimen orientation. It was not determined, for example, if strength anisotropy could be correlated with preferentially oriented residual stress or if the shape of strength-controlling microcracks or pores had an orientation bias. Anisotropic pore orientation has been observed and quantified by Chinnathambi (2011) for various grades of graphite.

Price plotted data (in normal probability coordinates) for individual data sets with sample sizes ranging between 24 and 48 specimens each. The data sets were segregated for height from the bottom of the log, radial distance from the centerline of the log, and orientation of the specimen relative to the extrusion direction. Price did not attempt to combine individual data sets into larger pooled data sets. Because of the small sample sizes that were examined, Price concluded that that the overall distribution of H–451 graphite strength was neither two-parameter-Weibull nor normal (gaussian) because the individual slab cumulative strength distributions could be fit equally well by either distribution. The authors of this report believe that this was an inconclusive finding because the data sets examined had too few specimens to make any contentions about distribution type with a reasonable degree of statistical confidence.

Price found that the value of the Weibull modulus m was lower for tensile tests than for flexure tests—particularly for the MOR values adjusted for the nonlinear stress-strain relationship used to model graphite response. The mean tensile strength of small tensile specimens (volume 724 mm^3) was higher than that of large tensile specimens (volume 9847 mm^3) by 3 percent for axial specimens and by 8 percent for radial specimens. These numbers disagreed with the differences of 28 and 38 percent, respectively, that Price predicted using a simplified Weibull model for an averaged m obtained from the individual data sets. Flexural strengths (nonlinear values) averaged 52 percent higher than the corresponding tensile strengths for axial specimens and averaged 55 percent higher for radial specimens. These values agreed well with Weibull theory predictions of 51 and 64 percent, respectively, according to Price.

Price concluded that these inconsistencies prevented the material from qualifying as a "Weibull solid." We, however, believe that the reported findings from Price do not conclusively indicate that the material is not Weibull behaved, but they do indicate that the situation is more complicated and that other factors must be considered. What is certain is that the variability in graphite strength must be considered in the mechanical design of graphite components. Price showed that a significant part of the variability is attributable to local fluctuations over distances on the order of 100 mm.

3.0 Weibull Analysis: Tools and Procedure

3.1 Software Tools and Data Reconstruction

The results and conclusions from Price are reexamined in this report using the more recently developed WeibPar and CARES/Life programs. This new analysis was performed from the perspective of the Weibull distribution. WeibPar was used to provide the Weibull parameters, confidence bounds on parameters, goodness-of-fit statistics, and Weibull plots of the data. The NASA-developed CARES/Life program was used to investigate the size effect and strength response relationship of the four-point-flexure specimens.

Price originally plotted data in normal probability coordinates and listed the fracture stresses σ_f for all specimens. For the flexure specimens, this included fracture stresses corrected for nonlinear stress-strain response and fracture stress with the assumption of linear-elastic behavior. Unfortunately, fracture loads were not provided in the tables, and fractography was not attempted in the Price study.

Fractography of graphite rarely yields the source of failure—except when large flaws or inhomogeneities are present. For the Weibull analysis in this report, we assumed that the critical flaws were volume distributed. The rupture data were reconstructed from the tables provided in Price. There were a few values that were difficult to read (primarily in the third significant digit) from the report; however, a comparison of mean and standard deviation from the individual slab data correlated very well with the published values (see Appendix F).

3.2 Weibull Parameters, Effective Volume, and Size Effect Relationships

All of the individual data sets were analyzed with the WeibPar program to obtain the Weibull modulus, characteristic strength, and 90-percent confidence intervals on estimated parameters—which are a function of sample size (Thoman et al. (1969)). Typically for brittle materials, the Weibull parameters are determined from simple specimen geometry and loading conditions, such as beams under flexure and either cylindrical or flat specimens under uniform uniaxial tension. For fast-fracture in an inert environment, the failure probability of the part can be expressed in terms of the maximum stress σ_f (for flexural loading σ_f is the extreme fiber stress, also known as the modulus of rupture (MOR)) at the moment of fracture by using the two-parameter Weibull form:

$$P_f = 1 - \exp\left[-\left(\frac{\sigma_f}{\sigma_\theta}\right)^m\right] = 1 - \exp\left[-V_e\left(\frac{\sigma_f}{\sigma_{oV}}\right)^{m_V}\right] \tag{3}$$

where the Weibull modulus estimated from the experimental data, m_V is the volume-based (and m_S is the area-based) fast-fracture Weibull modulus. The subscript V indicates a property that is associated with the volume, and here m and m_V are equivalent in value. The term σ_θ is the volume- or area-based specimen characteristic strength, and V_e is the effective volume. The Weibull scale parameter for volume σ_{oV} (or for surface cracks σ_{oS}) is determined from σ_θ, m, the specimen geometry, and the loading configuration (e.g., Pai and Gyekenyesi (1988)). The scale parameter σ_{oV} is considered to be a material property, whereas σ_θ includes the effects of the specimen dimensions and stress distribution. Note that dimensional

compatibility means that σ_{oV} has units of stress • volume$^{1/m_V}$. The characteristic strength σ_θ is defined as the uniform stress or extreme fiber stress at which the probability of failure is 0.6321. The component failure behavior in fast-fracture (Eq. (3)) is only a function of σ_f and the empirically determined parameters, m and σ_θ. Procedures such as the least-squares method or maximum-likelihood analysis are used to estimate m and σ_θ from experimental fracture data. For this report, the Weibull parameters were determined from maximum-likelihood analysis, and the effective volume was defined as

$$V_e = \int_V \left(\frac{\sigma_1(x,y,z) + \sigma_2(x,y,z) + \sigma_2(x,y,z)}{\sigma_f} \right)^{m_V} \mathrm{d}V = \left(\frac{\sigma_{oV}}{\sigma_{\theta V}} \right)^{m_V} \tag{4}$$

The effective volume is an equivalent volume that is a function of stress magnitude and Weibull modulus and not the true volume of the component. The effective volume is calculated in the CARES/*Life* program. It can be thought of as the volume of a baseline specimen subjected to a uniform uniaxial stress that is equal to the peak stress in the component.

Equation (4) uses the Principle of Independent Action (PIA) model (Barnett et al. (1967) and Freudenthal (1968) and as described in Nemeth et al. (2003)). Sookdeo et al. (2008) showed that the Batdorf failure model (Batdorf and Crose (1974) and Batdorf and Heinisch (1978)) better correlated with graphite multiaxial rupture data. However, when the first principal stress is significantly larger than the other principal stresses, the two failure criterion yield quite similar results. In this particular case, the first principal stress dominates the reliability response for all specimen geometries, so the simpler PIA criterion was chosen for our analysis. Components (or specimens) with different shapes and loading configurations are described by the scale parameter σ_o and V_e. The Weibull size effect is a direct consequence of Equation (3) and predicts that the average strength of a large component is lower than that of a smaller component for identical loading and geometry because of the increased probability of having a weaker flaw present. The magnitude of the size effect is a function of the effective volume (or area) and the Weibull modulus. For two different component geometry/loading combinations, the size effect strength ratio is obtained by equating the probabilities of failure for the two different components, resulting in

$$\left(\frac{\sigma_{f,2}}{\sigma_{f,1}} \right) = \left(\frac{V_{e,1}}{V_{e,2}} \right)^{\frac{1}{m_V}} \tag{5}$$

One can make a straightforward comparison between two components by taking the characteristic strength values $\sigma_{\theta,1}$ and $\sigma_{\theta,2}$ estimated from rupture data and substituting for $\sigma_{f,1}$ and $\sigma_{f,2}$, respectively, into Equation (5). This is an important way to test the applicability of the Weibull distribution for modeling the strength response of different specimen geometries.

4.0 Data Pooling

4.1 Data Pooling Sequence

This section of the report is organized such that the rupture data are pooled into progressively larger data sets. This is shown in Appendixes A to E. Statistical tests to justify data pooling, such as those described in the *Composite Materials Handbook* (Department of Defense (2002)), were not performed. Price (1976) had previously concluded that, in general, the strength variations observed with regard to the location and orientation within the graphite log were outside the range of what would be expected from normal statistical variation. On that basis, data pooling could not be justified. These systematic variations were prevalent throughout the log. However, from the design engineer perspective, not pooling the data is

impractical. One would be left with the choice of either (1) trying to account for all these local effects, which would quickly become an intractable problem when one considers that this would also include log-to-log variations, or (2) combining all the data in a way that averages or groups this variation in a systematic way. This latter choice was the route taken in this report in order to study the overall strength behavior for graphite.

The slab-to-slab variations in mean strength were smaller than center-to-edge and axial-to-radial variations. Therefore, for the first level of data pooling, the rupture data for specimen type—small tensile, large tensile, and flexure—were pooled from the four slabs (disks) of material that were removed from the graphite log. This created data sets of between 126 to 192 specimens for each specimen type. From there, comparisons, such as center to edge and radial to axial, were made. Finally, all data for the respective specimen types were combined into "superpooled" sets to see the distribution trends of data sets containing many hundreds of specimens. Note that this report did not investigate the relationship of strength versus density, although Price did report that such a relationship was evident with many of the samples.

4.2 Weibull Parameters and Confidence Bounds of Individual Slabs

Figure 7 shows the two-parameter Weibull modulus m and characteristic strength σ_θ for the individual sample sets of each slab for the various orientations and locations (see also Appendix A). The parameters were determined using maximum-likelihood estimation. The 90-percent confidence bounds on parameters (see Thoman et al. (1969)) are also shown in the figure. Each sample set represents a unique slab number, orientation, and location.

There are a number of things to notice in Figure 7. First is that the confidence bounds for the Weibull modulus are much broader than the confidence bonds for the characteristic strength. This was as expected since it is known that there is more variability in the estimates for the Weibull modulus than for the characteristic strength for a given number of specimens. The width of confidence bounds is also a function of sample size—the greater the number of specimens in a sample set, the narrower the bounds will be. If the confidence bands for the different slabs do not overlap (share common values), it is a very strong indication that at least some of the difference is real and not due solely to natural statistical variation. In this regard, the slab-to-slab differences in characteristic strength in Figure 7(b) tend to stand out more (with less overlap) than do the differences in the Weibull modulus in Figure 7(a). The procedure described in chapter 8 of the *Composites Materials Handbook* (Department of Defense (2002)) provides a more rigorous treatment to test whether or not batch-to-batch (or in this case slab-to-slab) variation is statistically significant. That exercise was not performed in this report. The authors contend here that individual cases where the confidence bands do not overlap provide a sufficiently strong indication that the observed differences were real and that, in this situation, further statistical tests would not be of much further value (or provide much more insight).

There is a large difference between the flexure and tensile specimen characteristic strength that is clearly statistically significant in Figure 7(b). This is true for flexural stresses for both the linear-elastic stress-strain response and the stress response corrected for the nonlinear-elastic stress-strain response. Henceforth, this is referred to as the linear-elastic and nonlinear-elastic stress-strain response. This difference is expected and is consistent with Weibull methodology as indicated in Equation (5). Figure 7(b) also shows a consistent pattern in that the trends in strength from slab 1 to slab 4 are consistent for the large tensile, small tensile, and four-point-flexure specimens for a given orientation and location. For example, slab 1 is stronger than slab 2, which is stronger than slab 3 for the axial specimens from the center of the log for the large tensile, small tensile, and four-point-flexure specimens. This adds credence to the argument that slab-to-slab strength variations are real. Another trend to note is that the strengths of the large and small tensile specimens are quite similar when similar slabs, specimen orientation, and specimen location are compared. This trend is not consistent with Weibull theory as

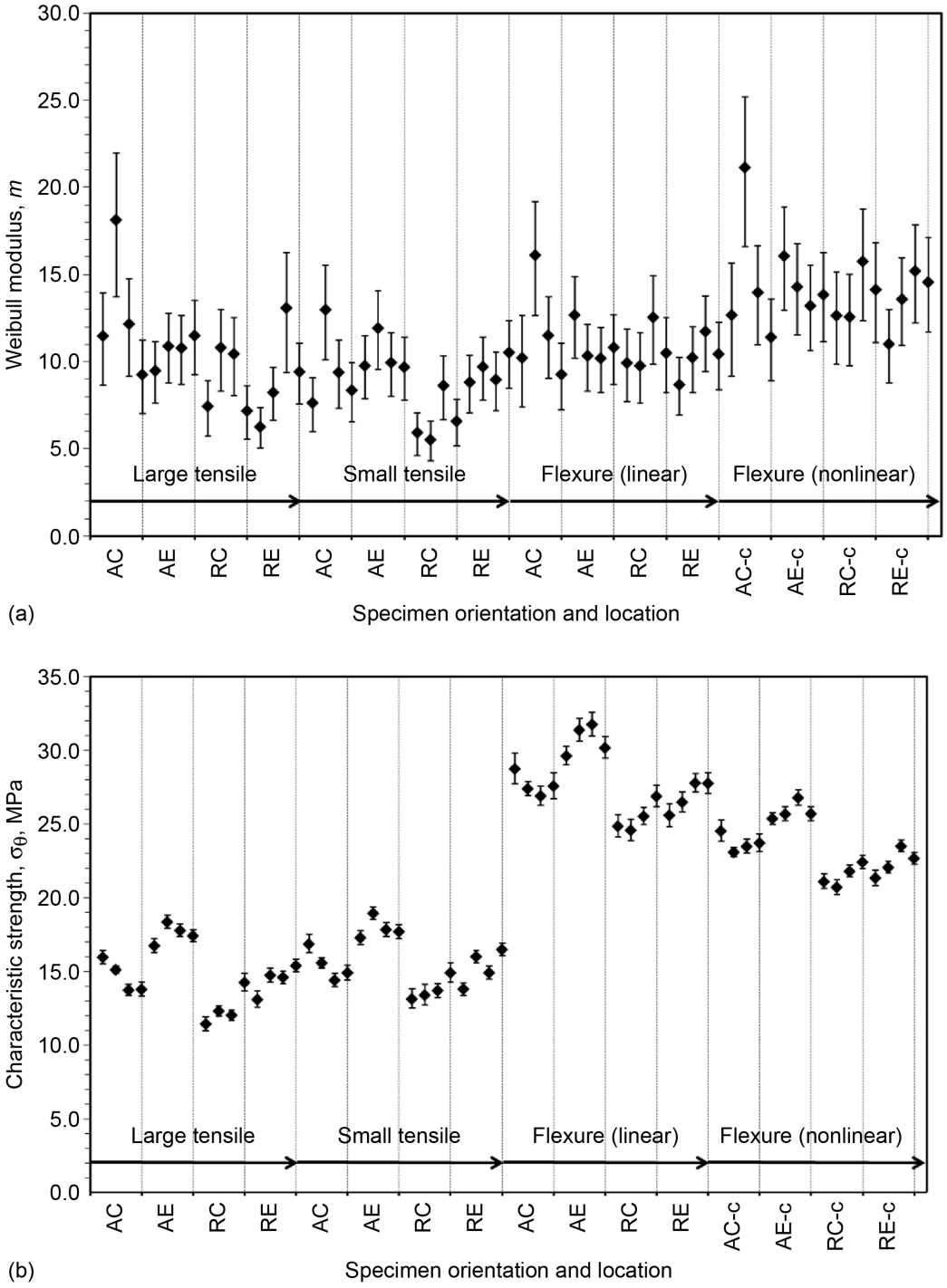

Figure 7.—Two-parameter model results for large tensile, small tensile, and four-point-flexure specimen sample sets. The 90-percent confidence bounds on the parameters are also shown. Specimen orientations and locations are designated as A = axial, C = center of slabs, E = edge of slabs, R = radial, and -c = stress corrected for the nonlinear stress-strain response. Slabs 1 to 4 are shown from left to right, respectively, for each grouping of common specimen orientation and location. (a) Weibull modulus. (b) Characteristic strength.

noted by Price. Another trend that is fairly distinct from Figure 7(b) is that the characteristic strengths for slabs 1 to 4 cluster together for a given orientation and location (versus some other orientation and/or location). In addition, for a given location (center or edge), the axial specimens are stronger than the radial specimens.

4.3 Comparison of Coefficients of Variation

Table 1 shows the coefficients of variation (COVs) of the characteristic strength and Weibull modulus for the large and small tensile specimens for various situations. The flexure specimens are not included, although the trends are similar. Including the flexure specimens adds the additional factor of stress gradient effects. In Table 1 the COV compares the large and small specimens that share similar slab number, location, and orientation. The other comparisons (slab-to-slab, center-to-edge, and axial-to-radial comparisons) are for specimens that share a common size, slab number, location, and orientation. Those results are a combined average of the COVs of the large and small specimens. Table 1 for the characteristic strength shows that the least amount of variability is between the large and small tensile specimens, followed by the slab-to-slab, center-to-edge, and axial-to-radial comparisons. The slab-to-slab COV is substantially smaller than the center-to-edge and axial-to-radial COVs. The axial-to-radial COV is only slightly larger than the center-to-edge COV. The COV for Weibull modulus in Table 1 shows relatively small changes for the various scenarios listed. This trend is closer to what would be expected if the natural statistical variation was the only factor.

Because the slab-to-slab COV for characteristic strength is significantly smaller than either the center-to-edge or axial-to-radial COV, it seems appropriate to use the average Weibull parameters for slabs 1 to 4 for comparison purposes. Tables 2 and 3 show these comparisons for the characteristic strength and Weibull modulus, respectively. For the specimen characteristic strength, Table 2 shows that the edge specimens are consistently stronger than the center specimens and that the axial specimens are consistently stronger than the radial specimens. The occasional inconsistencies of these trends from slab to slab are noted in the Price report and can be observed in Figure 7.

TABLE 1.—COEFFICIENT OF VARIATION OF WEIBULL PARAMETERS COMPARING VARIOUS SCENARIOS FOR VARIOUS LOCATION AND ORIENTATION COMBINATIONS
[Weibull two-parameter model.]

Weibull parameter	Coefficient of variation, COV			
	Comparisons			
	Large versus small	Slab versus slab	Center versus edge	Axial versus radial
Characteristic strength, σ_θ	4.05	6.52	10.31	11.38
Weibull modulus, m	15.93	19.28	17.42	18.97

TABLE 2.—AVERAGE CHARACTERISTIC STRENGTH OF SLABS 1 TO 4 FOR VARIOUS LOCATION AND ORIENTATION COMBINATIONS
[Weibull two-parameter model.]

Specimen type	Average of slabs 1 to 4 for characteristic strength, σ_θ, MPa				
	Specimen orientation and location				
	Axial center	Axial edge	Radial center	Radial edge	All specimens
Large	14.66	17.59	12.52	14.47	14.81
Small	15.45	17.96	13.79	15.31	15.63
Flexure, linear[a]	27.68	30.76	25.48	26.93	27.71
Flexure, nonlinear[b]	23.73	25.91	21.52	22.41	23.39

[a]Linear-elastic stress-strain response was assumed.
[b]Nonlinear-elastic stress-strain response was assumed.

4.4 Comparison of Weibull Modulus

Figure 7(a) shows the slab-to-slab variation for the Weibull modulus *m* for the two-parameter Weibull model. In the figure the confidence bands tend to show more overlap than for the characteristic strength shown in Figure 7(b), although three anomalously high values of *m* are noted for slab 2 for the axial and center locations for the large tensile, small tensile, and four-point-flexure specimens. Occasionally, the high and low values are outside of the main trend of the data. In Figure 7(a), the *m* from the small tensile specimens seems to trend a little lower than for the large tensile specimens, whereas the flexure specimens for linear-elastic stresses seem to have an *m* that is relatively similar to that of the large tensile specimens. The *m* for the flexure specimens with the linear-elastic and nonlinear-elastic stress-strain response trends higher than that for the tensile specimens.

These trends become more apparent in Table 3, although there are exceptions. For example, for the radial specimens from the edge of the log, the *m* for the small tensile specimens has a higher average value than it does for the large tensile specimens. Also, for the axial specimens from the center of the log, the *m* for the flexure specimens (for linear-elastic stress) are lower than for the large tensile specimens. Overall though, *m* is larger for axial specimens than for radial specimens. The flexure specimens (for linear-elastic response) tend to be slightly higher on average than the tensile specimens (more so for the radial orientation), although the flexure specimens corrected for the nonlinear stress-strain response are clearly higher. See Section 6.3 for further comments about this. The small tensile specimens tend to have a lower value of *m* than either the large tensile specimens or the flexure specimens. A general observation regarding Table 3 is that a single value of *m* can reasonably be used to characterize the large tensile, small tensile, and flexure specimens (for linear-elastic stress response for a given set of location and orientation conditions).

TABLE 3.—AVERAGE WEIBULL MODULUS OF SLABS 1 TO 4 FOR VARIOUS LOCATION AND ORIENTATION COMBINATIONS
[Weibull two-parameter model.]

Specimen type	Average Weibull modulus of slabs 1 to 4, *m*				
	Specimen orientation and location				
	Axial center	Axial edge	Radial center	Radial edge	All specimens
Large	12.76	10.67	8.97	9.25	10.41
Small	9.60	10.34	6.67	9.51	9.03
Flexure, linear[a]	11.78	11.01	10.69	10.28	10.94
Flexure, nonlinear[b]	14.81	14.36	13.78	13.60	14.13

[a]Linear-elastic stress-strain response was assumed.
[b]Nonlinear-elastic stress-strain response was assumed.

4.5 Weibull Plotting and the Pooling of Individual Slabs

The WeibPar software was used to create Weibull plots of the data for the individual slabs. Appendix A provides a full reproduction of the plots, and Figure 8 shows a representative plot of the individual slab data for the large tensile specimen. The individual specimen rupture stresses $\sigma_{f,i}$ were ranked from the lowest to highest value and assigned a failure probability according to the ranking formula $P_{f,i} = (i - 0.5)/n$, where i is the ranked value and n is the number of rupture specimens in a particular sample. This plot shows individual slabs 1 to 4 for the axial specimens from the edge of the log and the radial specimens from the center of the log. These examples represent two of the more extreme differences in the behavior of the overall data. The plot illustrates the slab-to-slab differences as well as overall differences regarding location and orientation.

Because the slab-to-slab COV for characteristic strength is significantly smaller than either the center-to-edge or axial-to-radial COV (see Table 1), it seems appropriate to first combine the data from the four slabs into single data sets segregated for location and orientation to better examine trends in the data. However, Price points out, and Figure 7(b) also shows, that slab-to-slab variations can be statistically

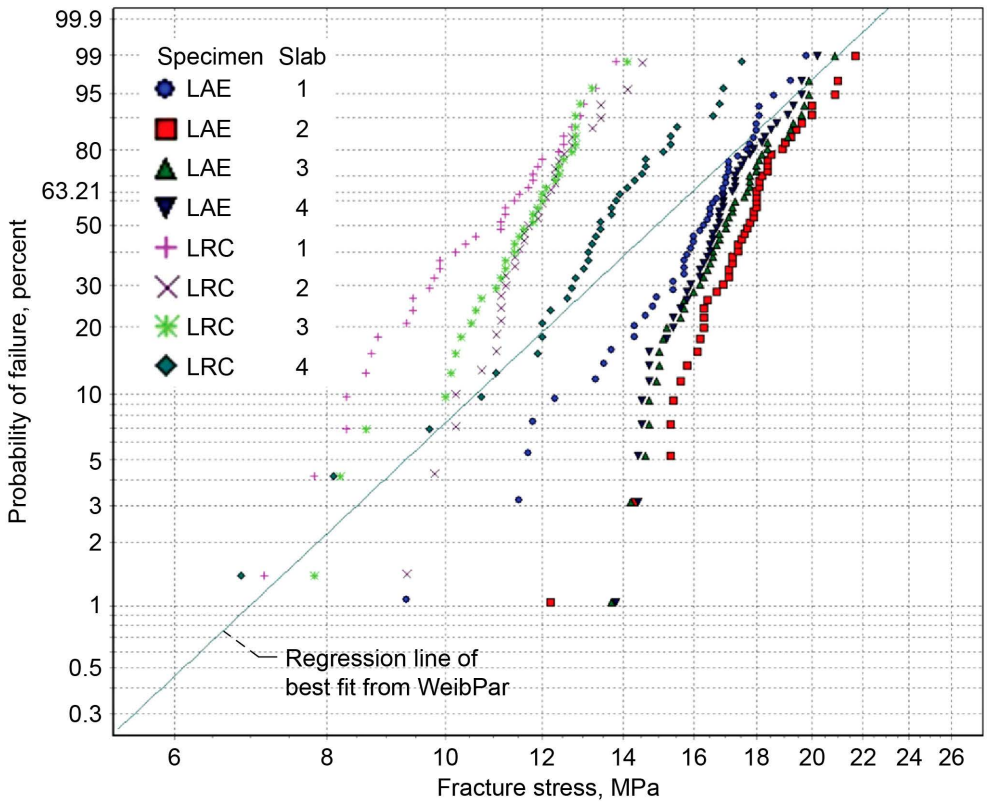

Figure 8.—Weibull plot of fracture stresses of individual slabs 1 to 4 for axial large tensile specimens from edge of slab and radial large tensile specimens from center of slabs. Specimen types, orientations, and locations are L = large tensile specimen, A = axial, E = edge of slabs, R = radial, and C = center of slabs.

significant (beyond the reasonable bounds of statistical expectation)—even for the same specimen orientation and (center or edge) location in the log. On that basis, the data for those slabs are not (from a statistical perspective) from the same source and, therefore, should not be combined. This restriction must be relaxed for this exercise. It can be seen from Figure 7 that it is very difficult (or next to impossible) to track and account for the differences in stochastic strength behavior depending on the origin (more so for the location and less so for the orientation) within a log showing where parts originated from. In other words, having a unique set of Weibull parameters applied to a part depending on where it came from within the log is impractical for the design of graphite reactor bricks, where thousands of tons of material are required. This is particularly true if these behaviors also change from log to log. Pooling data averages out local effects and allows overarching trends in the data to become more apparent. For this report, first slabs 1 to 4 were pooled into a single set for a given location and orientation, then data sets were pooled by orientation of the specimen only (i.e., edge and center data were pooled). Finally, all tensile specimen data were pooled so that the overall distribution of data could be examined.

4.6 Pooled Data Comparisons: Center, Edge, and Orientation

Appendixes B to E show the Weibull plots for the various combinations of pooled data. Highlights of this work are shown in the main body of the text. For the large tensile specimens, Figure 9 shows pooled data for slabs 1 to 4 for axial and radial specimens from the center and edge of the log. This figure illustrates the overall effect of location and orientation on the strength response of the graphite. Notice that the axial specimens tend to be stronger than the radial specimens and that their behaviors tend to diverge at the lower probabilities of failure. Plots for small tensile specimens and four-point-flexure

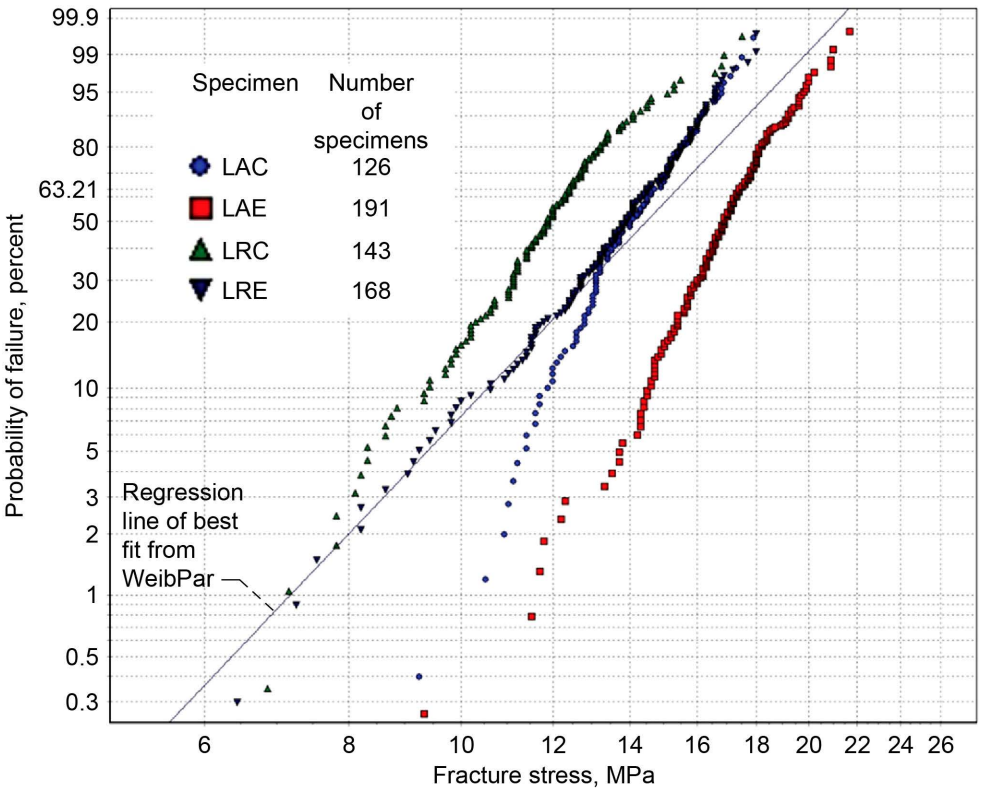

Figure 9.—Weibull plot of fracture stresses of pooled data from slabs 1 to 4 for axial and radial large tensile specimens from center and edge of slabs. Specimen types, orientations, and locations are L = large tensile, A = axial, C = center of slabs, E = edge of slabs, and R = radial,

specimens show very similar trends (see Appendix C for further comparisons). Because of the divergence in behaviors at the lower probabilities of failure, and because the COV of characteristic strength in Table 1 for orientation is larger than the COV for location, it seems more appropriate to pool data in terms of orientation rather than location. In other words, the next level of pooling should be to combine the center and edge data into two data sets segregated for axial and radial orientations.

Figure 10 is a Weibull plot contrasting the effects of axial and radial orientations for the large and small tensile specimens when the center and edge data are pooled. (The information in Appendix E is also relevant here.) For the axial orientation, the data for the large tensile specimens (m = 7.83 and σ_θ = 16.69) and small tensile specimens (m = 7.60 and σ_θ = 17.02) are nearly coincident, with the small tensile specimens only slightly stronger than the large tensile specimens. For the radial orientation, the small tensile specimens (m = 6.72 and σ_θ = 14.78) are noticeably stronger than the large tensile specimens (m = 6.42 and σ_θ = 13.74)—although not by a large amount. In both cases, the size effect is much smaller than what would be expected from Weibull analysis (see Eq. (5)). Another important item to note is that the data for the large and small tensile specimens show a similar slope, closely tracking one another. This adds confidence in the consistency of the data and in the Weibull modulus being constant with changing specimen size for the 14:1 difference in the tensile specimen volumes.

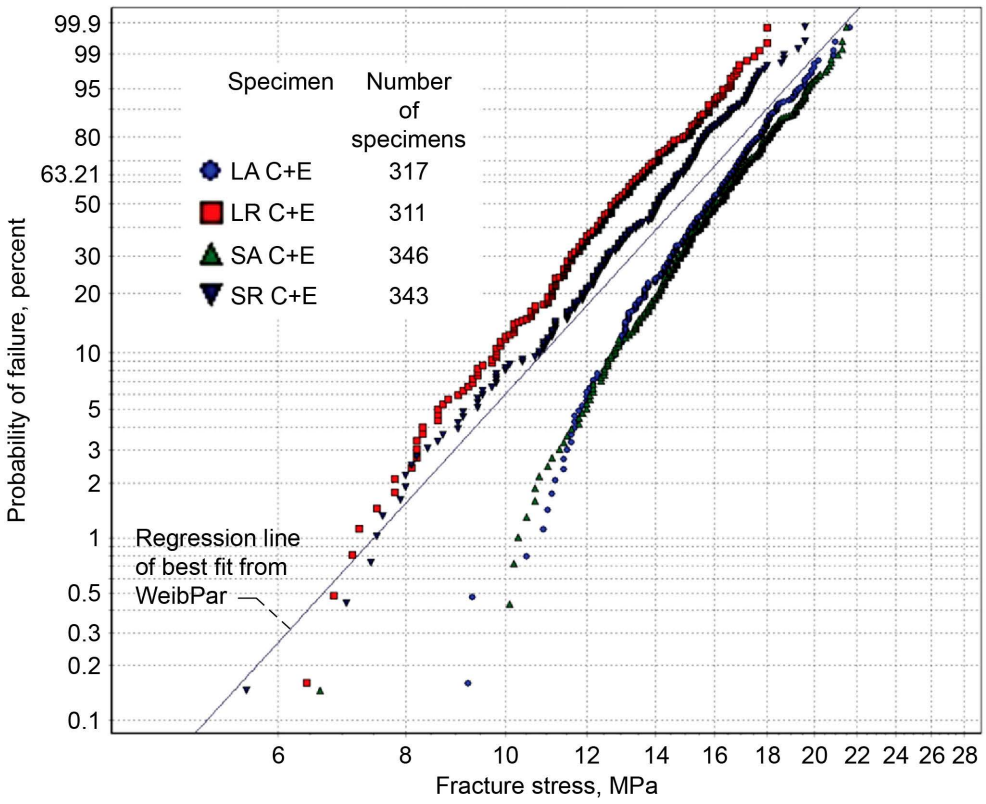

Figure 10.—Weibull plot of fracture stresses of pooled data from slabs 1 to 4 for axial and radial large and small tensile specimens pooled for center and edge of slabs. Specimen types, orientations, and locations are L = large tensile, A = axial, C = center of slabs, E = edge of slabs, R = radial, and S = small tensile.

4.7 Comparison to Three-Parameter Weibull Behavior

Similar to Figure 9, Figure 10 shows that the axial specimens are stronger than the radial specimens. In addition, the data for the axial specimens have a curved appearance more consistent with a three-parameter Weibull distribution or some other distribution. Price compared data for the individual slabs with best-fit two-parameter-Weibull and gaussian distributions. Here instead, we provide some limited comparison using the three-parameter Weibull distribution, which is expressed as

$$P_f = 1 - \exp\left[-\left(\frac{\sigma_f - \sigma_l}{\sigma_\theta}\right)^m\right] \tag{6}$$

where σ_l is known as the threshold or location parameter. When σ_l is zero, the two-parameter Weibull distribution is obtained.

Tables 4 to 9 list the maximum-likelihood estimated parameters for the two- and three-parameter distributions from WeibPar for the small tensile, large tensile, and four-point-flexure specimens. A three-parameter distribution would generally be expected to give better fit to the data than would the two-parameter distribution simply because of the additional degree of freedom. In the tables, the residual sum of squares (RSS) and the coefficient of determination R^2 are also listed. The RSS is the sum of the squares of the residuals. It is a measure of the discrepancy between the data and an estimation model. A small RSS indicates a tight fit of the model to the data, and R^2 is a statistic that gives some information about the goodness of fit of a model. In regression, R^2 is a statistical measure of how well the regression line

TABLE 4.—WEIBULL PARAMETERS OF POOLED SLABS 1 TO 4 FOR LARGE TENSILE SPECIMENS AND VARIOUS LOCATION AND ORIENTATION COMBINATIONS

[Weibull two-parameter model.]

Weibull parameter	Specimen orientation and location					
	Axial center	Axial edge	Radial center	Radial edge	Axial, center and edge	Radial, center and edge
Characteristic strength, σ_θ, MPa	14.80	17.63	12.65	14.52	16.69	13.74
Weibull modulus, m	9.47	10.05	6.50	7.52	7.83	6.42
Residual sum of squares, RSS	.0731	.0603	.224	.0749	.209	.132
Coefficient of determination, R^2	.960	.977	.944	.987	.970	.988

TABLE 5.—WEIBULL PARAMETERS OF POOLED SLABS 1 TO 4 FOR LARGE TENSILE SPECIMENS AND VARIOUS LOCATION AND ORIENTATION COMBINATIONS

[Weibull three-parameter model.]

Weibull parameter	Specimen orientation and location					
	Axial center	Axial edge	Radial center	Radial edge	Axial, center and edge	Radial, center and edge
Characteristic strength, σ_θ, MPa	7.02	11.64	6.93	14.52	9.30	10.06
Threshold parameter, σ_l, MPa	7.67	5.94	5.58	0.00	7.26	3.61
Weibull modulus, m	4.37	6.58	3.54	7.52	4.27	4.61
Residual sum of squares, RSS	.0123	.0546	.0689	.0749	.0183	.0330
Coefficient of determination, R^2	.993	.979	.983	.987	.997	.997

TABLE 6.—WEIBULL PARAMETERS OF POOLED SLABS 1 TO 4 FOR SMALL TENSILE SPECIMENS AND VARIOUS LOCATION AND ORIENTATION COMBINATIONS

[Weibull two-parameter model.]

Weibull parameter	Specimen orientation and location					
	Axial center	Axial edge	Radial center	Radial edge	Axial, center and edge	Radial, center and edge
Characteristic strength, σ_θ, MPa	15.56	17.98	13.85	15.43	17.02	14.78
Weibull modulus, m	7.58	9.73	6.11	8.02	7.60	6.72
Residual sum of squares, RSS	.122	.0441	.0568	.0664	.142	.0603
Coefficient of determination, R^2	.967	.984	.991	.987	.984	.995

TABLE 7.—WEIBULL PARAMETERS OF POOLED SLABS 1 TO 4 FOR SMALL TENSILE SPECIMENS AND VARIOUS LOCATION AND ORIENTATION COMBINATIONS

[Weibull three-parameter model.]

Weibull parameter	Specimen orientation and location					
	Axial center	Axial edge	Radial center	Radial edge	Axial, center and edge	Radial, center and edge
Characteristic strength, σ_θ, MPa	11.29	10.33	11.12	15.43	12.99	14.59
Threshold parameter, σ_l, MPa	4.21	7.57	2.68	0.00	3.98	0.185
Weibull modulus, m	5.47	5.48	4.87	8.02	5.74	6.63
Residual sum of squares, RSS	.0936	.0108	.0592	.0664	.0866	.0612
Coefficient of determination, R^2	.975	.996	.990	.987	.990	.995

TABLE 8.—WEIBULL PARAMETERS OF POOLED SLABS 1 TO 4 FOR LARGE AND SMALL TENSILE SPECIMENS AND VARIOUS LOCATION AND ORIENTATION COMBINATIONS

[Weibull two-parameter model.]

Weibull parameter	Specimen orientation and location					
	Axial center	Axial edge	Radial center	Radial edge	Axial, center and edge	Radial, center and edge
Characteristic strength, σ_θ, MPa	15.24	17.81	13.30	15.02	16.86	14.30
Weibull modulus, m	7.92	9.83	6.02	7.57	7.68	6.39
Residual sum of squares, RSS	.263	.0892	.305	.104	.316	.142
Coefficient of determination, R^2	.953	.984	.971	.991	.980	.994

TABLE 9.—WEIBULL PARAMETERS OF POOLED SLABS 1 TO 4 FOR LARGE AND SMALL TENSILE SPECIMENS AND VARIOUS LOCATION AND ORIENTATION COMBINATIONS

[Weibull three-parameter model.]

Weibull parameter	Specimen orientation and location					
	Axial center	Axial edge	Radial center	Radial edge	Axial, center and edge	Radial, center and edge
Characteristic strength, σ_θ, MPa	9.92	11.11	8.79	15.02	11.74	11.81
Threshold parameter, σ_l, MPa	5.25	6.64	4.41	0.00	5.04	2.45
Weibull modulus, m	5.14	6.06	3.94	7.57	5.28	5.23
Residual sum of squares, RSS	.122	.0474	.0854	.104	.0930	.056
Coefficient of determination, R^2	.978	.991	.992	.991	.994	.998

TABLE 10.—WEIBULL PARAMETERS OF POOLED SLABS 1 TO 4 FOR FOUR-POINT-FLEXURE SPECIMEN AND VARIOUS LOCATION AND ORIENTATION COMBINATIONS

[Weibull two-parameter model.]

Weibull parameter	Specimen orientation and location					
	Axial center	Axial edge	Radial center	Radial edge	Axial, center and edge	Radial, center and edge
Characteristic strength, σ_θ, MPa	27.63 23.69[a]	30.82 25.94[a]	25.56 21.59[a]	27.00 22.49[a]	29.61 25.10[a]	26.39 22.11[a]
Weibull modulus, m	10.79 13.07[a]	10.24 13.27[a]	9.82 12.65[a]	9.78 12.31[a]	9.12 11.54[a]	9.45 12.03[a]
Residual sum of squares, RSS	.103 .0761[a]	.247 .109[a]	.0855 .0264[a]	.0635 .0673[a]	.505 .249[a]	.0456 .0228[a]
Coefficient of determination, R^2	.929 .922[a]	.877 .911[a]	.958 .980[a]	.982 .971[a]	.885 .914[a]	.992 .994[a]

[a]Nonlinear-elastic stress-strain response was assumed.

TABLE 11.—WEIBULL PARAMETERS OF POOLED SLABS 1 TO 4 FOR FOUR-POINT-FLEXURE SPECIMEN AND VARIOUS LOCATION AND ORIENTATION COMBINATIONS

[Weibull three-parameter model.]

Weibull parameter	Axial-center	Axial-edge	Radial-center	Radial-edge	Axial, center and edge	Radial, center and edge
Characteristic strength, σ_θ, MPa	11.30 8.65[a]	9.64 7.29[a]	11.24 10.15[a]	27.00 22.49[a]	11.98 9.32[a]	19.41 18.46[a]
Threshold parameter, σ_l, MPa	16.13 14.91[a]	20.82 18.44[a]	14.13 11.36[a]	0.00 0.00[a]	17.34 15.60[a]	6.92 3.63[a]
Weibull modulus, m	4.35 4.71[a]	3.13 3.66[a]	4.22 5.82[a]	9.78 12.31[a]	3.66 4.22[a]	6.89 10.01[a]
Residual sum of squares, RSS	.0274 .0254[a]	.0124 .00411[a]	.0105 .00521[a]	.0635 .0673[a]	.0635 .0327[a]	.0413 .0289[a]
Coefficient of determination, R^2	.981 .974[a]	.994 .997[a]	.995 .996[a]	.982 .971[a]	.986 .989[a]	.993 .992[a]

[a]Nonlinear-elastic stress-strain response was assumed.

approximates the real data points. An R^2 of 1.0 indicates that the regression line fits the data perfectly. (Also see definitions in standard statistics textbooks or Web-based resources.) Note that RSS and R^2 are not associated with the maximum-likelihood estimation but are listed here because they provide useful information regarding the relative goodness of fit. The tables provide values for pooled data from slabs 1 to 4 for four types of specimens: (1) axial specimens from the center of the log, (2) axial specimens from the edge of the log, (3) radial specimens from the center of the log, and (4) radial specimens from the edge of the log. Also provided are values associated with the axial and radial specimens, where the center and edge specimens are pooled for the given orientation.

Tables 4 and 5 provide the two- and three-parameter values, respectively, for the large tensile specimens. Tables 6 and 7 provide these values for the small tensile specimens; Tables 8 and 9 provide these values for the pooled large and small tensile specimens; and Tables 10 and 11 provide these values for the four-point-flexure specimens. For all specimen geometries, the threshold stress σ_l tends to be

higher for the axial specimens than for the radial specimens. This is consistent with the trend that the data for the axial specimens generally show more visible curvature on a Weibull plot than do the data for the radial specimens. For radial specimens from the edge of the log, σ_l is essentially zero for all geometries. (Note that WeibPar does not consider, or allow estimation for, negative threshold values.)

Tables 5, 7, 9, and 11 provide the three-parameter Weibull values obtained from the maximum-likelihood estimation. Generally σ_l is less than half the two-parameter σ_θ value for the tensile specimens but greater than half this value for the four-point-flexure specimens, except for the radial specimens from the edge of the log. A comparison of RSS and R^2 for the two-parameter and three-parameter values of the flexure specimens in Tables 10 and 11, respectively, seems to indicate a stronger correlation to a three-parameter distribution than to a two-parameter distribution. This trend is somewhat less apparent for the tensile specimens.

There is quite a bit of variation in σ_l, but this is to be expected because a larger number of specimens is required to sufficiently reduce uncertainty in this parameter estimate. Generally R^2 is high for all the data sets: 0.94 or greater. This means that the data closely follow the best-fit regression curves for two- or three-parameter Weibull distributions. However, the three-parameter best fit measured by RSS and R^2 tends to be better than the two-parameter best fit. For R^2, values approaching 1.0 indicate better correlation with a value of 1.0, which indicates a perfect fit to the data. For RSS, the closer the value is to zero, the better the fit to the data is. A comparison of the two- and three-parameter values in Tables 4 and 5 for axial large tensile specimens from the edge of the log shows a relatively small difference for RSS and R^2. This means that the two- and three-parameter distributions fit the data equally well. Conversely, a larger difference in values means that one distribution fits better than the other. However, if σ_l is relatively small, these differences probably have less significance, as is the case for the pooled data for the radial large tensile specimens from the center and edge of the log (Tables 4 and 5).

Since a large number of data points are available, a visual interpretation of the behavior of the data on a Weibull plot seems to provide a good basis, along with the RSS and R^2 (or other goodness-of-fit statistics), for supporting a particular argument. However, when a small number of specimens are involved, arguing that the data are behaving according to one distribution is practically groundless because of the natural statistical variation involved (see graphical examples of this behavior in Danzer et al. (2008)). Larger numbers of specimens are needed to even begin to discern one distribution from another. This is an important reason for pooling data wherever possible.

4.8 Weibull Modulus and Specimen Geometry

In Tables 4 and 6, the Weibull modulus m for the small tensile specimens tends to be smaller than for the large tensile specimens, although this is not true for radial specimens from the edge of the log. This trend was also borne out in Table 3 for slab-averaged parameters. Data for the pooled center and edge locations have differences that appear to be negligible, and overall, m is quite similar for the large and small tensile specimens of a given orientation. (A similar, although less clear, trend is evident in Table 3.) Contrasting Table 3 with Tables 4 and 6 for m indicates that data pooling decreases the estimated values of m. This is to be expected since the characteristic strengths σ_θ for the individual slabs varied more than what would be expected from natural statistical variation. This increased the relative scatter in the pooled data and, therefore, reduced the Weibull modulus. This phenomenon may also have ramifications for the size effect expected on the basis of Weibull analysis. A comparison of Table 2 with Tables 4 and 6 shows negligible differences between the averaged and pooled σ_θ. This is as expected.

Another noteworthy trend, less apparent in Table 3 than in Tables 4, 6, 7, and 10, is that m tends to be larger for the four-point-flexure specimens than for the two tensile specimen geometries. This is particularly evident for the flexure specimen fracture stresses that were corrected for nonlinear stress-strain response as discussed previously. Again, this difference could be due to the changing effective volume V_e with load, but it cannot be discounted that imperfections at the surface of the specimen may behave differently than the imperfections embedded within the volume of the specimen.

4.9 Effect of a Residual Compressive Stress (or Location Parameter)

A clear trend in the data in Tables 4 to 9 is that, for the two-parameter Weibull distribution, *m* is consistently smaller for the axial specimens than for the radial specimens. This is probably not a coincidence. It could mean that there are subtle differences in the flaw population being sampled or that a residual compressive stress is present in the axial specimens and absent (or smaller) in the radial specimens. One contributor to this behavior is that slab 2 has an anomalously high Weibull modulus for the axial specimens from the center of the log. This helps to truncate the behavior of the pooled slabs at a low probability of failure. (See Appendix A for additional plots and tables regarding this behavior.) Note that the relative scatter is reduced (the estimated two-parameter Weibull modulus *m* increases) when, for an underlying three-parameter-behaved data set, the threshold stress σ_l increases.

In Figure 10 the data for the radial specimens appear to be more linear and consistent with a two-parameter Weibull distribution, whereas the data for the axial specimens appear to be more consistent with a three-parameter distribution. This trend is consistent for the data for the four-point-flexure specimens as well (see Appendix E for additional plots). This tendency toward three-parameter behavior is considerably more difficult to discern from the individual slab data of the axial tensile specimens shown in Appendix A. However, in examining Figures 29, 32, 38, and 41 from Appendix A, there appears to be a slight overall bias in the curvature in the data consistent with three-parameter behavior, although we would not claim that this was a distinct trend and certainly exceptions could be noted. Data pooling helps to bring out these global trends, although it also smears out the local fluxuations.

A three-parameter distribution can indicate that a residual compressive stress is affecting the observed fracture strengths, where the fracture strength is increased by the amount of the residual compressive stress. A residual compressive stress would only affect the threshold or location parameter σ_l of the Weibull distribution. A residual stress would not affect the Weibull modulus (see Eq. (6)). Bias in the orientation of elongated pores would also be expected to have an effect on the characteristic strength σ_θ (the percentage of porosity would be a contributing factor by changing the net section stress with orientation). However, this is a conjecture here. Further investigation would be needed, and as previously noted, there is physical evidence of pore shape orientation bias in other graphite grades (Chinnathambi (2011)).

An interesting exercise, therefore, would be to examine how similar *m* is for the axial and radial specimens. Here, we do this by assuming that a residual compressive stress is larger in the axial direction than in the radial direction. This is considered for the tensile specimens only. (The flexure specimens are not considered because of the confounding effects of the nonlinear stress-strain response). Note that this only involves manipulation of the σ_l parameter. If the Weibull modulus were different in the axial direction than in the radial direction, it would indicate that other phenomena are present, such as different flaw populations or R-curve behavior (see Nemeth and Bratton (2010, 2011) for example). Other statistical effects could appear similar to three-parameter behavior, as shown in the example in Section 5.12.

Mapping the axial specimen data onto the radial specimen data by subtracting the assumed residual stress, allows the data to be further pooled into a larger set of equivalent radial specimens. Figure 11 shows a plot of Figure 10 data where an assumed residual stress of 2.95 or 2.24 MPa has been subtracted from the rupture strength of each specimen for the axial large and small tensile specimens, respectively. The values of 2.95 and 2.24 MPa were obtained by subtracting σ_θ for the radial specimens from the axial specimens (for pooled center and edge locations) for the two-parameter values shown in Tables 4 and 6. Two different values of residual stress were chosen (rather than a single averaged value of the two specimen geometries) so that the small specimen data could be superimposed on the large specimen data for direct comparison. Figure 11 shows that the axial specimen data, with a residual stress subtracted, largely falls directly over the data for the radial specimens. For the axial large tensile specimens, $m = 6.41$ and $\sigma_\theta = 13.70$; for the radial large tensile specimens, $m = 6.42$ and $\sigma_\theta = 13.74$; for the axial small tensile specimens, $m = 6.56$ and $\sigma_\theta = 14.75$; and for the radial small tensile specimens, $m = 6.72$ and $\sigma_\theta = 14.78$.

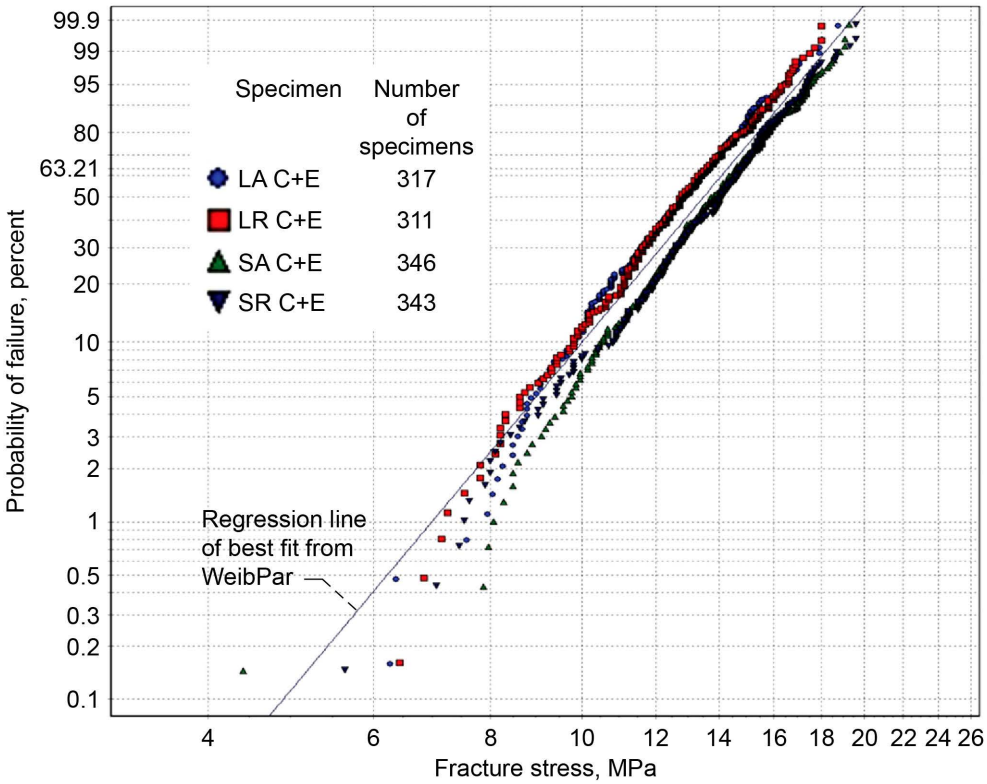

Figure 11.—Weibull plot of fracture stresses of pooled data from slabs 1 to 4 for large and small tensile specimens, contrasting the axial and radial specimen orientations when an assumed residual stress of 2.95 or 2.24 MPa has been subtracted from the data for the axial large or small specimens, respectively. Specimen types, orientations, and locations are L = large tensile, A = axial, C = center of slabs, E = edge of slabs, R = radial, and S = small tensile.

It is significant that the *m* values are quite close to one another, and it is an indication that the axial and radial specimens have an underlying common behavior.

4.10 Large-Scale Superpooling of Tensile Specimens

Figure 12 shows the pooled data for the axial (with residual stress subtracted) and radial large and small tensile specimens from Figure 11. The figure shows that the large and small tensile specimens have nearly identical behavior. For the large tensile specimens, $m = 6.41$ and $\sigma_\theta = 13.72$, and for the small tensile specimens, $m = 6.64$ and $\sigma_\theta = 14.76$. Figure 13 combines the small and large tensile specimen data. Equation (5), the size-effect equation, was used for $m = (6.64 + 6.41)/2 = 6.53$ to transform the small tensile specimen data to equivalent large tensile specimen data. It was assumed that the small tensile specimens had a volume that was 0.621 times the size of the large tensile specimens, so Equation (5) could be used to transform the characteristic strength of the small tensile specimens to that of the large tensile specimens. Note that the actual volume ratio between the small and large tensile specimens was 0.074. However, using this size difference in the transformation would yield unusual results because the actual size effect is substantially smaller than what would be predicted from the Weibull equation. For these simulated large tensile specimen data, the WeibPar algorithm yields $m = 6.53$ and $\sigma_\theta = 13.72$ for the two-parameter model.

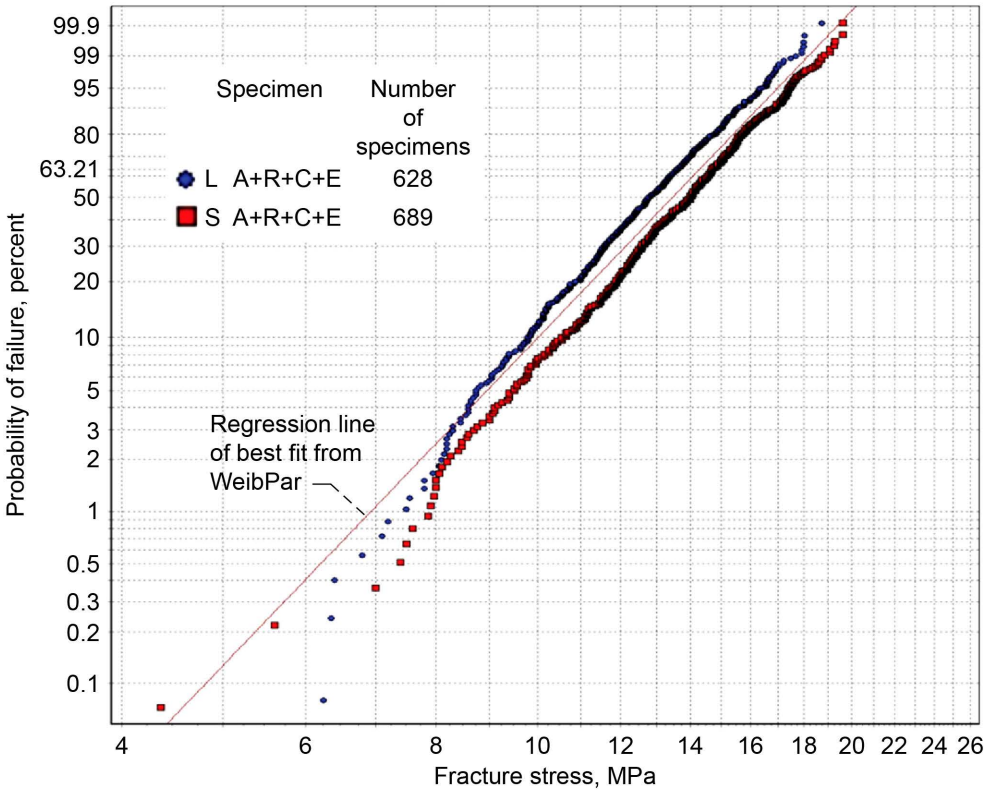

Figure 12.—Weibull plot of fracture stresses for data from Figure 11 pooled into single data sets for the large and small tensile specimens. Specimen types, orientations, and locations are L = large tensile, A = axial, R = radial, C = center of slabs, E = edge of slabs, and S = small tensile.

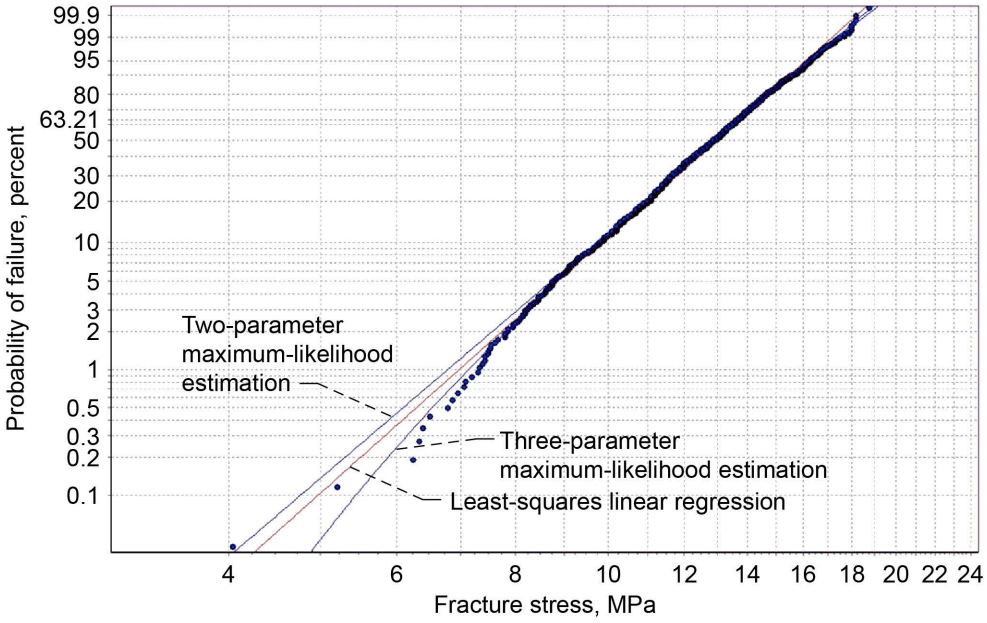

Figure 13.—Large and small tensile specimen data from Figure 12 pooled into a single data set of 1317 equivalent large tensile specimens.

TABLE 12.—WEIBULL PARAMETERS OF POOLED DATA FOR ALL LARGE AND SMALL TENSILE SPECIMENS (1317 SPECIMENS)

Weibull parameter	Pooled large and small (equivalent large tensile geometry)		Pooled large and small (with no scaling)	
	Two-parameter model	Three-parameter model	Two-parameter model	Three-parameter model
Characteristic strength, σ_θ, MPa	13.73	11.40	15.70	12.22
Threshold parameter, σ_l, MPa	------	2.30	------	3.41
Weibull modulus, m	6.53	5.37	6.16	4.73
Residual sum of squares, RSS	.241	.0847	.398	.0769
Coefficient of determination, R^2	.995	.998	.992	.998

Table 12 shows the respective two- and three-parameter maximum-likelihood estimates for the Weibull parameters. The R^2 statistic is above 0.99 regardless of the distribution. Note also that the value of σ_l is relatively low at 2.30. Figure 13 also illustrates the prudence of using a two-parameter distribution instead of a three-parameter distribution. The figure shows that there are two low-strength rupture stresses at the lowest probabilities of failure. This is consistent with two-parameter behavior. A less likely, though plausible, scenario is that the two data points are outliers, possibly indicating the presence of another failure mode with a lower m. It is unknown how the actual data would have behaved at lower probabilities of failure. This uncertainty warrants the more conservative approach of predicting material behavior with the two-parameter distribution (instead of using another distribution) at low probabilities of failure—consistent with the conclusions of Liu (1997) for smaller specimen sample sizes. The point of developing Figure 13 was to examine the overall distribution of the graphite rupture data for a large equivalent sample size of over 1000. Even with such a large sample size it is difficult to draw firm conclusions regarding the type of distribution the data follows, although again, use of the two-parameter Weibull distribution seems the prudent choice and it certainly seems to approximate the behavior of the data rather well. Table 12 also shows the Weibull parameter values for the small and large tensile specimens pooled without consideration of a residual stress or size effect. Again a two- or three-parameter distribution fit the data well. The plot, which is not shown here (see Figure 211 in Appendix E for the plot), is similar to Figure 13 in shape except for some more exaggerated truncation at the lower tail of the distribution for the very lowest strength specimens. Note that m is lower than the transformed data in the table although not dramatically so.

4.11 Anomalous Behavior of Slab 1 Edge-of-Log Specimens

For this report, the fracture behavior of slab 1 specimens from the edge of the log is worth considering. Figure 14 shows a Weibull plot of individual specimen fracture stresses for the pooled data of radial specimens from the edge of the log of slabs 1 to 4 for large and small tensile specimens and four-point-flexure specimens. The linear-elastic flexure specimen fracture stresses are shown. The knee in the curve at the lower failure probability is due to the contribution from slab 1 for all specimen geometries (see Figure 15). Slab 2 also contributes to the knee for the small tensile specimens. This deviation may also exist for axial specimens at the same location, although this is less clear (Appendix A shows the complete set of Weibull plots for the individual slabs, and Figure 90 in Appendix B—a plot of the bend fracture stresses corrected for a nonlinear stress-strain response—shows a similar knee in the data.)

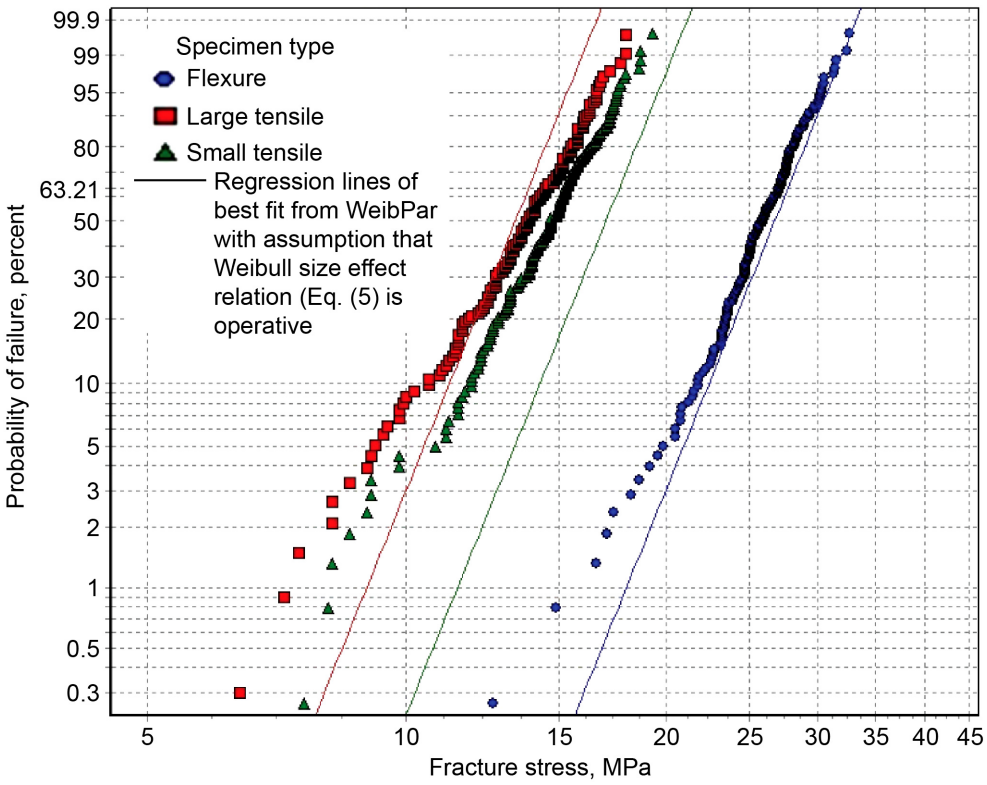

Figure 14.—Weibull plot of fracture stresses of data pooled from slabs 1 to 4 for radial large tensile, small tensile, and four-point-flexure specimens (linear-elastic flexure-specimen fracture stresses) from edge of slab.

In Weibull analysis, a knee in the data is indicative of bimodal behavior or the presence of two or more flaw distributions (see Johnson (1983)). The inflection point at the knee occurs between 5- and 10-percent probability of failure for all specimen geometries in Figure 14. In this case the knee occurred in the data because of the systematic difference in the behavior of slab 1. Slab 1 shows more scatter in fracture strength at lower probabilities of failure (locally a lower value of Weibull modulus m, as shown in Figure 15). Since the other slabs did not typically display this behavior (see Appendix A), pooling the rupture data from the four slabs should show an overall distribution similar to that of partially concurrent or mutually exclusive flaw populations (again see Johnson (1983)). It is unclear why the inflection point in Figure 15 (at about 40-percent probability of failure) does not appear to shift to higher probabilities of failure as the effective volume increases (from flexure, to small tensile, to large tensile), which would be the case if the flaw populations were concurrent (simultaneously present in all specimens throughout the graphite log). The effect seems to be independent of the amount of material under load—perhaps because of a localized density variation (an effect independent of volume), where a more localized region of slab 1 has low strength and low Weibull modulus behavior. The behavior of slab 1 at the edge of the log appears to have been an isolated effect that was not reproduced in the rest of the log.

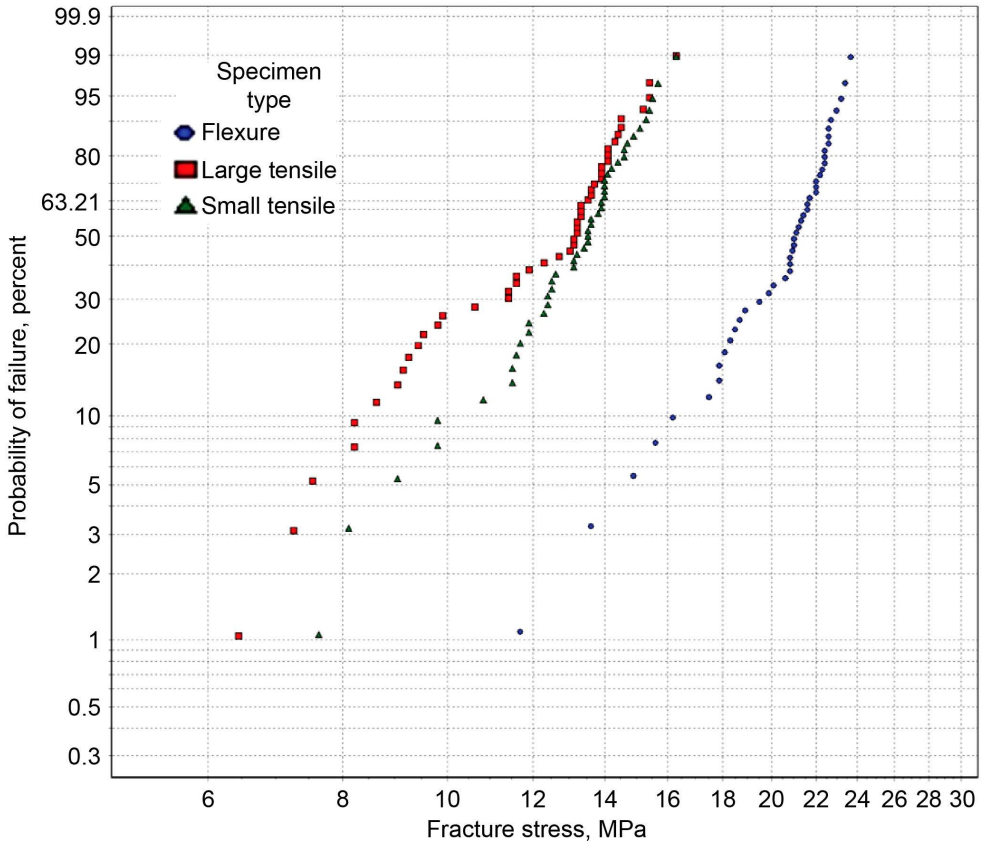

Figure 15.—Weibull plot of fracture stresses of slab 1 for radial large tensile, small tensile, and four-point-flexure specimens (linear-elastic flexure) from edge of slabs. Note the divergent behavior below 40-percent probability of failure for all three specimen geometries.

4.12 Monte-Carlo Simulation: Effect of Characteristic Strength Variability on Strength Distribution

As previously mentioned, there was significant slab-to-slab scatter in the characteristic strength σ_θ beyond what would be expected from natural statistical variation (see Figure 7(b)). Consequently, the data pooling contains this additional effect on the scatter in strength. This is evidenced by the reduction of Weibull modulus from the individual-slab-averaged m in Table 3 relative to the pooled m shown in Tables 4, 6, 8, 10, and 12. A Monte-Carlo simulation was performed to illustrate the potential effect of this scatter in the individual slab σ_θ on pooled strength distribution. Figure 7(a) shows that m is relatively constant (that is, with a fair amount of overlap in the individual slab confidence bounds). The value of σ_θ was assumed to be uniformly distributed within the bounds of the maximum and minimum values of σ_θ for the individual slab data. Simulated fracture data were generated from this random distribution of σ_θ and a fixed value of m. This simple approximation illustrates one possible effect of Weibull parameter scatter on the overall strength distribution.

The simulation was run in MatLab as follows: First a random number r between 0 and 1 was generated. Then $\sigma_{\theta,r}$ was calculated as $\sigma_{\theta,r} = \sigma_{\theta,1} + (\sigma_{\theta,2} - \sigma_{\theta,1})r$, where $\sigma_{\theta,1}$ and $\sigma_{\theta,2}$ are the lower and upper bounds, respectively, of the possible range of $\sigma_{\theta,r}$. Another random number s between 0 and 1 was generated to represent the probability of failure. Equation (3) was used to calculate σ_f. This process was repeated until 100 000 randomly chosen values of σ_f were generated. The individual values of $\sigma_{f,i}$ were ranked from lowest to highest and assigned a failure probability according to the ranking formula $P_{f,i} = (i - 0.5)/n$, where i is the number of the ranked value and n is the number of trials performed, which in this case is 100 000. These simulated data were then plotted in Weibull coordinates.

Figure 16 compares the results from a Monte-Carlo simulation for the 100 000 data points for pooled data (without regard to size effect) for the axial and radial large and small tensile specimens (pooling all tensile specimen data without regard to specimen size, location, or orientation within the log). In the simulation, the average *m* value of the individual slabs was used. Figure 16 also lists the *m* values and the bounds for $\sigma_{\theta,1}$ and $\sigma_{\theta,2}$. The simulated results show a reasonable fit to the data, but what is important to

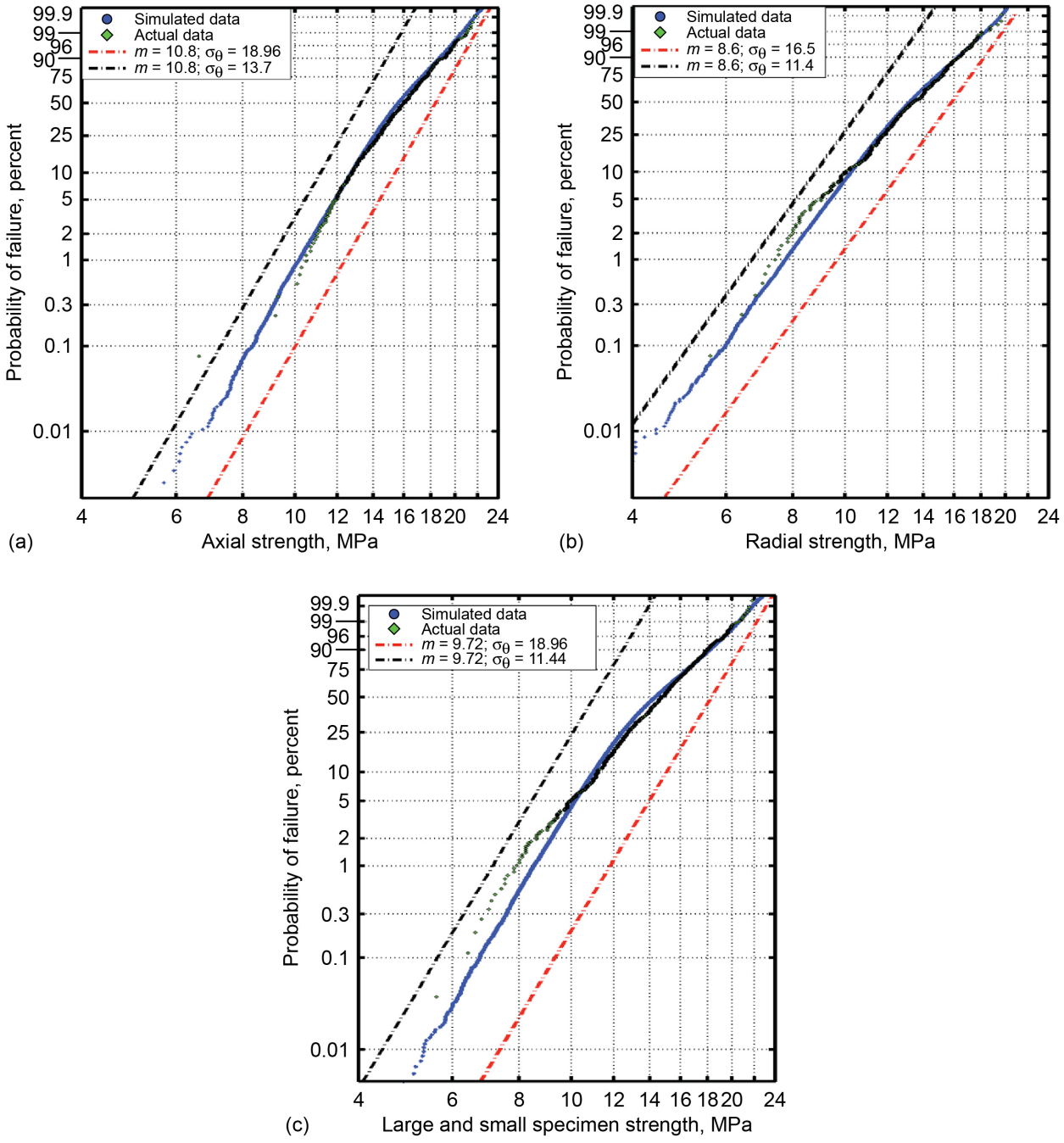

Figure 16.—Monte-Carlo simulated data (100 000 data points) for a constant Weibull modulus, *m*, and a uniform distribution of characteristic strength, σ_θ, between the bounds indicated. This first-order approximation of the scatter observed in the characteristic strength shows pooled data for large and small tensile specimens. (a) Axial specimens. (b) Radial specimens. (c) All data pooled together (regardless of specimen orientation and location within the slabs).

note is that the behavior is asymptotically two-parameter Weibull at high and low probabilities of failure. Between probabilities of failure of 1 and 99 percent, there is increased scatter in strength (the observed *m* is lower than the value used for the simulation), and the results have a downward curvature similar to that of a three-parameter Weibull distribution. The overall behavior of the simulated data is very similar to that described in Johnson (1983) for two mutually exclusive flaw population distributions.

The point of this exercise was to show that the localized scatter in the characteristic strength σ_θ on an overall (pooled) distribution of data lowers the experimentally observed Weibull modulus. Also, experimental data that exhibit a downward curvature similar to that of a three-parameter Weibull distribution may not actually originate from a three-parameter distribution. Although the experimental data may appear to imply the existence of a threshold stress σ_l, the true behavior could be different—in this case, asymptotic according to a two-parameter Weibull distribution. In addition, this behavior could only be detected at sufficiently low probabilities of failure, as seen in Figure 16, and the predicted size effect using the experimentally observed *m* would overpredict the actual size effect by some degree. Finally, the prudent practice for the design engineer would be to always assume a two-parameter Weibull distribution for the sake of conservatism (for design at low probabilities of failure) unless strong evidence (empirical or theoretical) exists otherwise. However, even in that case, use of the two-parameter distribution may still be warranted if there are not a lot of rupture data available (e.g., 20 or fewer specimens) because of the inherent statistical uncertainties associated with smaller size data sets as described by Liu (1997).

5.0 CARES/LIFE Analysis of Four-Point-Flexure Specimens

5.1 Finite Element Model for Linear-Elastic Stress Response of Flexure Specimens

A finite element model for the linear-elastic stress-strain response of cylindrical four-point-flexure specimens was generated with COMSOL version 3.5a. Linear brick elements were used. The finite element mesh is shown in Figure 17. The model consisted of 107 352 elements for a quarter symmetry model. The diameter was 6.4 mm, the total length was 51 mm, and the distance between the loads was 12.7 mm (loading points equally spaced). The Price report did not clearly state the location of the support points, so this distance was assumed to be 38.1 mm (12.7 mm between the load and support point), which was corroborated by Ho (1979). The distance between the end of the specimen and the support point was therefore 6.45 mm (so the support point was not at the very end of the specimen). For this exercise only, the relative distribution of stresses was needed. Note that Price only reported failure stresses and not failure loads. The mesh density is highest at the location of peak stresses between the loading points (see Figure 17(b)). CARES/Life failure probability predictions are very sensitive to the mesh size; stress gradients are present at the highly stressed regions, and therefore, mesh density must be greatest at those locations.

The support and load blocks were modeled to be 1.2 mm long and span a total arc of 10° (5° for the quarter symmetry model), with a maximum height of 0.5 mm (at the edge). The width of the block was 0.28 mm for the quarter symmetry model, and the total width was 0.56 mm. The load and support blocks were centered on the cited load and support distances. The blocks were arbitrarily sized for a bearing area that sufficiently reduced hertzian stresses below the value of the highest flexural stresses at the center of the specimen. Figure 17(c) shows the mesh details at a support block (the loading block is similar). A relatively coarse mesh was needed to help damp out unwanted hertzian stresses. The Poisson's ratio was 0.167. The Young's modulus, specified as 11.508 GPa, was assumed to be the same in both tension and compression. The support and load blocks were set to mimic a soft material to help mitigate stress concentrations from hertzian contact. The support blocks had a Young's modulus of 1.1 GPa and a Poisson's ratio of 0.35. The load blocks had a Young's modulus of 11.0 GPa (110×10^8 Pa) and a Poisson's ratio of 0.35. The pressure load on the block was arbitrarily 14.06 N/m^2 (Pa), which resulted

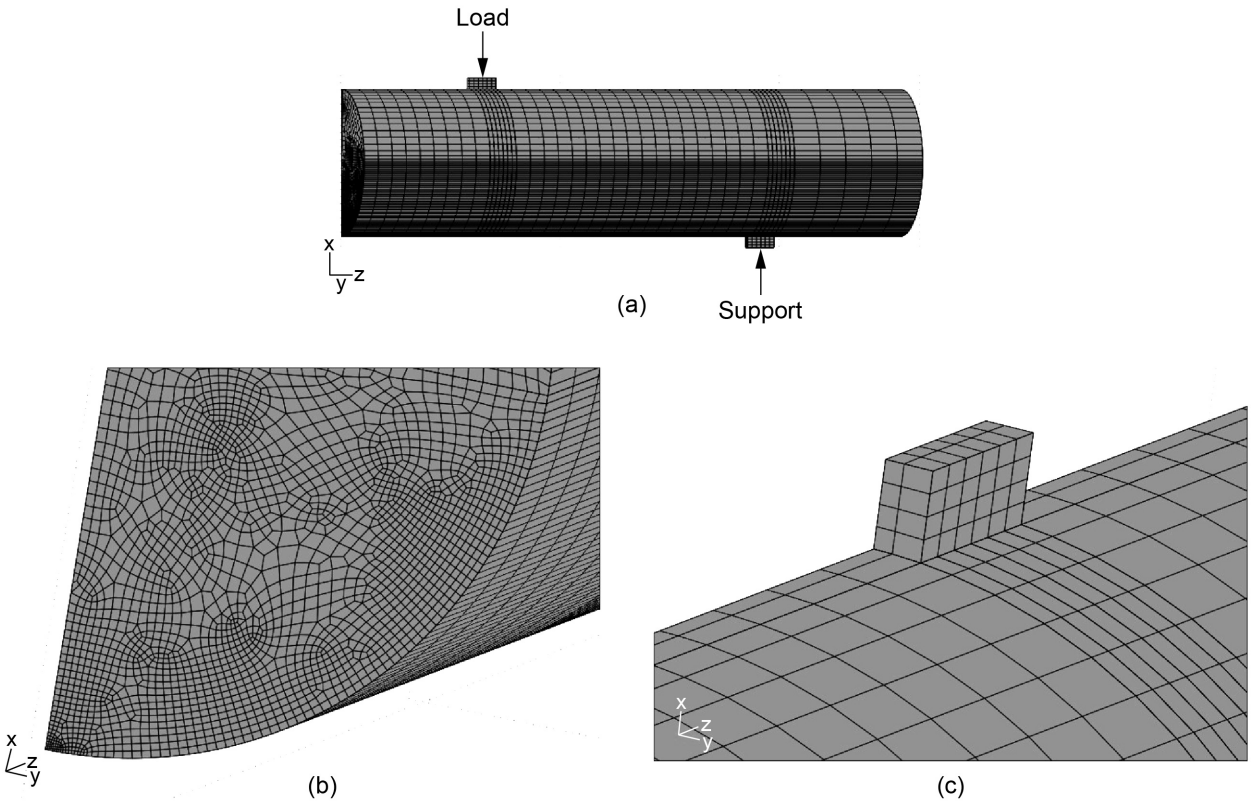

Figure 17.—Quarter symmetry finite element mesh of the cylindrical four-point-flexure specimen. (a) Overall model with support blocks. (b) Mesh details at the high tensile stress region. (c) Mesh details at the support block.

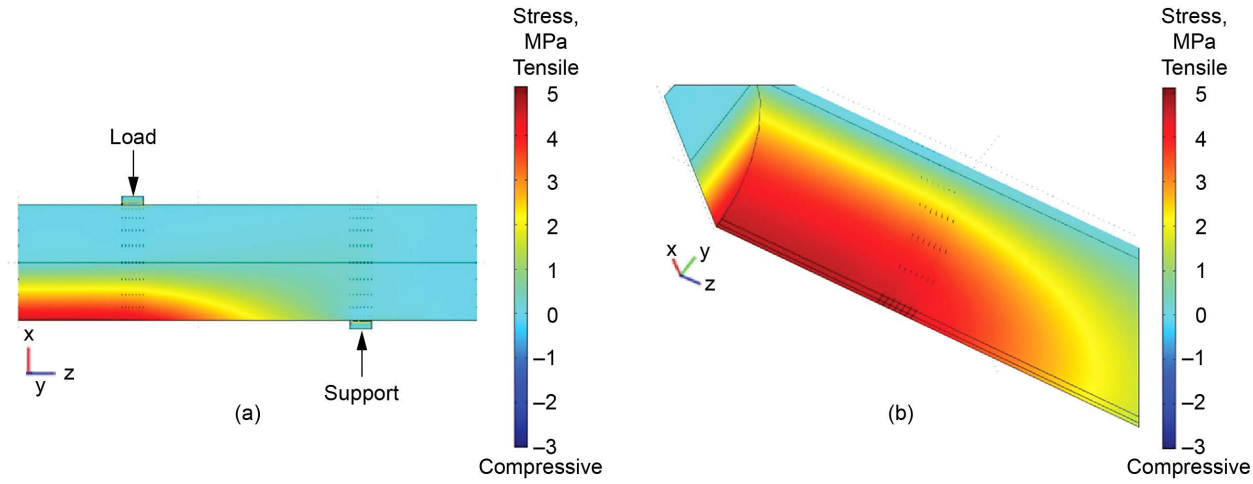

Figure 18.—First principal stress distribution in the cylindrical four-point-flexure specimen (linear-elastic response). (a) Full model view. (b) Close-up of tensile stress distribution.

in a maximum stress (from the finite element model) of 4.78 Pa obtained from the CARES maximum effective stress with the PIA model output. The maximum stress in the finite element model, 8.545 Pa, was located in the support block. Note that the support block was not considered in the CARES/Life analysis. The distribution of the first principal stress σ_1 is shown in Figure 18. The stress distribution in the specimen is primarily uniaxial and oriented in the direction parallel to the specimen length.

5.2 CARES/Life Prediction for Linear-Elastic Stress Distributions

For the CARES/Life analysis, only the relative distribution of stresses throughout the flexure specimen volume was needed to compute the effective volume V_e for the PIA criterion (Eq. (4)). As stated previously, the first principal stress dominates over the second and third principal stresses in the computation of V_e for the flexure specimen. This means that all three specimen geometries involve only uniaxial loading, so any additional effects from multiaxial loading are not a concern here. For this flexure specimen geometry and loading configuration, the effective volume was constant regardless of the magnitude of the load for a linear-elastic stress solution. Therefore, only a single finite element solution for some arbitrarily specified load was needed to compute V_e. With this information, Equation (3) was then used to determine the specimen probability of failure P_f versus the MOR σ_f in the specimen.

Size effect, as predicted from Weibull analysis, depends on the amount of material under stress or the effective volume V_e (see Eq. (4)). For uniform uniaxial tension, the effective volume is simply the gauge volume of the specimen and is independent of the Weibull modulus. For situations involving a stress gradient, such as the four-point-flexure specimen, the effective volume is a more complicated quantity that is a function of m. Figure 19 shows the relation of the effective volume with the Weibull modulus for the three specimen geometries. The effective volumes for the four-point-flexure specimens were calculated from CARES/Life for a linear-elastic stress response of the specimen finite element model. Figure 19 shows that there is approximately a 14:1 difference between the large and small tensile specimens and approximately a 1000:1 difference between the effective volumes for m = 10 for the large tensile and four-point-flexure specimens. For a proper size-effect study, a broad range of specimen sizes (spanning orders of magnitude in effective volume) are needed to clearly stand out from the statistical noise in the data. Typically 30 or more specimens are needed for each specimen size. Ideally, at least a third tensile specimen geometry having 2 orders of magnitude or more difference in V_e is needed.

Figures 20 to 23 show experimental rupture data versus the predictions from WeibPar and CARES/Life (additional plots and tables are provided in Appendixes B and E). In the figures, lines of best fit are shown that were determined from WeibPar with the assumption that the Weibull size effect (Eq. (5)) was operational. The probability of failure response for the three individual specimen geometries was predicted from a single value of m and σ_o that WeibPar determined as the best fit to the overall experimental data (for the particular figure) by using simple closed-form solutions for the tensile specimen geometries (using Eq. (3), where the tensile specimen volume is also the effective volume V_e) and the results from the CARES/Life analysis of the four-point-flexure specimen for the PIA fracture criterion (Eq. (3) and (4)). According to Weibull theory, the probability of failure response for any component geometry and loading can be predicted from m and σ_o, which are regarded as material

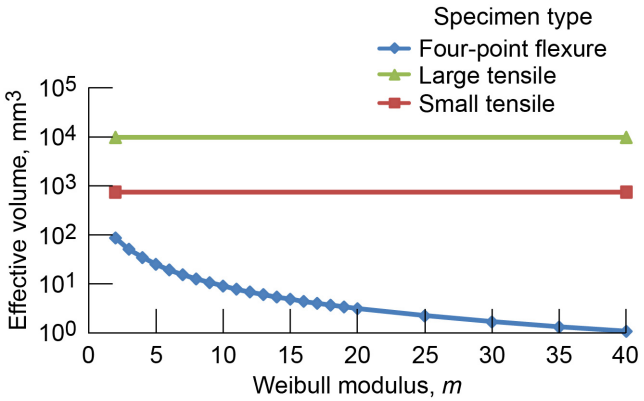

Figure 19.—Calculation of the effective volume (using Eq. (4)) for the three specimen geometries. The effective volume for the four-point-flexure specimen was calculated from CARES/Life for a linear-elastic stress response.

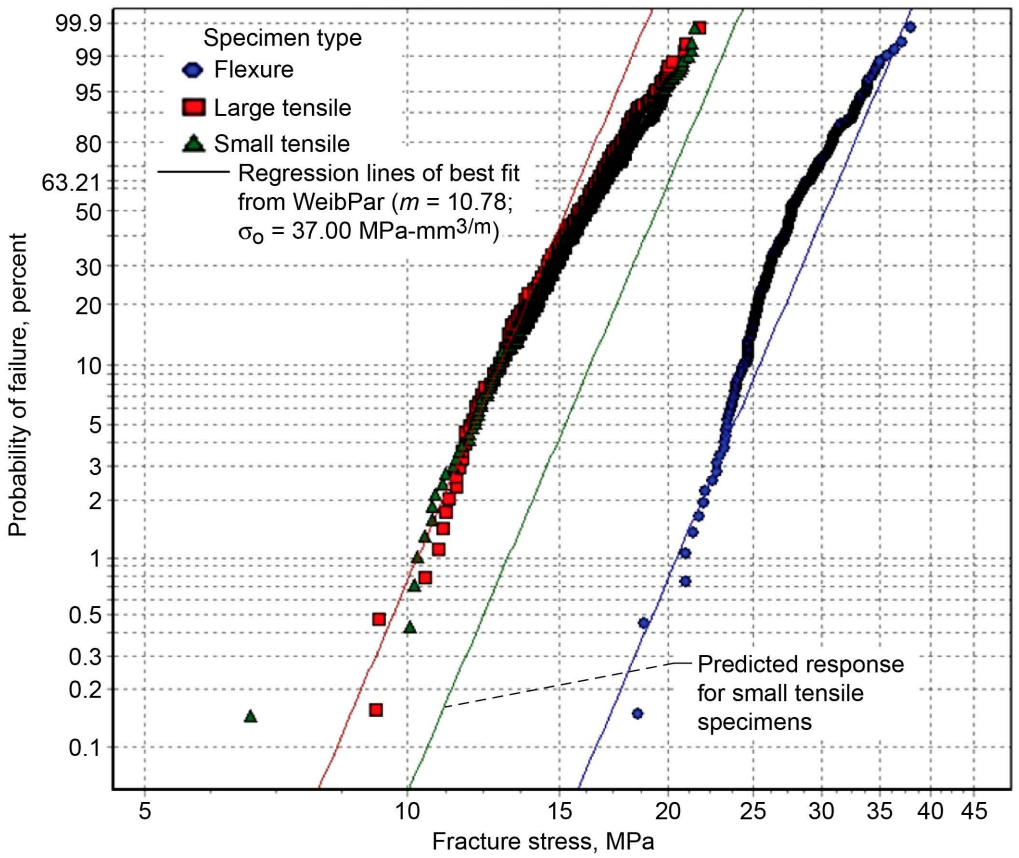

Figure 20.—Weibull plot of fracture stresses of axial large tensile, small tensile, and four-point-flexure specimens pooled for center and edge of slabs. Flexure specimen rupture data assume a linear-elastic response. Regression lines consider the stress distribution from the finite element analysis in conjunction with the CARES/Life probability of failure predictions for the flexure specimens.

properties. The linear-elastic finite element model of the four-point-flexure specimen was used with CARES/Life to determine the flexure specimen probability of failure versus σ_f response in all the analysis cases shown in the figures.

Figure 20 shows the WeibPar results predicted for the three specimen geometries versus the experimental rupture data for the axial specimens that includes pooled data from the center and edge of the log. The four-point-flexure specimen rupture data assume a linear-elastic response. The pooled rupture data for the axial specimens show a distinct nonlinear appearance on the Weibull plot—particularly for the four-point-flexure specimens. As noted previously, the tensile specimen rupture data for the two different size geometries basically fall on top of one another. To achieve a best fit to the data, WeibPar used $m = 10.78$ and a scale parameter of $\sigma_o = 37.00$ MPa-mm$^{3/m}$. This value of m is comparable to those in Table 3 for the averaged values from the individual slabs for the axial specimens. The m from the pooled data in Tables 4, 6, 8, and 10 tend to be a little lower because of the increased scatter from the pooling. From the figure, the size effect between the large tensile specimens and the four-point-flexure specimens is reasonably predicted by the Weibull relation. However, the flexure specimen rupture data in this report are used "as is" and are not verified for accuracy. Even though for these data, the rupture stresses were computed for a linear-elastic stress response, the data were still affected by the nonlinear stress-strain response of the material (for example, the changing effective volume with load was not accounted for). The predicted size effect between the large and small tensile specimens is much larger than that displayed by the experimental data.

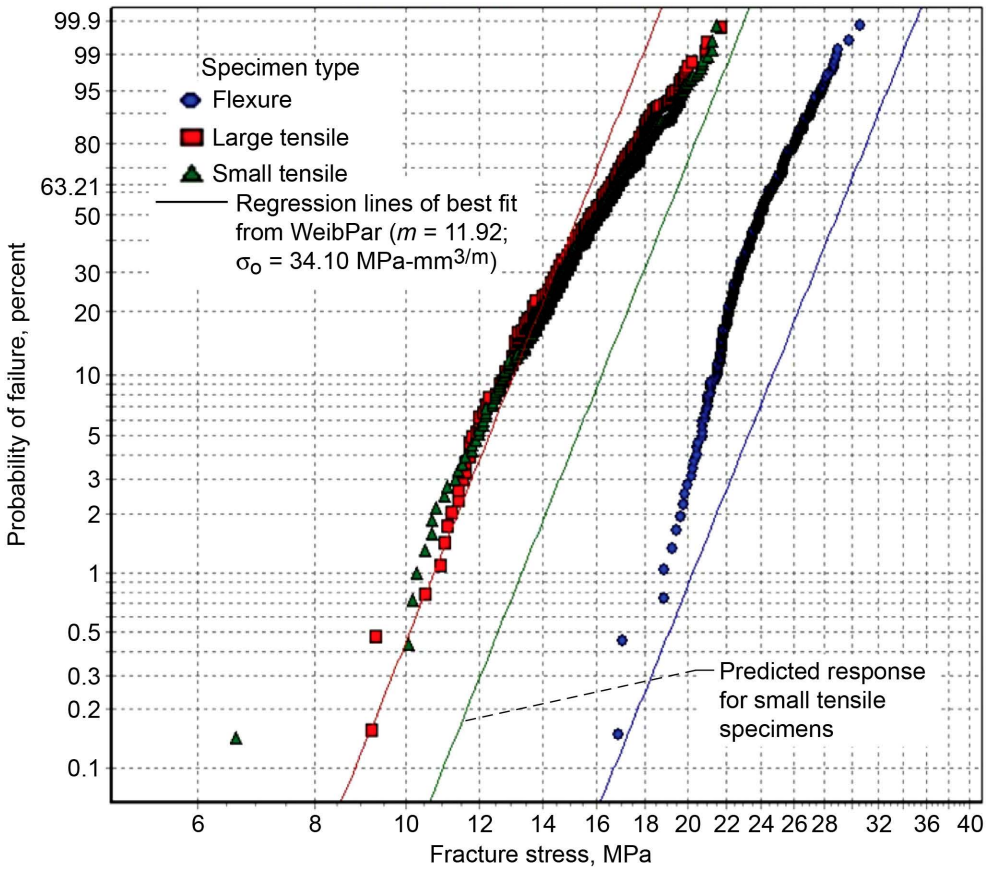

Figure 21.—Weibull plot of fracture stresses of axial large tensile, small tensile, and four-point-flexure specimens pooled for center and edge of slabs. Flexure specimen rupture stresses were corrected for nonlinear stress-strain response. Regression lines consider the stress distribution from the finite element analysis in conjunction with the CARES/Life probability of failure predictions for the flexure specimens. The finite element stress distribution was based on results from linear-elastic stress analysis. Note that WeibPar cannot use results from nonlinear-elastic stress analysis.

Figure 21 shows the same plot as Figure 20, except that the stresses corrected for the nonlinear stress-strain response for the four-point-flexure specimens are substituted. In this figure, the line of best fit was determined to be for $m = 11.92$ and $\sigma_o = 34.10$ MPa-mm$^{3/m}$. The nonlinear-elastic stresses show a weaker material in flexure with a higher m than for the linear-elastic stresses (see Tables 3 and 10). The fit to the data from WeibPar is less satisfactory, although the experimental data still show an appreciable size effect between the data for the large tensile and the four-point-flexure specimens. In this case WeibPar overpredicts the size effect. Size effect is a function of m such that the larger m is, the smaller the size effect is. In this plot, m would have to be larger to reduce the size effect, but the increased slope of the line would fit more poorly to the collective slope of the experimental data.

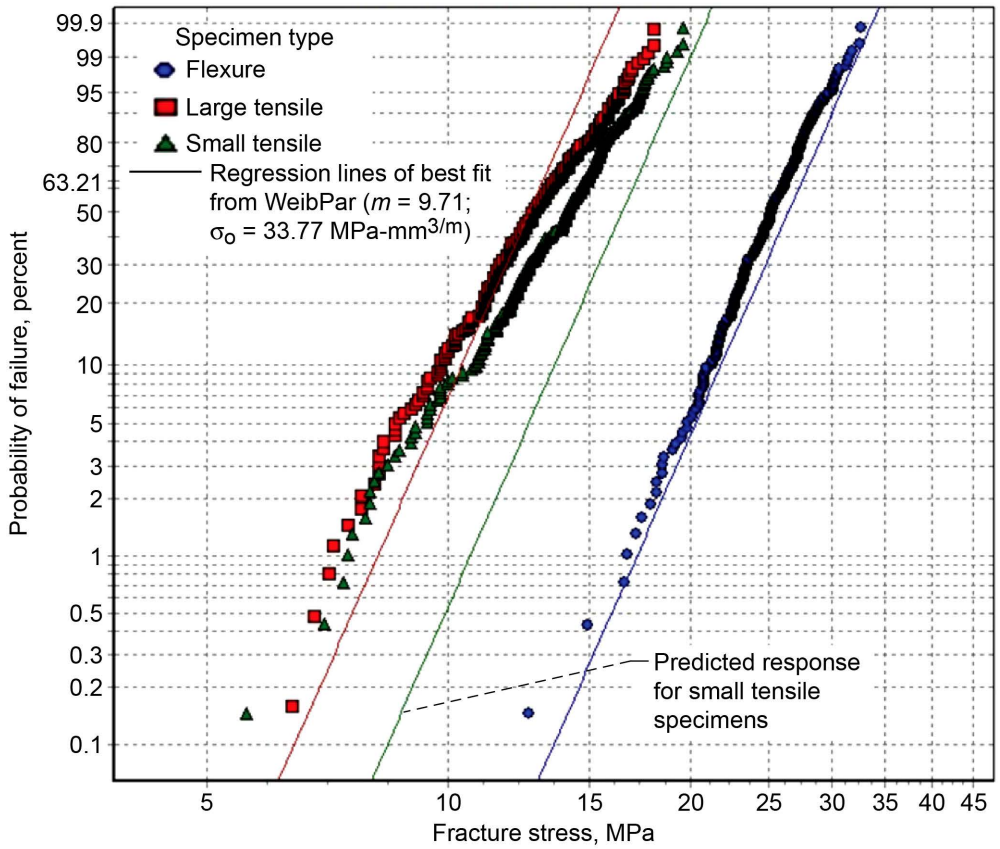

Figure 22.—Weibull plot of fracture stresses of radial large tensile, small tensile, and four-point-flexure specimens pooled for center and edge of slabs. Flexure specimen rupture data assume a linear-elastic response. Regression lines consider the stress distribution from the finite element analysis in conjunction with the CARES/Life probability of failure predictions for the flexure specimens.

Figure 22 shows the WeibPar results predicted for the three specimen geometries versus the experimental rupture data for the pooled radial specimens from the center and edge of the log. Again, the four-point-flexure specimen rupture data assume a linear-elastic response. The pooled rupture data for the axial specimens show a distinct linear appearance on the Weibull plot for all three specimen geometries. However, it can be seen more easily than in Figure 20 that the Weibull slope for the four-point-flexure specimens is larger than for the tensile specimens. As noted previously, the tensile specimen rupture data for the two size geometries are quite similar in Weibull slope m, with the smaller specimens being only marginally stronger than the larger specimens. To achieve a best fit to the data, WeibPar used $m = 9.71$ and $\sigma_o = 33.77$ MPa-mm$^{3/m}$. This Weibull modulus is a little larger than those of Table 3 for the averaged values from the individual slabs for the radial specimens. The m from the pooled data in Tables 4, 6, 8, and 10 tend to be even lower because of the increased scatter from the pooling. Figure 20 shows that the Weibull relation reasonably predicts the size effect between the large tensile and four-point-flexure specimens. The predicted size effect between the large and small tensile specimens is significantly larger than that displayed by the experimental data.

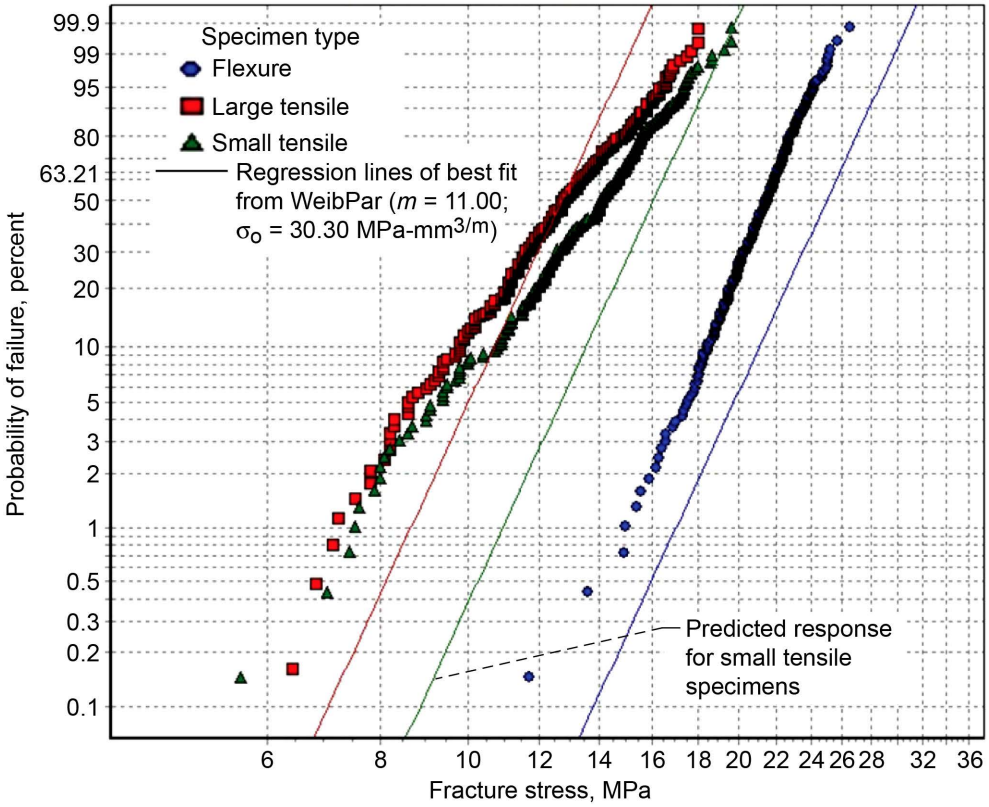

Figure 23.—Weibull plot of fracture stresses of radial large tensile, small tensile, and four-point-flexure specimens pooled for center and edge of slabs. Specimen rupture stresses were corrected for nonlinear stress-strain response. Flexure specimen rupture data assume a linear-elastic response. Regression lines consider the stress distribution from the finite element analysis in conjunction with the CARES/Life probability of failure predictions for the flexure specimens.

Figure 23 shows the same plot as Figure 22 except that the stresses corrected for the nonlinear stress-strain response for the four-point-flexure specimens are substituted. In this figure, the line of best fit was determined to be m = 11.00 and σ_o = 30.30 MPa-mm$^{3/m}$. The nonlinear-elastic stresses show a weaker material in flexure with a higher m than for the linear-elastic stresses (see Tables 3 and 10). The fit to the data from WeibPar is less satisfactory, although the experimental data still show an appreciable size effect between the large tensile and the four-point-flexure specimens. In this case, WeibPar overpredicts the size effect. Size effect is a function of m, such that the larger m is, the smaller the size effect is. In this plot, m would have to be larger to reduce the size effect, but the increased slope of the line would fit more poorly to the collective slope of the experimental data.

5.3 Nonlinear-Elastic Stress Distribution Effect on Weibull Modulus

The possibility that the higher observed m for the flexure specimens corrected for nonlinear stress-strain response could be a result of changing effective volume V_e with load was investigated briefly herein. A changing V_e with load implies a changing size effect with load via Equation (5). For a linear-elastic response, V_e is constant with load for the four-point-flexure specimen geometry. The effect of changing V_e with load is explored in Nemeth et al. (2007), where the observed m (from the simulation) became lower when the effective area A_e decreased with increasing load. Conversely, when A_e (or equivalently V_e) increases with increasing load, the observed m will get larger. Note that typically the observed Weibull modulus is constant regardless of geometry but that exceptions, such as changing

effective volume with changing load, can occur (for example the shifting of the neutral axis with load). Another important scenario to consider is that the Weibull modulus in flexure and the Weibull modulus in tension can be different because different flaw populations may be sampled. This is where fractography is useful, provided that the strength-controlling flaws can be identified.

5.3.1 Finite Element Model for a Nonlinear-Elastic Stress Response

The development of a robust nonlinear material model for graphite is beyond the scope of this report; however, results are presented from the ANSYS finite element analysis using the nonlinear material model from Price (see Eq. (1)). In addition, a linear-elastic material model is included for comparison to the nonlinear results. Graphite is known to have different elastic behaviors in tension and compression (see Arai and Oku (1979) for example), and this response has some variability from specimen to specimen (although this response is not considered here). The nonlinear-elastic material model used here does not include any hysteresis behavior. Upon unload, the material response retraces the nonlinear curve back down to zero strain. This behavior was modeled in ANSYS through the use of the MELAS material property, which allows the input of a multiple (piecewise) linear-elastic modulus segments. The linear-elastic material model applied to all cases included a Young's modulus of 11 508 MPa and a Poisson's ratio of 0.167. The nonlinear-elastic model was based on Equation (1). Parameter values were taken to be E = 11 508 MPa and ε_o = 0.004. Figure 24 depicts the linear and nonlinear stress-strain curves for a cylindrical rod in tension for progressive loading and unloading. The nonlinear stress-strain response was approximated by 100 piecewise linear segments up to a strain of 0.01 mm/mm. Note that the response is symmetrical in tension and compression and that, therefore, this model will not predict a neutral axis shift with increasing load.

An ANSYS finite element model of a four-point-flexure specimen was prepared. Figure 25 shows the mesh. This mesh is coarser than the COMSOL mesh of Figure 17 but is sufficient for demonstration purposes. The model consisted of 31 744 SOLID45 eight-noded hexahedral elements. Solution convergence for the nonlinear model was successfully obtained with this element type. Figure 26 shows the response of the model for load, stress, and strain located inside the inner span along the surface opposite the inner load span loading location. In Figure 26(a), the model indicates that, for a nonlinear solution, maximum stress for a given load is lower than that for the linear solution and that this difference increases with increasing load.

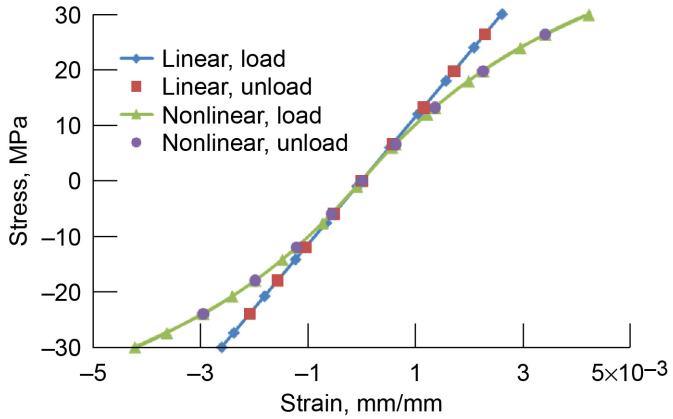

Figure 24.—ANSYS results for the nonlinear- and linear-elastic response of a cylindrical specimen in pure tension. Nonlinear indicates that nonlinear-elastic stress-strain response was assumed; linear indicates that linear-elastic stress-strain response was assumed.

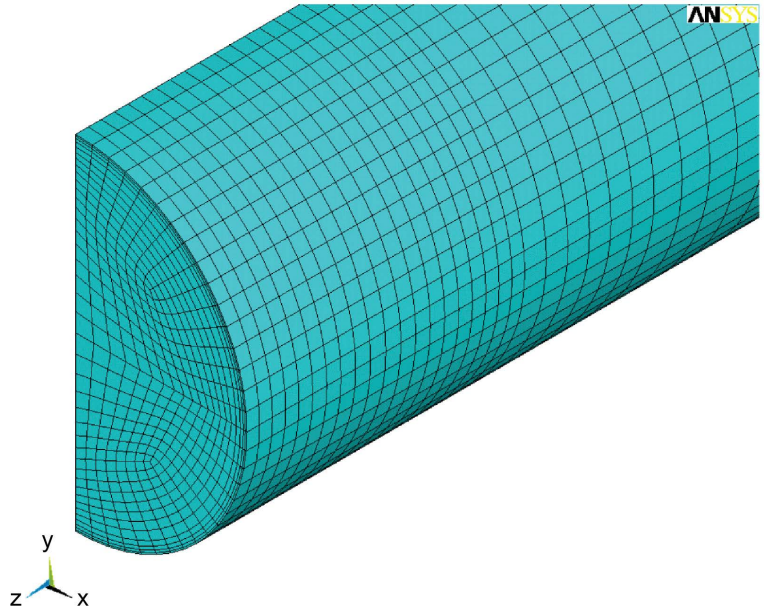

Figure 25.—ANSYS quarter-symmetry finite element model of the cross section of a four-point-flexure specimen.

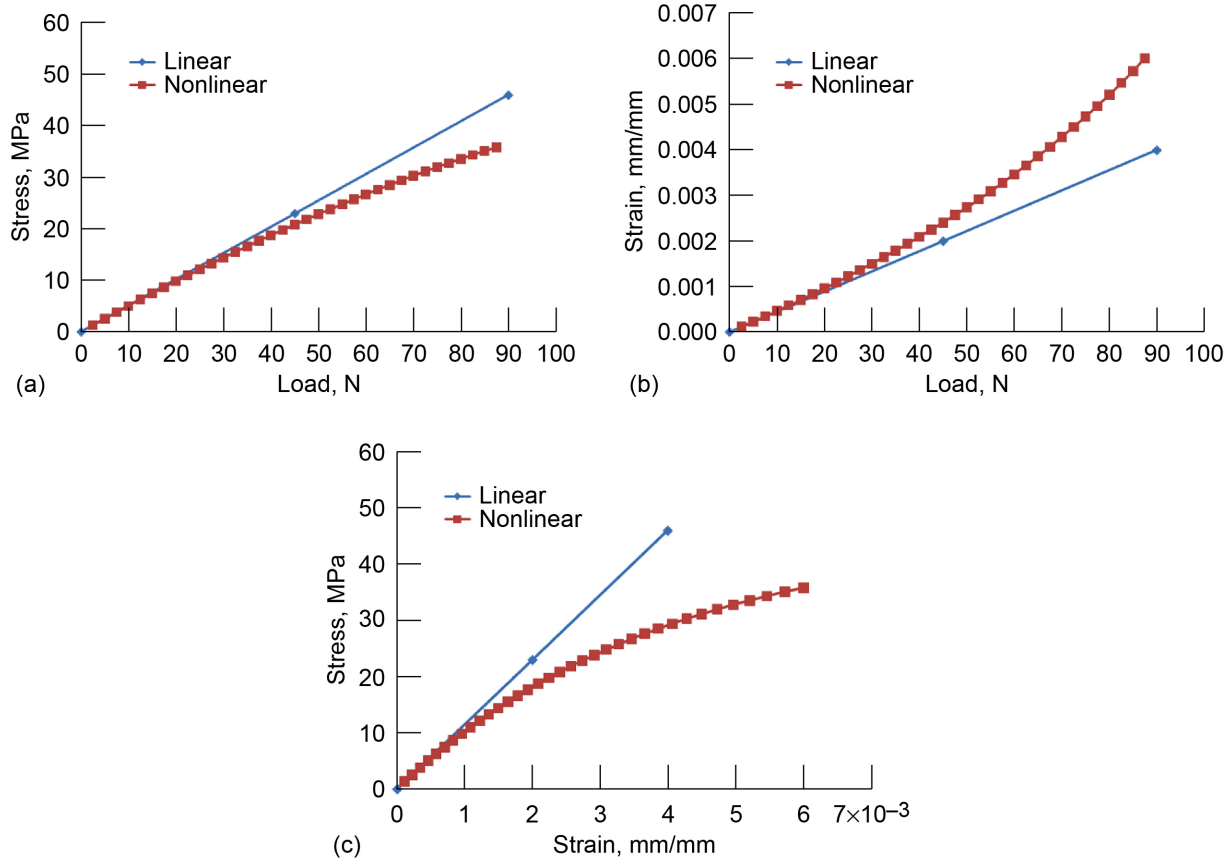

Figure 26.—ANSYS results for the nonlinear- and linear-elastic response of the cylindrical four-point-flexure specimens at the point of maximum stress on the specimen surface centered between the loading points. Nonlinear indicates that nonlinear-elastic stress-strain response was assumed; linear indicates that linear-elastic stress-strain response was assumed. (a) Stress versus loading response. (b) Strain versus loading response. (c) Stress versus strain response.

5.3.2 CARES/Life Prediction for a Nonlinear-Elastic Stress Distribution

Figure 27 plots effective volume V_e versus load (Fig. 27(a)) and the maximum stress σ_f (at the element integration point) shown in Figure 27(b) for m of 5.0, 10.0, 15.0, and 20.0. The figure shows that V_e increases as load (and stress) increases. From Equation (5), this implies that size effect will change with load. Figure 28 shows an example of how this response manifests. For this figure, m = 10.0 and σ_o = 33.0 MPa-mm$^{3/m}$ were assumed, so that the figure would correlate closely with the fracture data for the linear-elastic model. This acts as the baseline result. The results for the nonlinear model show a small

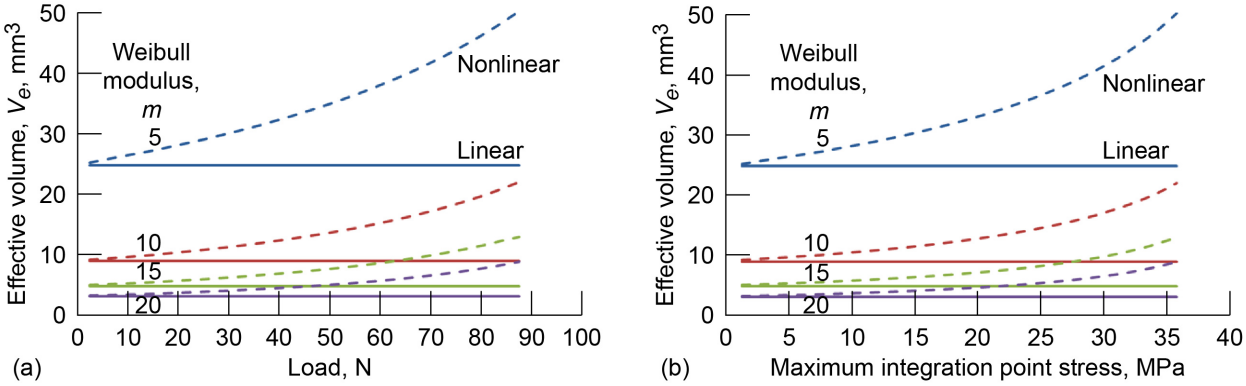

Figure 27.—Effective volume, V_e, versus applied load and maximum stress. Note that V_e is not constant with load or stress. (a) Applied load for various values of m. (b) Maximum stress (at the element integration point) in the finite element model.

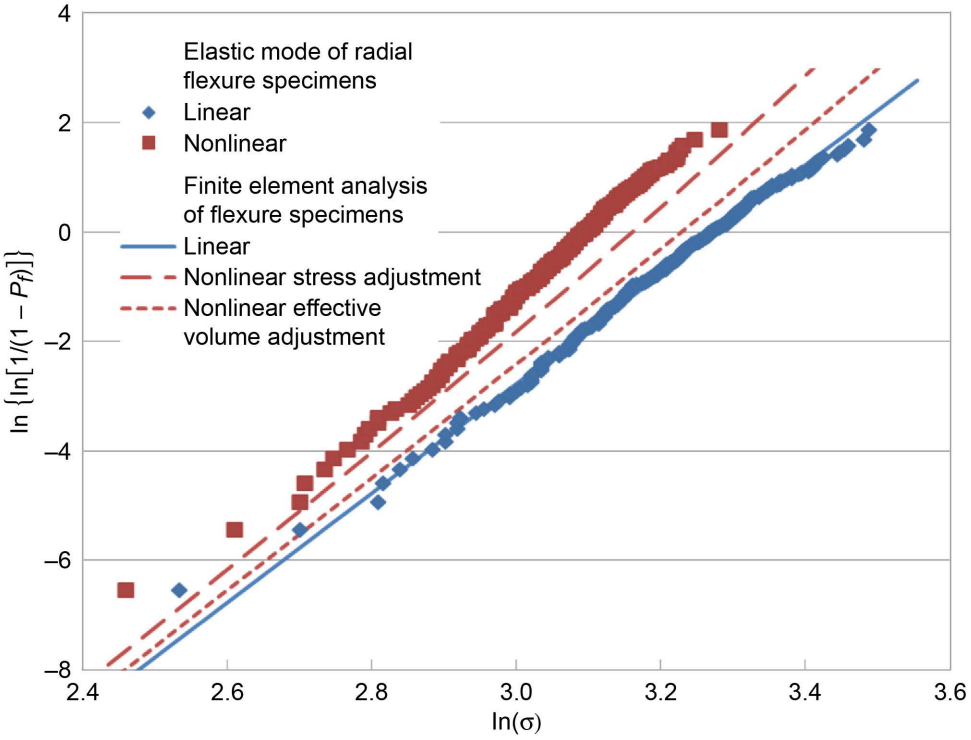

Figure 28.—CARES/Life failure probability, P_f, predictions versus peak stress, σ, for the linear- and nonlinear-elastic response models for Weibull modulus, m = 10.0, and scale parameter, σ_o = 33.0 MPa-mm$^{3/m}$. Also shown are the computed fracture stresses from Price (1976) for the linear- and nonlinear-elastic response for pooled radial four-point-flexure specimens. The nonlinear stress adjustment line is the response predicted from the finite element (FE) model that compares to the nonlinear fracture stresses. Nonlinear indicates that nonlinear-elastic stress-strain response was assumed; linear indicates that linear-elastic stress-strain response was assumed.

but noticeable response whereby *m* (which is the slope of a line in a Weibull plot) appears to increase slightly. This is due to the effective volume changing with load and to the nonlinear stress-strain response. The predicted response is not actually linear on the Weibull plot. A linear regression on the predicted curve shows that it has an approximate *m* of 10.3. Therefore, the predicted effect of the reduction in scatter of strength is relatively small—on the order of 3 percent. It also can be seen in Figure 28 that the predicted nonlinear response (for the adjusted effective volume) does not approach the results for the experimental fracture stresses corrected for nonlinear stress response. Also shown in Figure 28, for comparison and model validation purposes, is a line showing the nonlinear stress adjustment from the line for the linear model. The line was obtained by transforming the linear elastic stress for a given probability of failure to the nonlinear stress according to the FE model. From the figure it can be seen that the FE model line approaches the nonlinear fracture stresses from Price (1976). However, the reason for any remaining discrepancy is unknown.

Note that Arai and Oku (1979) indicated better correlation to data when nonlinear-elastic response was accounted for. Here the opposite trend seemed to hold: better correlation was achieved to the data for the Weibull model when a linear-elastic stress response was assumed. An improved nonlinear-elastic model might show a more significant response, for example, if neutral axis shifting is considered. One thing that should be pointed out is the implication that the linear-elastic computed specimen experimental fracture stresses were affected by the effective volume that changed with load. This trend is reflected in Figure 21 (and in Tables 4, 6, and 10), where the *m* estimated from the experimental fracture stresses for the flexure specimens is higher than that estimated for the tensile specimens.

Li and Fok (2009) offered an alternative explanation for the difference in strength and Weibull modulus between tension and flexure due to the nature of damage progression in quasi-brittle materials. Their model was based on a Weibull-distributed critical strain failure criterion with strain-softening behavior from damage accumulation based on an approach from Bazant and Li (1995). It predicted the observed Weibull modulus (based on an effective stress from linear-elastic beam theory), which increased from tension to flexural loading. In their model, the material stress-strain response was assumed to be linear until a threshold strain level when damage accumulation began. The stress in the damaged region was assumed to decrease with increasing strain, and for pure flexure, a neutral axis shift occurred. The classical Weibull model shown herein indicates that observed Weibull modulus also can be affected by effective volume changing with load, although the effect was predicted to be small in this particular model. An improved model of the stress-strain response would help to achieve a better understanding of the potential effect. It would be an interesting exercise to also apply the Li and Fok model to the Price data; however, that is beyond the scope of this report.

6.0 Grain Size Effects on Small Sized Specimens

The smaller-than-expected size effect between the large and small tensile specimen geometries could have a variety of explanations: (1) the behavior is real and stochastic failure models of graphite need to account for this—including possible porosity effects, (2) there were systemic errors in the testing, such as load eccentricities, that could account for some or all of the discrepancy, or (3) the large average grain size relative to the diameter of the small tensile specimens had a knock-down effect on the specimen strength. These items will be discussed briefly, but the most likely explanation, in the opinion of the authors, is grain size effect. There is evidence in the technical literature for the contention that the lack of size effect is real. This is discussed further in the review article by Nemeth and Bratton (2010) and in somewhat greater detail in Nemeth and Bratton (2011). The overall trend that has been reported is that, for tensile specimens, the strength is fairly constant with increasing size (or it shows a smaller-than-expected size effect), but when specimen size is roughly within an order-of-magnitude of the grain size, strength decreases. Tucker et al. (1986) explained that strength falls off with small diameter because the characteristic flaw size penetrates a greater fraction of the specimen diameter.

Ho (1979) introduced a correction factor to the Weibull scale parameter to empirically account for the effect of grain size relative to tensile specimen dimension for nuclear-grade graphite. In Ho's relation, specimen dimensions on the order of the maximum grain size weaken the specimen. The correction factor was introduced because small-sized tensile specimens were often observed to be weaker than larger size specimens—contrary to the expectation based on the Weibull theory (e.g., see Strizak (1991)). For instance, grade H–451 graphite has a mean grain size of 1.6 mm, so a 6.4-mm-diameter tensile specimen is only 4 times this size and a 12.8-mm-diameter specimen is only 8 times this size. In Ho's relation, the Weibull scale parameter is modified by

$$P_{fV} = 1 - \exp\left[-V\left(\frac{\sigma}{\sigma_o f\left(h_o, d\right)} \right)^m \right]$$

$$f(h_o, d) = \frac{2}{\pi}\cos^{-1}\left(\frac{h_o}{d}\right) \tag{7}$$

where h_o is the characteristic grain size and d is the diameter of the specimen. Ho found good correlation with this relation for the reported strength ratios of the tensile specimens from Price. As an aside, it is worth pointing out that m remained constant between the large and small tension specimens (see Fig. 12), so it appears that there was little effect of large grain size relative to specimen diameter on m.

Another potential source for the discrepancy in the tensile specimen size effect could be the load eccentricity due to improper alignment of the load train. It is very difficult to apply a pure tensile force such that stress distribution is completely uniform throughout the volume of the specimen. There has been much research and development in this area in the ceramics community since the Price report. Unfortunately, the degree of load eccentricity in the Price data is unknown because even a few percent variation in stress across the specimen diameter can have a significant impact on size effect. Finally, the diameters of the four-point-flexure specimens were the same as those of the small tensile specimens. Therefore, grain size could have affected the flexural strength in this case.

7.0 Additional Comments

The flexure specimen rupture stresses were used "as is" from the Price report. They were not checked for accuracy because fracture loads were not available. Other systematic testing errors may also be reflected in the flexural rupture data. It is somewhat atypical that cylindrical specimens were used for the four-point-flexure tests. The usual practice is to use a beam with a rectangular cross section. Also, the specimen diameter was large relative to the support span. This meant that large hertzian stresses were generated at the support and loading points. In addition, the Price report did not provide the details of the flexure specimen testing apparatus. Modern testing rigs use rollers at the support and load points to reduce frictional effects. Therefore, the degree of error from systematic testing effects is unknown, but it is potentially significant. Another source of concern was that the small tensile specimen diameter was less than 10 times the size of the average graphite grain size. This biases the size effect, as discussed by Ho (1979), and may help to explain the small size effect observed between the small and large tensile specimens. This exercise also illustrated the need for using improved testing techniques and a better designed experimental matrix with a larger range of specimen sizes and sufficiently large specimen dimensions so that microstructural and statistical effects become a less significant factor.

8.0 Conclusions

The WeibPar and CARES/Life analysis software were used to perform a new analysis of fracture strength data that were originally reported by Price (1976) for H–451 near-isotropic petroleum-coke-based nuclear-grade graphite. Both tension and four-point-flexure test data were used for the analysis. To obtain the data, Price had used over 2000 cylindrical specimens that had been excised from a large cylindrical billet (or "log"). In this study, the original data were replotted in terms of a Weibull distribution and pooled into progressively larger data sets to establish trends with greater statistical confidence. The statistical strength distribution, strength variation versus specimen orientation and location within the log, and the effect of specimen size and stress gradient on strength (size effect) were investigated. Experimental results were compared with the predicted strength based on the Weibull stress-volume integration performed with CARES/Life and a finite element model of the four-point-flexure specimen.

The major findings of the new analysis follow:

(1) There were significant variations in average strength, but the Weibull modulus was relatively constant with regard to specimen location and orientation within the log.

(2) The Weibull moduli for the flexure tests were higher than those for the tension tests, and this result was partially confirmed from modeling.

(3) The Weibull moduli for the small and large tensile specimens were similar.

(4) A significant size effect existed between the flexure specimens and the tensile specimens, consistent with predictions from the Weibull theory.

(5) The flexure specimen fracture stresses for the linear-elastic stress-strain response correlated better with the expected size effect from the Weibull theory than did the flexure specimens corrected for nonlinear stress-strain response.

(6) A small to negligible size effect existed between the two different sizes of tensile specimens, which was not consistent with Weibull theory but might be explained by microstructural effects.

(7) Specimens that had a radial orientation relative to the graphite log were weaker and behaved more consistent with a two-parameter Weibull distribution than did the axial specimens, which behaved more consistent with a three-parameter Weibull distribution.

(8) The Weibull moduli were similar for the axial and radial specimens.

(9) Because of fluctuations in the characteristic strength of the individual data sets, the Weibull moduli for the pooled data sets were lower than the average for the individual data segregated for location and/or orientation.

(10) A Monte-Carlo simulation showed how this effect could be manifested.

(11) The Monte-Carol simulation also showed how nonlinear behavior could result on a Weibull plot, but this simulation was also asymptotically two-parameter Weibull in behavior at the tails of the distribution.

A very good approximation to a two-parameter Weibull distribution, or to a three-parameter distribution with a relatively low threshold stress, was obtained for a pooled data set containing 1317 tensile specimens. The overall distribution of the data demonstrated the prudence of using the two-parameter Weibull distribution for the structural design and analysis of graphite components because at the lowest probabilities of failure there were data points that best followed the two-parameter distribution. If less data were available for this study, say for example about 30 specimens of a given geometry (a typical case), use of a three-parameter Weibull, a normal, or a log-normal distribution would likely have yielded nonconservative predictions at low probabilities of failure because of the behavior in the lower tail of those distributions. Because of the large number of rupture tests that were performed, this study provided an opportunity to demonstrate this contention with actual data.

This study also helped to illustrate the shortfalls in the experimental results database—such as not having enough variation in sample size for a proper size-effect study or not having the data available from multiaxial stress states. Potential systematic experimental errors were not reported, such as putting strain gauges on tensile specimens to check for load eccentricity or errors associated with the four-point-flexure rig. The experimental data, although extensive in the number of samples, were insufficient to conclude whether or not this material behaved according to the Weibull theory for size effect. Contrary to the conclusions of Price (1976), the reported results do not invalidate the material from being Weibull behaved, but they do indicate that other factors, such as grain-size effects, variation (or drift) in material properties, nonlinear processes (stress-strain response), residual stresses, and porosity need to be considered or investigated further. In particular, physically based models are needed that properly account for the size effect in graphite. This report also showed that a conservative approach of using a two-parameter Weibull distribution is the best for the design of graphite components with low probability of failure for the in-core structures in the proposed Generation IV (Gen IV) high-temperature gas-cooled nuclear reactors.

Appendix A.—Data for Individual Slabs 1 to 4 for Specimen Type, Orientation, and Location Within the Slabs From the Graphite Log

The level of scatter in Figure 29 is lower for slab 2 than for the other slabs. See Table 13 for a listing of the Weibull parameters and the 90-percent confidence bounds on parameters.

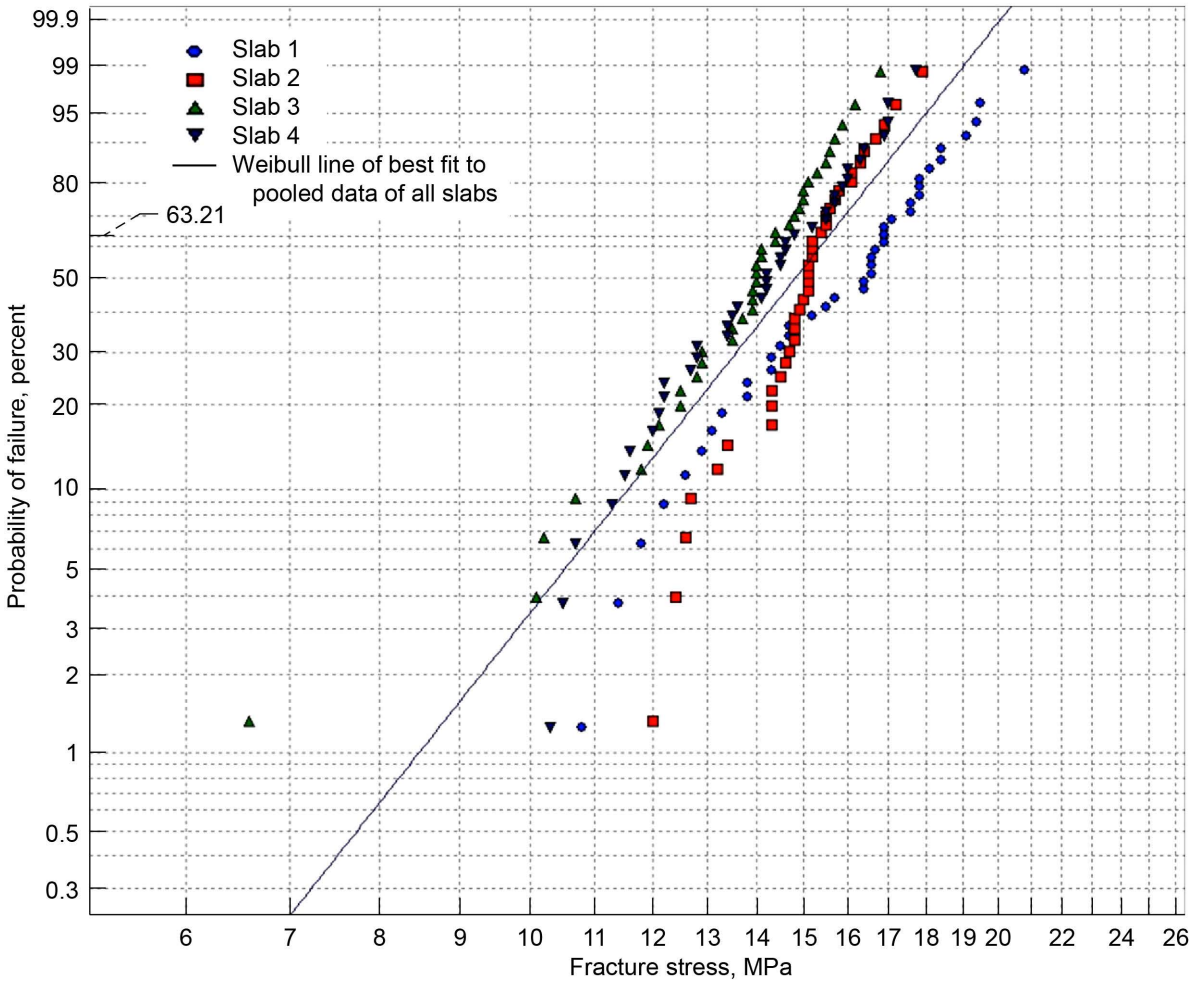

Figure 29.—Weibull plot of fracture stresses of individual slabs 1 to 4 for axial small tensile specimens from center of slabs.

The level of scatter in Figure 30 is lower for slab 2 than for the other slabs. See Table 13 for a listing of the Weibull parameters and the 90-percent confidence bounds on parameters.

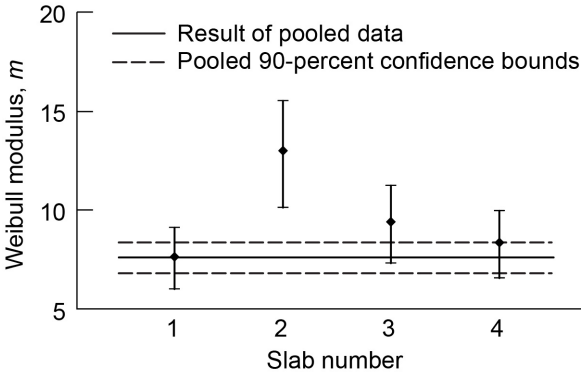

Figure 30.—Weibull modulus and 90-percent confidence bounds of individual slabs 1 to 4 for axial small tensile specimens from center of slabs.

In Figure 31, slab-to-slab variation of the characteristic strength appears to be statistically significant with a high degree of confidence since there is little overlapping of confidence bounds. See Table 13 for a listing of the Weibull parameters and the 90-percent confidence bounds on the parameters.

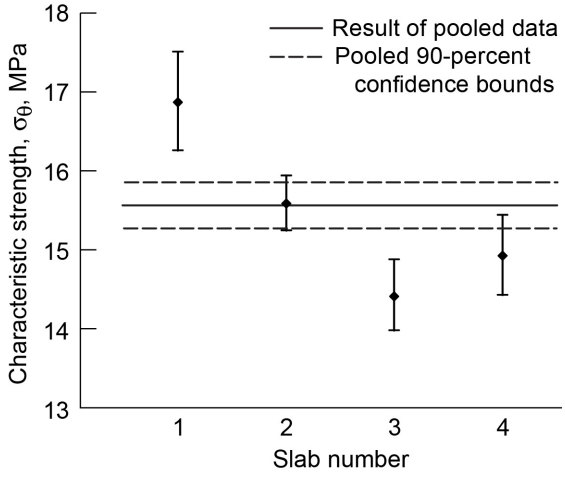

Figure 31.—Characteristic strength and 90-percent confidence bounds of individual slabs 1 to 4 for axial small tensile specimens from center of slabs.

TABLE 13.—WEIBULL PARAMETERS AND 90-PERCENT CONFIDENCE BOUNDS ON INDIVIDUAL AND POOLED DATA FROM SLABS 1 TO 4 FOR AXIAL SMALL TENSILE SPECIMENS FROM CENTER OF SLABS

Slab	Number of specimens	Weibull modulus, m		Characteristic strength, σ_θ, MPa	
		MLE biased[a]	90-percent confidence	MLE biased[a]	90-percent confidence
1	40	7.64	5.99/9.09	16.87	16.26/17.51
2	38	12.99	10.11/15.52	15.59	15.24/15.94
3	38	9.39	7.31/11.22	14.41	13.97/14.87
4	40	8.36	6.55/9.95	14.92	14.42/15.44
Mean	39.00	9.60	----------	15.45	----------
Pooled	156	7.58	6.78/8.33	15.56	15.27/15.85

[a]Maximum-likelihood estimation.

The level of scatter in Figure 32 is lower for slab 2 than for the other slabs, and there is a relative separation between slabs 1 and 2, and slabs 3 and 4. See Table 14 for a listing of Weibull parameters and 90-percent confidence bounds on parameters.

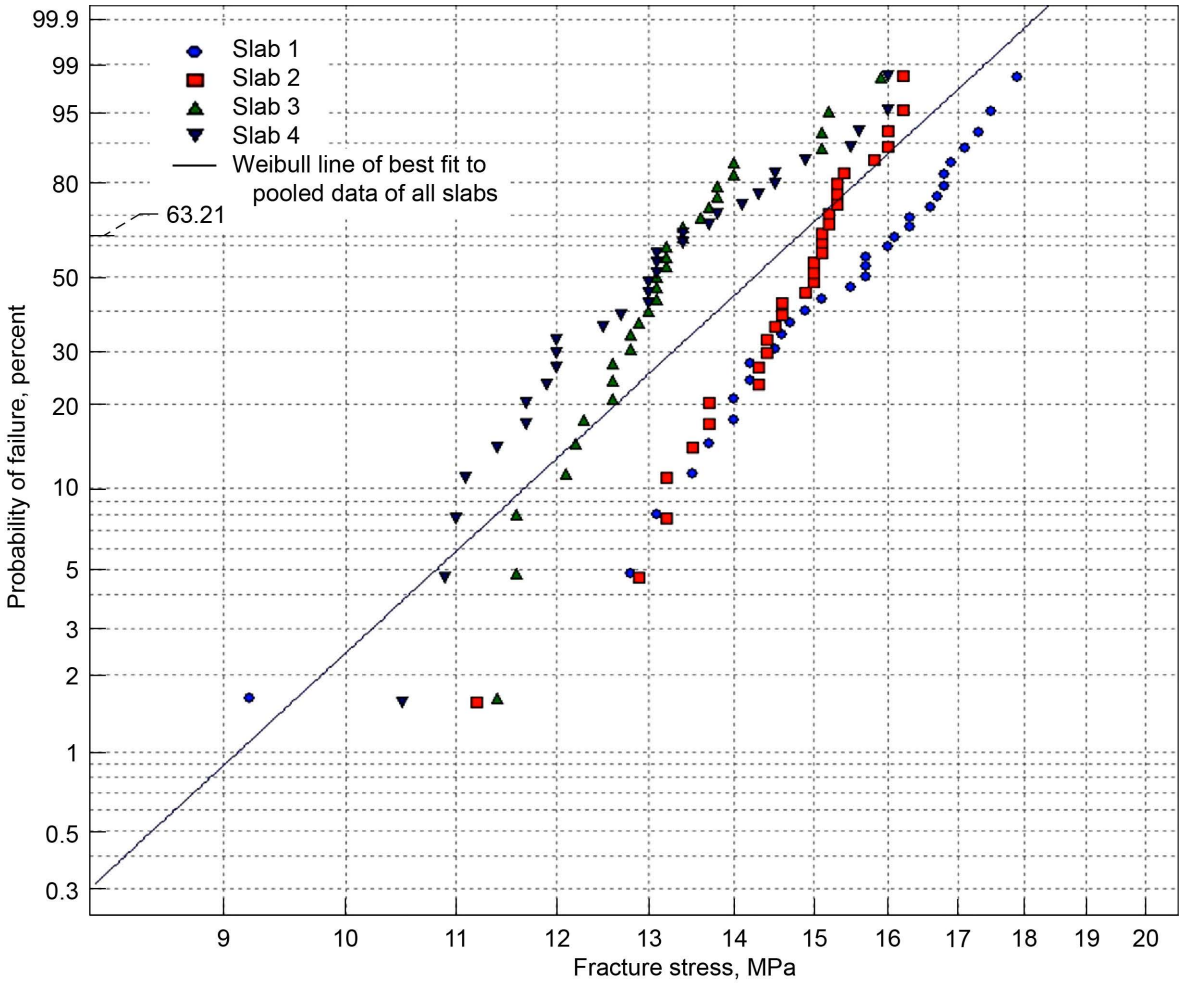

Figure 32.—Weibull plot of fracture stresses of individual slabs 1 to 4 for axial large tensile specimens from center of slabs.

In Figure 33, the Weibull modulus is higher for slab 2 than for the other slabs. See Table 14 for a listing of Weibull parameters and 90-percent confidence bounds on parameters.

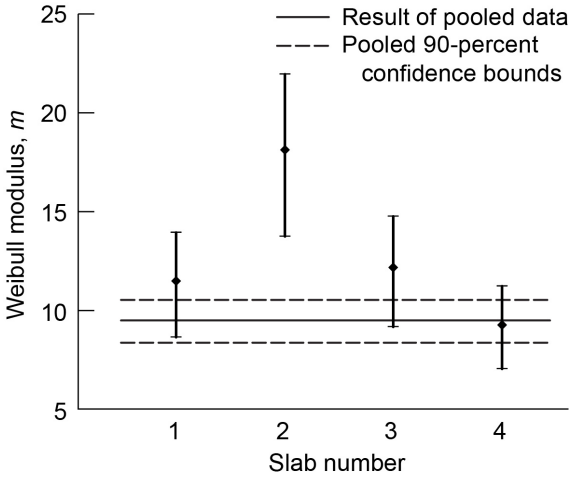

Figure 33.—Weibull modulus and 90-percent confidence bounds of individual slabs 1 to 4 for axial large tensile specimens from center of slabs.

In Figure 34, the slab-to-slab variation of characteristic strength appears to be statistically significant with a high degree of confidence because there is little overlapping of confidence bounds. See Table 14 for a listing of Weibull parameters and 90-percent confidence bounds on parameters.

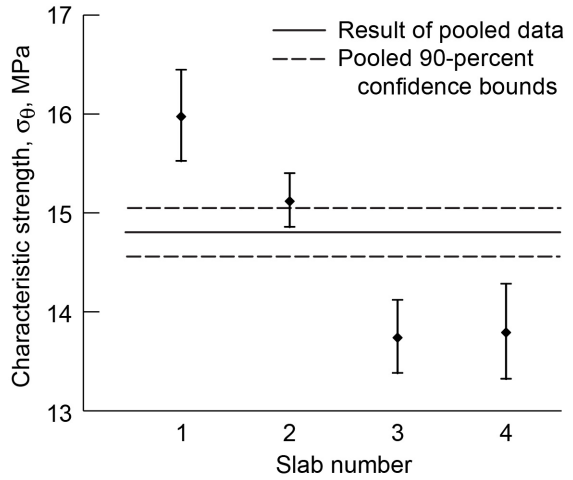

Figure 34.—Characteristic strength and 90-percent confidence bounds of individual slabs 1 to 4 for axial large tensile specimens from center of slabs.

TABLE 14.—WEIBULL PARAMETERS AND 90-PERCENT CONFIDENCE BOUNDS ON INDIVIDUAL AND POOLED DATA FROM SLABS 1 TO 4 FOR AXIAL LARGE TENSILE SPECIMENS FROM CENTER OF SLABS

Slab	Number of specimens	Weibull modulus, m		Characteristic strength, σ_θ, MPa	
		MLE biased[a]	90-percent confidence	MLE biased[a]	90-percent confidence
1	31	11.48	8.64/13.93	15.98	15.53/16.45
2	32	18.14	13.74/21.96	15.12	14.86/15.40
3	31	12.17	9.15/14.77	13.74	13.38/14.12
4	32	9.26	7.02/11.21	13.79	13.32/14.28
Mean	31.50	12.76	----------	14.66	----------
Pooled	126	9.47	8.34/10.52	14.80	14.56/15.05

[a]Maximum-likelihood estimation.

The level of scatter in Figure 35 is lower for slab 2 than for the other slabs. See Table 15 for a listing of the Weibull parameters and 90-percent confidence bounds on the parameters.

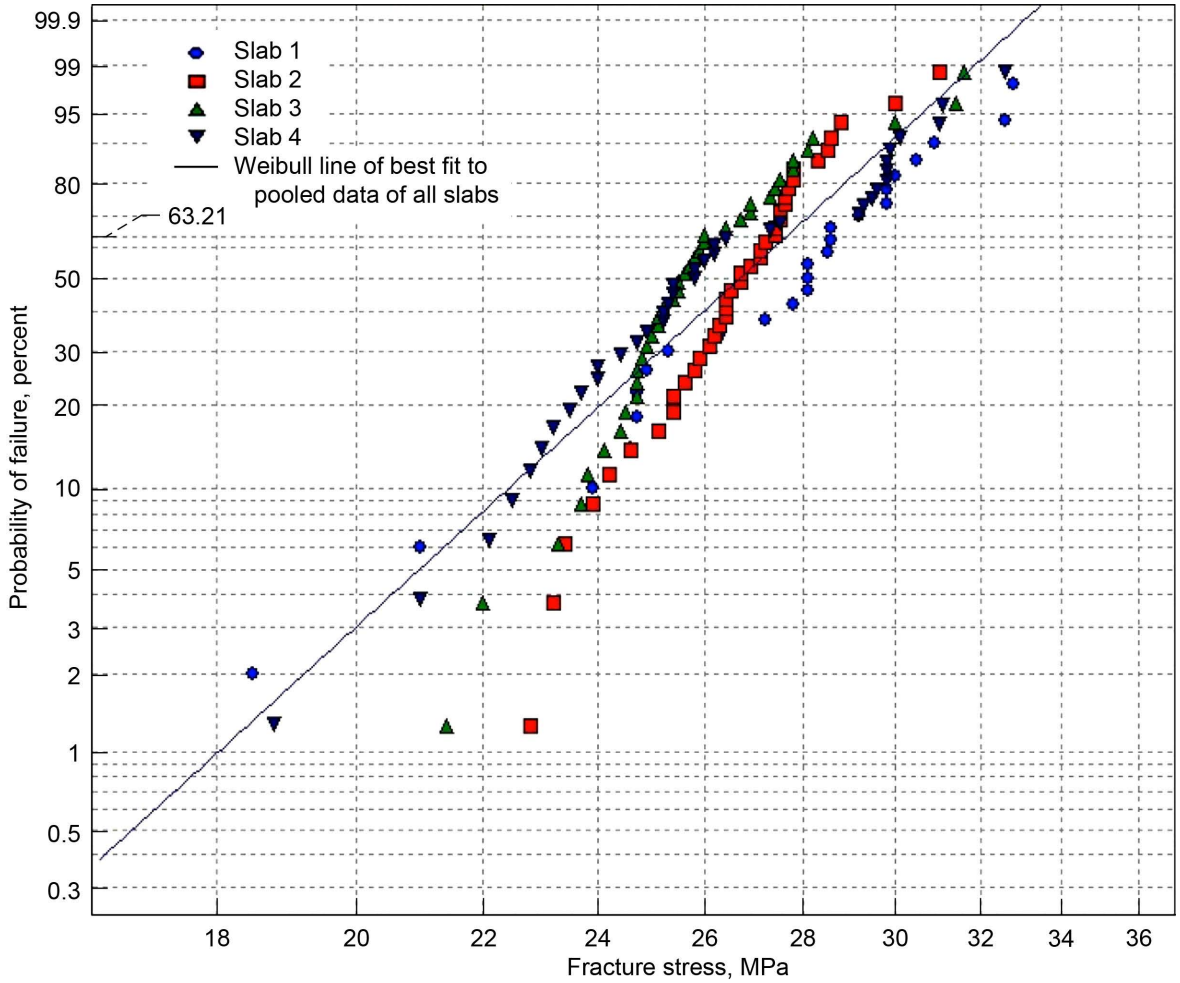

Figure 35.—Weibull plot of fracture stresses of individual slabs 1 to 4 for axial flexure specimens (with linear-elastic stress response) from center of slabs.

In Figure 36, the Weibull modulus is higher for slab 2 than for the other slabs. See Table 15 for a listing of the Weibull parameters and the 90-percent confidence bounds on the parameters.

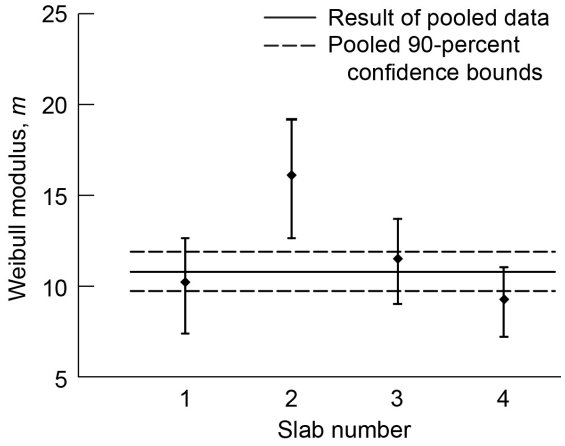

Figure 36.—Weibull modulus and 90-percent confidence bounds of individual slabs 1 to 4 for axial flexure specimens (with linear-elastic stress response) from center of slabs.

In Figure 37, the slab-to-slab variation of characteristic strength is less severe and may be substantially due to natural statistical variation. See Table 15 for a listing of the Weibull parameters and the 90-percent confidence bounds on the parameters.

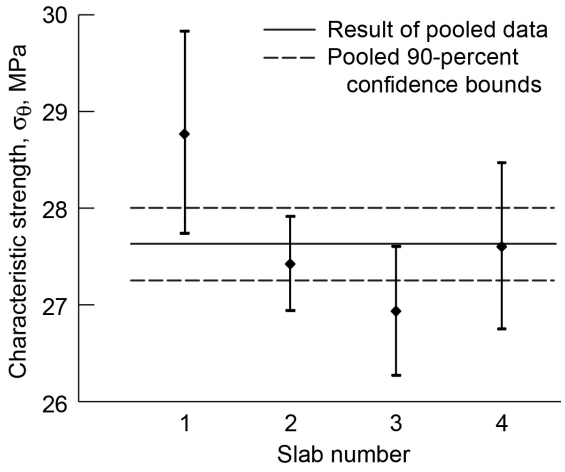

Figure 37.—Characteristic strength and 90-percent confidence bounds of individual slabs 1 to 4 for axial flexure specimens (with linear-elastic stress response) from center of slabs.

TABLE 15.—WEIBULL PARAMETERS AND 90-PERCENT CONFIDENCE BOUNDS ON INDIVIDUAL AND POOLED DATA FROM SLABS 1 TO 4 FOR AXIAL FLEXURE SPECIMENS (WITH LINEAR-ELASTIC STRESS RESPONSE) FROM CENTER OF SLABS

Slab	Number of specimens	Weibull modulus, *m*		Characteristic strength, σ_0, MPa	
		MLE biased[a]	90-percent confidence	MLE biased[a]	90-percent confidence
1	25	10.22	7.39/12.63	28.77	27.74/29.83
2	40	16.12	12.64/19.19	27.42	26.94/27.91
3	40	11.51	9.02/13.70	26.93	26.27/27.60
4	39	9.27	7.24/11.05	27.60	26.75/28.47
Mean	36	11.78	----------	27.68	----------
Pooled	144	10.79	9.60/11.91	27.63	27.25/28.00

[a]Maximum-likelihood estimation.

The level of scatter in Figure 38 is lower for slab 2 than for the other slabs. See Table 16 for a listing of the Weibull parameters and the 90-percent confidence bounds on the parameters.

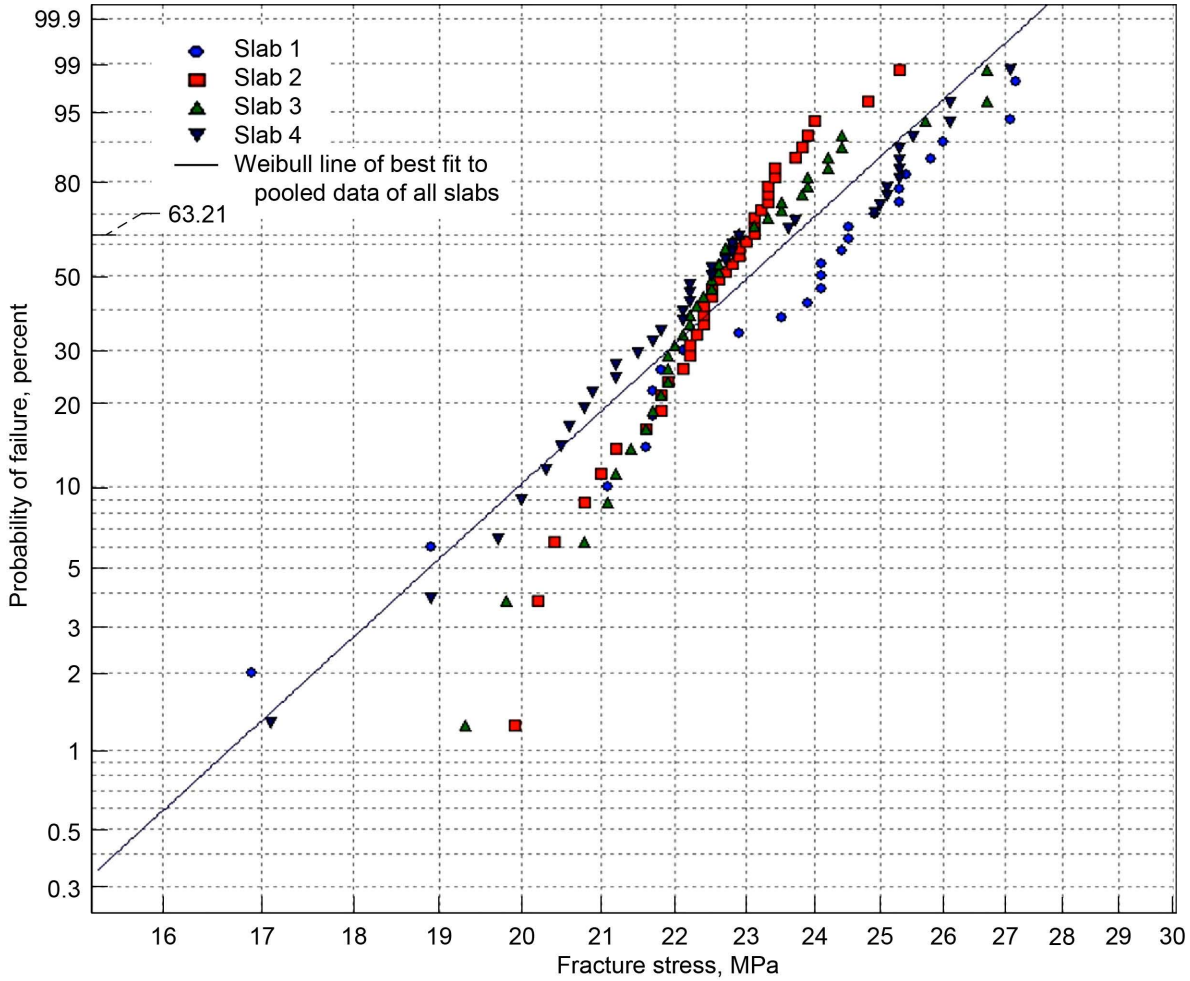

Figure 38.—Weibull plot of fracture stresses of slabs 1 to 4 for axial flexure specimens (with nonlinear-elastic stress response) from center of slabs.

In Figure 39, the Weibull modulus is higher for slab 2 than for the other slabs.

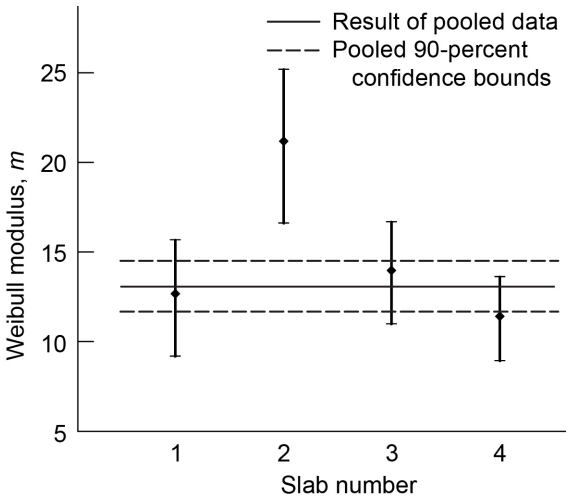

Figure 39.—Weibull modulus and 90-percent confidence bounds of individual slabs 1 to 4 for axial flexure specimens (with nonlinear-elastic stress response) from center of slabs.

In Figure 40, there appears to be some slab-to-slab variation that is beyond what is expected with natural statistical variation, although the difference does not appear to be large. See Table 16 for a listing of the Weibull parameters and the 90-percent confidence bounds on the parameters.

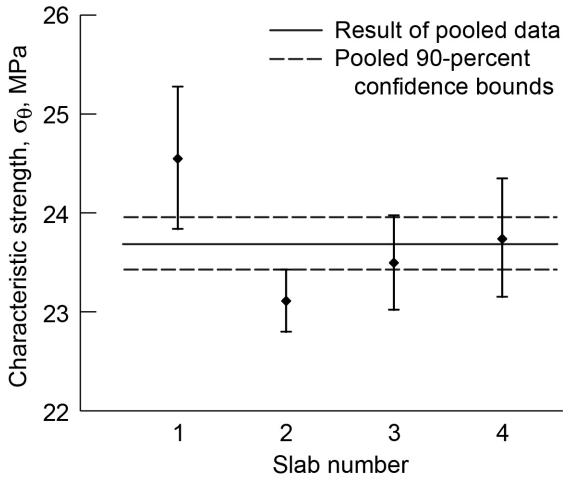

Figure 40.—Characteristic strength and 90-percent confidence bounds of individual slabs 1 to 4 for axial flexure specimens (with nonlinear-elastic stress response) from center of slabs.

TABLE 16.—WEIBULL PARAMETERS AND 90-PERCENT CONFIDENCE BOUNDS ON INDIVIDUAL AND POOLED DATA FROM SLABS 1 TO 4 FOR AXIAL FLEXURE SPECIMENS (WITH NONLINEAR-ELASTIC STRESS RESPONSE) FROM CENTER OF SLABS

Slab	Number of specimens	Weibull parameter, m		Characteristic strength, σ_θ, MPa	
		MLE biased	90-percent confidence	MLE biased[a]	90-percent confidence
1	25	12.68	9.16/15.67	24.55	23.84/25.28
2	40	21.15	16.59/25.18	23.11	22.80/23.43
3	40	13.98	10.97/16.65	23.50	23.02/23.98
4	39	11.41	8.91/13.60	23.74	23.15/24.35
Mean	36.00	14.81	----------	23.73	----------
Pooled	144	13.07	11.62/14.42	23.69	23.43/23.96

Figure 41 shows individual data for slabs 1 to 4. See Table 17 for a listing of the Weibull parameters and the 90-percent confidence bounds on the parameters.

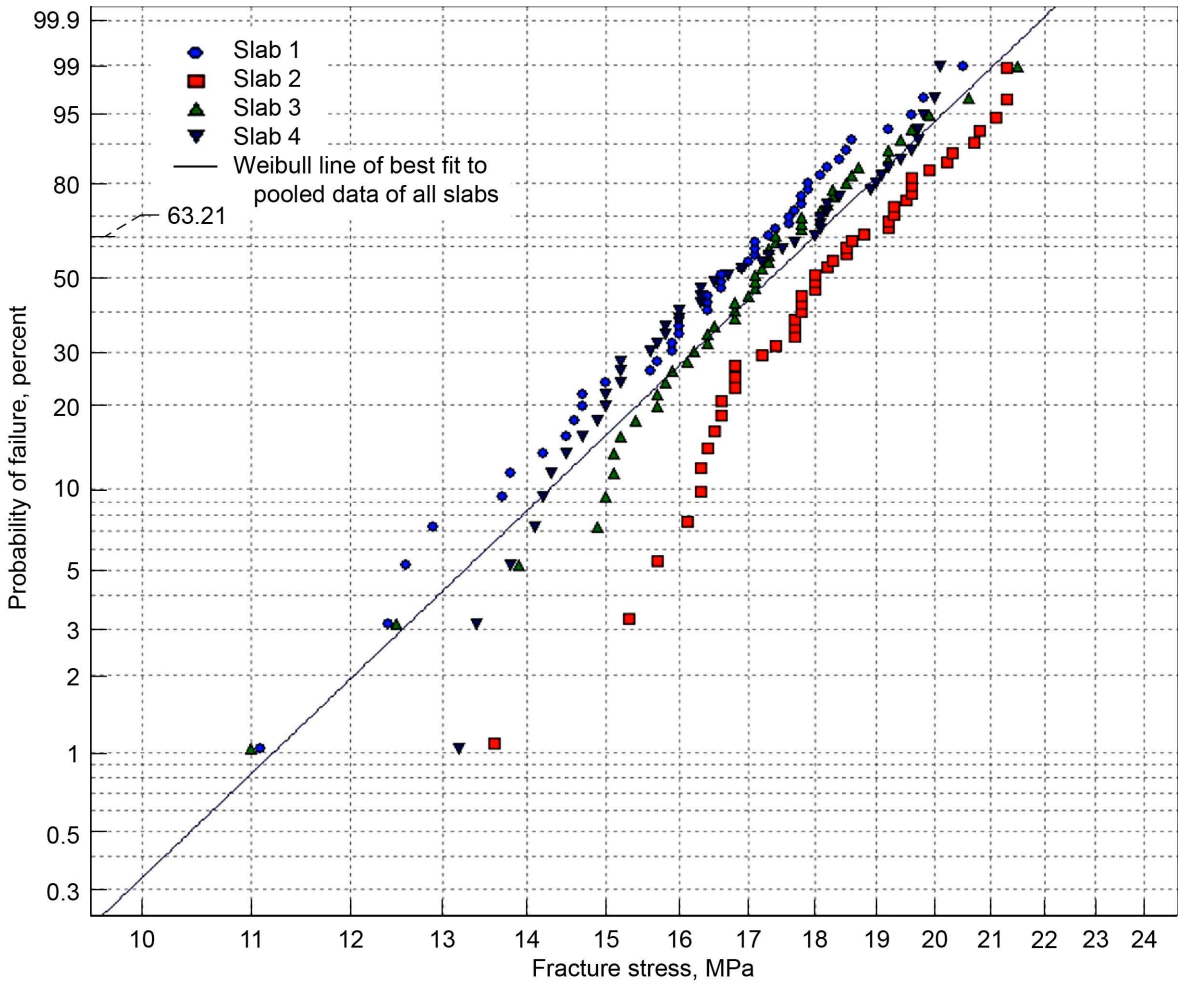

Figure 41.—Weibull plot of fracture stresses of individual slabs 1 to 4 for axial small tensile specimens from edge of slabs.

Figure 42 has a relatively consistent set of data, and the scatter in the Weibull modulus is within statistical expectation. See Table 17 for a listing of the Weibull parameters and the 90-percent confidence bounds on the parameters.

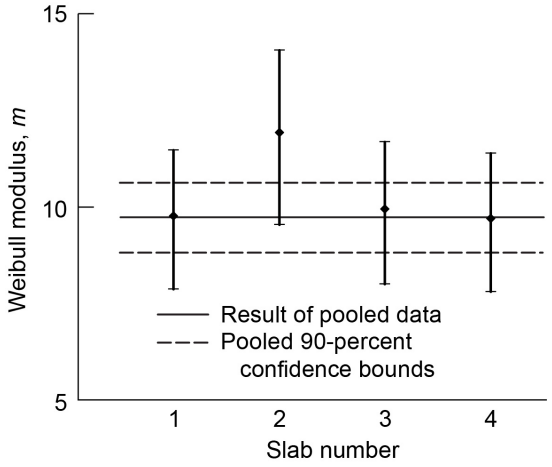

Figure 42.—Weibull modulus and 90-percent confidence bounds of individual slabs 1 to 4 for axial small tensile specimens from edge of slabs.

In Figure 43, the characteristic strength of slab 1 is higher than what would be expected from natural statistical variation with a high degree of confidence. See Table 17 for a listing of the Weibull parameters and the 90-percent confidence bounds on the parameters.

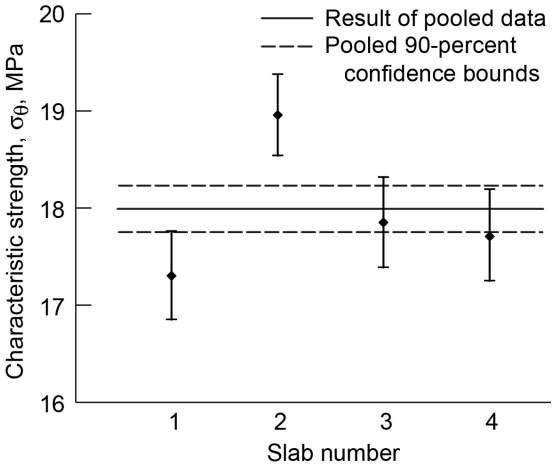

Figure 43.—Characteristic strength and 90-percent confidence bounds of individual slabs 1 to 4 for axial small tensile specimens from edge of slabs.

TABLE 17.—WEIBULL PARAMETERS AND 90-PERCENT CONFIDENCE BOUNDS ON INDIVIDUAL AND POOLED DATA FROM SLABS 1 TO 4 FOR AXIAL SMALL TENSILE SPECIMENS FROM EDGE OF SLABS

Slab	Number of specimens	Weibull parameter, m		Characteristic strength, σ_θ, MPa	
		MLE biased[a]	90-percent confidence	MLE biased[a]	90-percent confidence
1	48	9.77	7.86/11.47	17.30	16.85/17.76
2	46	11.93	9.54/14.05	18.96	18.54/19.38
3	48	9.95	8.00/11.67	17.85	17.39/18.32
4	48	9.69	7.80/11.38	17.71	17.25/18.19
Mean	47.50	10.34	----------	17.96	----------
Pooled	190	9.73	8.80/10.62	17.98	17.75/18.22

[a]Maximum-likelihood estimation.

The data in Figure 44 appear to be fairly tight and well behaved. See Table 18 for a listing of the Weibull parameters and the 90-percent confidence bounds on the parameters.

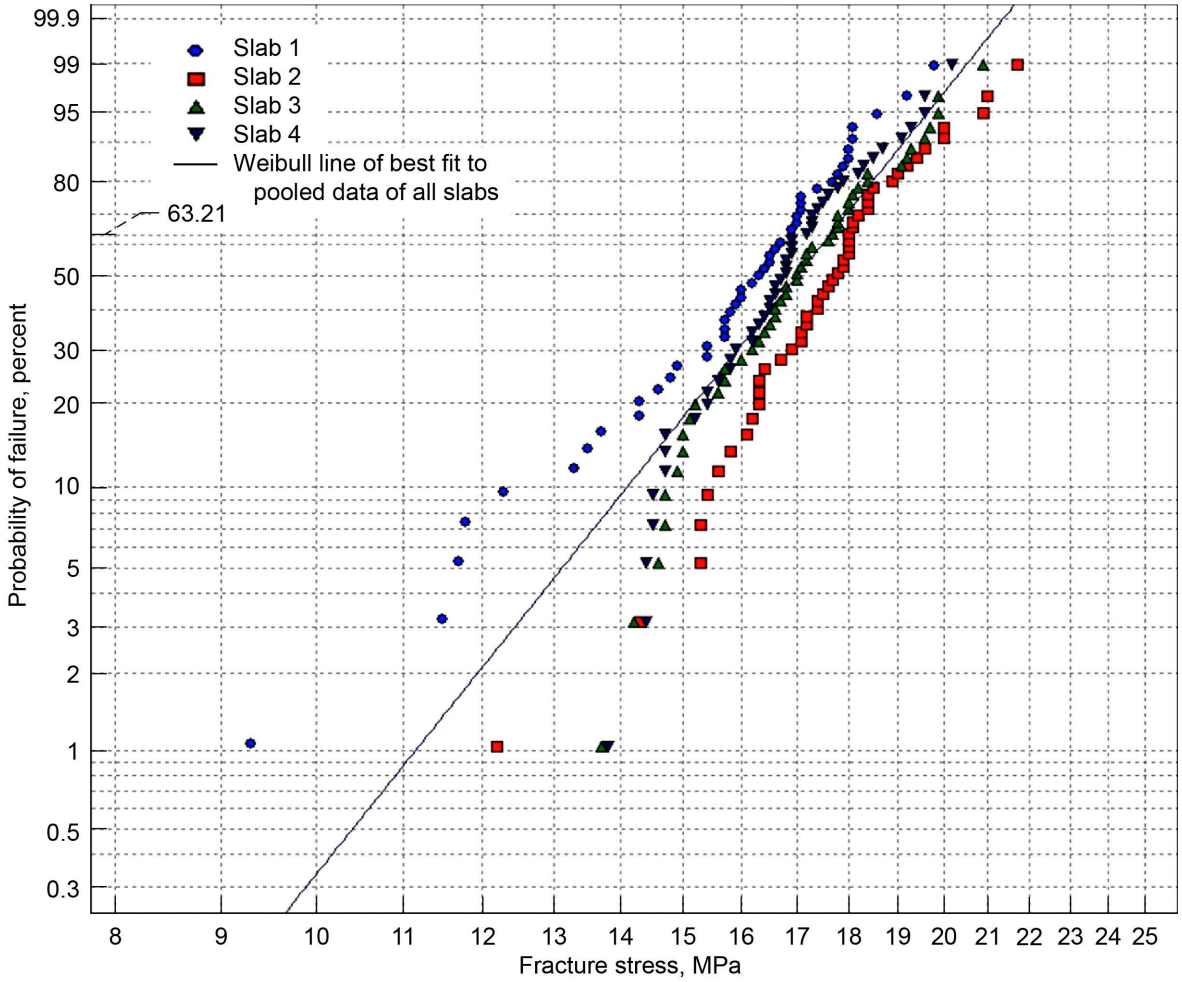

Figure 44.—Weibull plot of fracture stresses of individual slabs 1 to 4 for axial large tensile specimens from edge of slabs.

The data in Figure 45 are well behaved, and the scatter in the Weibull modulus is within statistical expectation. See Table 18 for a listing of the Weibull parameters and the 90-percent confidence bounds on the parameters.

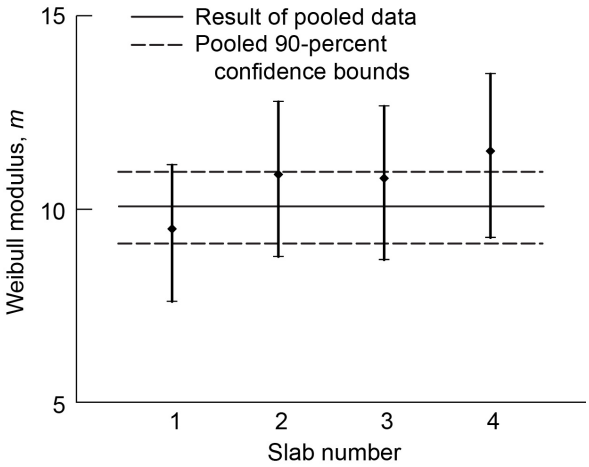

Figure 45.—Weibull modulus and 90-percent confidence bounds of individual slabs 1 to 4 for axial large tensile specimens from edge of slabs.

In Figure 46, there appears to be some slab-to-slab variation in the characteristic strength that is beyond what is expected with natural statistical variation. See Table 18 for a listing of the Weibull parameters and the 90-percent confidence bounds on the parameters.

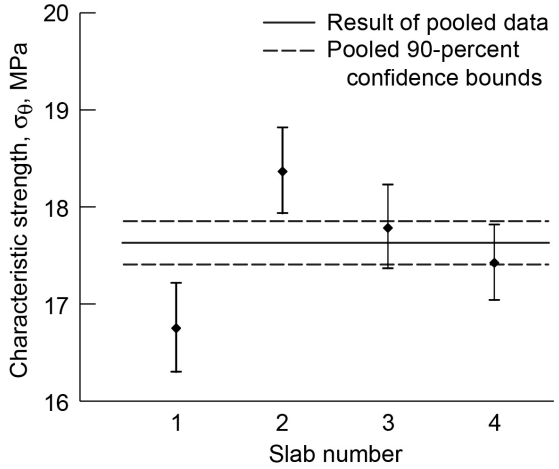

Figure 46.—Characteristic strength and 90-percent confidence bounds of individual slabs 1 to 4 for axial large tensile specimens from edge of slabs.

TABLE 18.—WEIBULL PARAMETERS AND 90-PERCENT CONFIDENCE BOUNDS ON INDIVIDUAL AND POOLED DATA FROM SLABS 1 TO 4 FOR AXIAL LARGE TENSILE SPECIMENS FROM EDGE OF SLABS

Slab	Number of specimens	Weibull parameter, *m*		Characteristic strength, σ_0, MPa	
		MLE biased[a]	90-percent confidence	MLE biased[a]	90-percent confidence
1	47	9.48	7.60/11.14	16.75	16.30/17.22
2	48	10.89	8.76/12.78	18.37	17.94/18.82
3	48	10.79	8.68/12.66	17.79	17.37/18.23
4	48	11.50	9.25/13.50	17.43	17.04/17.82
Mean	47.75	10.67	----------	17.59	----------
Pooled	191	10.05	9.09/10.96	17.63	17.41/17.85

[a]Maximum-likelihood estimation.

The data in Figure 47 appear to be fairly tight and well behaved. Note the collective downward curvature of the data. See Table 19 for a listing of the Weibull parameters and the 90-percent confidence bounds on the parameters.

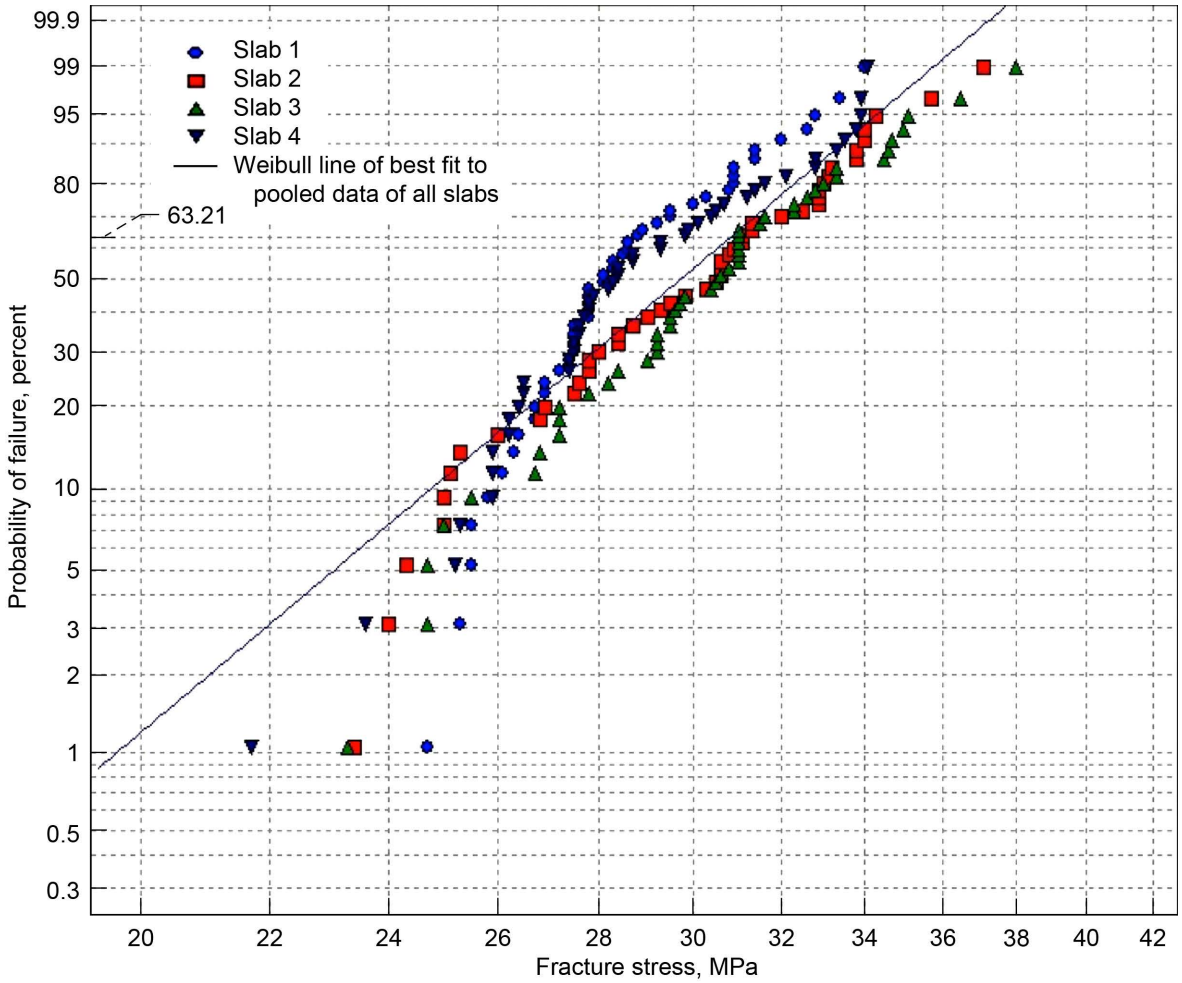

Figure 47.—Weibull plot of fracture stresses of individual slabs 1 to 4 for axial flexure specimens (with linear-elastic stress response) from edge of slabs.

The data in Figure 48 are fairly well behaved, and the scatter in the Weibull modulus is within statistical expectation. See Table 19 for a listing of the Weibull parameters and the 90-percent confidence bounds on the parameters.

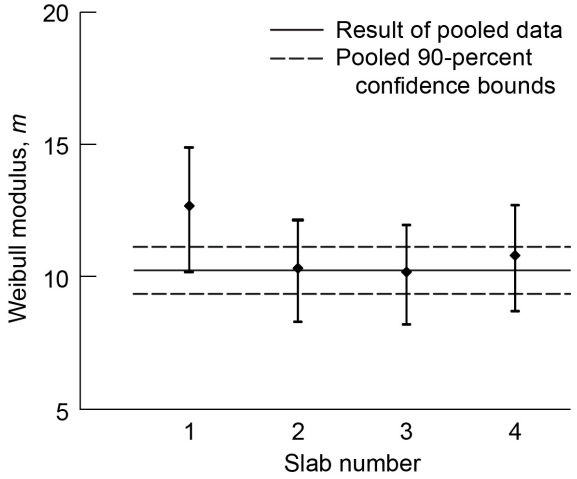

Figure 48.—Weibull modulus and 90-percent confidence bounds of individual slabs 1 to 4 for axial flexure specimens (with linear-elastic stress response) from edge of slabs.

In Figure 49, there seems to be some slab-to-slab variation in characteristic strength that is beyond what is expected from natural statistical variation. See Table 19 for a listing of the Weibull parameters and the 90-percent confidence bounds on the parameters.

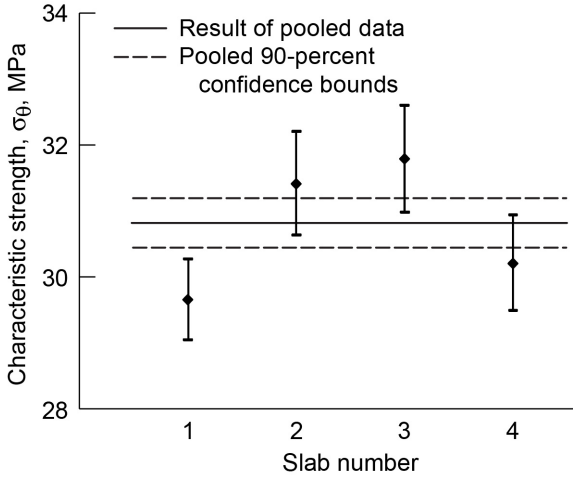

Figure 49.—Characteristic strength and 90-percent confidence bounds of individual slabs 1 to 4 for axial flexure specimens (with linear-elastic stress response) from edge of slabs.

TABLE 19.—WEIBULL PARAMETERS AND 90-PERCENT CONFIDENCE BOUNDS ON INDIVIDUAL AND POOLED DATA FROM SLABS 1 TO 4 FOR AXIAL FLEXURE SPECIMENS (WITH LINEAR-ELASTIC STRESS RESPONSE) FROM EDGE OF SLABS

Slab	Number of specimens	Weibull modulus, m		Characteristic strength, σ_θ, MPa	
		MLE biased[a]	90-percent confidence	MLE biased[a]	90-percent confidence
Pooled	191	10.05	9.09/10.96	17.63	17.41/17.85
1	48	12.68	10.20/14.88	29.65	29.05/30.27
2	48	10.34	8.32/12.14	31.41	30.64/32.21
3	48	10.20	8.21/11.97	31.79	30.99/32.61
4	48	10.82	8.71/12.70	30.20	29.49/30.94
Mean	48	11.01	----------	30.76	----------
Pooled	192	10.24	9.27/11.17	30.82	30.44/31.20

[a]Maximum-likelihood estimation.

The data in Figure 50 appear to be fairly tight and well behaved. Note the apparent collective downward curvature of the data. See Table 20 for a listing of the Weibull parameters and the 90-percent confidence bounds on the parameters.

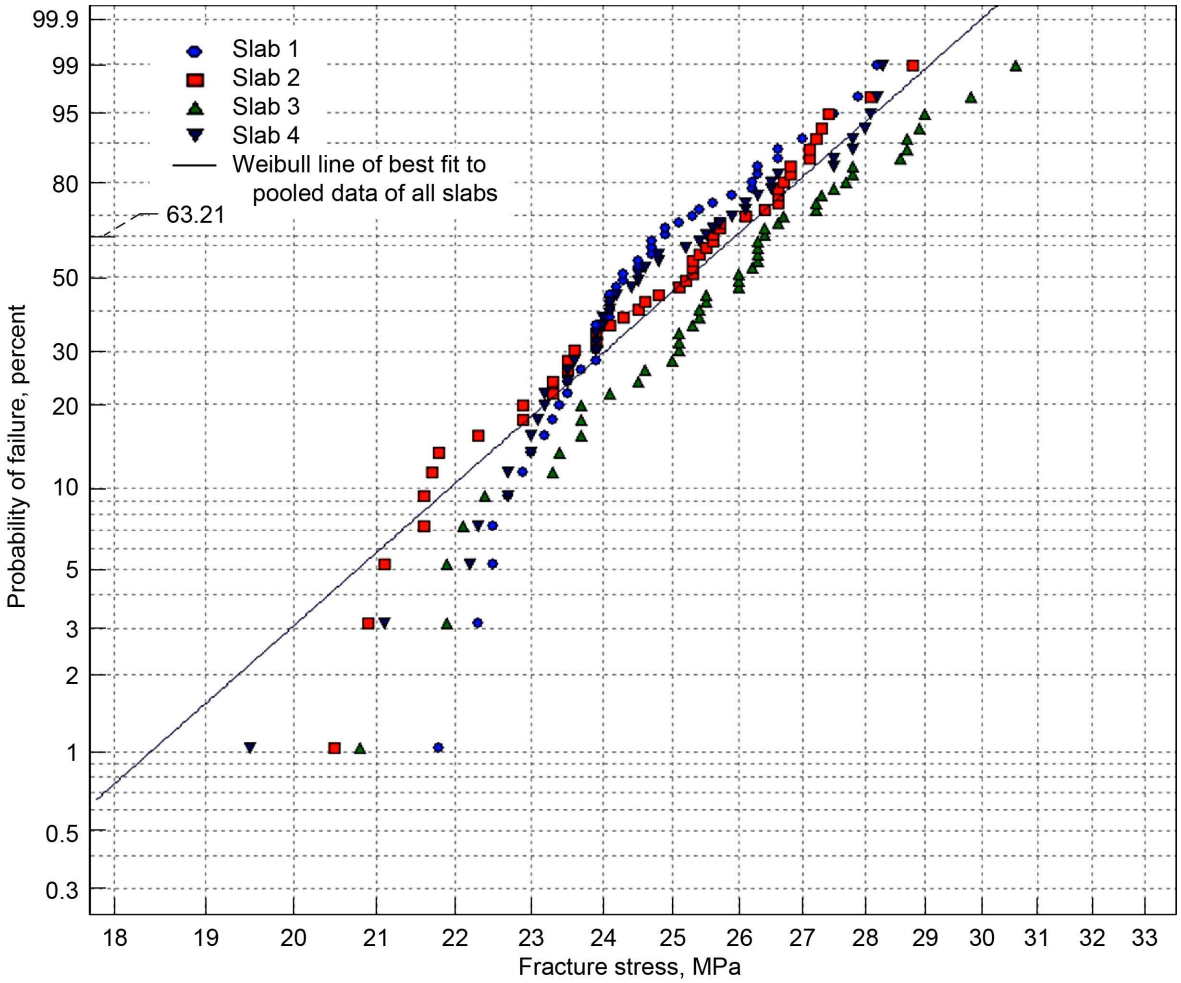

Figure 50.—Weibull plot of fracture stresses of individual slabs 1 to 4 for axial flexure specimens (with nonlinear-elastic stress response) from edge of slabs.

The data in Figure 51 are well behaved, and the scatter in the Weibull modulus is within statistical expectation. See Table 20 for a listing of the Weibull parameters and the 90-percent confidence bounds on the parameters.

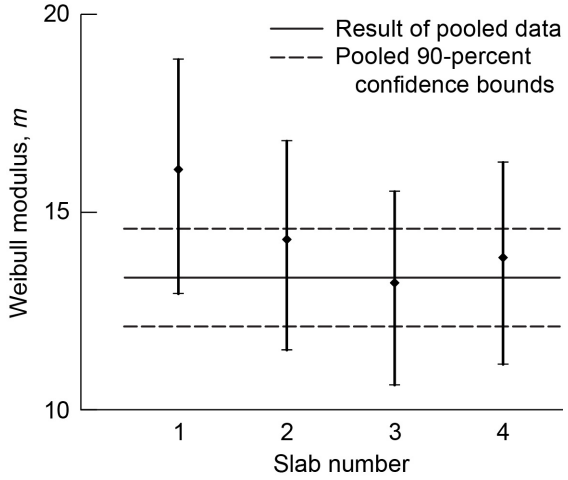

Figure 51.—Weibull modulus and 90-percent confidence bounds on individual slabs 1 to 4 for axial flexure specimens (with nonlinear-elastic stress response) from edge of slabs.

In Figure 52, the characteristic strength of slab 3 seems to be a little higher than what is expected from natural statistical variation. See Table 20 for a listing of the Weibull parameters and the 90-percent confidence bounds on the parameters.

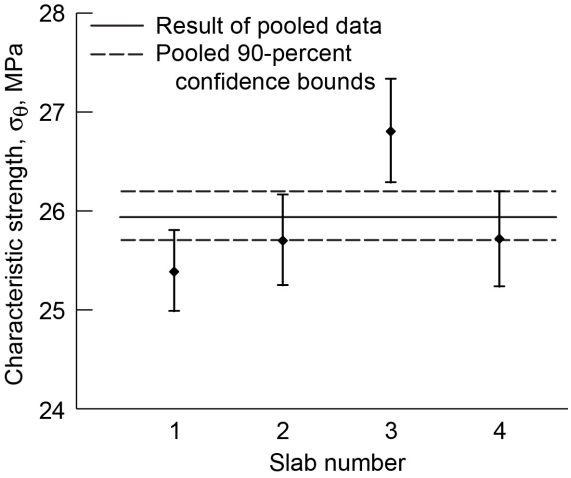

Figure 52.—Characteristic strength and 90-percent confidence bounds of individual slabs 1 to 4 for axial flexure specimens (with nonlinear-elastic stress response) from edge of slabs.

TABLE 20.—WEIBULL PARAMETERS AND 90-PERCENT CONFIDENCE BOUNDS ON INDIVIDUAL AND POOLED DATA FROM SLABS 1 TO 4 FOR AXIAL FLEXURE SPECIMENS (WITH NONLINEAR-ELASTIC STRESS RESPONSE) FROM EDGE OF SLABS

Slab	Number of specimens	Weibull modulus, m		Characteristic strength, σ_θ, MPa	
		MLE biased[a]	90-percent confidence	MLE biased[a]	90-percent confidence
1	48	16.07	12.93/18.86	25.39	24.99/25.81
2	48	14.30	11.51/16.79	25.70	25.25/26.17
3	48	13.21	10.63/15.51	26.81	26.29/27.34
4	48	13.85	11.14/16.25	25.72	25.24/26.20
Mean	48.00	14.36	----------	25.91	----------
Pooled	192	13.36	12.09/14.57	25.94	25.70/26.19

[a]Maximum-likelihood estimation.

In Figure 53, the strength data of slab 2 are relatively low at lower probabilities of failure. See Table 21 for a listing of the Weibull parameters and the 90-percent confidence bounds on the parameters.

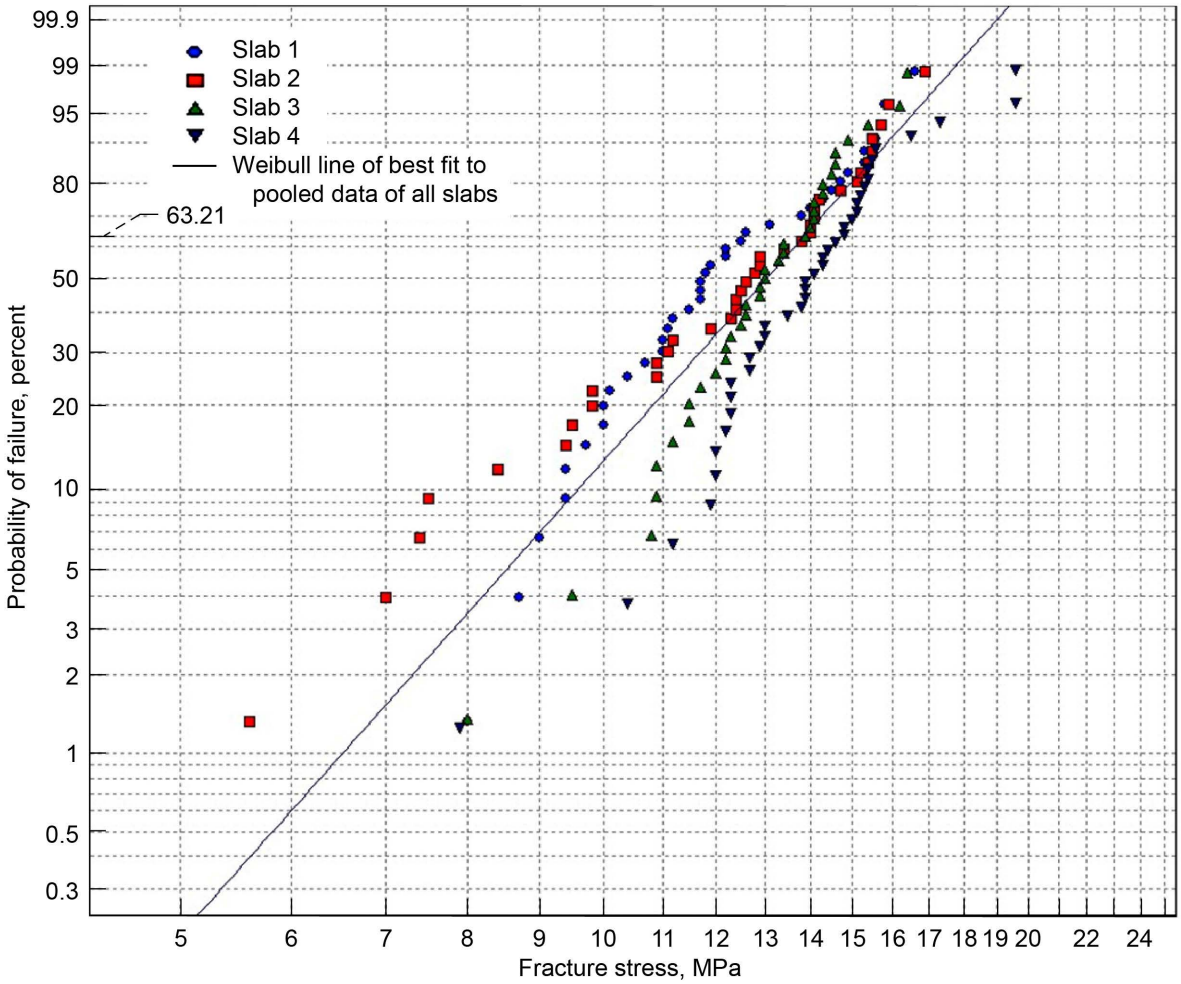

Figure 53.—Weibull plot of fracture stresses of individual slabs 1 to 4 for radial small tensile specimens from center of slabs.

In Figure 54, slab 3 has somewhat less scatter in strength and, hence, a higher Weibull modulus than that of the other slabs. The difference appears to be statistically significant. See Table 21 for a listing of the Weibull parameters and the 90-percent confidence bounds on the parameters.

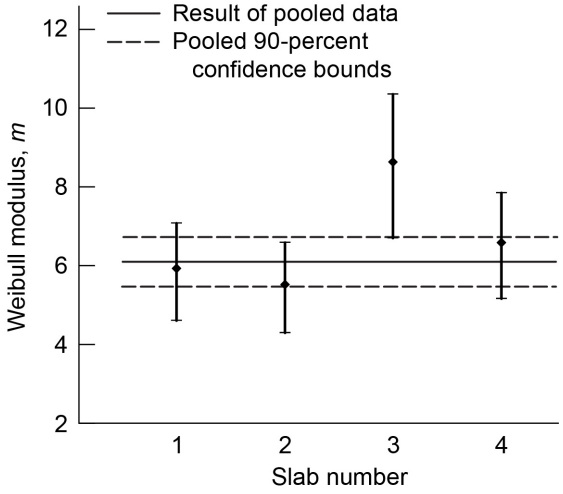

Figure 54.—Weibull modulus and 90-percent confidence bounds of individual slabs 1 to 4 for radial small tensile specimens from center of slabs.

In Figure 55, slab 4 has characteristic strength that is higher than what is expected from natural statistical variation. See Table 21 for a listing of the Weibull parameters and the 90-percent confidence bounds on the parameters.

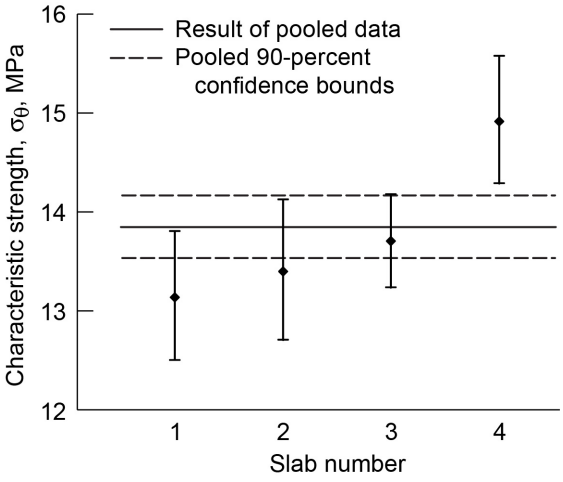

Figure 55.—Characteristic strength and 90-percent confidence bounds of individual slabs 1 to 4 for radial small tensile specimens from center of slabs.

TABLE 21.—WEIBULL PARAMETERS AND 90–PERCENT CONFIDENCE BOUNDS ON INDIVIDUAL AND POOLED DATA FROM SLABS 1 TO 4 FOR RADIAL SMALL TENSILE SPECIMENS FROM CENTER OF SLABS

Slab	Number of specimens	Weibull modulus, *m*		Characteristic strength, σ_θ, MPa	
		MLE biased[a]	90-percent confidence	MLE biased[a]	90-percent confidence
1	38	5.93	4.61/7.08	13.14	12.51/13.81
2	38	5.52	4.29/6.59	13.40	12.71/14.13
3	37	8.63	6.69/10.34	13.71	13.24/14.18
4	40	6.58	5.16/7.84	14.92	14.29/15.58
Mean	38.25	6.67	----------	13.79	----------
Pooled	153	6.11	5.46/6.72	13.85	13.53/14.17

[a]Maximum-likelihood estimation.

In Figure 56, there is a wide difference in strength between slab 1 and slab 4, with distinctly less scatter in strength for slabs 2 and 3 than for slabs 1 and 4. See Table 22 for a listing of the Weibull parameters and the 90-percent confidence bounds on the parameters.

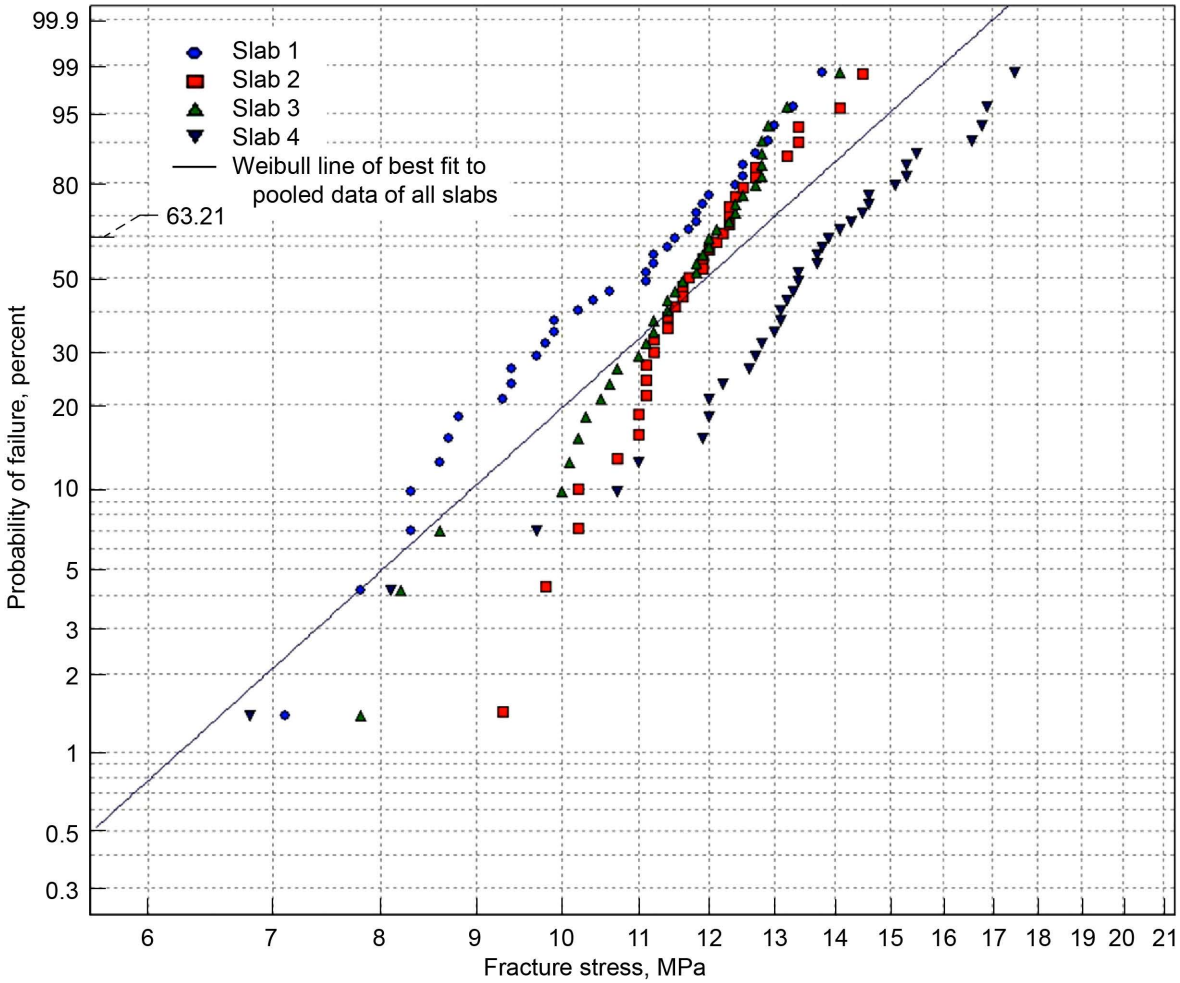

Figure 56.—Weibull plot of fracture stresses of individual slabs 1 to 4 for radial large tensile specimens from center of slabs.

In Figure 57, the Weibull modulus is relatively higher for slabs 2 and 3 than for slabs 1 and 4, but the difference is not too far beyond what is expected from natural statistical variation. See Table 22 for a listing of the Weibull parameters and the 90-percent confidence bounds on the parameters.

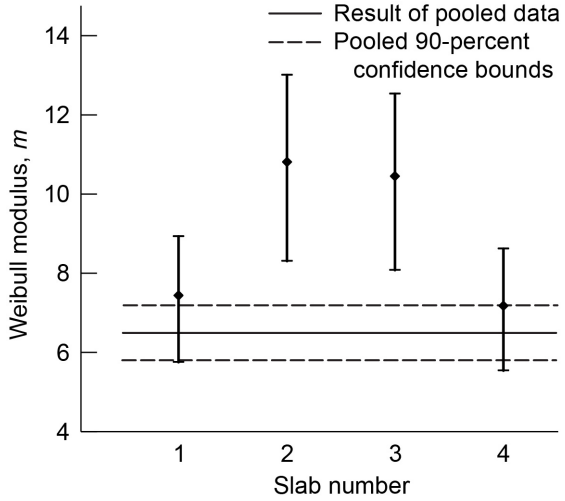

Figure 57.—Weibull modulus and 90-percent confidence bounds of individual slabs 1 to 4 for radial large tensile specimens from center of slabs.

In Figure 58, slabs 1 and 4, and particularly slab 4, have characteristic strengths well beyond what is expected from natural statistical variation. See Table 22 for a listing of the Weibull parameters and the 90-percent confidence bounds on the parameters.

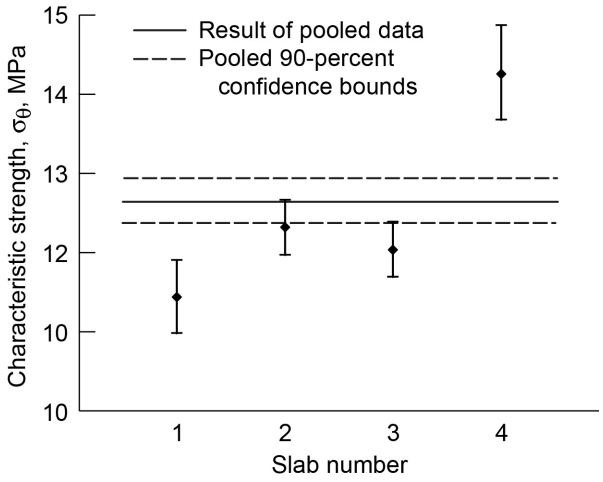

Figure 58.—Characteristic strength and 90-percent confidence bounds of individual slabs 1 to 4 for radial large tensile specimens from center of slabs.

TABLE 22.—WEIBULL PARAMETERS AND 90-PERCENT CONFIDENCE BOUNDS ON INDIVIDUAL AND POOLED DATA FROM SLABS 1 TO 4 FOR RADIAL LARGE TENSILE SPECIMENS FROM CENTER OF SLABS

Slab	Number of specimens	Weibull modulus, m		Characteristic strength, σ_θ, MPa	
		MLE biased[a]	90-percent confidence	MLE biased[a]	90-percent confidence
1	36	7.44	5.75/8.92	11.44	10.98/11.91
2	35	10.81	8.31/13.00	12.32	11.97/12.67
3	36	10.45	8.07/12.53	12.04	11.69/12.39
4	36	7.18	5.54/8.61	14.26	13.68/14.88
Mean	35.75	8.97	----------	12.52	----------
Pooled	143	6.50	5.78/7.17	12.65	12.37/12.94

[a]Maximum-likelihood estimation.

The data in Figure 59 appear to be fairly well behaved. See Table 23 for a listing of the Weibull parameters and the 90-percent confidence bounds on the parameters.

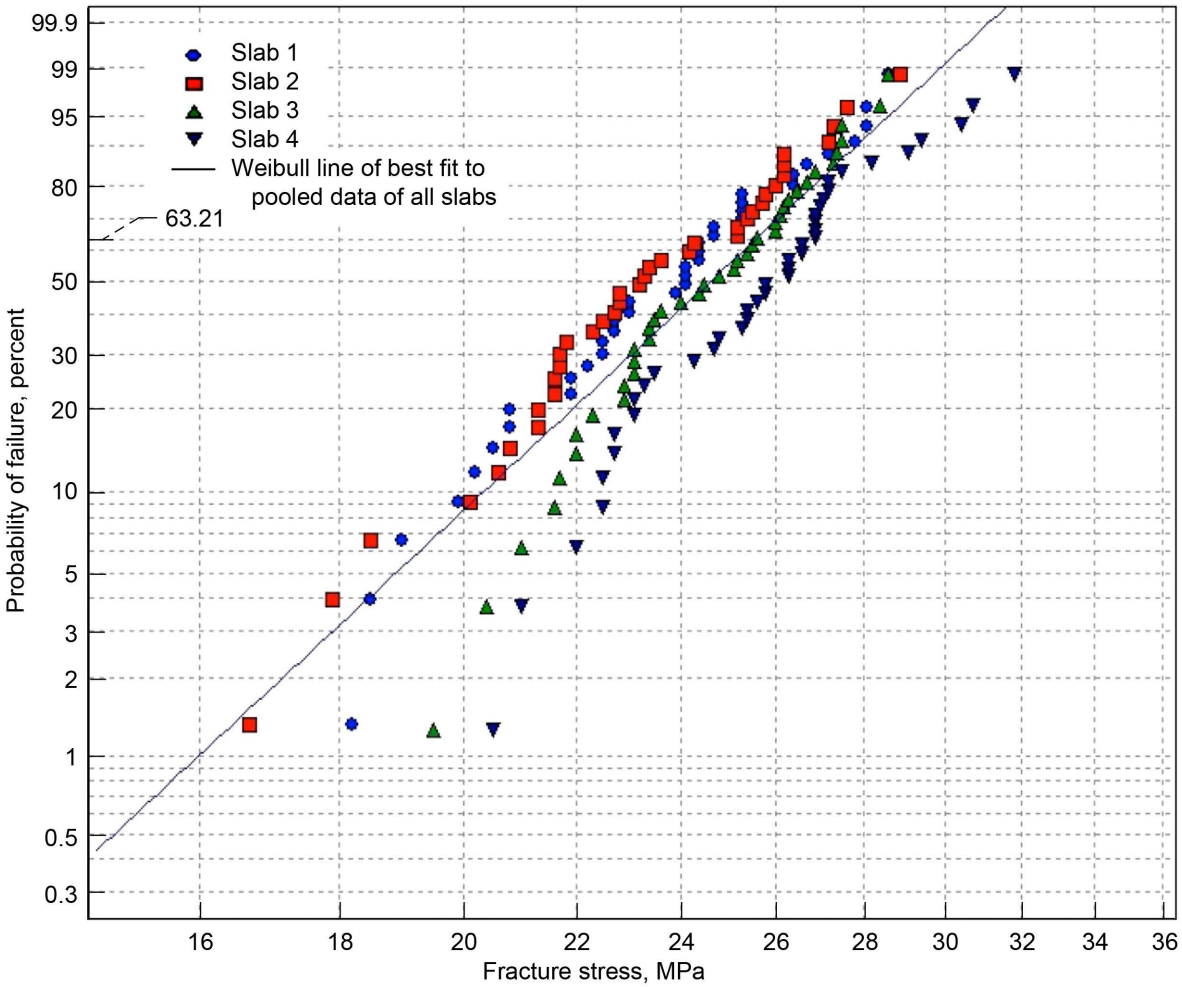

Figure 59.—Weibull plot of fracture stresses of individual slabs 1 to 4 for radial flexure specimens (with linear-elastic stress response) from center of slabs.

The data in Figure 60 are well-behaved, and the scatter in the Weibull modulus is within statistical expectation. See Table 23 for a listing of the Weibull parameters and the 90-percent confidence bounds on the parameters.

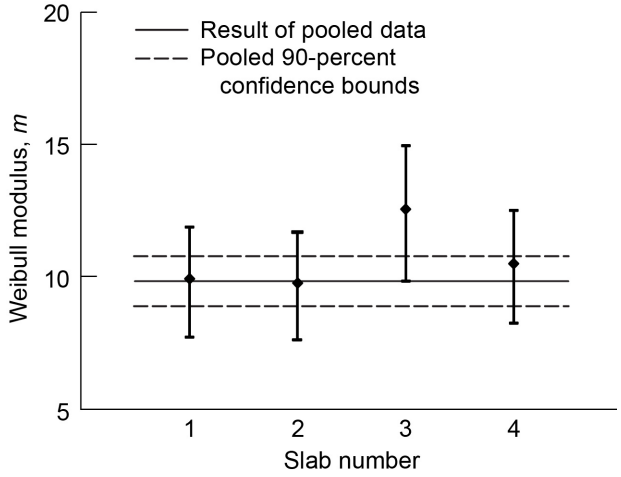

Figure 60.—Weibull modulus and 90-percent confidence bounds of individual slabs 1 to 4 for radial flexure specimens (with linear-elastic stress response) from center of slabs.

In Figure 61, the slab-to-slab variation in characteristic strength appears to be beyond what is expected from natural statistical variation—particularly for slab 4. See Table 23 for a listing of the Weibull parameters and the 90-percent confidence bounds on the parameters.

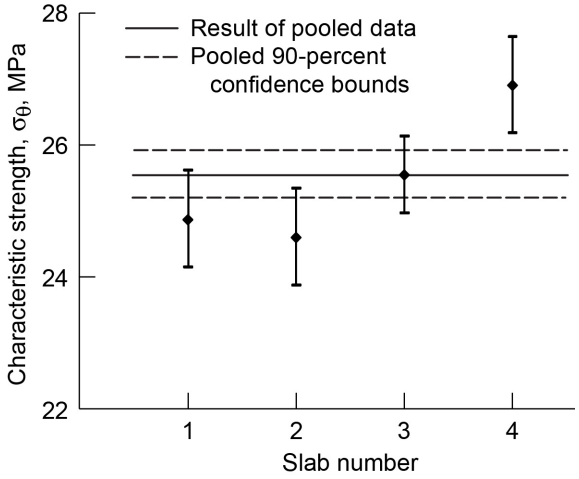

Figure 61.—Characteristic strength and 90-percent confidence bounds of individual slabs 1 to 4 for radial flexure specimens (with linear-elastic stress response) from center of slabs.

TABLE 23.—WEIBULL PARAMETERS AND 90-PERCENT CONFIDENCE BOUNDS ON INDIVIDUAL AND POOLED DATA FROM SLABS 1 TO 4 FOR RADIAL FLEXURE SPECIMENS (WITH LINEAR-ELASTIC STRESS RESPONSE) FROM CENTER OF SLABS

Slab	Number of specimens	Weibull modulus, m		Characteristic strength, σ_θ, MPa	
		MLE biased[a]	90-percent confidence	MLE biased[a]	90-percent confidence
1	38	9.93	7.72/11.86	24.87	24.15/25.62
2	38	9.77	7.60/11.67	24.60	23.88/25.35
3	40	12.55	9.84/14.94	25.55	24.98/26.14
4	40	10.50	8.24/12.50	26.91	26.19/27.65
Mean	39	10.69	----------	25.48	----------
Pooled	156	9.82	8.78/10.79	25.56	25.20/25.93

[a]Maximum-likelihood estimation.

The data shown in Figure 62 appear to be a fairly well behaved. See Table 24 for a listing of the Weibull parameters and the 90-percent confidence bounds on the parameters.

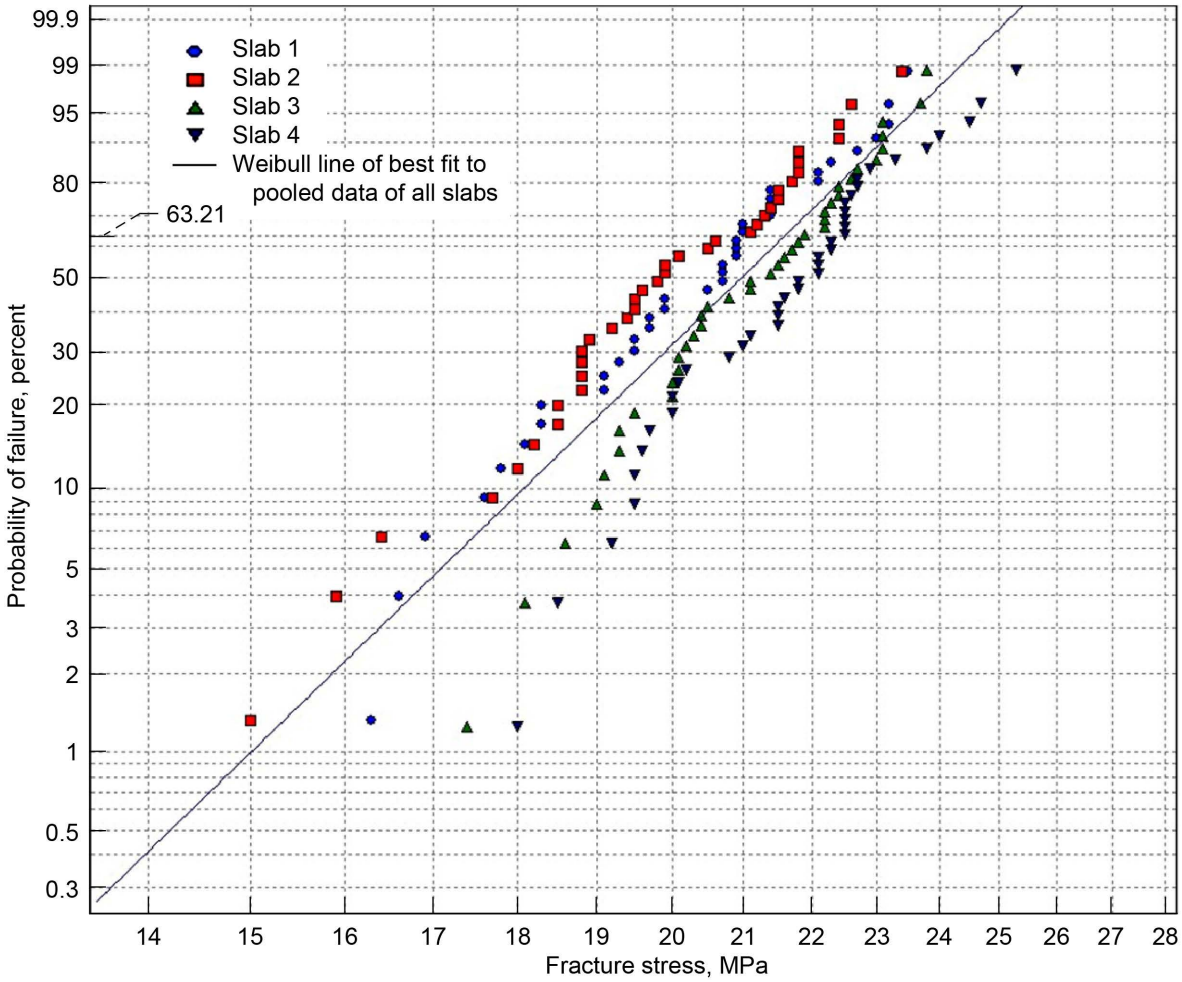

Figure 62.—Weibull plot of fracture stresses of individual slabs 1 to 4 for radial flexure specimens (with nonlinear-elastic stress response) from center of slabs.

The data in Figure 63 are well behaved, and the scatter in the Weibull modulus is within statistical expectation. See Table 24 for a listing of the Weibull parameters and the 90-percent confidence bounds on the parameters.

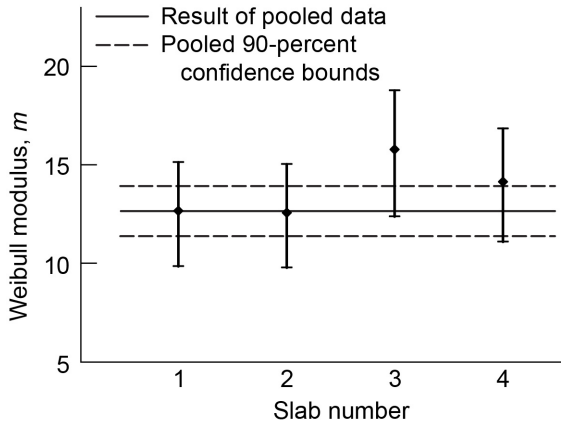

Figure 63.—Weibull modulus and 90-percent confidence bounds of individual slabs 1 to 4 for radial flexure specimens (with nonlinear-elastic stress response) from center of slabs.

In Figure 64, the slab-to-slab variation in characteristic strength appears to be beyond what is expected from natural statistical variation. See Table 24 for a listing of the Weibull parameters and the 90-percent confidence bounds on the parameters.

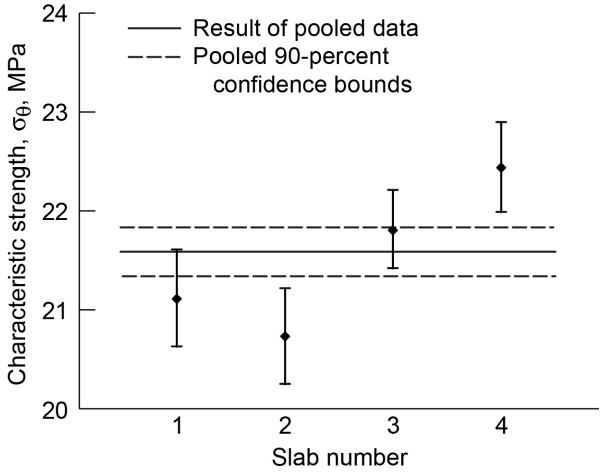

Figure 64.—Characteristic strength and 90-percent confidence bounds of individual slabs 1 to 4 for radial flexure specimens (with nonlinear-elastic stress response) from center of slabs.

TABLE 24.—WEIBULL PARAMETERS AND 90-PERCENT CONFIDENCE BOUNDS ON INDIVIDUAL AND POOLED DATA FROM SLABS 1 TO 4 FOR RADIAL FLEXURE SPECIMENS (WITH NONLINEAR-ELASTIC STRESS RESPONSE) FROM CENTER OF SLABS

Slab	Number of specimens	Weibull parameter, *m*		Characteristic strength, σ_θ, MPa	
		MLE biased[a]	90-percent confidence	MLE biased[a]	90-percent confidence
1	38	12.65	9.85/15.12	21.11	20.63/21.61
2	38	12.57	9.78/15.02	20.73	20.25/21.22
3	40	15.76	12.36/18.76	21.81	21.42/22.21
4	40	14.14	11.09/16.83	22.44	21.99/22.90
Mean	39.00	13.78	----------	21.52	----------
Pooled	156	12.65	11.32/13.91	21.59	21.35/21.83

[a]Maximum-likelihood estimation.

In Figure 65, note that slab 1 and slab 3 seem to show lower strength failures below the 10-percent probability of failure. Also, slab 1 seems to be significantly weaker than the other slabs. See Table 25 for a listing of the Weibull parameters and the 90-percent confidence bounds on the parameters.

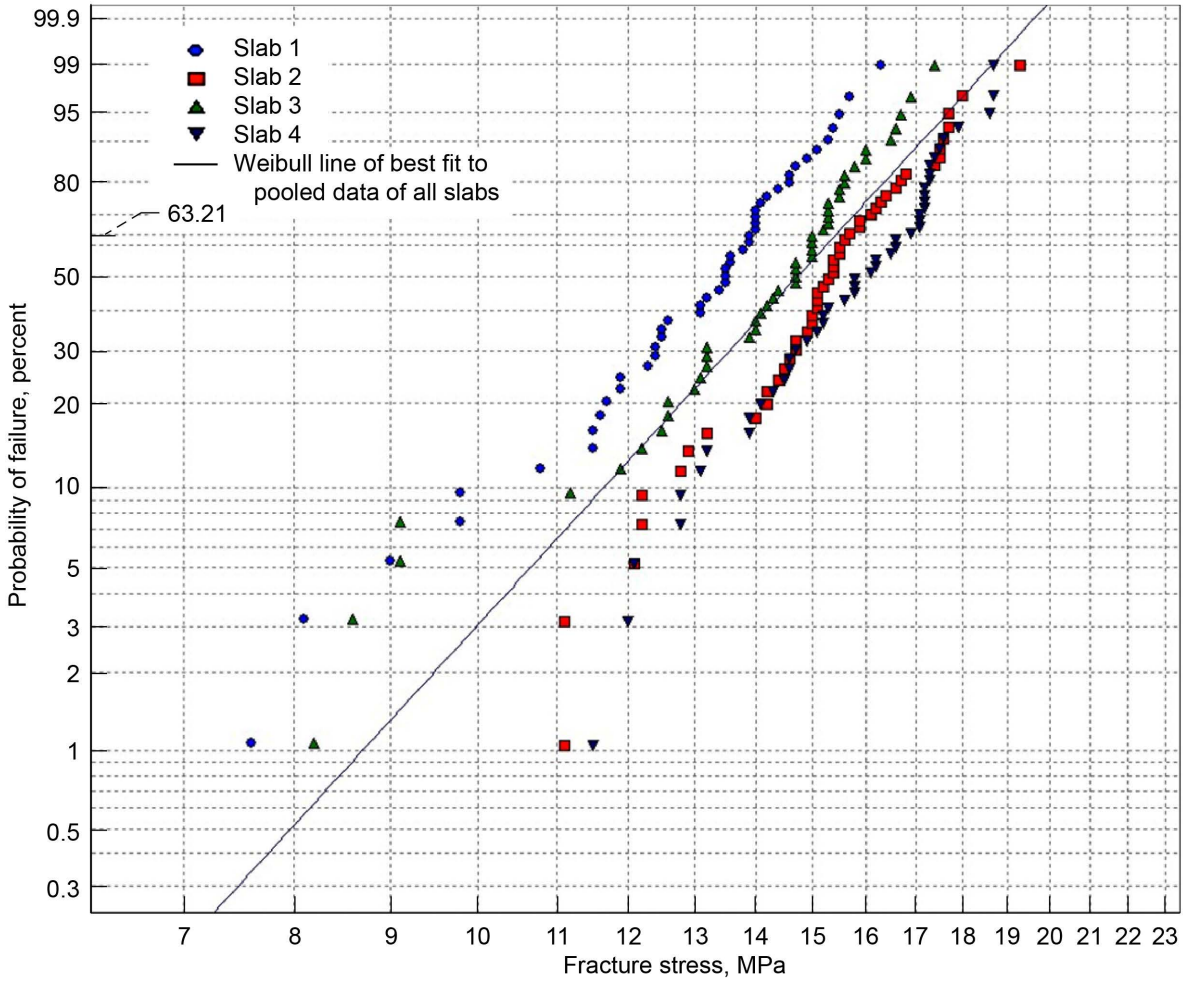

Figure 65.—Weibull plot of fracture stresses of individual slabs 1 to 4 for radial small tensile specimens from edge of slabs.

The Weibull moduli in Figure 66 are well behaved and within the expected statistical uncertainty. See Table 25 for a listing of the Weibull parameters and the 90-percent confidence bounds on the parameters.

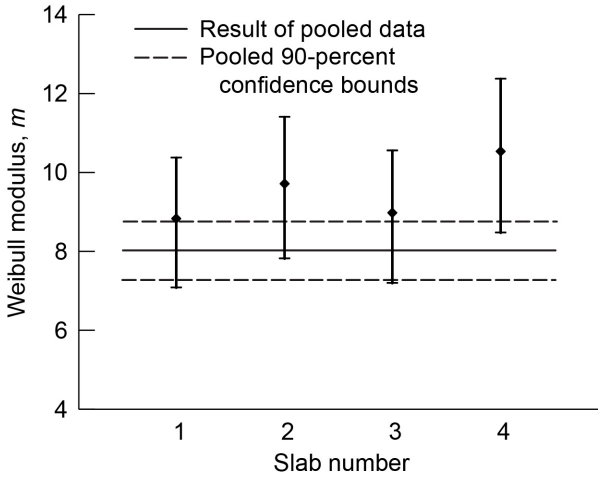

Figure 66.—Weibull modulus and 90-percent confidence bounds of individual slabs 1 to 4 for radial small tensile specimens from edge of slabs.

In Figure 67, the slab-to-slab variation in characteristic strength appears to be well beyond what is expected from natural statistical variation. Note the low characteristic strength of slab 1. See Table 25 for a listing of the Weibull parameters and the 90-percent confidence bounds on the parameters.

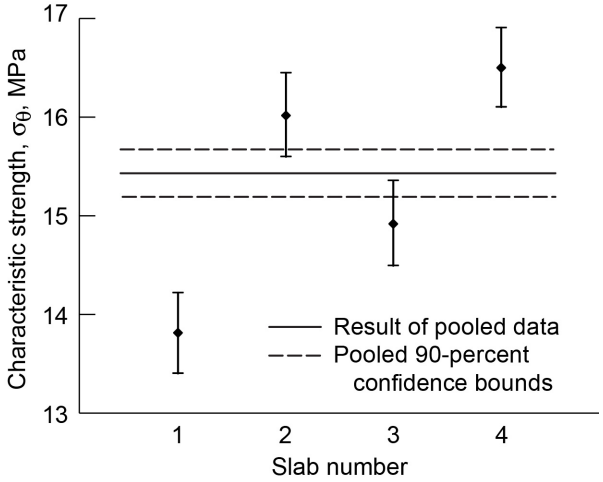

Figure 67.—Characteristic strength and 90-percent confidence bounds of individual slabs 1 to 4 for radial small tensile specimens from edge of slabs.

TABLE 25.—WEIBULL PARAMETERS AND 90-PERCENT CONFIDENCE BOUNDS ON INDIVIDUAL AND POOLED DATA FROM SLABS 1 TO 4 FOR RADIAL SMALL TENSILE SPECIMENS FROM EDGE OF SLABS

Slab	Number of specimens	Weibull modulus, m		Characteristic strength, σ_θ, MPa	
		MLE biased[a]	90-percent confidence	MLE biased[a]	90-percent confidence
1	47	8.82	7.08/10.37	13.81	13.40/14.22
2	48	9.71	7.81/11.40	16.02	15.60/16.45
3	47	8.97	7.19/10.54	14.92	14.49/15.36
4	48	10.53	8.47/12.36	16.50	16.10/16.91
Mean	47.50	9.51	----------	15.31	----------
Pooled	190	8.02	7.25/8.75	15.43	15.19/15.67

[a]Maximum-likelihood estimation.

In Figure 68, slab 1 has distinctly different behavior at lower probabilities of failure. See Table 26 for a listing of the Weibull parameters and the 90-percent confidence bounds on the parameters.

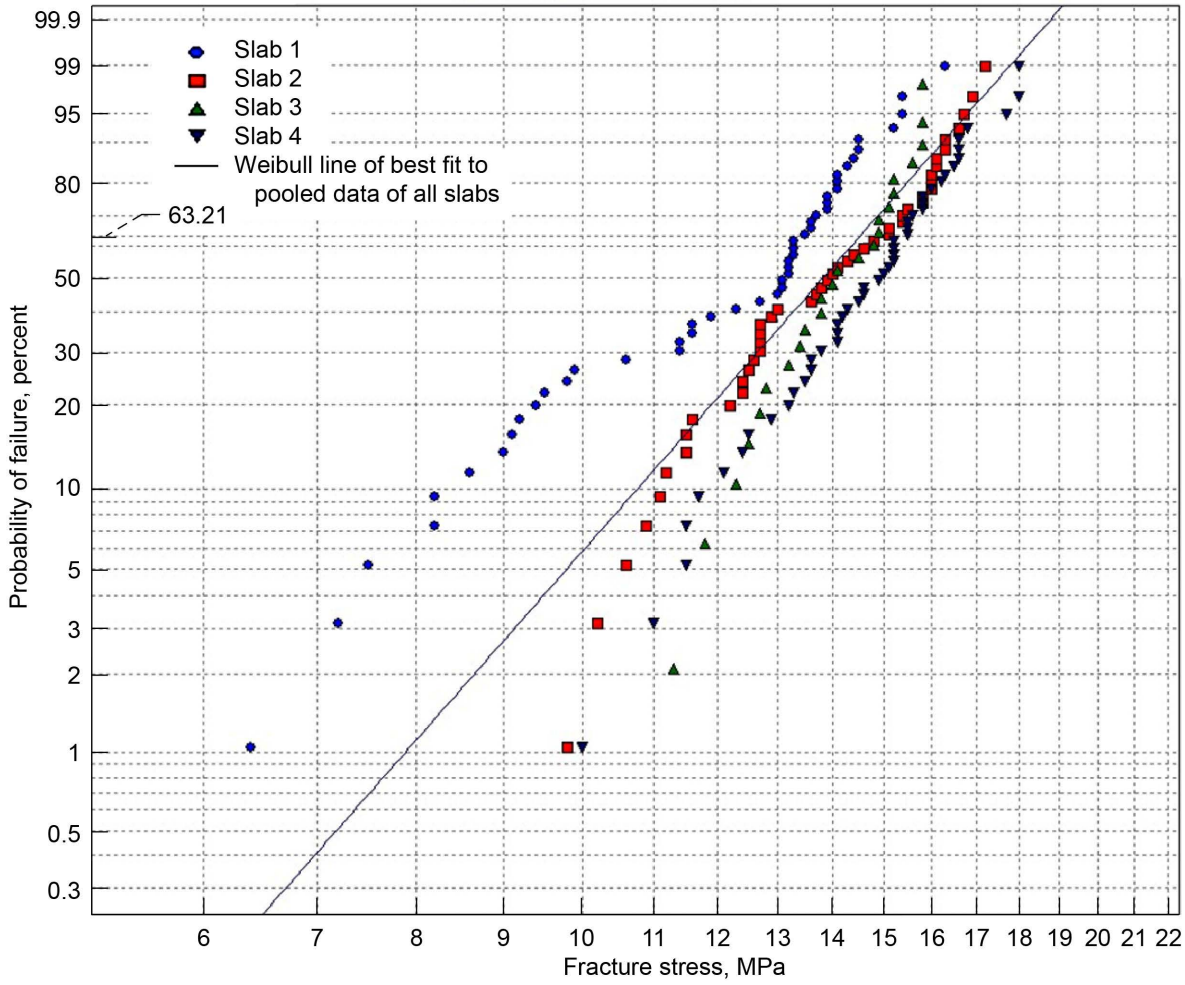

Figure 68.—Weibull plot of fracture stresses of individual slabs 1 to 4 for radial large tensile specimens from edge of slabs.

In Figure 69, note the low Weibull modulus of slab 1 versus the high Weibull modulus of slab 3, indicating significant slab-to-slab variation in the Weibull modulus. See Table 26 for a listing of the Weibull parameters and the 90-percent confidence bounds on the parameters.

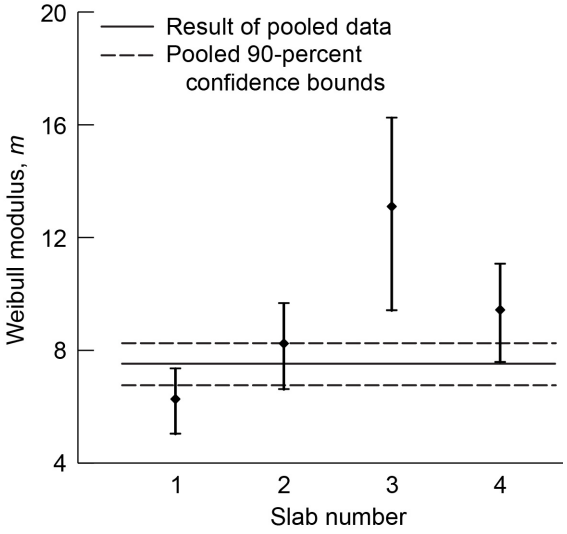

Figure 69.—Weibull modulus and 90-percent confidence bounds of individual slabs 1 to 4 for radial large tensile specimens from edge of slabs.

In Figure 70, the low characteristic strength of slab 1 is statistically significant. See Table 26 for a listing of the Weibull parameters and the 90-percent confidence bounds on the parameters.

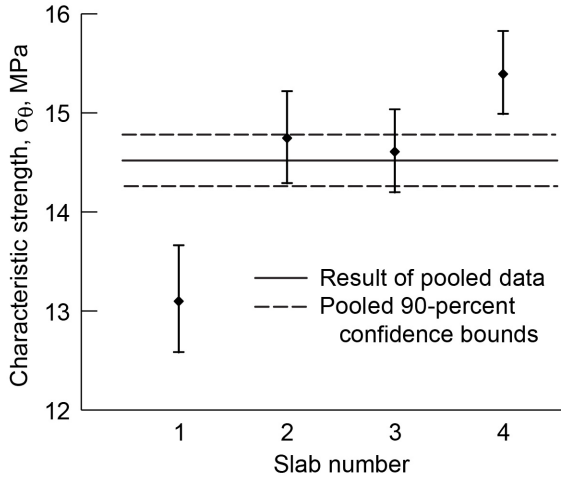

Figure 70.—Characteristic strength and 90-percent confidence bounds on individual slabs 1 to 4 for radial large tensile specimens from edge of slabs.

TABLE 26.—WEIBULL PARAMETERS AND 90-PERCENT CONFIDENCE BOUNDS ON INDIVIDUAL AND POOLED DATA FROM SLABS 1 TO 4 FOR RADIAL LARGE TENSILE SPECIMENS FROM EDGE OF SLABS

Slab	Number of specimens	Weibull modulus, *m*		Characteristic strength, σ_θ, MPa	
		MLE[a] biased	90-percent confidence	MLE biased[a]	90-percent confidence
1	48	6.26	5.04/7.35	13.10	12.58/13.66
2	48	8.23	6.62/9.66	14.75	14.29/15.22
3	24	13.09	9.40/16.24	14.61	14.20/15.04
4	48	9.42	7.58/11.06	15.40	14.99/15.83
Mean	42.00	9.25	----------	14.47	----------
Pooled	168	7.52	6.75/8.25	14.52	14.26/14.78

[a]Maximum-likelihood estimation.

In Figure 71, slab 1 has distinctly different behavior at lower probabilities of failure—possibly indicating bimodal Weibull behavior. See Table 27 for a listing of the Weibull parameters and the 90-percent confidence bounds on the parameters.

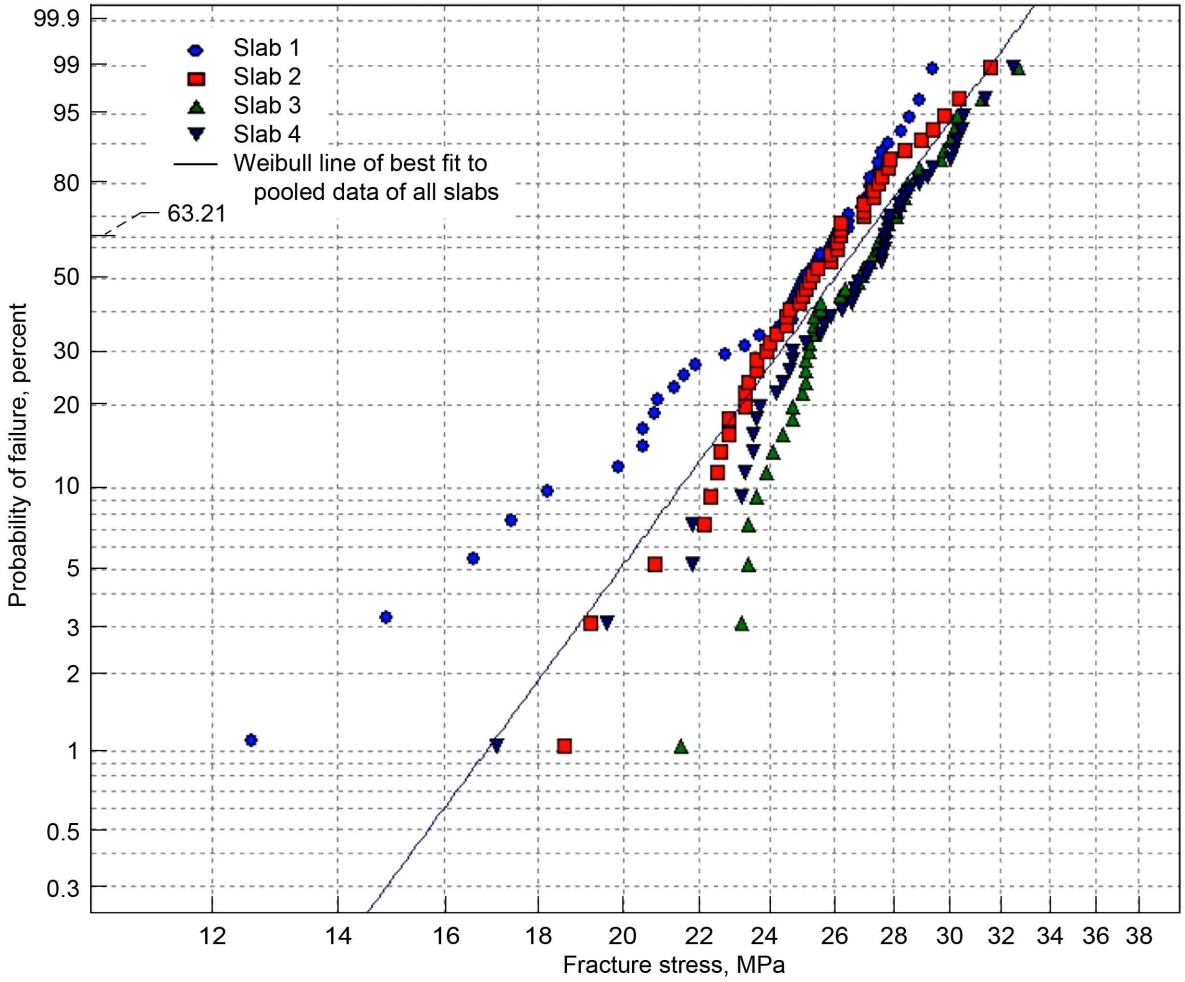

Figure 71.—Weibull plot of fracture stresses of individual slabs 1 to 4 for radial flexure specimens (with linear-elastic stress response) from edge of slabs.

In Figure 72, the Weibull modulus for slab 1 is somewhat lower than for the other slabs, but the variation between the slabs is actually quite consistent and can be largely explained by natural statistical variation. This is a little surprising given the visual appearance of the Weibull plot in Figure 71, but it must be kept in mind that the Weibull parameter estimates for slab 1 are a best fit to all the data and, therefore, represent an averaging of all the data for slab 1. See Table 27 for a listing of the Weibull parameters and the 90-percent confidence bounds on the parameters.

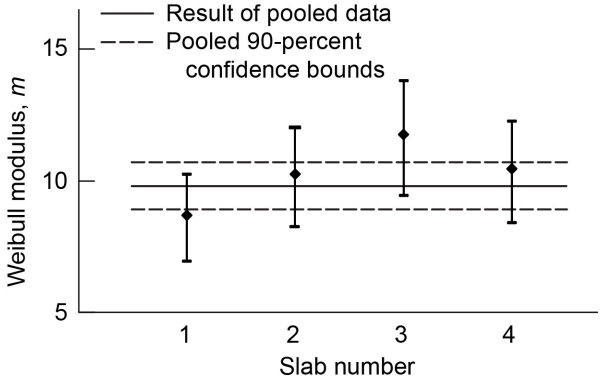

Figure 72.—Weibull modulus and 90-percent confidence bounds of individual slabs 1 to 4 for radial flexure specimens (with linear-elastic stress response) from edge of slabs.

In Figure 73, note the low characteristic strength of slab 1 versus slab 3, indicating that there is some slab-to-slab variation beyond what is expected from natural statistical variation. See Table 27 for a listing of the Weibull parameters and the 90-percent confidence bounds on the parameters.

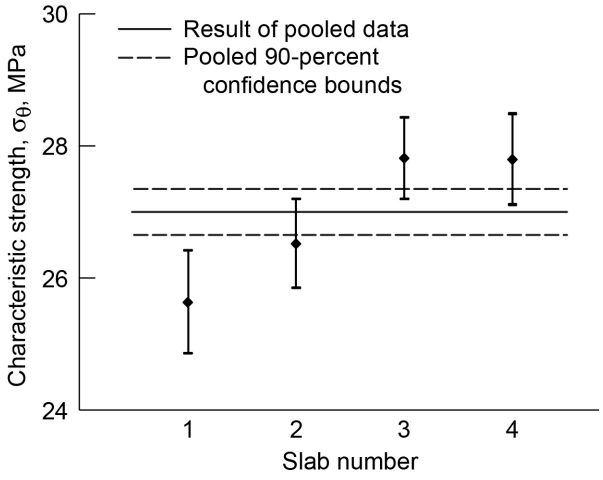

Figure 73.—Characteristic strength and 90-percent confidence bounds of individual slabs 1 to 4 for radial flexure specimens (with linear-elastic stress response) from edge of slabs.

TABLE 27.—WEIBULL PARAMETERS AND 90-PERCENT CONFIDENCE BOUNDS ON INDIVIDUAL AND POOLED DATA FROM SLABS 1 TO 4 FOR RADIAL FLEXURE SPECIMENS (WITH LINEAR-ELASTICSTRESS RESPONSE) FROM EDGE OF SLABS

Slab	Number of specimens	Weibull modulus, m		Characteristic strength, σ_θ, MPa	
		MLE biased[a]	90-percent confidence	MLE biased[a]	90-percent confidence
1	46	8.68	6.94/10.23	25.62	24.85/26.41
2	48	10.24	8.24/12.02	26.51	25.85/27.19
3	48	11.74	9.44/13.77	27.81	27.20/28.43
4	48	10.44	8.40/12.25	27.79	27.11/28.49
Mean	47.50	10.28	----------	26.93	----------
Pooled	190	9.78	8.84/10.66	27.00	26.66/27.35

[a]Maximum-likelihood estimation.

In Figure 74, slab 1 has distinctly different behavior at lower probabilities of failure that possibly indicates bimodal Weibull behavior. See Table 28 for a listing of the Weibull parameters and the 90-percent confidence bounds on the parameters.

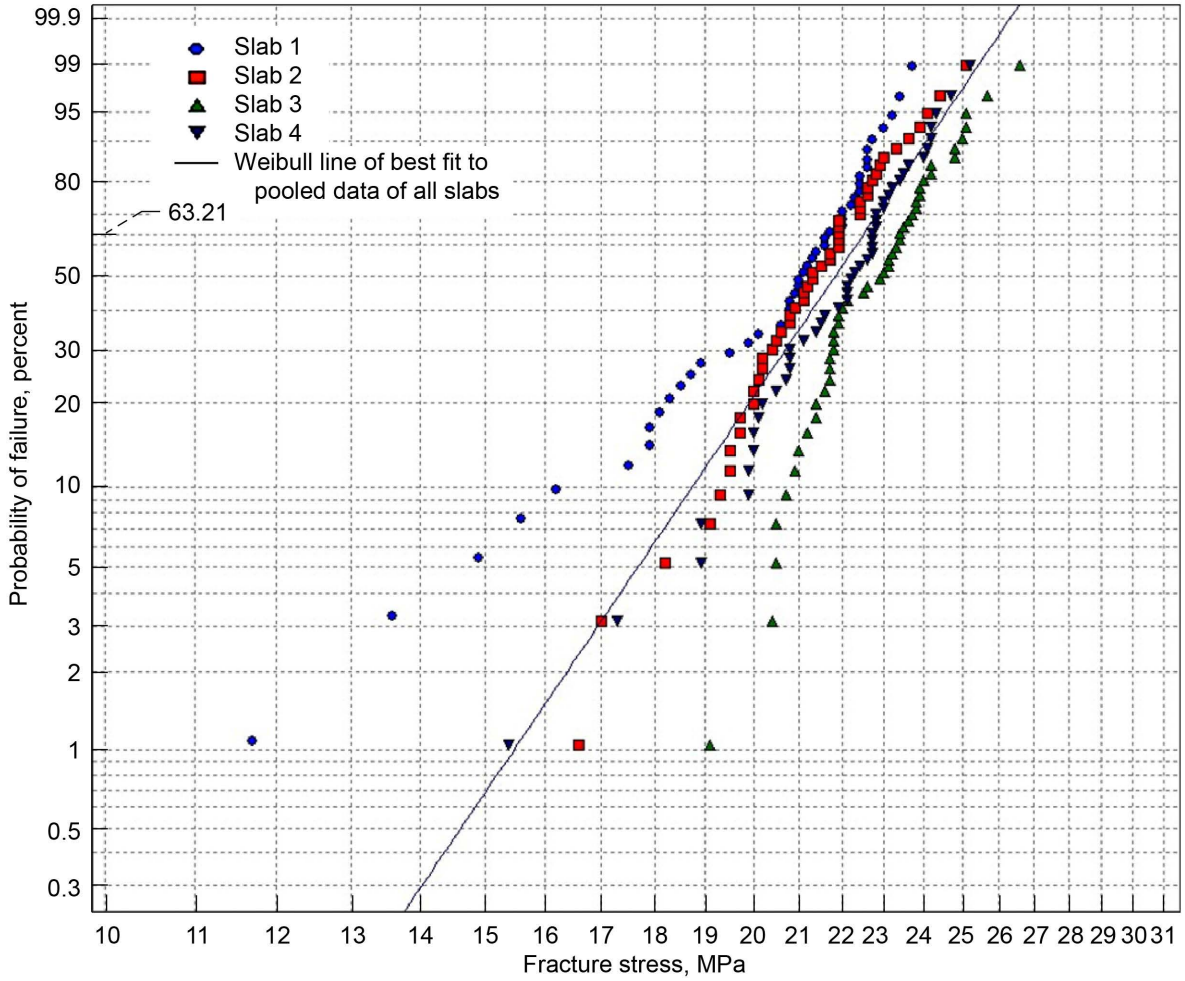

Figure 74.—Weibull plot of fracture stresses of individual slabs 1 to 4 for radial flexure specimens (with nonlinear-elastic stress response) from edge of slabs.

In Figure 75, the Weibull modulus is lower for slab 1 than for the other slabs but not dramatically lower. In this case, there appears to be slab-to-slab variation significantly beyond what is expected from natural statistical variation. The fact that the Weibull modulus for slab 1 is not dramatically lower is a little surprising given the visual appearance of the Weibull plot in Figure 74, but it must be kept in mind that the Weibull parameter estimates for slab 1 are a best fit to all the data and, therefore, represent an averaging of all the data for slab 1. See Table 28 for a listing of the Weibull parameters and the 90-percent confidence bounds on the parameters.

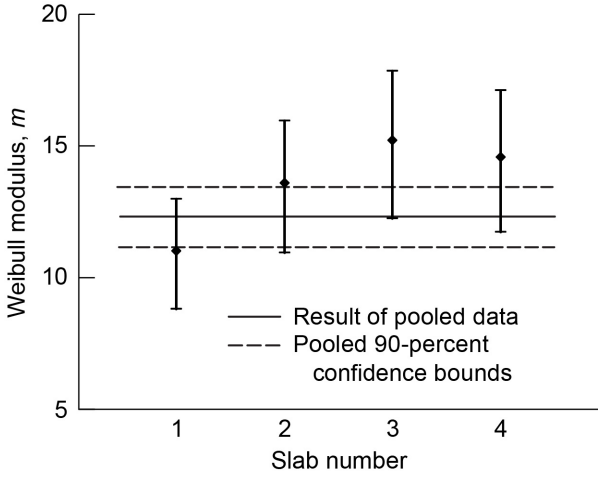

Figure 75.—Weibull modulus and 90-percent confidence bounds of individual slabs 1 to 4 for radial flexure specimens (with nonlinear-elastic stress response) from edge of slabs.

In Figure 76, slab 1 has a low characteristic strength in comparison to slab 3, indicating that there is some slab-to-slab variation beyond what is expected from natural statistical variation. See Table 28 for a listing of the Weibull parameters and the 90-percent confidence bounds on the parameters.

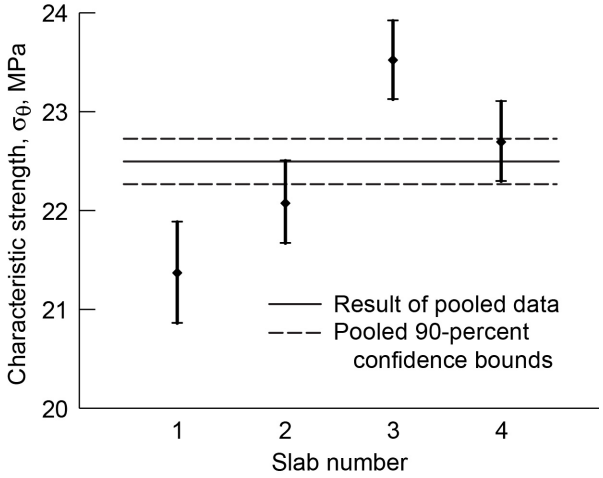

Figure 76.—Characteristic strength and 90-percent confidence bounds of individual slabs 1 to 4 for radial flexure specimens (with nonlinear-elastic stress response) from edge of slabs.

TABLE 28.—WEIBULL PARAMETERS AND 90-PERCENT CONFIDENCE BOUNDS ON INDIVIDUAL AND POOLED DATA FROM SLABS 1 TO 4 FOR RADIAL FLEXURE SPECIMENS (WITH NONLINEAR-ELASTIC STRESS RESPONSE) FROM EDGE OF SLABS

Slab	Number of specimens	Weibull number, *m*		Characteristic strength, σ_θ, MPa	
		MLE biased[a]	90-percent confidence	MLE biased[a]	90-percent confidence
1	46	11.01	8.80/12.97	21.36	20.85/21.88
2	48	13.59	10.93/15.95	22.07	21.66/22.50
3	48	15.21	12.23/17.85	23.52	23.12/23.92
4	48	14.57	11.72/17.10	22.69	22.29/23.10
Mean	47.50	13.60	----------	22.41	----------
Pooled	190	12.31	11.13/13.43	22.49	22.26/22.72

[a]Maximum-likelihood estimation.

Appendix B.—Pooled Data for Slabs 1 to 4 Comparing Strength Versus Specimen Location and Orientation Within Slabs of the Graphite Log for Small Tensile, Large Tensile, and Flexure Specimens

In Figure 77, the Weibull best-fit lines were determined by assuming that all the data had the same Weibull modulus and that the Weibull size effect was operating (by accounting for the geometry and loading of the specimens). A linear stress-strain response was assumed in determining the fracture stresses (from Price (1976)), and a linear-elastic finite element model of the four-point cylindrical flexure specimen was used in conjunction with WeibPar to determine the best-fit Weibull modulus and scale parameter (m = 10.77 and σ_o = 32.85 MPa-mm$^{3/m}$). See Table 29 for a listing of the Weibull parameters and the 90-percent confidence bounds on the parameters.

The WeibPar/CARES analysis shows that the size effect for the experimental fracture stress data for the two tensile specimen geometries is much smaller than what is expected from the Weibull stress-volume integration, whereas a large size effect exists between the tensile and flexure specimens that is adequately predicted with Weibull stress-volume integration.

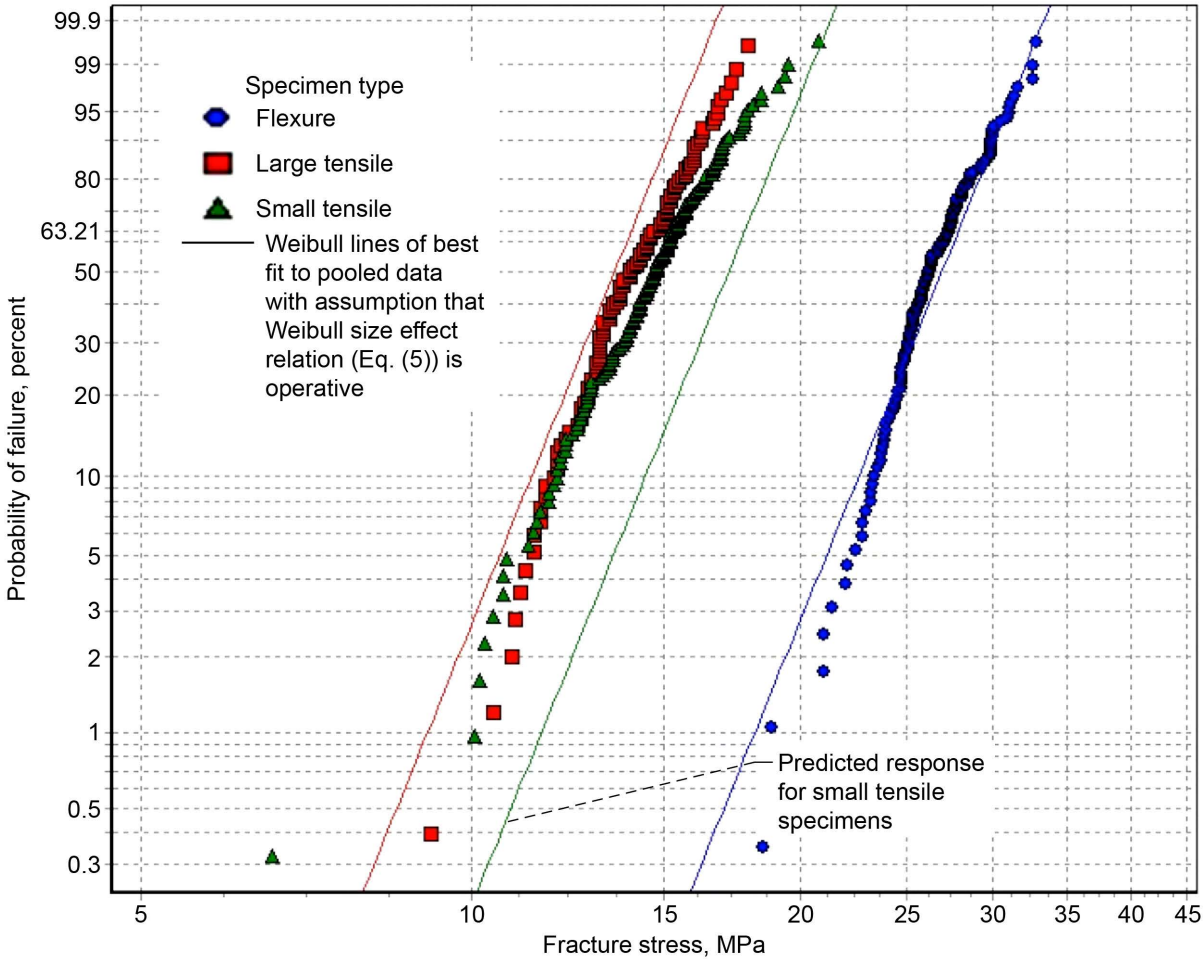

Figure 77.—Weibull plot of fracture stresses of pooled data from slabs 1 to 4 for axial small tensile, large tensile, and flexure specimens (with linear-elastic stresses) from center of slabs for a linear stress-strain response.

In Figure 78, the Weibull best-fit lines were determined by assuming that all the data had the same Weibull modulus and that the Weibull size effect was operating (by accounting for the geometry and loading of the specimens). A nonlinear stress-strain response was assumed in determining the fracture stresses (from Price (1976)), and a linear-elastic finite element model of a four-point cylindrical flexure specimen was used in conjunction with WeibPar to determine the best-fit Weibull modulus and scale parameter (m = 13.93 and σ_o = 27.57 MPa-mm$^{3/m}$). The predictions for the strength response from the WeibPar/CARES analysis do not account for the changing effective volume with load that would be expected from a nonlinear stress-strain response. See Table 29 for a listing of the Weibull parameters and the 90-percent confidence bounds on the parameters.

The WeibPar/CARES analysis shows that the experimental fracture stress data for the two tensile specimen geometries is much smaller than what is expected from the Weibull stress-volume integration, whereas a large size effect exists between the tensile and flexure specimens that is slightly overpredicted with the Weibull stress-volume integration.

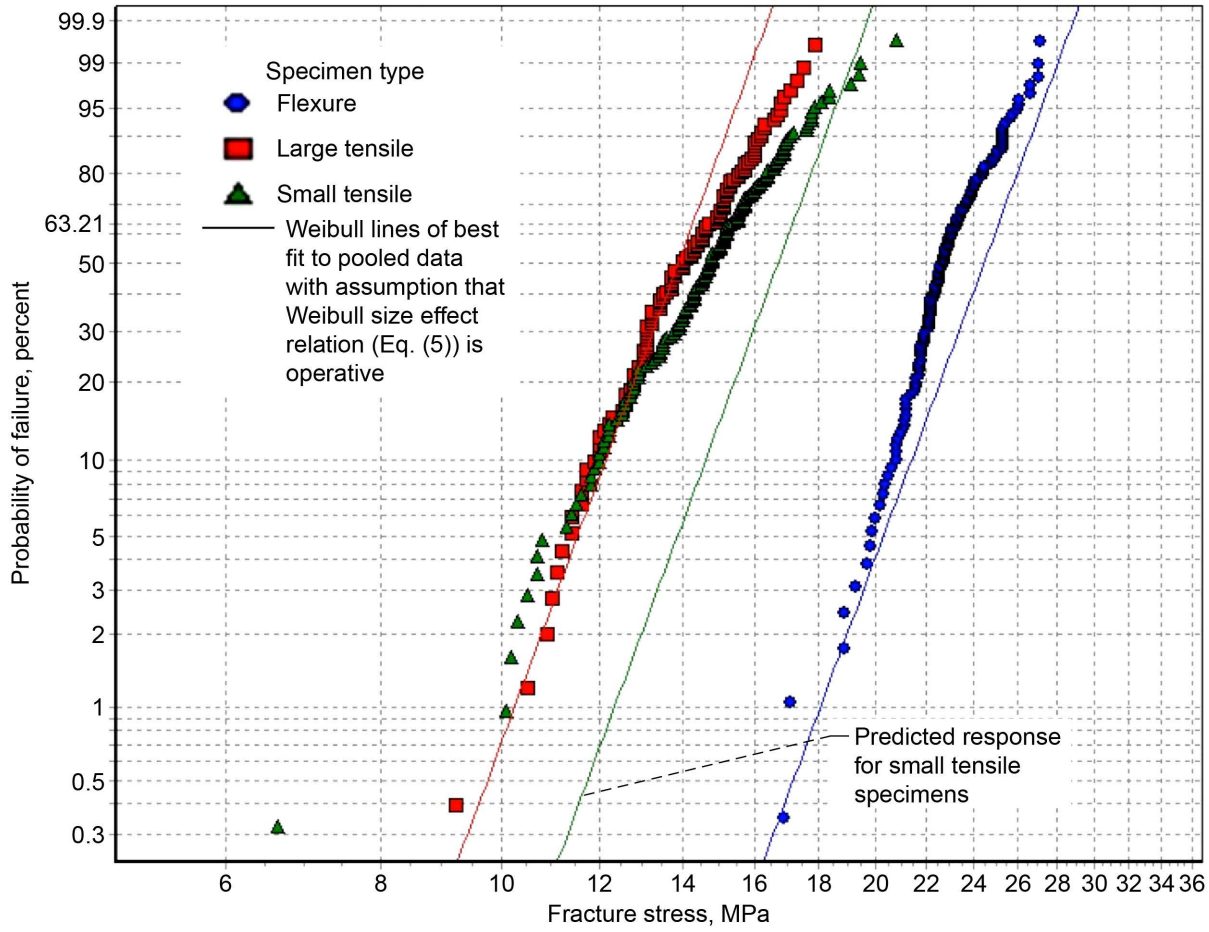

Figure 78.—Weibull plot of fracture stresses of slabs 1 to 4 for pooled data from axial small tensile, large tensile, and flexure specimens (with nonlinear-elastic stresses) from center of slabs for a nonlinear stress-strain response. See Table 29 for a listing of the Weibull parameters and the 90-percent confidence bounds on the parameters.

In Figure 79, the Weibull modulus for the nonlinear correction of stresses is higher for the flexure specimens than for the tensile specimens. It has not been established how much of this difference could be attributed to the nonlinear stress-strain response of H–451. An alternative explanation is that a different failure mode with a separate set of Weibull parameters was operating at the surface when the material was loaded under flexure. There is some difference indicated between the large and small tensile specimen geometries, but examination of Figures 77 and 78 shows that the fracture data of the two geometries are quite similar.

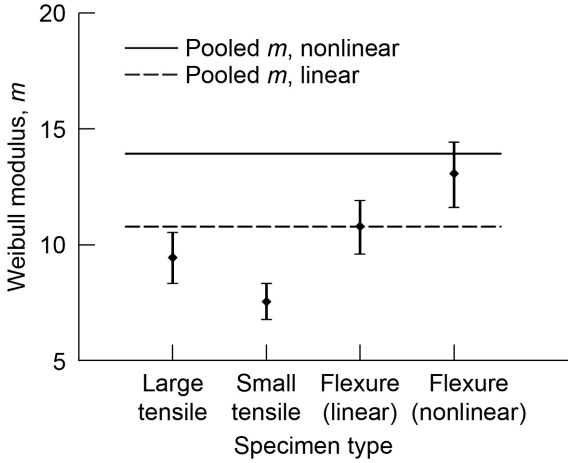

Figure 79.—Weibull modulus and 90-percent confidence bounds of pooled slabs 1 to 4 for axial small tensile, large tensile, and flexure specimens from center of slabs. See Table 29 for a listing of Weibull parameters and 90-percent confidence bounds on parameters.

The higher characteristic strength of the flexure specimens in Figure 80 cannot be explained from natural statistical variation, and the size effect must be explained by other means such as with Weibull stress-volume integration. On the other hand, the size effect between the small and large tensile specimens is less than what is expected with the Weibull distribution (see Figs. 77 and 78). When the fracture stresses were computed from Price (1976), the nonlinear stress-strain response reduced the characteristic strength of the flexure specimen. Table 29 reproduces the data from Tables 13 to 16 and is shown here for convenience.

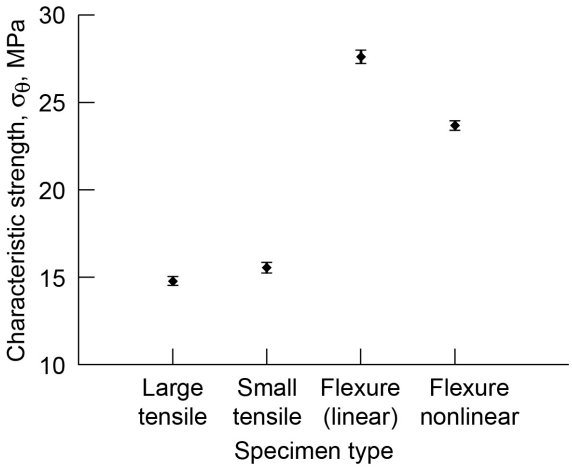

Figure 80.—Characteristic strength and 90-percent confidence bounds of pooled slabs 1 to 4 for axial small tensile, large tensile, and flexure specimens from center of slabs. See Table 29 for a listing of Weibull parameters and 90-percent confidence bounds on parameters.

In Table 29 (and 13 to 16), slab 1 seems to be consistently stronger and slab 3 is consistently weaker. Slab 2 consistently shows a higher Weibull modulus than for the other slabs. This may have contributed to the somewhat nonlinear appearance of the plots. The average (mean) Weibull modulus for the four slabs is always higher than the Weibull modulus for the pooled data. This is largely because the slab-to-slab variation in the average strength (or alternatively, the characteristic strength in Table 29) of the individual slabs is beyond what is expected from natural statistical variation. Hence, pooling (combining) the data from the four slabs, which incorporated the additional slab-to-slab strength variation, increased the apparent scatter in strength of the pooled data. This resulted in a lower estimated Weibull modulus for the pooled data set.

TABLE 29.—WEIBULL PARAMETERS AND 90-CONFIDENCE BOUNDS ON INDIVIDUAL AND POOLED DATA OF SLABS 1 TO 4 FOR AXIAL SMALL TENSILE, LARGE TENSILE, AND FLEXURE SPECIMENS FROM CENTER OF SLABS

Specimen type	Slab	Number of specimens	Weibull modulus, *m*		Characteristic strength, σ_θ, MPa	
			MLE biased[a]	90-percent confidence	MLE biased[a]	90-percent confidence
Small tensile	1	40	7.64	5.99/9.09	16.87	16.26/17.51
	2	38	12.99	10.11/15.52	15.59	15.24/15.94
	3	38	9.39	7.31/11.22	14.41	13.97/14.87
	4	40	8.36	6.55/9.95	14.92	14.42/15.44
	Mean	39.00	9.60	----------	15.45	----------
	Pooled	156	7.58	6.78/8.33	15.56	15.27/15.85
Large tensile	1	31	11.48	8.64/13.93	15.98	15.53/16.45
	2	32	18.14	13.74/21.96	15.12	14.86/15.40
	3	31	12.17	9.15/14.77	13.74	13.38/14.12
	4	32	9.26	7.02/11.21	13.79	13.32/14.28
	Mean	31.50	12.76	----------	14.66	----------
	Pooled	126	9.47	8.34/10.52	14.80	14.56/15.05
Flexure, linear[c]	1	25	10.22	7.39/12.63	28.77	27.74/29.83
	2	40	16.12	12.64/19.19	27.42	26.94/27.91
	3	40	11.51	9.02/13.70	26.93	26.27/27.60
	4	39	9.27	7.24/11.05	27.60	26.75/28.47
	Mean	36	11.78	----------	27.68	----------
	Pooled	144	10.79	9.60/11.91	27.63	27.25/28.00
Flexure, nonlinear[d]	1	25	12.68	9.16/15.67	24.55	23.84/25.28
	2	40	21.15	16.59/25.18	23.11	22.80/23.43
	3	40	13.98	10.97/16.65	23.50	23.02/23.98
	4	39	11.41	8.91/13.60	23.74	23.15/24.35
	Mean	36.00	14.81	----------	23.73	----------
	Pooled	144	13.07	11.62/14.42	23.69	23.43/23.96
Pooled, linear[c]	All data	570	10.77	(b)	-------	----------
Pooled, nonlinear[d]	All data	570	13.93	(b)	-------	----------

[a]Maximum-likelihood estimation.
[b]Not applicable for finite element model.
[c]Linear-elastic stress-strain response was assumed.
[d]Nonlinear-elastic stress-strain response was assumed.

In Figure 81, the Weibull best-fit lines were determined by assuming that all the data had the same value of Weibull modulus and that the Weibull size effect was operating (by accounting for the geometry and loading of the specimens). A linear stress-strain response was assumed in determining the fracture stresses (from Price (1976)), and a linear-elastic finite element model of the four-point cylindrical flexure specimen was used in conjunction with WeibPar to determine the best-fit Weibull modulus and scale parameter (m = 12.02 and σ_o = 36.06 MPa-mm$^{3/m}$. See Table 30 for a listing of Weibull parameters and 90-percent confidence bounds on parameters.

The WeibPar/CARES analysis shows that the size effect for the experimental fracture stress data for the two tensile specimen geometries is much smaller than what is expected from the Weibull stress-volume integration and that a large size effect exists between the tensile and flexure specimens that is adequately predicted with Weibull stress-volume integration.

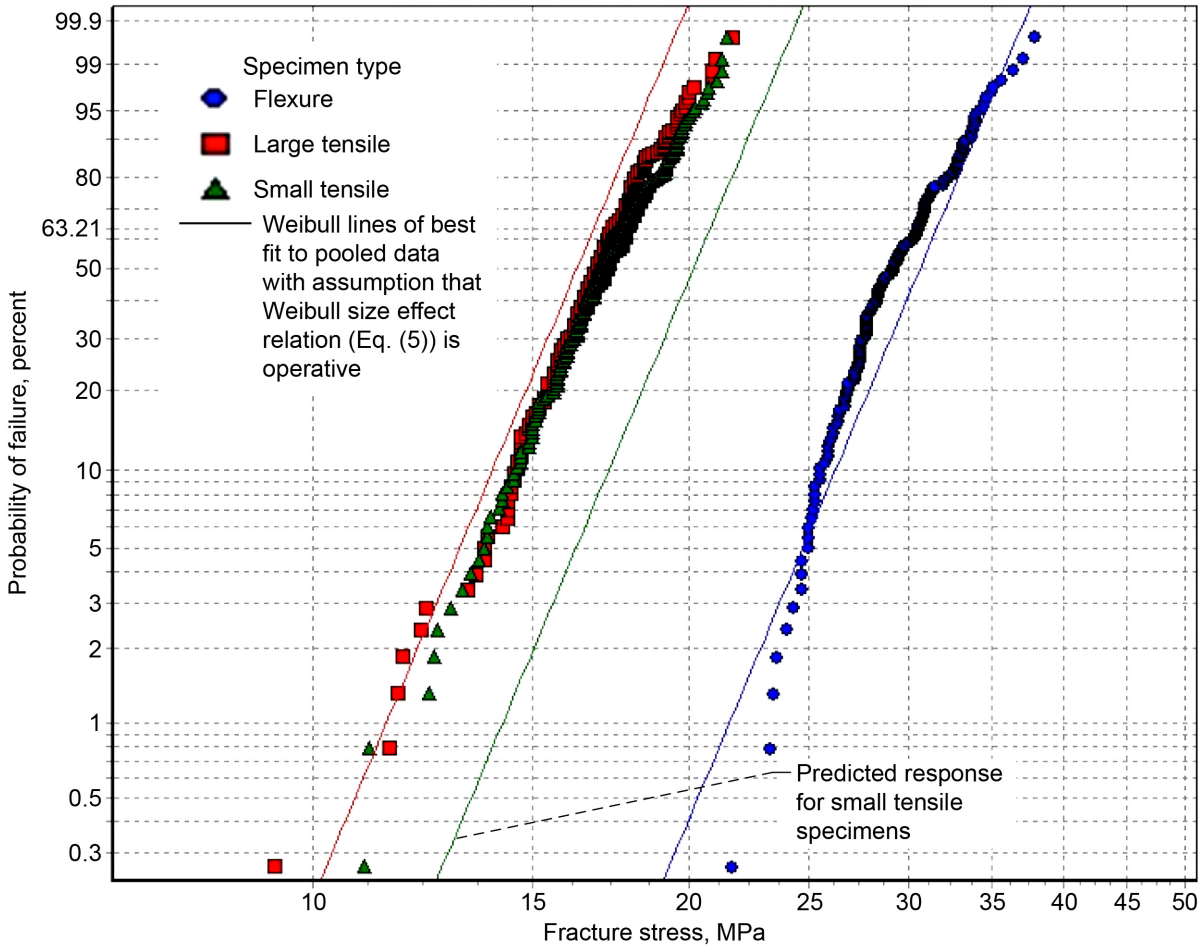

Figure 81.—Weibull plot of fracture stresses of pooled data from slabs 1 to 4 for axial small tensile, large tensile, and flexure specimens (with linear-elastic stresses) from edge of slabs. See Table 30 for a listing of Weibull parameters and 90-percent confidence bounds on parameters.

In Figure 82, the Weibull best-fit lines were determined by assuming that all the data had the same value of Weibull modulus and that the Weibull size effect was operating (by accounting for the geometry and loading of the specimens). A nonlinear stress-strain response was assumed in determining the fracture stresses (from Price (1976)), and a linear-elastic finite element model of the four-point cylindrical flexure specimen was used in conjunction with WeibPar to determine the best-fit Weibull modulus and scale parameter (m = 15.79 and σ_o = 30.50 MPa-mm$^{3/m}$). The predictions for the strength response from the WeibPar/CARES analysis do not account for changing effective volume with load that would be expected from a nonlinear stress-strain response. See Table 30 for a listing of Weibull parameters and 90-percent confidence bounds on parameters.

The WeibPar/CARES analysis shows that the experimental fracture stress data for the two tensile specimen geometries is much smaller than what is expected from the Weibull stress-volume integration and that a large size effect exists between the tensile and flexure specimens that is slightly overpredicted with Weibull stress-volume integration.

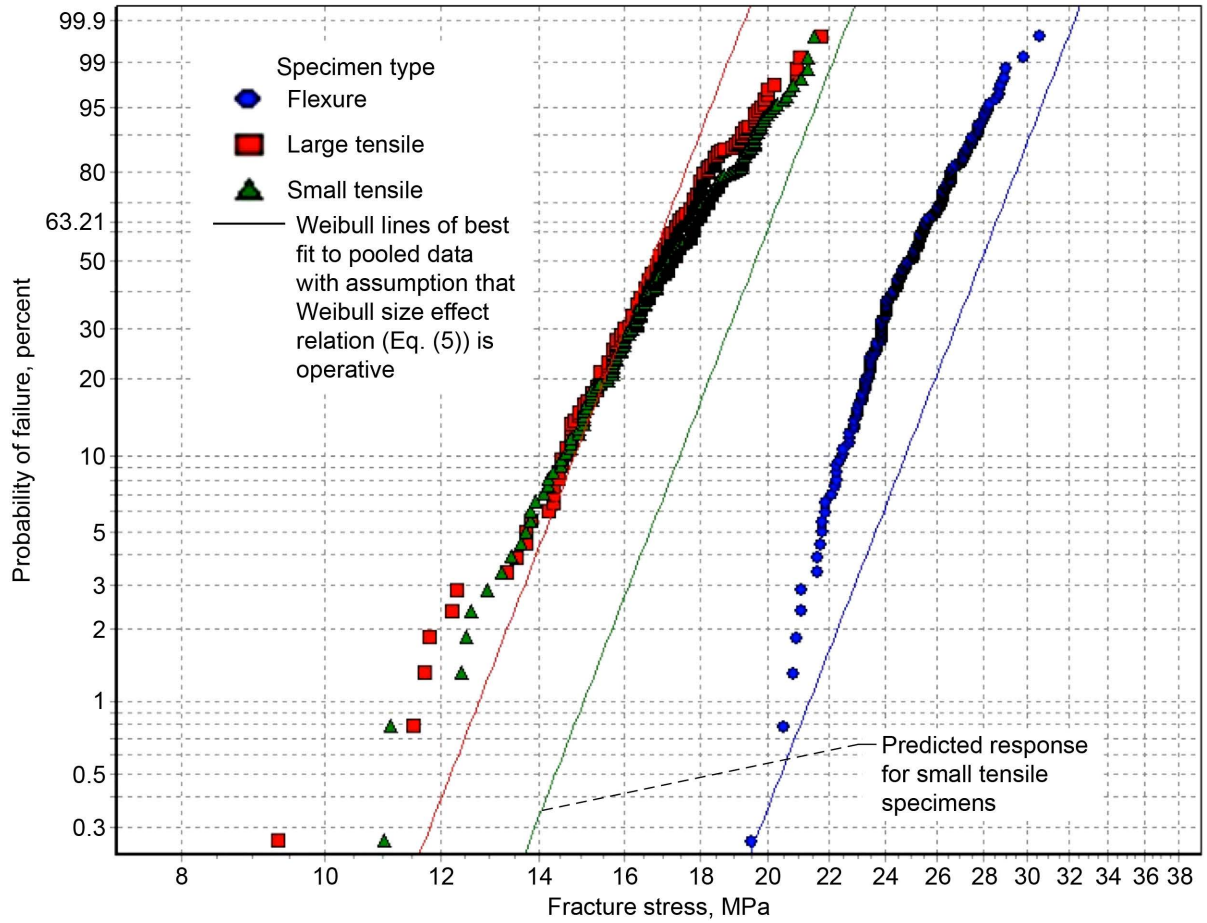

Figure 82.—Weibull plot of fracture stresses of pooled data from slabs 1 to 4 for axial small tensile, large tensile, and flexure specimens (with nonlinear-elastic stresses) from edge of slabs.

In Figure 83, the Weibull modulus for the flexure specimens with nonlinear-elastic stresses is higher than for the tensile specimens. It has not been established how much of this difference could be attributed to the nonlinear stress-strain response of H–451. The Weibull modulus for the small tensile, large tensile, and flexure specimens assuming a linear-elastic stress response are quite similar. See Table 30 for a listing of Weibull parameters and 90-percent confidence bounds on parameters.

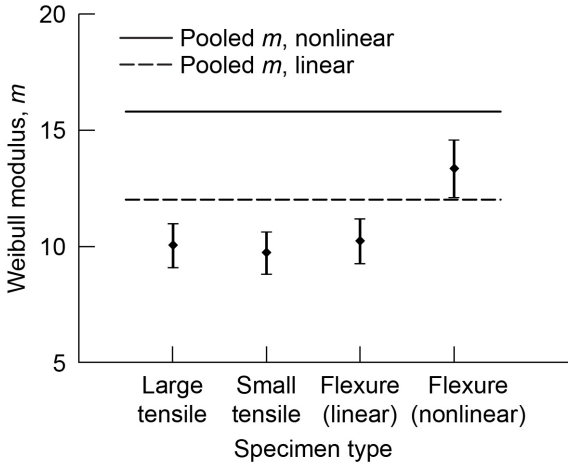

Figure 83.—Weibull modulus and 90-percent confidence bounds of pooled slabs 1 to 4 for axial small tensile, large tensile, and flexure specimens from edge of slabs. See Table 30 for a listing of Weibull parameters and 90-percent confidence bounds on parameters.

The higher characteristic strength of the flexure specimens in Figure 84 cannot be explained from natural statistical variation, and the size effect must be explained by other means such as with the Weibull distribution. On the other hand, the size effect between the small and large tensile specimens is less than what is expected with the Weibull distribution (see Figs. 82 and 83). When the fracture stresses were computed from Price (1976), the nonlinear stress-strain response reduced the characteristic strength of the flexure specimen. Table 30 reproduces the data from Tables 17 to 20 and is shown here for convenience.

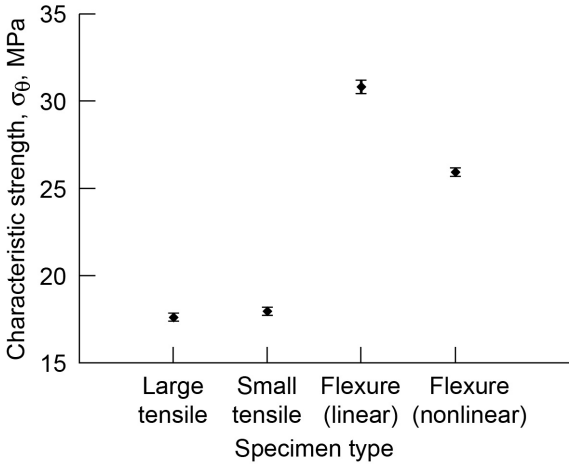

Figure 84.—Characteristic strength and 90-percent confidence bounds of pooled slabs 1 to 4 for axial small tensile, large tensile, and flexure specimens from edge of slabs. See Table 30 for a listing of Weibull parameters and 90-percent confidence bounds on parameters.

In Tables 30 and 17 to 20, slab 1 seems to be consistently weaker and slab 2 seems to be consistently stronger for large and small tensile specimens. Slabs 1 and 4 do not show as much difference in strength. The average (mean) Weibull modulus for the four slabs is always higher than the Weibull modulus for the pooled data. This is largely because the slab-to-slab variation in the average strength (or alternatively, the characteristic strength shown in Table 30) of the individual slabs is beyond what is expected from natural statistical variation. Hence, pooling (combining) the data from the four slabs, which incorporated the additional slab-to-slab strength variation, increased the apparent scatter in strength of the pooled data. This resulted in a lower estimated Weibull modulus for the pooled data set.

TABLE 30.—WEIBULL PARAMETERS AND 90-CONFIDENCE BOUNDS ON INDIVIDUAL AND POOLED DATA OF SLABS 1 TO 4 FOR AXIAL SMALL TENSILE, LARGE TENSILE, AND FLEXURE SPECIMENS FROM EDGE OF SLABS

Specimen type	Slab	Number of specimens	Weibull modulus, *m*		Characteristic strength, σ_θ, MPa	
			MLE biased[a]	90-percent confidence	MLE biased[a]	90-percent confidence
Small tensile	1	48	9.77	7.86/11.47	17.30	16.85/17.76
	2	46	11.93	9.54/14.05	18.96	18.54/19.38
	3	48	9.95	8.00/11.67	17.85	17.39/18.32
	4	48	9.69	7.80/11.38	17.71	17.25/18.19
	Mean	47.50	10.34	----------	17.96	----------
	Pooled	190	9.73	8.80/10.62	17.98	17.75/18.22
Large tensile	1	47	9.48	7.60/11.14	16.75	16.30/17.22
	2	48	10.89	8.76/12.78	18.37	17.94/18.82
	3	48	10.79	8.68/12.66	17.79	17.37/18.23
	4	48	11.50	9.25/13.50	17.43	17.04/17.82
	Mean	47.75	10.67	----------	17.59	----------
	Pooled	191	10.05	9.09/10.96	17.63	17.41/17.85
Flexure, linear[b]	1	48	12.68	10.20/14.88	29.65	29.05/30.27
	2	48	10.34	8.32/12.14	31.41	30.64/32.21
	3	48	10.20	8.21/11.97	31.79	30.99/32.61
	4	48	10.82	8.71/12.70	30.20	29.49/30.94
	Mean	48	11.01	----------	30.76	----------
	Pooled	192	10.24	9.27/11.17	30.82	30.44/31.20
Flexure, nonlinear[c]	1	48	16.07	12.93/18.86	25.39	24.99/25.81
	2	48	14.30	11.51/16.79	25.70	25.25/26.17
	3	48	13.21	10.63/15.51	26.81	26.29/27.34
	4	48	13.85	11.14/16.25	25.72	25.24/26.20
	Mean	48.00	14.36	----------	25.91	----------
	Pooled	192	13.36	12.09/14.57	25.94	25.70/26.19
Pooled, linear[b]	All data	765	12.02	N/A for FE model	-------	----------
Pooled, nonlinear[c]	All data	765	15.79	N/A for FE model	-------	----------

[a]Maximum-likelihood estimation.
[b]Linear-elastic stress-strain response was assumed.
[c]Nonlinear-elastic stress-strain response was assumed.

In Figure 85, the Weibull best-fit lines were determined by assuming that all the data had the same value of Weibull modulus and that the Weibull size effect was operating (by accounting for the geometry and loading of the specimens). A linear stress-strain response was assumed in determining the fracture stresses (from Price (1976)), and a linear-elastic finite element model of the four-point cylindrical flexure specimen was used in conjunction with WeibPar to determine the best-fit Weibull modulus and scale parameter (m = 9.01 and σ_o = 33.40 MPa-mm$^{3/m}$. See Table 31 for a listing of Weibull parameters and 90-percent confidence bounds on parameters.

The WeibPar/CARES analysis shows that the size effect for the experimental fracture stress data for the two tensile specimen geometries is much smaller than what is expected from the Weibull stress-volume integration and that a large size effect exists between the tensile and flexure specimens that is adequately predicted with Weibull stress-volume integration.

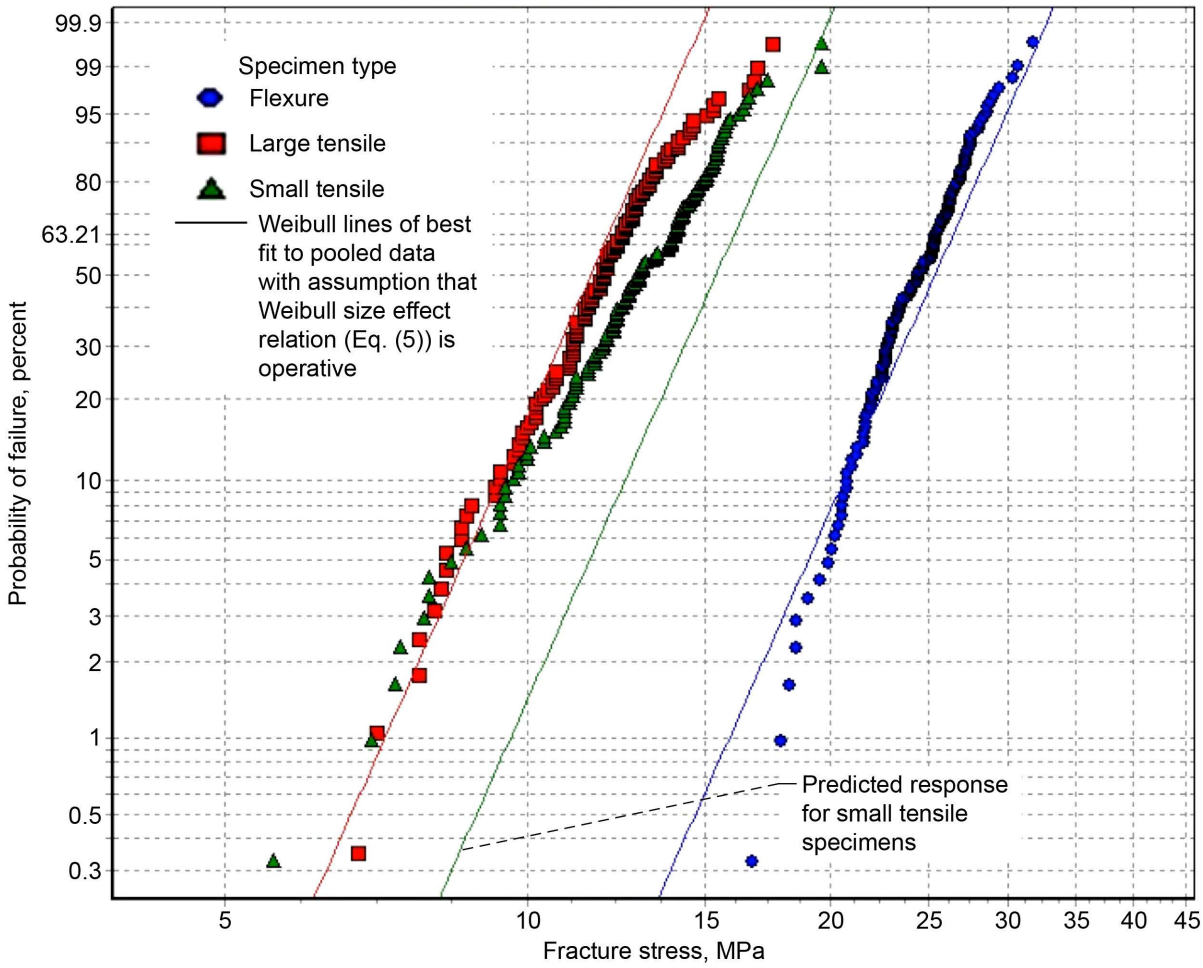

Figure 85.—Weibull plot of fracture stresses of pooled data from slabs 1 to 4 for radial small tensile, large tensile, and flexure specimens (with linear-elastic stress response) from center of slabs. See Table 31 for a listing of Weibull parameters and 90-percent confidence bounds on parameters.

In Figure 86, the Weibull best-fit lines were determined by assuming that all the data had the same value of Weibull modulus and that the Weibull size effect was operating (by accounting for the geometry and loading of the specimens). A nonlinear stress-strain response was assumed in determining the fracture stresses (from Price (1976)), and a linear-elastic finite element model of the four-point cylindrical flexure specimen was used in conjunction with WeibPar to determine the best-fit Weibull modulus and scale parameter (m = 10.06 and σ_o = 30.06 MPa-mm$^{3/m}$). The predictions for the strength response from the WeibPar/CARES analysis do not account for changing effective volume with load that would be expected from a nonlinear stress-strain response. See Table 31 for a listing of Weibull parameters and 90-percent confidence bounds on parameters.

The WeibPar/CARES analysis shows that the experimental fracture stress data for the two tensile specimen geometries is much smaller than what is expected from the Weibull stress-volume integration and that a large size effect exists between the tensile and flexure specimens that is slightly overpredicted with Weibull stress-volume integration.

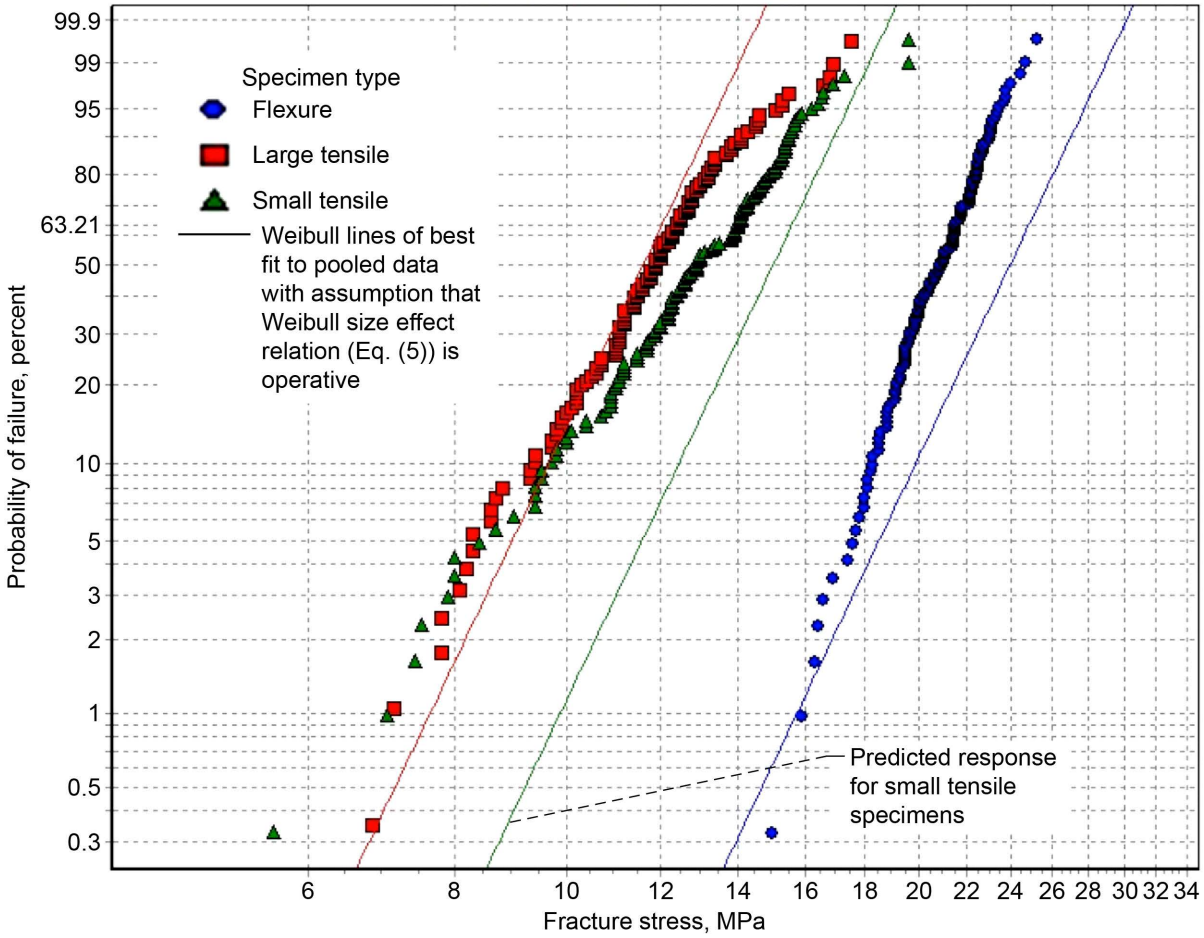

Figure 86.—Weibull plot of fracture stresses of pooled data from slabs 1 to 4 for radial small tensile, large tensile, and flexure specimens (with nonlinear-elastic stress-strain response) from center of slabs. See Table 31 for a listing of Weibull parameters and 90-percent confidence bounds on parameters.

In Figure 87, the Weibull modulus for the flexure specimens is significantly higher than for the tensile specimens—beyond what is expected from natural statistical variation. It has not been established how much of this difference could be attributed to the nonlinear stress-strain response of H–451. An alternative explanation is that a different failure mode with a separate set of Weibull parameters was operating at the surface when the material was loaded under flexure. The Weibull moduli for the two different sizes of tensile specimens are quite similar. See Table 31 for a listing of Weibull parameters and 90-percent confidence bounds on parameters.

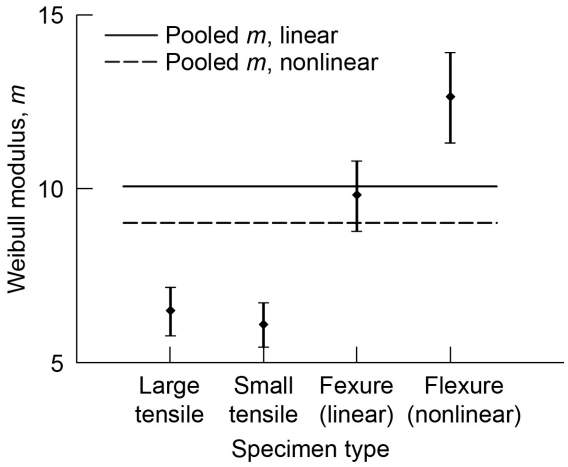

Figure 87.—Weibull modulus and 90-percent confidence bounds of pooled slabs 1 to 4 for radial small tensile, large tensile, and flexure specimens from center of slabs. See Table 31 for a listing of Weibull parameters and 90-percent confidence bounds on parameters.

The higher characteristic strength of the flexure specimens in Figure 88 cannot be explained from natural statistical variation, and the size effect must be explained by other means such as with the Weibull distribution. On the other hand, the size effect between the small and large tensile specimens is less than what is expected with the Weibull distribution (see Figs. 86 and 87). When the fracture stresses were computed from Price (1976), the nonlinear stress-strain response reduced the characteristic strength of the flexure specimen. Table 31 reproduces the data from Tables 21 to 24 and is shown here for convenience.

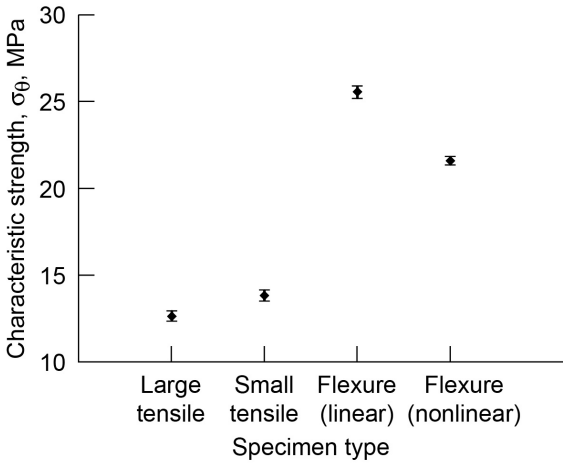

Figure 88.—Characteristic strength and 90-percent confidence bounds of pooled slabs 1 to 4 for radial small tensile, large tensile, and flexure specimens from center of slabs. See Table 31 for a listing of Weibull parameters and 90-percent confidence bounds on parameters. Linear indicates that linear-elastic stress-strain response was assumed, and nonlinear indicates that nonlinear-elastic stress-strain response was assumed.

In Tables 31 and 21 to 24, slab 1 is consistently weaker than slab 4 and strength generally increases with slab number. Slab 3 tends to have a higher Weibull modulus than the other slabs. The average (mean) Weibull moduli for the four slabs are always higher than the Weibull moduli for the pooled data. This is largely because the slab-to-slab variation in the average strength (or alternatively, the characteristic strength shown in Table 31) of the individual slabs is beyond what is expected from natural statistical variation. Hence, pooling (combining) the data from the four slabs, which incorporated the additional slab-to-slab strength variation, increased the apparent scatter in strength of the pooled data. This resulted in a lower estimated Weibull modulus for the pooled data set.

TABLE 31.—WEIBULL PARAMETERS AND 90-PERCENT CONFIDENCE BOUNDS ON INDIVIDUAL AND POOLED DATA FROM SLABS 1 TO 4 FOR RADIAL SMALL TENSILE, LARGE TENSILE, AND FLEXURE SPECIMENS FROM CENTER OF SLABS

Specimen type	Slab	Number of specimens	Weibull modulus, m		Characteristic strength, σ_θ, MPa	
			MLE biased[a]	90-percent confidence	MLE biased[a]	90-percent confidence
Small tensile	1	38	5.93	4.61/7.08	13.14	12.51/13.81
	2	38	5.52	4.29/6.59	13.40	12.71/14.13
	3	37	8.63	6.69/10.34	13.71	13.24/14.18
	4	40	6.58	5.16/7.84	14.92	14.29/15.58
	Mean	38.25	6.67	----------	13.79	----------
	Pooled	153	6.11	5.46/6.72	13.85	13.53/14.17
Large tensile	1	36	7.44	5.75/8.92	11.44	10.98/11.91
	2	35	10.81	8.31/13.00	12.32	11.97/12.67
	3	36	10.45	8.07/12.53	12.04	11.69/12.39
	4	36	7.18	5.54/8.61	14.26	13.68/14.88
	Mean	35.75	8.97	----------	12.52	----------
	Pooled	143	6.50	5.78/7.17	12.65	12.37/12.94
Flexure, linear[b]	1	38	9.93	7.72/11.86	24.87	24.15/25.62
	2	38	9.77	7.60/11.67	24.60	23.88/25.35
	3	40	12.55	9.84/14.94	25.55	24.98/26.14
	4	40	10.50	8.24/12.50	26.91	26.19/27.65
	Mean	39	10.69	----------	25.48	----------
	Pooled	156	9.82	8.78/10.79	25.56	25.20/25.93
Flexure, nonlinear[c]	1	38	12.65	9.85/15.12	21.11	20.63/21.61
	2	38	12.57	9.78/15.02	20.73	20.25/21.22
	3	40	15.76	12.36/18.76	21.81	21.42/22.21
	4	40	14.14	11.09/16.83	22.44	21.99/22.90
	Mean	39.00	13.78	----------	21.52	----------
	Pooled	156	12.65	11.32/13.91	21.59	21.35/21.83
Pooled, linear[b]	All data	608	9.01	N/A for FE model	-------	----------
Pooled, nonlinear[c]	All data	608	10.06	N/A for FE model	-------	----------

[a]Maximum-likelihood estimation.
[b]Linear-elastic stress-strain response was assumed.
[c]Nonlinear-elastic stress-strain response was assumed.

In Figure 89, the Weibull best-fit lines were determined by assuming that all the data had the same value of Weibull modulus and that the Weibull size effect was operating (by accounting for the geometry and loading of the specimens). A linear stress-strain response was assumed in determining the fracture stresses (from Price (1976)), and a linear-elastic finite element model of the four-point cylindrical flexure specimen was used in conjunction with WeibPar to determine the best-fit Weibull modulus and scale parameter (m = 10.65 and σ_o = 32.83 MPa-mm$^{3/m}$. See Table 32 for a listing of Weibull parameters and 90-percent confidence bounds on parameters.

The knee in the data at smaller probability of failure could be indicative of bimodal Weibull behavior. However, the fact that the knee appears at approximately the same probability of failure (at approximately 5 to 10 percent) is not consistent with predictions from Weibull stress-volume integration for competing failure modes. If it were consistent, then the flaw population with the smaller Weibull modulus would dominate at larger effective volumes (in the tensile specimens) and the flaw population with the higher Weibull modulus would dominate at smaller effective volumes (the flexure specimen). Instead, what is seen is that there is no apparent shifting of the knee in the data to lower or higher probabilities of failure with changing effective volume. This is contrary to the assumption of concurrent flaw populations as competing failure modes acting in accordance with the prediction from Weibull stress-volume integration. This may mean that some other systematic variation, independent of geometry and loading, that affects the strength at lower probabilities of failure is present.

The WeibPar/CARES analysis shows that the size effect for the experimental fracture stress data for the two tensile specimen geometries is much smaller than what is expected from the Weibull stress-volume integration and that a large size effect exists between the tensile and flexure specimens that is adequately predicted with Weibull stress-volume integration.

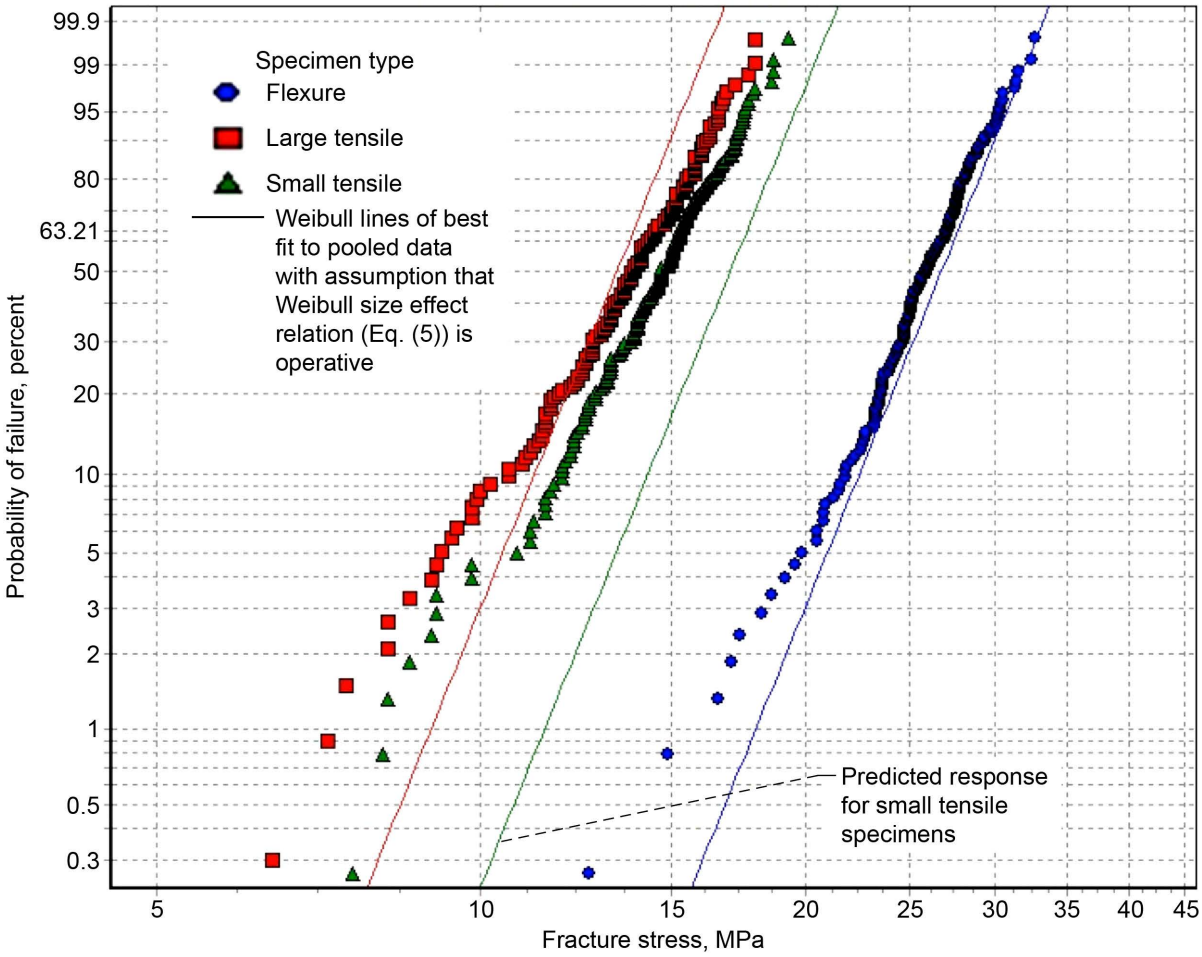

Figure 89.—Weibull plot of fracture stresses of pooled data from slabs 1 to 4 for radial small tensile, large tensile, and flexure specimens (with linear-elastic stresses) from edge of slabs. See Table 32 for a listing of Weibull parameters and 90-percent confidence bounds on parameters.

In Figure 90, the Weibull best-fit lines were determined by assuming that all the data had the same value of Weibull modulus and that the Weibull size effect was operating (by accounting for the geometry and loading of the specimens). A linear stress-strain response was assumed in determining the fracture stresses (from Price (1976)), and a linear-elastic finite element model of the four-point cylindrical flexure specimen was used in conjunction with WeibPar to determine the best-fit Weibull modulus and scale parameter (m = 13.67 and σ_o = 27.56 MPa-mm$^{3/m}$. See Table 32 for a listing of Weibull parameters and 90-percent confidence bounds on parameters.

The knee in the data at smaller probabilities of failure could be indicative of a concurrent competing failure mode, such as bimodal Weibull behavior. From Figures 56, 59, and 62 this seems to be primarily an effect from slab 1. However, the fact that the knee appears at approximately the same probability of failure (at approximately 5 to 10 percent) is not consistent with predictions from Weibull stress-volume integration for competing failure modes. If it were consistent, then the flaw population with the smaller Weibull modulus would dominate at larger effective volumes (in the tensile specimens) and the flaw population with the higher Weibull modulus would dominate at smaller effective volumes (the flexure specimens). Instead, what is seen is that there is no apparent shifting of the knee in the data to lower or higher probabilities of failure with changing effective volume. This is contrary to the assumption of concurrent flaw populations as competing failure modes acting in accordance with the prediction from Weibull stress-volume integration. This may mean that some other systematic variation is present, independent of geometry and loading, that affects the strength at lower probabilities of failure.

The WeibPar/CARES analysis shows that the size effect for the experimental fracture stress data for the two tensile specimen geometries is much smaller than what is expected from the Weibull stress-volume integration and that a large size effect exists between the tensile and flexure specimens which is adequately predicted with Weibull stress-volume integration.

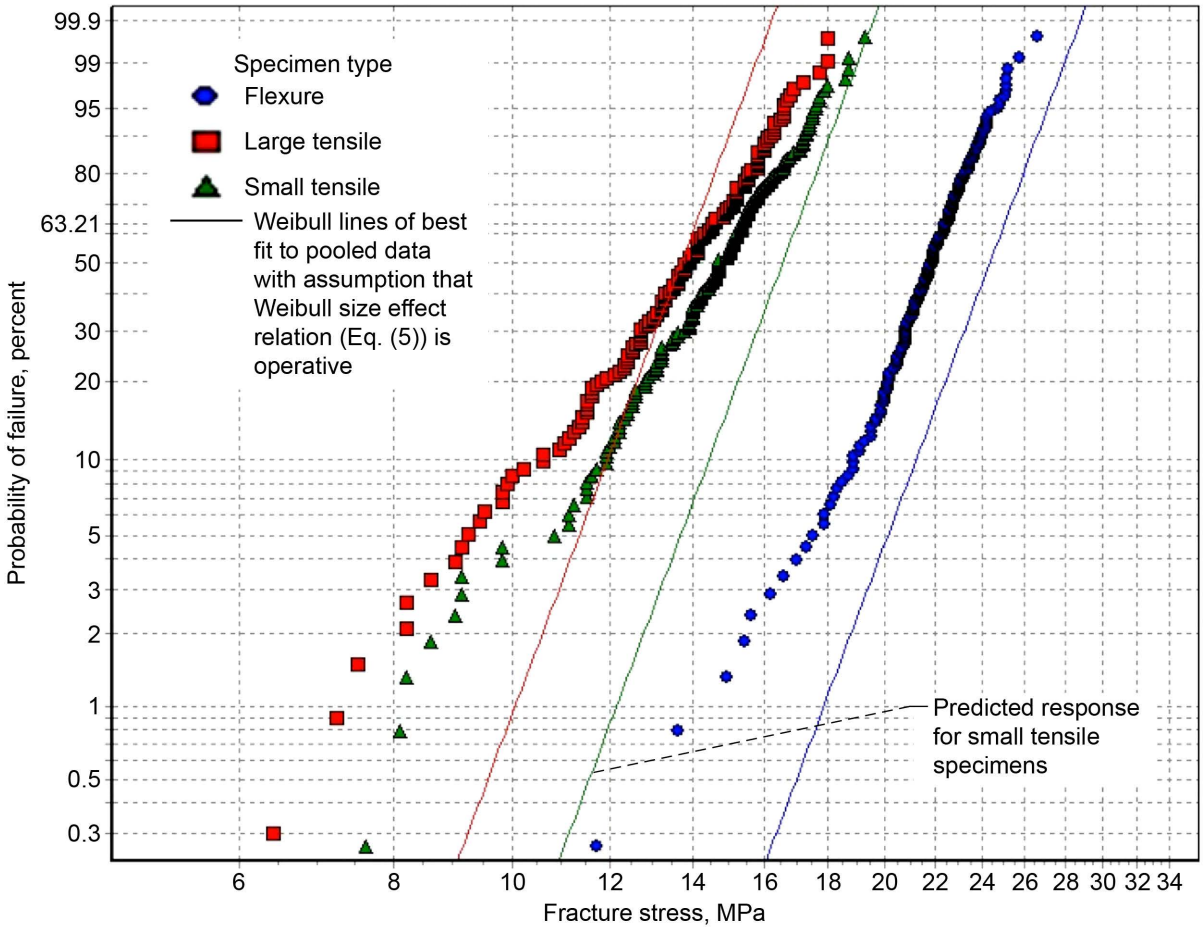

Figure 90.—Weibull plot of fracture stresses of pooled data from slabs 1 to 4 for radial small tensile, large tensile, and flexure specimens (with nonlinear-elastic stress response) from edge of slabs. See Table 32 for a listing of Weibull parameters and 90-percent confidence bounds on parameters.

In Figure 91, the Weibull modulus for the flexure specimens is significantly higher than for the tensile specimens—beyond what is expected from natural statistical variation. It has not been established how much of this difference could be attributed to the nonlinear stress-strain response of H–451. An alternative explanation is that a different failure mode with a separate set of Weibull parameters was operating at the surface when the material was loaded under flexure. The Weibull moduli for the two different sizes of tensile specimens are quite similar. See Table 32 for a listing of Weibull parameters and 90-percent confidence bounds on parameters.

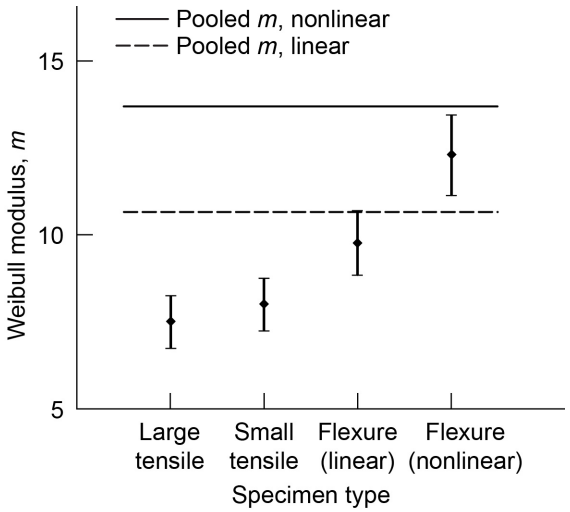

Figure 91.—Weibull modulus and 90-percent confidence bounds of pooled slabs 1 to 4 for radial small tensile, large tensile, and flexure specimens from edge of slabs. See Table 32 for a listing of Weibull parameters and 90-percent confidence bounds on parameters.

The higher characteristic strength of the flexure specimens in Figure 92 cannot be explained from natural statistical variation, and the size effect must be explained by other means such as with the Weibull distribution. On the other hand, the size effect between the small and large tensile specimens is less than what is expected with the Weibull distribution. When the fracture stresses were computed from Price (1976), the nonlinear stress-strain response reduced the characteristic strength of the flexure specimen. Table 32 reproduces the data from Tables 25 to 28 and is shown here for convenience.

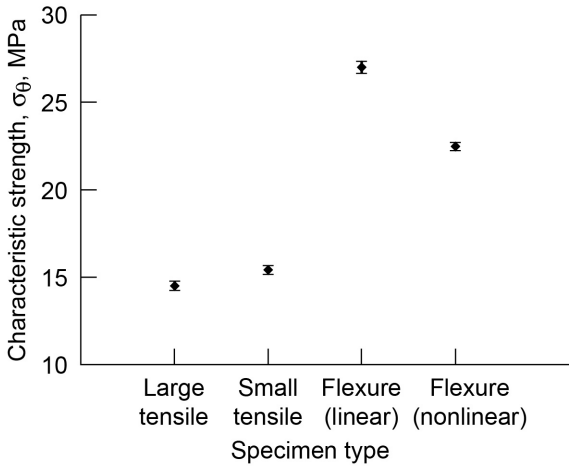

Figure 92.—Characteristic strength and 90-percent confidence bounds of pooled slabs 1 to 4 for radial small tensile, large tensile, and flexure specimens from edge of slabs. See Table 32 for a listing of Weibull parameters and 90-percent confidence bounds on parameters.

TABLE 32.—WEIBULL PARAMETERS AND 90-PERCENT CONFIDENCE BOUNDS ON INDIVIDUAL AND POOLED DATA FROM SLABS 1 TO 4 FOR RADIAL SMALL TENSILE, LARGE TENSILE, AND FLEXURE SPECIMENS FROM EDGE OF SLABS

Specimen type	Slab	Number of specimens	Weibull modulus, m		Characteristic strength, σ_θ, MPa	
			MLE biased[a]	90-percent confidence	MLE biased[a]	90-percent confidence
Small tensile	1	47	8.82	7.08/10.37	13.81	13.40/14.22
	2	48	9.71	7.81/11.40	16.02	15.60/16.45
	3	47	8.97	7.19/10.54	14.92	14.49/15.36
	4	48	10.53	8.47/12.36	16.50	16.10/16.91
	Mean	47.50	9.51	----------	15.31	----------
	Pooled	190	8.02	7.25/8.75	15.43	15.19/15.67
Large tensile	1	48	6.26	5.04/7.35	13.10	12.58/13.66
	2	48	8.23	6.62/9.66	14.75	14.29/15.22
	3	24	13.09	9.40/16.24	14.61	14.20/15.04
	4	48	9.42	7.58/11.06	15.40	14.99/15.83
	Mean	42.00	9.25	----------	14.47	----------
	Pooled	168	7.52	6.75/8.25	14.52	14.26/14.78
Flexure, linear[b]	1	46	8.68	6.94/10.23	25.62	24.85/26.41
	2	48	10.24	8.24/12.02	26.51	25.85/27.19
	3	48	11.74	9.44/13.77	27.81	27.20/28.43
	4	48	10.44	8.40/12.25	27.79	27.11/28.49
	Mean	47.50	10.28	----------	26.93	----------
	Pooled	190	9.78	8.84/10.66	27.00	26.66/27.35
Flexure, nonlinear[c]	1	46	11.01	8.80/12.97	21.36	20.85/21.88
	2	48	13.59	10.93/15.95	22.07	21.66/22.50
	3	48	15.21	12.23/17.85	23.52	23.12/23.92
	4	48	14.57	11.72/17.10	22.69	22.29/23.10
	Mean	47.50	13.60	----------	22.41	----------
	Pooled	190	12.31	11.13/13.43	22.49	22.26/22.72
Pooled, linear[b]	All data	738	10.65	NA for FE model	-------	----------
Pooled, nonlinear[c]	All data	738	13.68	NA for FE model	-------	----------

[a]Maximum-likelihood estimation.
[b]Linear-elastic stress-strain response was assumed.
[c]Nonlinear-elastic stress-strain response was assumed.

In Tables 32 and 25 to 28, slab 1 is consistently weaker and slab 4 is usually the strongest. Slabs 2 and 3 are usually between slabs 1 and 4 except for the flexure specimen. The average (mean) Weibull modulus for the four slabs is always higher than the Weibull modulus for the pooled data. This is largely because the slab-to-slab variation in the average strength (or alternatively, the characteristic strength shown in Table 32) of the individual slabs is beyond what is expected from natural statistical variation. Hence, pooling (combining) the data from the four slabs, which incorporated the additional slab-to-slab strength variation, increased the apparent scatter in strength of the pooled data. This resulted in a lower estimated Weibull modulus for the pooled data set.

Appendix C.—Tables and Figures of Pooled Data for Slabs 1 to 4 Comparing Effects of Specimen Location and Orientation in the Graphite Log

In Figure 93, the edge of the graphite log is stronger than the center.

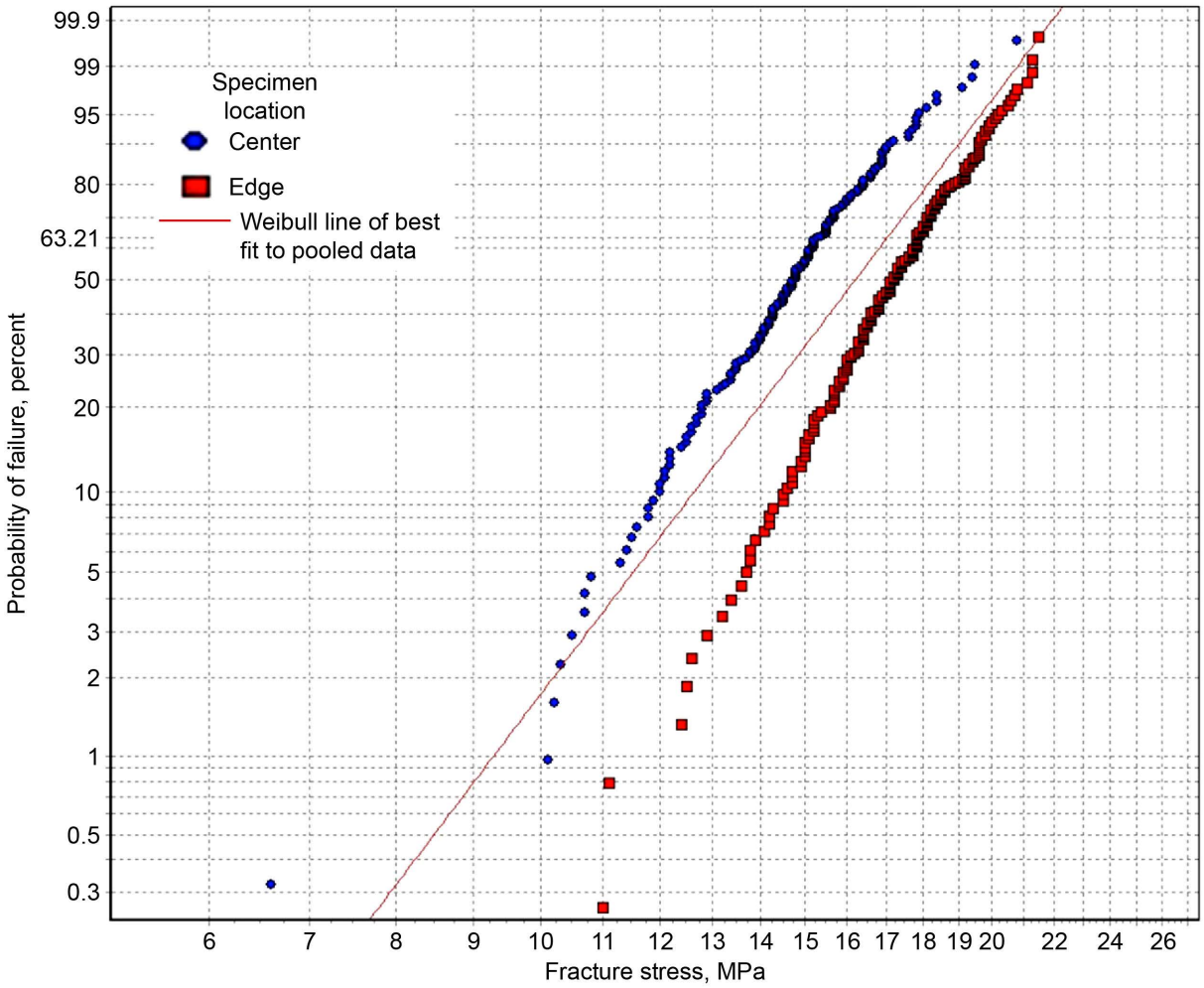

Figure 93.—Weibull plot of fracture stresses of pooled data from slabs 1 to 4 for axial small tensile specimens, comparing data from center and edge of slabs. See Table 33 for a listing of Weibull parameters and 90-percent confidence bounds on parameters.

There is a significant difference in Weibull modulus in Figure 94—beyond what is expected from natural statistical variation.

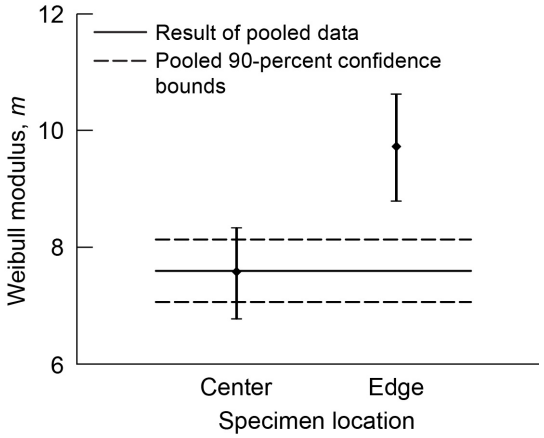

Figure 94.—Weibull modulus and 90-percent confidence bounds on pooled data from slabs 1 to 4 for axial small tensile specimens, comparing data from center and edge of slabs. See Table 33 for a listing of Weibull parameters and 90-percent confidence bounds on parameters.

There is a significant difference in the characteristic strengths in Figure 95—beyond what is expected from natural statistical variation. See Table 33 for a listing of the Weibull parameters and the 90-percent confidence bounds on parameters.

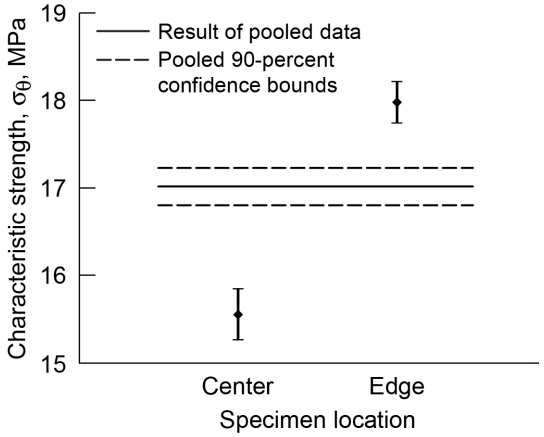

Figure 95.—Characteristic strength and 90-percent confidence bounds on pooled data from slabs 1 to 4 for axial small tensile specimens, comparing data from center and edge of slabs. See Table 33 for a listing of Weibull parameters and 90-percent confidence bounds on parameters.

TABLE 33.—WEIBULL PARAMETERS AND 90-PERCENT CONFIDENCE BOUNDS ON POOLED DATA FROM SLABS 1 TO 4 FOR AXIAL SMALL TENSILE SPECIMENS, COMPARING DATA FROM CENTER AND EDGE OF SLABS

Specimen type	Number of specimens	Weibull modulus, *m*		Characteristic strength, σ_θ, MPa	
		MLE biased[a]	90-percent confidence	MLE biased[a]	90-percent confidence
Center	156	7.58	6.78/8.33	15.56	15.27/15.85
Edge	190	9.73	8.80/10.62	17.98	17.75/18.22
Pooled	346	7.60	7.07/8.14	17.02	16.81/17.23

[a]Maximum-likelihood estimation.

In Figure 96, the edge of the graphite log is stronger than the center.

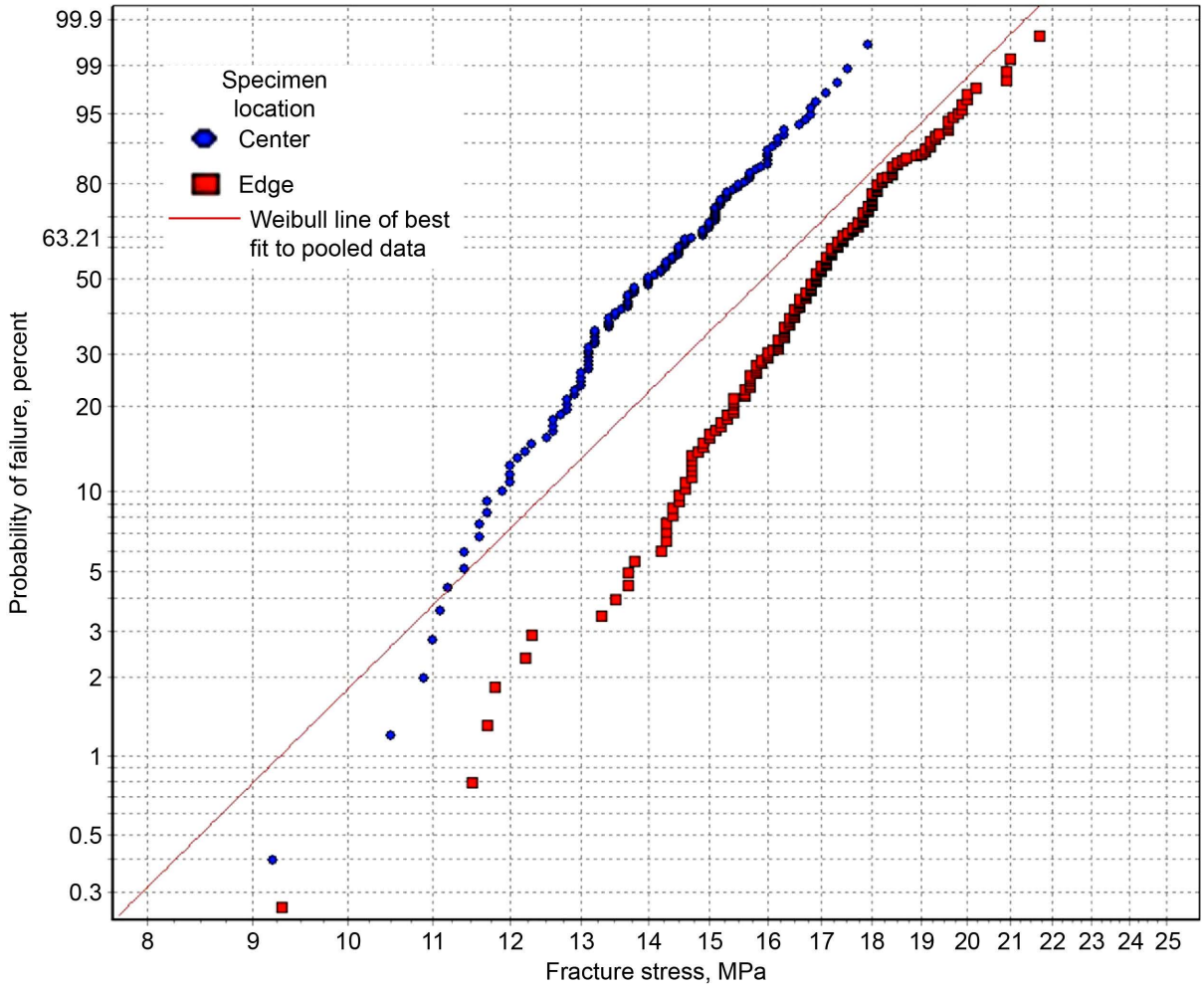

Figure 96.—Weibull plot of fracture stresses of pooled data from slabs 1 to 4 for axial large tensile specimens, comparing data from center and edge of slabs. See Table 34 for a listing of the Weibull parameters and the 90-percent confidence bounds on parameters.

In Figure 97, the values for the Weibull modulus are within statistical uncertainty.

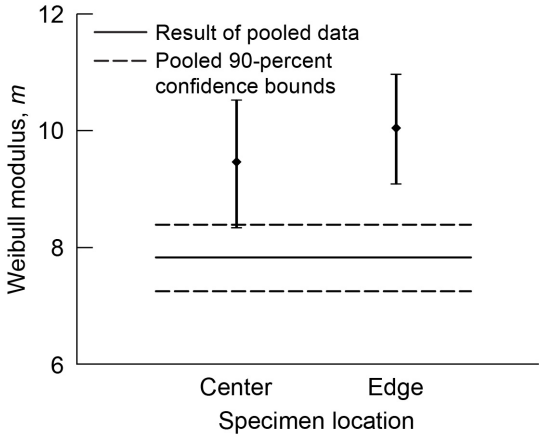

Figure 97.—Weibull modulus and 90-percent confidence bounds on pooled data from slabs 1 to 4 for axial large tensile specimens, comparing data from center and edge of slabs. See Table 34 for a listing of the Weibull parameters and the 90-percent confidence bounds on parameters.

There is a significant difference in the characteristic strengths in Figure 98—beyond what is expected from natural statistical variation. See Table 34 for a listing of the Weibull parameters and the 90-percent confidence bounds on the parameters.

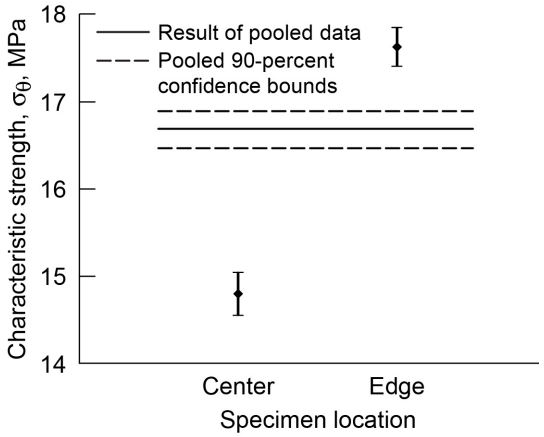

Figure 98.—Characteristic strength and 90-percent confidence bounds on pooled data from slabs 1 to 4 for axial large tensile specimens, comparing data from center and edge of slabs. See Table 34 for a listing of Weibull parameters and 90-percent confidence bounds on parameters.

TABLE 34.—WEIBULL PARAMETERS AND 90-PERCENT CONFIDENCE BOUNDS ON POOLED DATA FROM SLABS 1 TO 4 FOR AXIAL LARGE TENSILE SPECIMENS, COMPARING DATA FROM CENTER AND EDGE OF SLABS

Specimen type	Number of specimens	Weibull modulus, *m*		Characteristic strength, σ_θ, MPa	
		MLE biased[a]	90-percent confidence	MLE biased[a]	90-percent confidence
Center	126	9.47	8.34/10.52	14.80	14.56/15.05
Edge	191	10.05	9.09/10.96	17.63	17.41/17.85
Pooled	317	7.83	7.25/8.39	16.69	16.47/16.89

[a]Maximum-likelihood estimation.

The data have a distinctly nonlinear appearance in Figure 99, and this trend is consistent for the axial flexure specimens from both the center and edge of the slabs. The edge of the graphite log is stronger than the center.

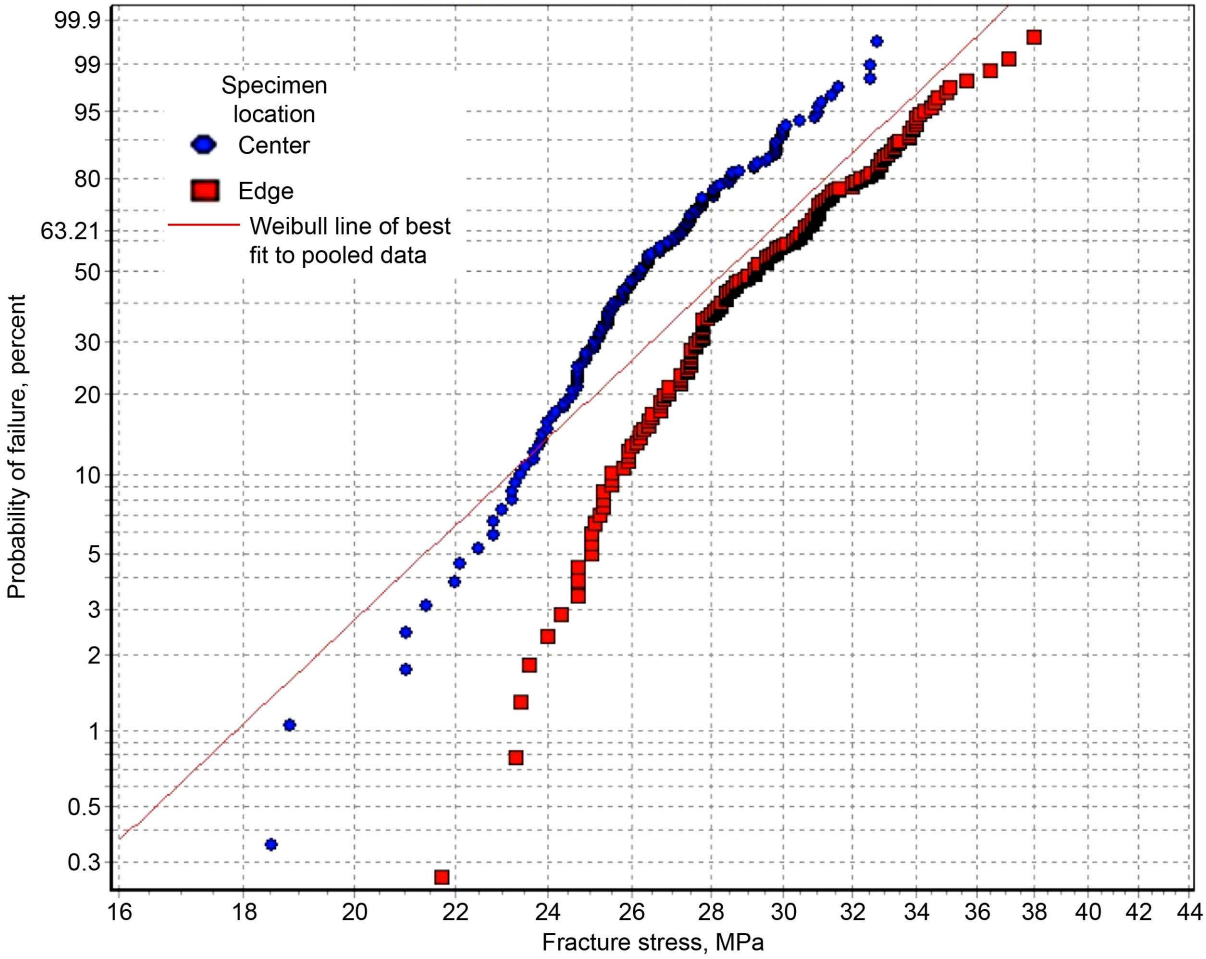

Figure 99.—Weibull plot of fracture stresses of pooled data from slabs 1 to 4 for axial flexure specimens (with linear-elastic stress response), comparing data from center and edge of slabs. See Table 35 for a listing of the Weibull parameters and the 90-percent confidence bounds on parameters.

In Figure 100, the differences in the Weibull moduli are within statistical uncertainty.

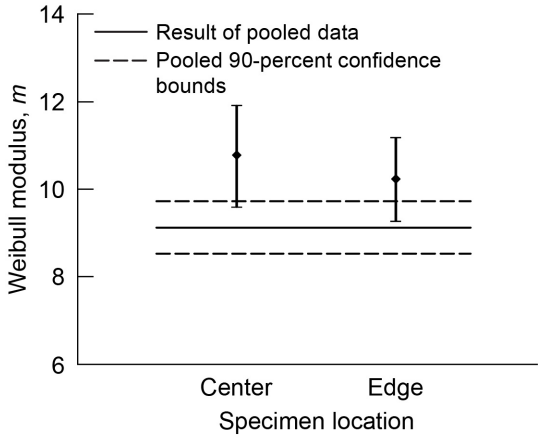

Figure 100.—Weibull modulus and 90-percent confidence bounds on pooled data from slabs 1 to 4 for axial flexure specimens (with linear-elastic stress response), comparing data from center and edge of slabs. See Table 35 for a listing of the Weibull parameters and the 90-percent confidence bounds on parameters.

There is a significant difference in the characteristic strengths in Figure 101—beyond what is expected from natural statistical variation. See Table 35 for a listing of the Weibull parameters and the 90-percent confidence bounds on the parameters.

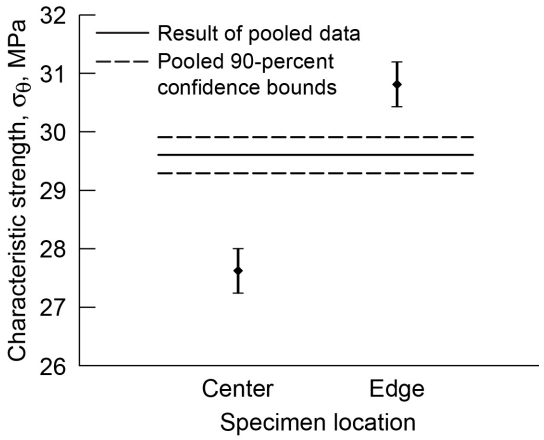

Figure 101.—Characteristic strength and 90-percent confidence bounds on pooled data from slabs 1 to 4 for axial flexure specimens (with linear-elastic stress response), comparing data from center and edge of slabs. See Table 35 for a listing of the Weibull parameters and the 90-percent confidence bounds on parameters.

TABLE 35.—WEIBULL PARAMETERS AND 90-PERCENT CONFIDENCE BOUNDS ON POOLED DATA FROM SLABS 1 TO 4 FOR AXIAL FLEXURE SPECIMENS (WITH LINEAR-ELASTIC STRESS RESPONSE), COMPARING DATA FROM CENTER AND EDGE OF SLABS

Specimen type	Number of specimens	Weibull modulus, *m*		Characteristic strength, σ_θ, MPa	
		MLE biased[a]	90-percent confidence	MPa	90-percent confidence
Center	144	10.79	9.60/11.91	27.63	27.25/28.00
Edge	192	10.24	9.27/11.17	30.82	30.44/31/20
Pooled	336	9.12	8.53/9.73	29.61	29.30/29.92

[a]Maximum-likelihood estimation.

The data have a nonlinear appearance in Figure 102, and this trend is consistent for axial flexure specimens from both the center and edge of the slabs. The edge of the graphite log is stronger than the center. See Table 36 for a listing of Weibull parameters and 90-percent confidence bounds on parameters.

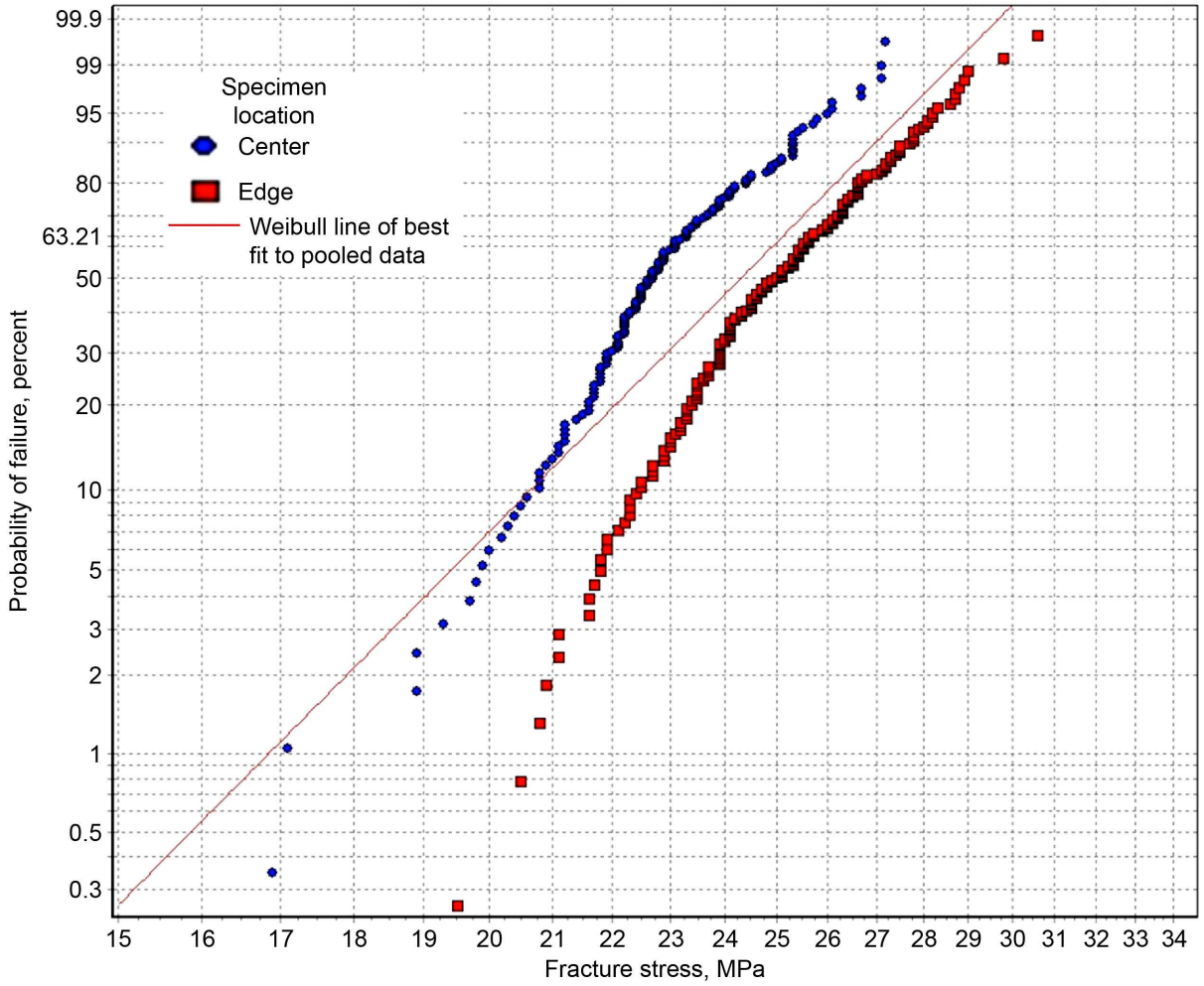

Figure 102.—Weibull plot of fracture stresses of pooled data from slabs 1 to 4 for axial flexure specimens (with nonlinear-elastic stress response), comparing data from center and edge of slabs. See Table 36 for a listing of Weibull parameters and 90-percent confidence bounds on parameters.

The differences in Weibull moduli are within statistical uncertainty in Figure 103. See Table 36 for a listing of Weibull parameters and 90-percent confidence bounds on parameters.

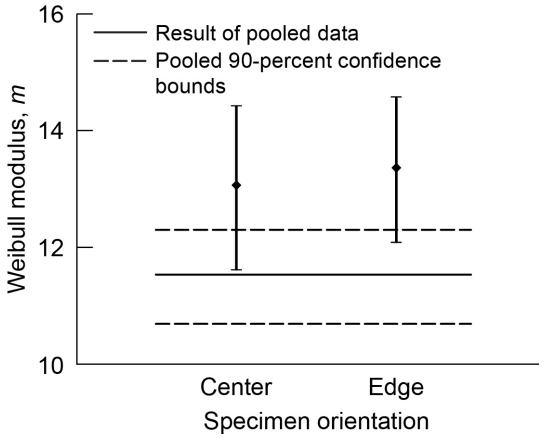

Figure 103.—Weibull modulus and 90-percent confidence bounds on individual slabs 1 to 4 for axial flexure specimens (with nonlinear-elastic stress response), comparing data from center and edge of slabs. See Table 36 for a listing of Weibull parameters and 90-percent confidence bounds on parameters.

There is a significant difference in the characteristic strengths in Figure 104—beyond what is expected from natural statistical variation. See Table 36 for a listing of Weibull parameters and 90-percent confidence bounds on parameters.

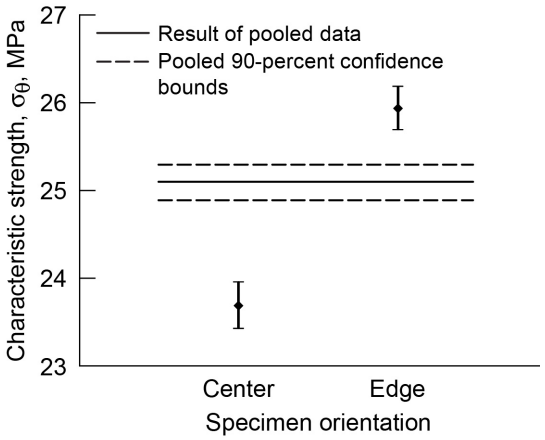

Figure 104.—Characteristic strength and 90-percent confidence bounds on individual slabs 1 to 4 for axial flexure specimens (with nonlinear-elastic stress response), comparing data from center and edge of slabs. See Table 36 for a listing of Weibull parameters and 90-percent confidence bounds on parameters.

TABLE 36.—WEIBULL PARAMETERS AND 90-PERCENT CONFIDENCE BOUNDS ON POOLED DATA FROM SLABS 1 TO 4 FOR AXIAL FLEXURE SPECIMENS (WITH NONLINEAR-ELASTIC STRESS RESPONSE), COMPARING DATA FROM CENTER AND EDGE OF SLABS

Specimen type	Number of specimens	Weibull modulus, *m*		Characteristic strength, σ_θ, MPa	
		MLE biased[a]	90-percent confidence	MPa	90-percent confidence
Center	144	13.07	11.62/14.42	23.69	23.43/23.96
Edge	192	13.36	12.09/14.57	25.94	25.70/26.19
Pooled	336	11.54	10.69/12.30	25.10	24.89/25.30

[a]Maximum-likelihood estimation.

In Figure 105, the data have a distinctly linear appearance. The edge of the graphite log is stronger than the center. See Table 37 for a listing of Weibull parameters and 90-percent confidence bounds on parameters.

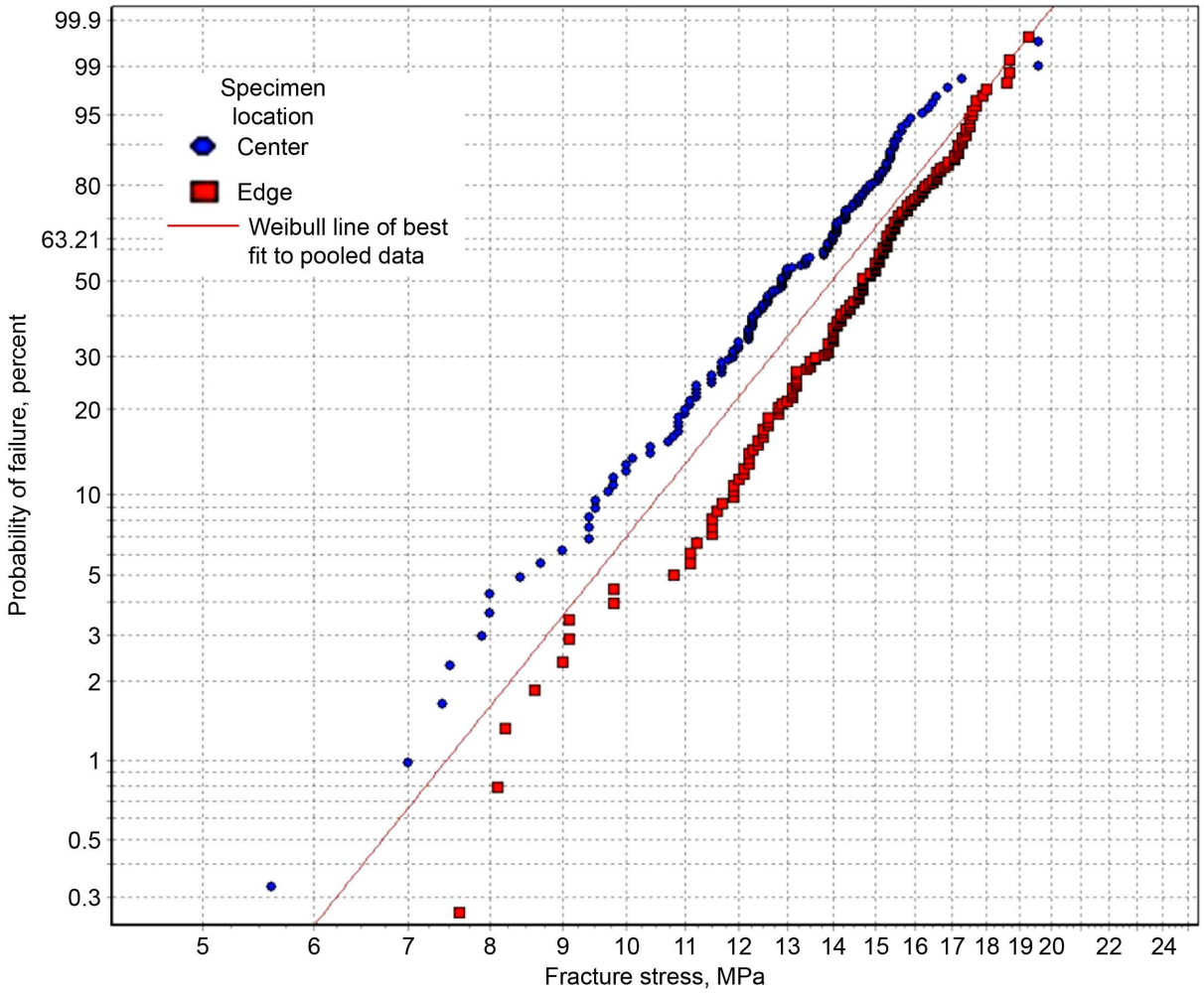

Figure 105.—Weibull plot of fracture stresses of pooled data from slabs 1 to 4 for radial small tensile specimens, comparing specimens from center and edge of slabs. See Table 37 for a listing of Weibull parameters and 90-percent confidence bounds on parameters.

There is a significant difference in Weibull moduli in Figure 106—beyond what is expected from natural statistical variation, but examination of Figure 105 shows that the data are quite similar in appearance. See Table 37 for a listing of Weibull parameters and 90-percent confidence bounds on parameters.

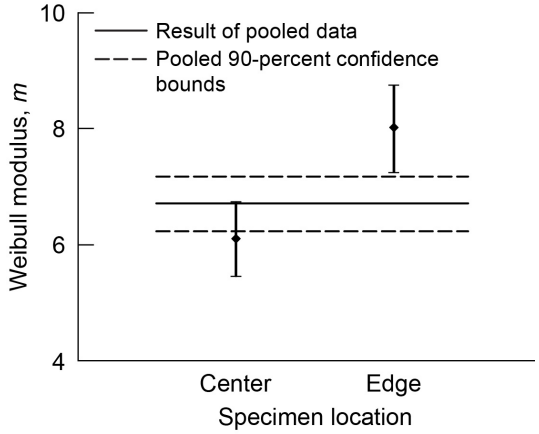

Figure 106.—Weibull modulus and 90-percent confidence bounds on pooled data from slabs 1 to 4 for radial small tensile specimens, comparing data from center and edge of slabs. See Table 37 for a listing of Weibull parameters and 90-percent confidence bounds on parameters.

There is a significant difference in the characteristic strengths in Figure 107—beyond what is expected from natural statistical variation. See Table 37 for a listing of the Weibull parameters and the 90-percent confidence bounds on the parameters.

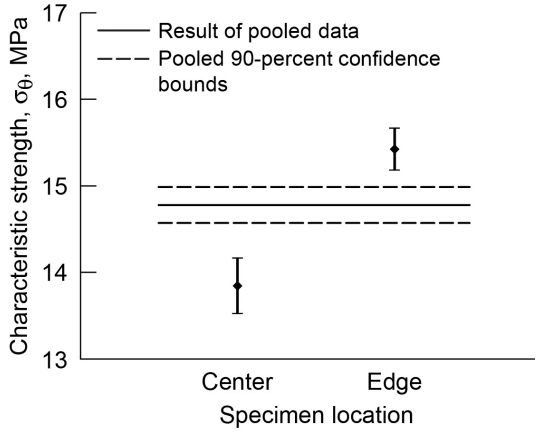

Figure 107.—Characteristic strength and 90-percent confidence bounds on pooled data from slabs 1 to 4 for radial small tensile specimens, comparing data from center and edge of slabs. See Table 37 for a listing of Weibull parameters and 90-percent confidence bounds on parameters.

TABLE 37.—WEIBULL PARAMETERS AND 90-PERCENT CONFIDENCE BOUNDS ON POOLED DATA FROM SLABS 1 TO 4 FOR RADIAL SMALL TENSILE SPECIMENS, COMPARING DATA FROM CENTER AND EDGE OF SLABS

Specimen type	Number of specimens	Weibull modulus, m		Characteristic strength, σ_θ, MPa	
		MLE biased[a]	90-percent confidence	MPa	90-percent confidence
Center	153	6.11	5.46/6.72	13.85	13.53/14.17
Edge	190	8.02	7.25/8.75	15.43	15.19/15.67
Pooled	343	6.72	6.23/7.18	14.78	14.57/14.99

[a]Maximum-likelihood estimation.

The data show a reasonably linear trend in Figure 108. Note that the edge of the graphite log is stronger than the center, except perhaps at lower probabilities of failure.

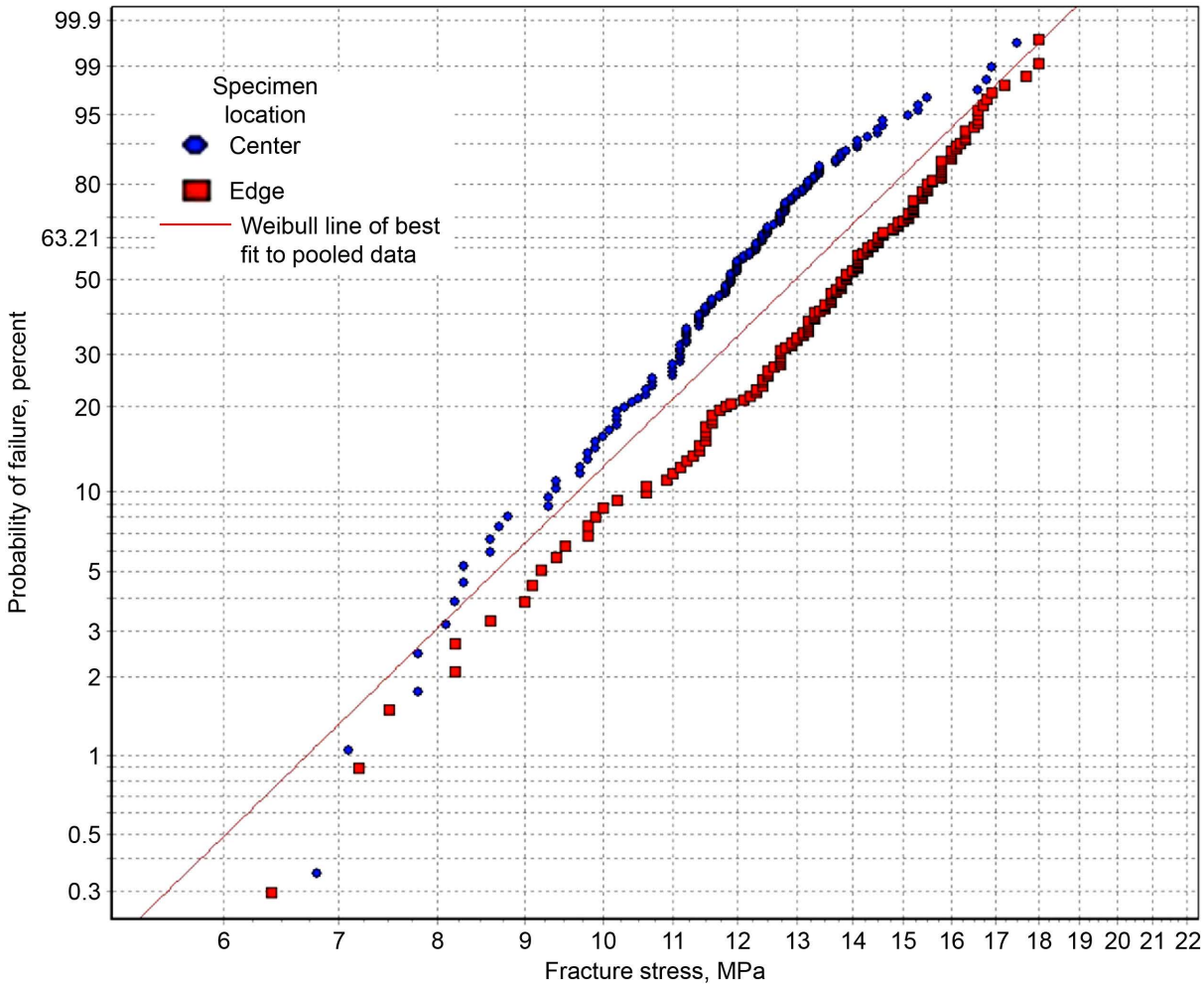

Figure 108.—Weibull plot of fracture stresses of pooled data from slabs 1 to 4 for radial large tensile specimens, comparing data from center and edge of slabs. See Table 38 for a listing of Weibull parameters and 90-percent confidence bounds on parameters.

In Figure 109, the difference in Weibull moduli is not large and can be considered to be within statistical uncertainty.

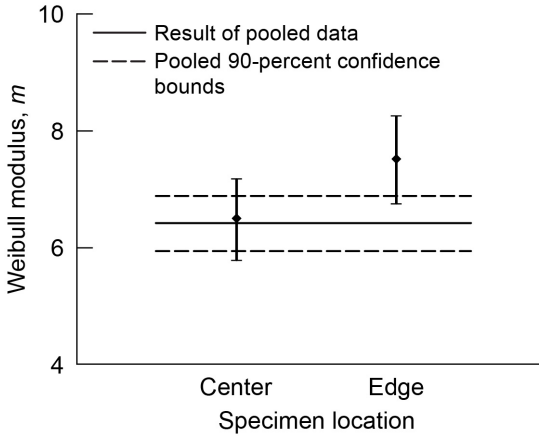

Figure 109.—Weibull modulus and 90-percent confidence bounds on pooled data from slabs 1 to 4 for radial large tensile specimens, comparing data from center and edge of slabs See Table 38 for a listing of Weibull parameters and 90-percent confidence bounds on parameters.

There is a significant difference in the characteristic strengths in Figure 110—beyond what is expected from natural statistical variation. See Table 38 for a listing of Weibull parameters and 90-percent confidence bounds on parameters.

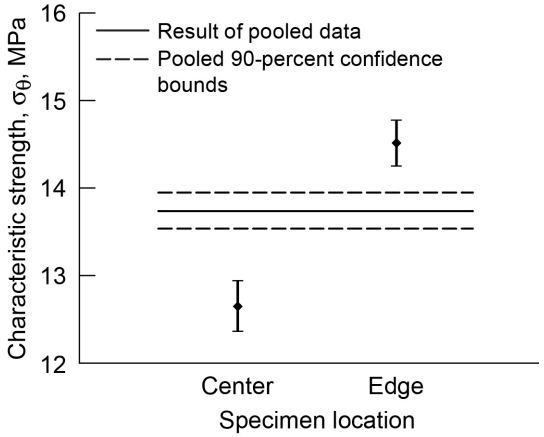

Figure 110.—Characteristic strength and 90-percent confidence bounds on pooled data from slabs 1 to 4 for radial large tensile specimens, comparing data from center and edge of slabs See Table 38 for a listing of Weibull parameters and 90-percent confidence bounds on parameters.

TABLE 38.—WEIBULL PARAMETERS AND 90-PERCENT CONFIDENCE BOUNDS ON POOLED DATA FROM SLABS 1 TO 4 FOR RADIAL LARGE TENSILE SPECIMENS, COMPARING DATA FROM CENTER AND EDGE OF SLABS

Specimen type	Number of specimens	Weibull modulus, *m*		Characteristic strength, σ_θ, MPa	
		MLE biased[a]	90-percent confidence	MPa	90-percent confidence
Center	143	6.50	5.78/7.17	12.65	12.37/12.94
Edge	168	7.52	6.75/8.25	14.52	14.26/14.78
Pooled	311	6.42	5.94/6.88	13.74	13.54/13.95

[a]Maximum-likelihood estimation.

It is interesting how the tails of the distributions in Figure 111 cross one another at lower probabilities of failure, but this could well be a random occurrence. Note that the edge of the graphite log is stronger than the center, except perhaps at lower probabilities of failure.

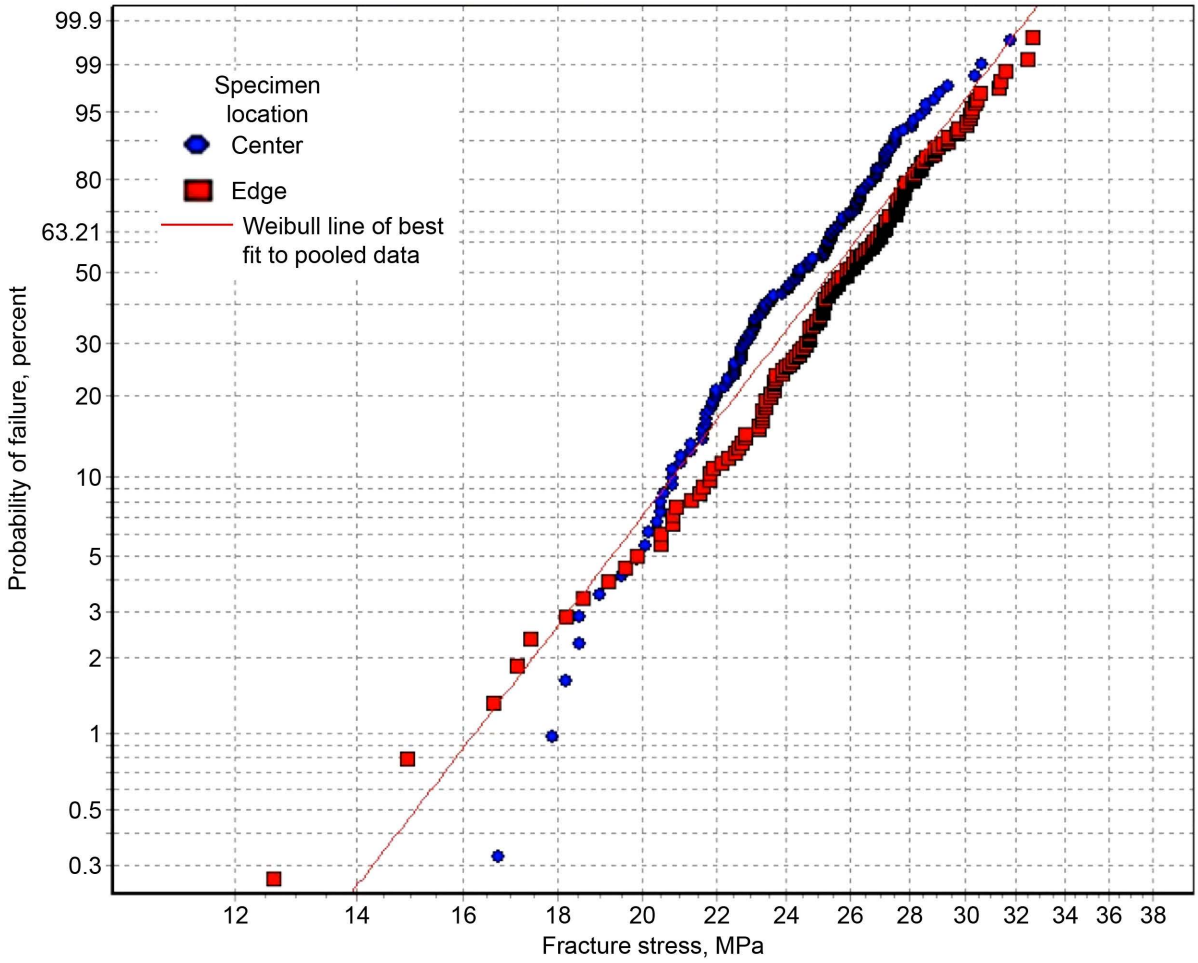

Figure 111.—Weibull plot of fracture stresses of pooled data from slabs 1 to 4 for radial flexure specimens (with linear-elastic stress response), comparing data from center and edge of slabs. See Table 39 for a listing of Weibull parameters and 90-percent confidence bounds on parameters.

The Weibull moduli in Figure 112 are well within statistical uncertainty.

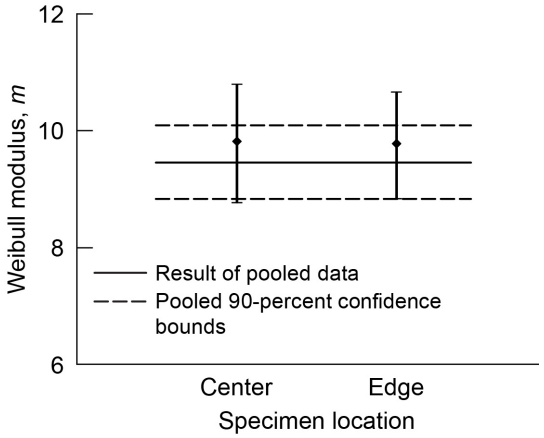

Figure 112.—Weibull modulus and 90-percent confidence bounds on pooled data from slabs 1 to 4 for radial flexure specimens (with linear-elastic stress response), comparing data from center and edge of slabs. See Table 39 for a listing of Weibull parameters and 90-percent confidence bounds on parameters.

In Figure 113, the difference in characteristic strength is statistically significant—beyond what is expected from natural statistical variation; however, the relative difference is not that large. See Table 39 for a listing of Weibull parameters and 90-percent confidence bounds on parameters.

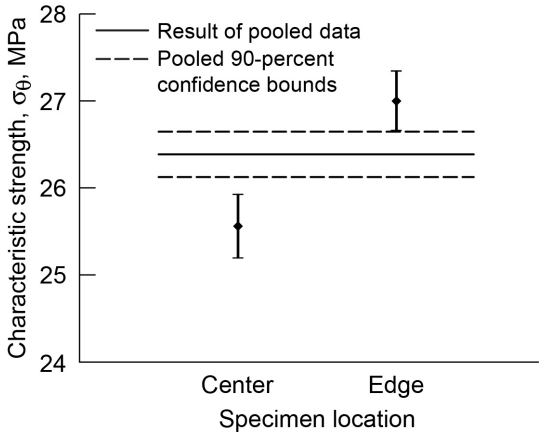

Figure 113.—Characteristic strength and 90-percent confidence bounds on pooled data from slabs 1 to 4 for radial flexure specimens (with linear-elastic stress response), comparing data from center and edge of slabs. See Table 39 for a listing of Weibull parameters and 90-percent confidence bounds on parameters.

TABLE 39.—WEIBULL PARAMETERS AND 90-PERCENT CONFIDENCE BOUNDS OF POOLED DATA FROM SLABS 1 TO 4 FOR RADIAL FLEXURE SPECIMENS (WITH LINEAR-ELASTIC STRESS RESPONSE), COMPARING DATA FROM CENTER AND EDGE OF SLABS

Specimen type	Number of specimens	Weibull modulus, *m*		Characteristic strength, σ_θ, MPa	
		MLE biased	90-percent confidence	MPa	90-percent confidence
Center	156	9.82	8.78/10.79	25.56	25.20/25.93
Edge	190	9.78	8.84/10.66	27.00	26.66/27.35
Pooled	346	9.45	8.83/10.09	26.39	26.13/26.65

[a]Maximum-likelihood estimation.

It is interesting how the tails of the distributions in Figure 114 cross one another at lower probabilities of failure, but this could well be a random occurrence. Note that the edge of the graphite log is stronger than the center, except perhaps at lower probabilities of failure.

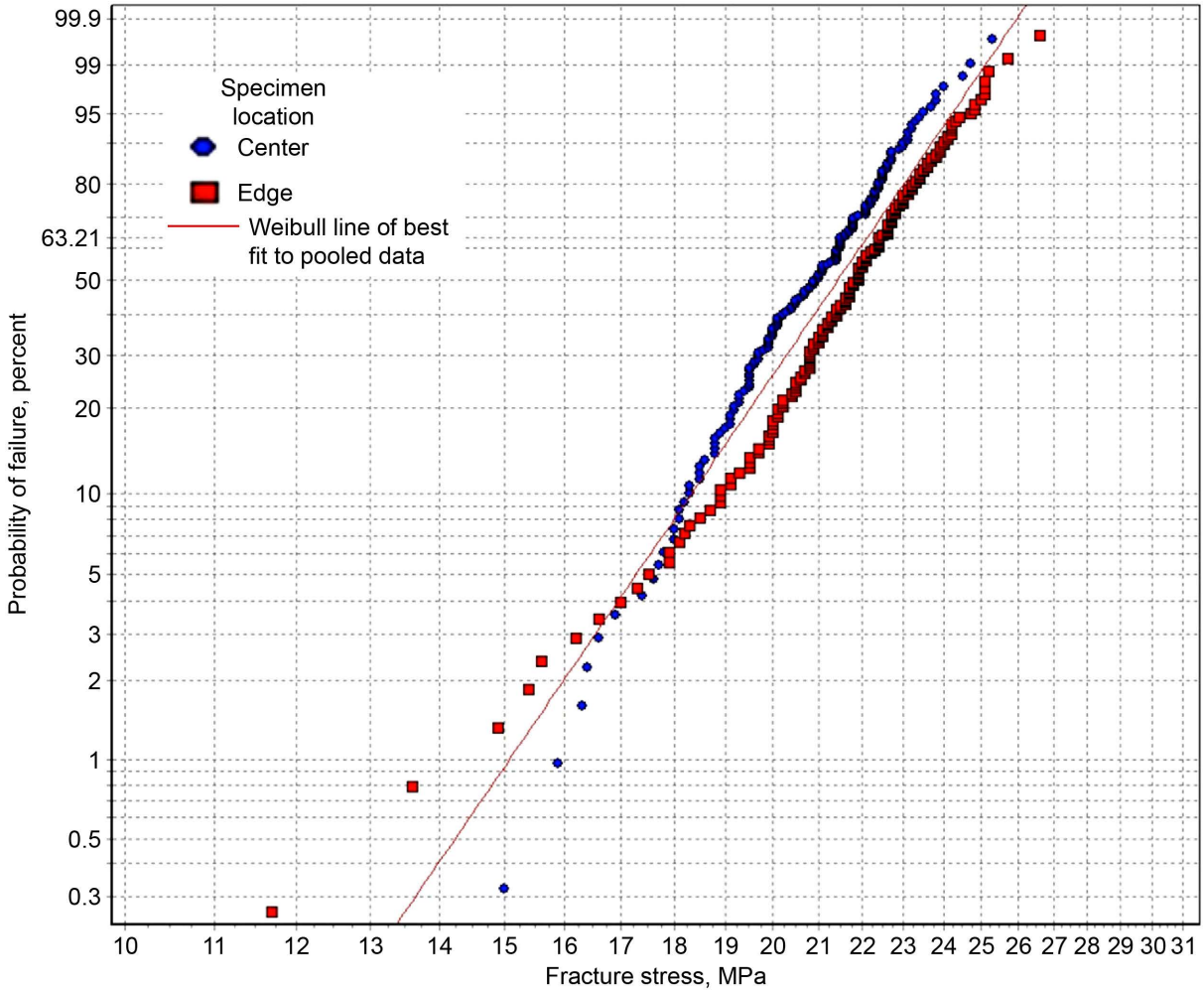

Figure 114.—Weibull plot of fracture stresses of pooled data from slabs 1 to 4 for radial flexure specimens (with nonlinear-elastic stress response), comparing data from center and edge of slabs. See Table 40 for a listing of Weibull parameters and 90-percent confidence bounds on parameters.

The Weibull moduli in Figure 115 are well within statistical uncertainty.

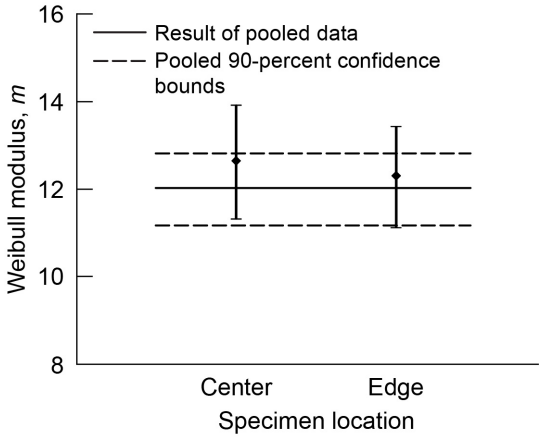

Figure 115.—Weibull modulus and 90-percent confidence bounds on pooled data from slabs 1 to 4 for radial flexure specimens (with nonlinear-elastic stress response), comparing data from center and edge of slabs. See Table 40 for a listing of Weibull parameters and 90-percent confidence bounds on parameters.

The difference in characteristic strength is statistically significant in Figure 116—beyond what is expected from natural statistical variation; however, the relative difference is not that large. See Table 40 for a listing of Weibull parameters and 90-percent confidence bounds on parameters.

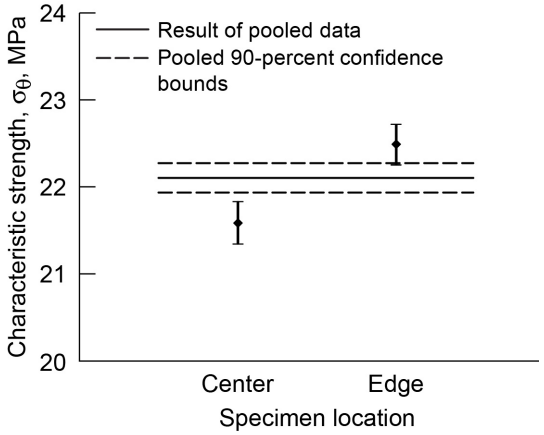

Figure 116.—Characteristic strength and 90-percent confidence bounds on pooled data from slabs 1 to 4 for radial flexure specimens (with nonlinear-elastic stress response), comparing data from center and edge of slabs. See Table 40 for a listing of Weibull parameters and 90-percent confidence bounds on parameters.

TABLE 40.—WEIBULL PARAMETERS AND 90-PERCENT CONFIDENCE BOUNDS ON POOLED DATA FROM SLABS 1 TO 4 FOR RADIAL FLEXURE SPECIMENS (WITH NONLINEAR-ELASTIC STRESS RESPONSE), COMPARING DATA FROM CENTER AND EDGE OF SLABS

Specimen type	Number of specimens	Weibull modulus, *m*		Characteristic strength, σ_θ, MPa	
		MLE biased[a]	90-percent confidence	MPa	90-percent confidence
Center	156	12.65	11.32/13.91	21.59	21.35/21.83
Edge	190	12.31	11.13/13.43	22.49	22.26/22.72
Pooled	346	12.03	11.17/12.81	22.11	21.94/22.28

[a]Maximum-likelihood estimation.

In Figure 117, the radial specimens are weaker than the axial specimens, and the data for the radial specimens appear to be more linear than that for the axial specimens.

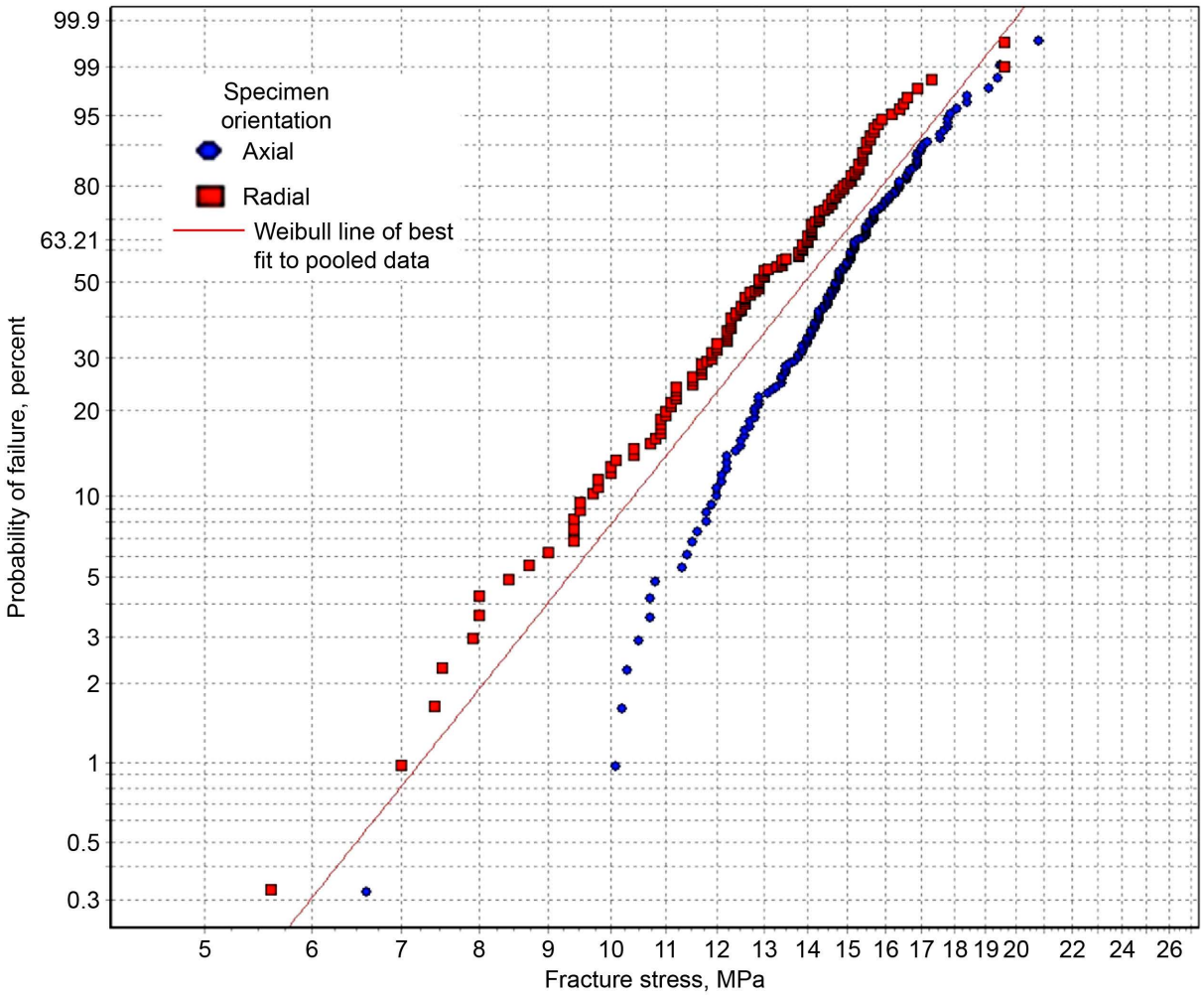

Figure 117.—Weibull plot of fracture stresses of pooled data from slabs 1 to 4 for small tensile specimens from center of slabs, comparing axial and radial orientations. See Table 41 for a listing of Weibull parameters and 90-percent confidence bounds on parameters.

The difference in Weibull moduli is not that large in Figure 118, but it appears to be beyond what is expected from natural statistical variation.

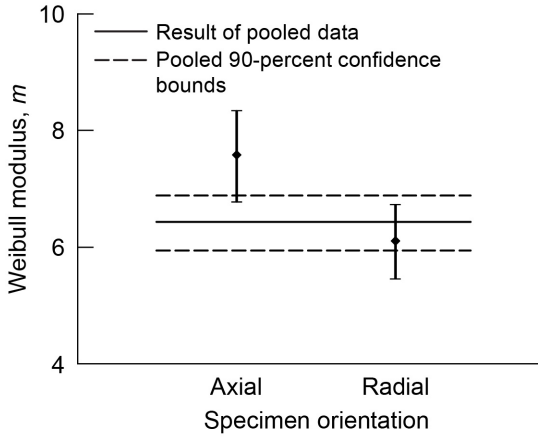

Figure 118.—Weibull modulus and 90-percent confidence bounds on pooled data from slabs 1 to 4 for small tensile specimens from center of slabs, comparing axial and radial orientations. See Table 41 for a listing of Weibull parameters and 90-percent confidence bounds on parameters.

The difference in the characteristic strength is statistically significant in Figure 119—beyond what is expected from natural statistical variation. See Table 41 for a listing of Weibull parameters and 90-percent confidence bounds on parameters.

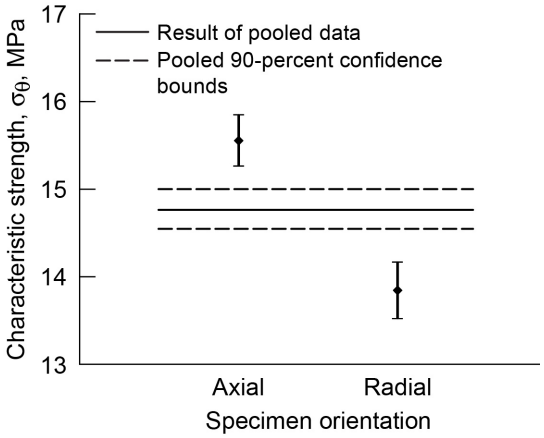

Figure 119.—Characteristic strength and 90-percent confidence bounds on pooled data from slabs 1 to 4 for small tensile specimens from center of slabs, comparing axial and radial orientations. See Table 41 for a listing of Weibull parameters and 90-percent confidence bounds on parameters.

TABLE 41.—WEIBULL PARAMETERS AND 90-CONFIDENCE BOUNDS ON POOLED DATA FROM SLABS 1 TO 4 FOR SMALL TENSILE SPECIMENS FROM CENTER OF SLABS, COMPARING AXIAL AND RADIAL ORIENTATIONS

Specimen type	Number of specimens	Weibull modulus, *m*		Characteristic strength, σ_θ, MPa	
		MLE biased[a]	90-percent confidence	MPa	90-percent confidence
Axial	156	7.58	6.78/8.33	15.56	15.27/15.85
Radial	153	6.11	5.46/6.72	13.85	13.53/14.17
Pooled	309	6.43	5.94/6.88	14.77	14.55/15.00

[a]Maximum-likelihood estimation.

In Figure 120, the radial specimens are weaker than the axial specimens, and the data for the radial specimens appears to be somewhat more linear than that for the axial specimens.

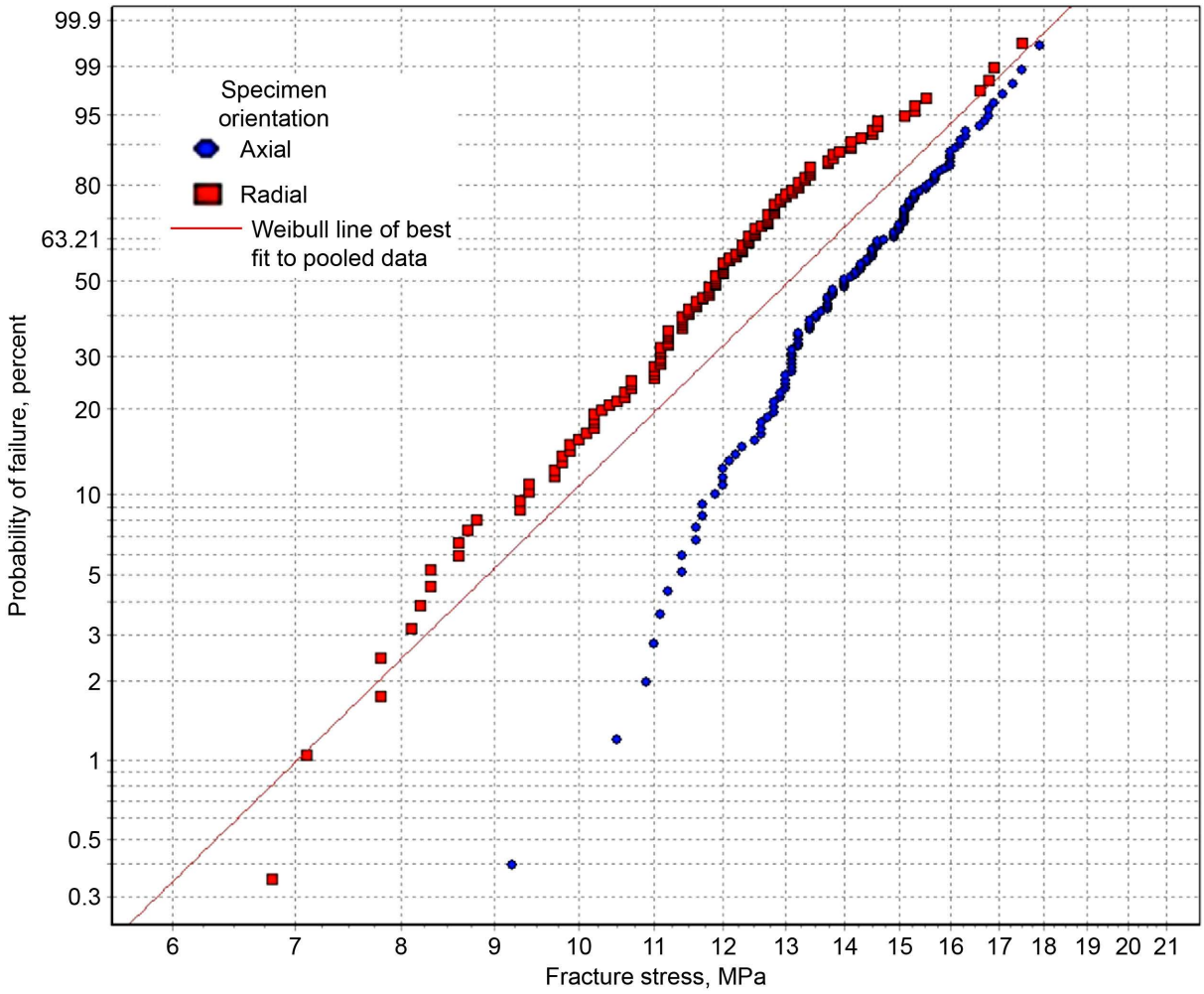

Figure 120.—Weibull plot of fracture stresses of pooled data from slabs 1 to 4 for large tensile specimens from center of slabs. See Table 42 for a listing of Weibull parameters and 90-percent confidence bounds on parameters.

The difference in Weibull moduli appears to be statistically significant in Figure 121—beyond what is expected from natural statistical variation.

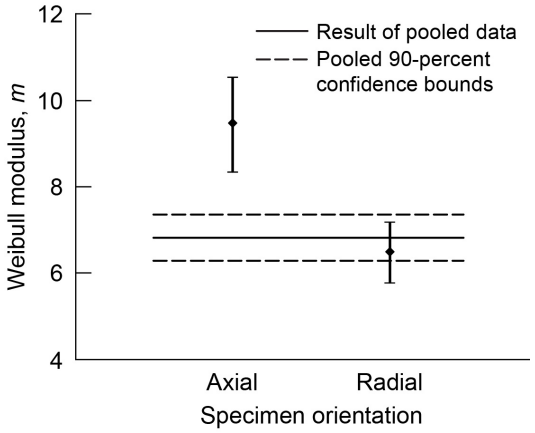

Figure 121.—Weibull modulus and 90-percent confidence bounds on pooled data from slabs 1 to 4 for large tensile specimens from center of slabs comparing axial and radial orientations. See Table 42 for a listing of Weibull parameters and 90-percent confidence bounds on parameters.

The difference in characteristic strength is statistically significant in Figure 122—beyond what is expected from natural statistical variation. See Table 42 for a listing of Weibull parameters and 90-percent confidence bounds on parameters.

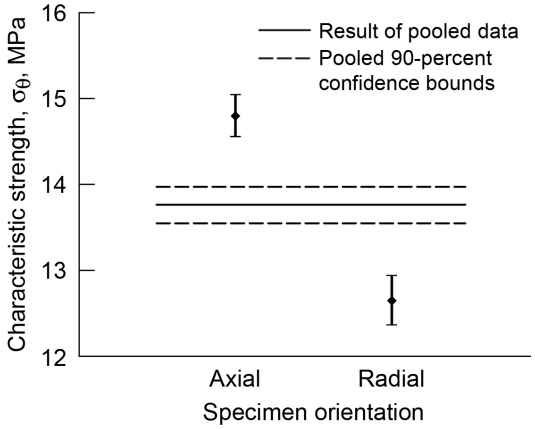

Figure 122.—Characteristic strength and 90-percent confidence bounds on pooled data from slabs 1 to 4 for large tensile specimens from center of slabs, comparing axial and radial orientations. See Table 42 for a listing of Weibull parameters and 90-percent confidence bounds on parameters.

TABLE 42.—WEIBULL PARAMETERS AND 90-PERCENT CONFIDENCE BOUNDS ON POOLED DATA FROM SLABS 1 TO 4 FOR LARGE TENSILE SPECIMENS FROM CENTER OF SLABS, COMPARING AXIAL AND RADIAL ORIENTATIONS

Specimen type	Number of specimens	Weibull modulus, *m*		Characteristic strength, σ_θ, MPa	
		MLE biased[a]	90-percent confidence	MPa	90-percent confidence
Axial large tensile	126	9.47	8.34/10.52	14.80	14.56/15.05
Radial large tensile	143	6.50	5.78/7.17	12.65	12.37/12.94
Pooled	269	6.82	6.29/7.36	13.77	13.55/13.98

[a]Maximum-likelihood estimation.

In Figure 123, the radial specimens are weaker than the axial specimens, and the plots for both data sets appear to have some nonlinearity. See Table 43 for a listing of Weibull parameters and 90-percent confidence bounds on parameters.

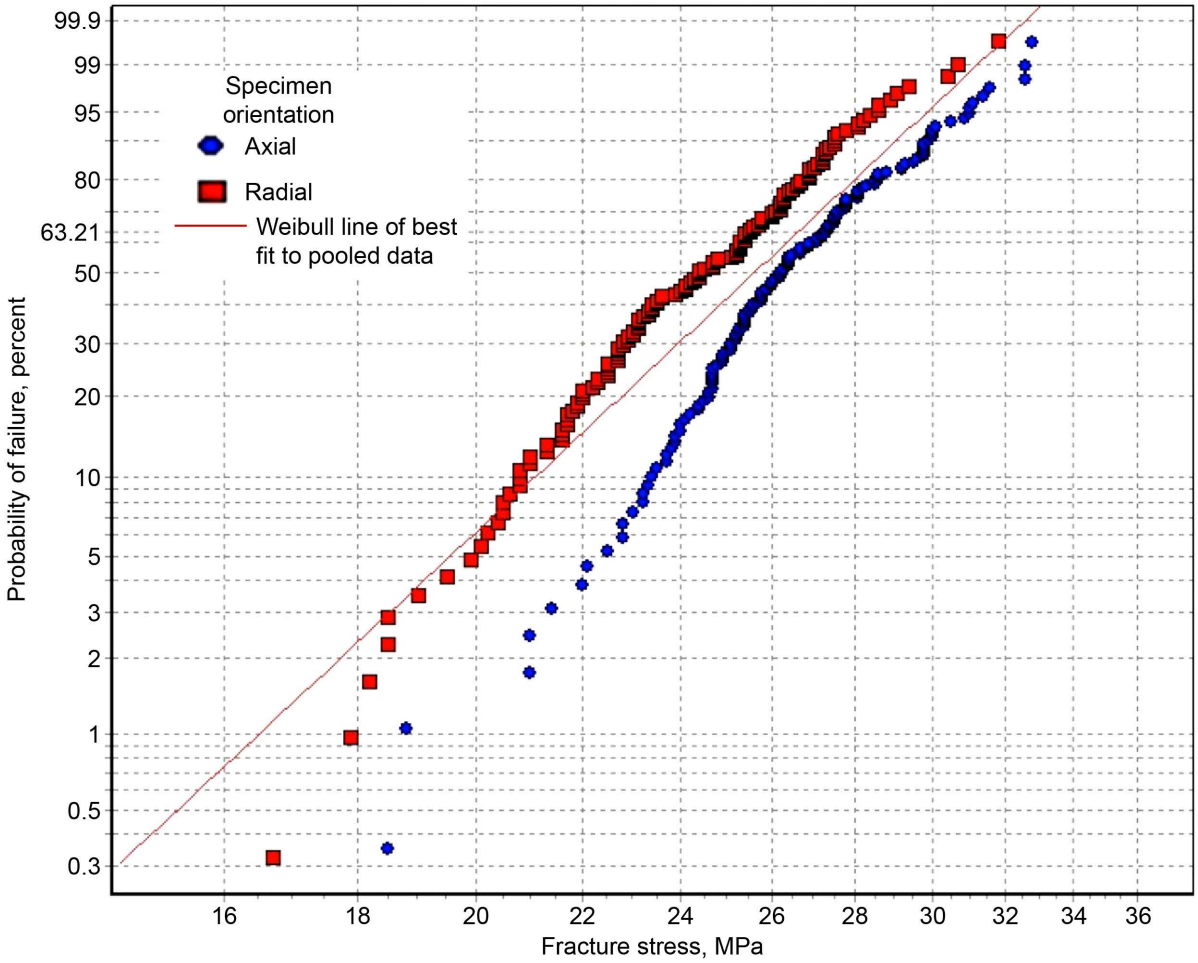

Figure 123.—Weibull plot of fracture stresses of pooled data from slabs 1 to 4 for flexure specimens (with linear-elastic stress response) from center of slabs, comparing axial and radial orientations.

The difference in Weibull moduli is not statistically significant in Figure 124 and is within what is reasonably expected from natural statistical variation.

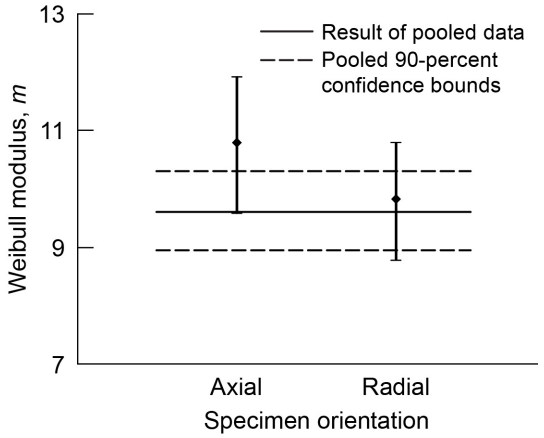

Figure 124.—Weibull modulus and 90-percent confidence bounds on pooled data from slabs 1 to 4 for flexure specimens (with linear-elastic stress response) from center of slabs, comparing axial and radial orientations. See Table 43 for a listing of Weibull parameters and 90-percent confidence bounds on parameters.

The difference in characteristic strengths is statistically significant in Figure 125—beyond what is expected from natural statistical variation. See Table 43 for a listing of Weibull parameters and 90-percent confidence bounds on parameters.

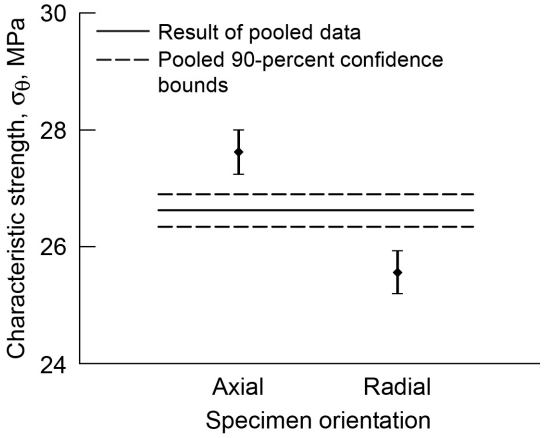

Figure 125.—Characteristic strength and 90-percent confidence bounds on pooled data from slabs 1 to 4 for flexure specimens (with linear-elastic stress response) from center of slabs, comparing axial and radial orientations. See Table 43 for a listing of Weibull parameters and 90-percent confidence bounds on parameters.

TABLE 43.—WEIBULL PARAMETERS AND 90-PERCENT CONFIDENCE BOUNDS ON POOLED DATA FROM SLABS 1 TO 4 FOR FLEXURE SPECIMENS (WITH LINEAR-ELASTIC STRESS RESPONSE) FROM CENTER OF SLABS, COMPARING AXIAL AND RADIAL ORIENTATIONS

Specimen type	Number of specimens	Weibull modulus, *m*		Characteristic strength, σ_θ, MPa	
		MLE biased[a]	90-percent confidence	MPa	90-percent confidence
Axial flexure	144	10.79	9.60/11.91	27.63	27.25/28.00
Radial flexure	156	9.82	8.78/10.79	25.56	25.20/25.93
Pooled	300	9.61	8.95/10.30	26.63	26.35/26.91

[a]Maximum-likelihood estimation.

In Figure 126, the radial specimens are weaker than axial specimens, and the plots for both data sets appear to have some nonlinearity.

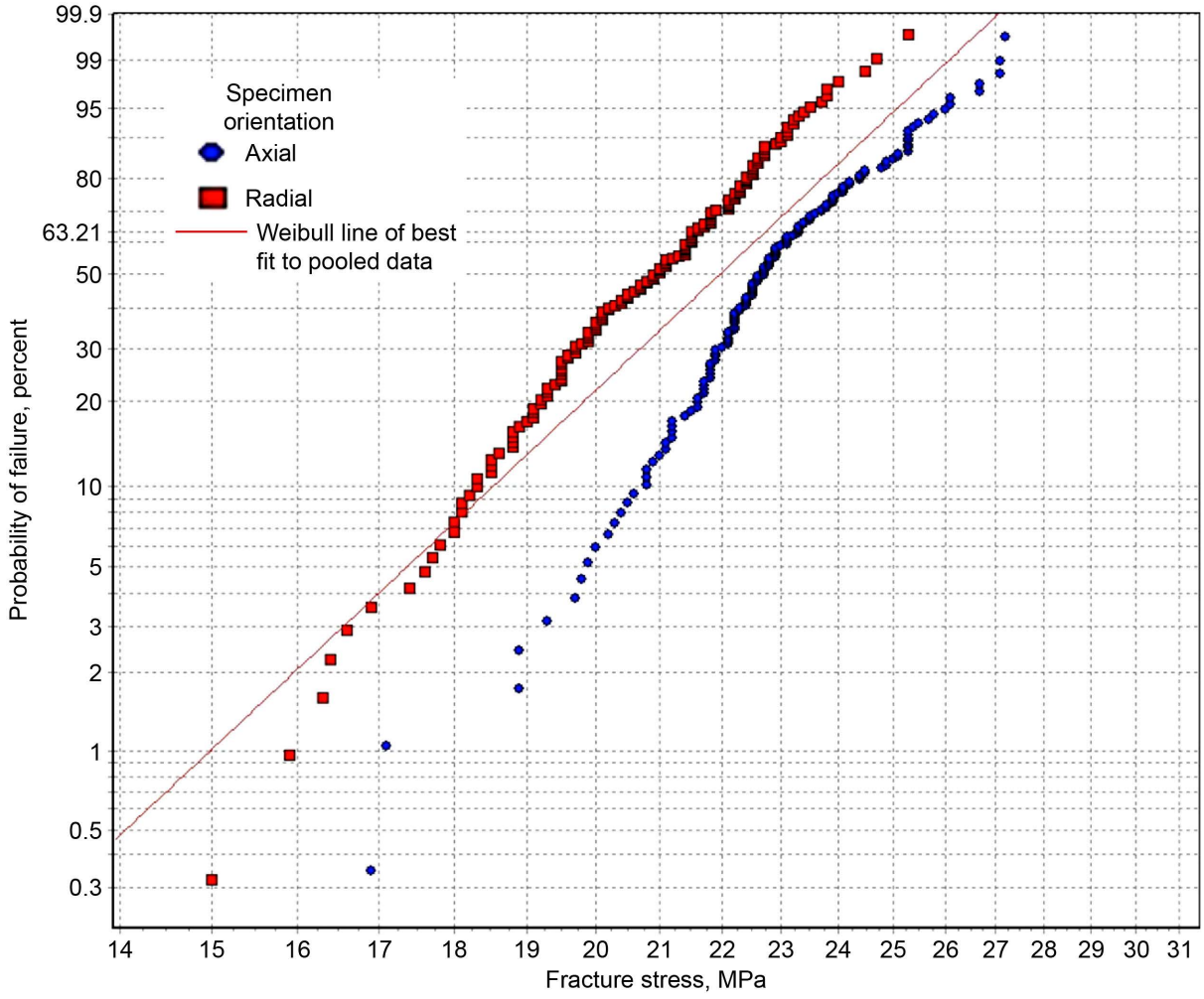

Figure 126.—Weibull plot of fracture stresses of pooled data from slabs 1 to 4 for flexure specimens (with nonlinear-elastic stress response) from center of slabs, comparing axial and radial orientations. See Table 44 for a listing of Weibull parameters and 90-percent confidence bounds on parameters.

The difference in Weibull moduli is not statistically significant in Figure 127 and is within what is reasonably expected from natural statistical variation, comparing axial and radial orientations.

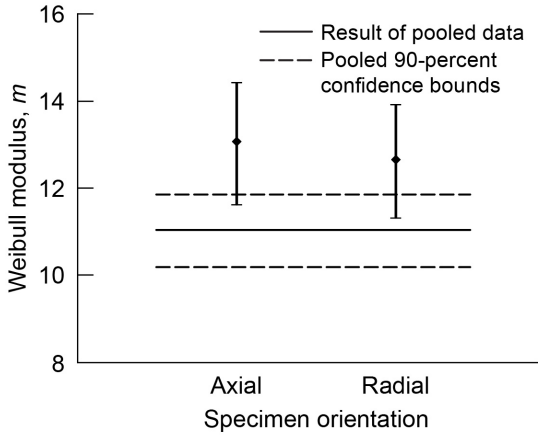

Figure 127.—Weibull modulus and 90-percent confidence bounds on pooled data from slabs 1 to 4 for flexure specimens (with nonlinear-elastic stress response) from center of slabs, comparing axial and radial orientations. See Table 44 for a listing of Weibull parameters and 90-percent confidence bounds on parameters.

The difference in characteristic strength is statistically significant in Figure 128—beyond what is expected from natural statistical variation. See Table 44 for a listing of Weibull parameters and 90-percent confidence bounds on parameters.

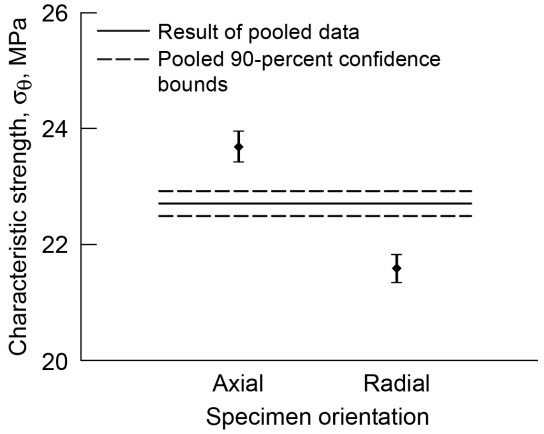

Figure 128.—Characteristic strength and 90-percent confidence bounds on pooled data from slabs 1 to 4 for flexure specimens (with nonlinear-elastic stress response) from center of slabs, comparing axial and radial orientations. See Table 44 for a listing of Weibull parameters and 90-percent confidence bounds on parameters.

TABLE 44.—WEIBULL PARAMETERS AND 90-PERCENT CONFIDENCE BOUNDS ON POOLED DATA FROM SLABS 1 TO 4 FOR FLEXURE SPECIMENS (WITH NONLINEAR-ELASTIC STRESS RESPONSE) FROM CENTER OF SLABS, COMPARING AXIAL AND RADIAL ORIENTATIONS

Specimen type	Number of specimens	Weibull modulus, *m*		Characteristic strength, σ_θ, MPa	
		MLE biased[a]	90-percent confidence	MPa	90-percent confidence
Axial flexure	144	13.07	11.62/14.42	23.69	23.43/23.96
Radial flexure	156	12.65	11.32/13.91	21.59	21.35/21.83
Pooled	300	11.04	10.19/11.85	22.71	22.5/22.93

[a]Maximum-likelihood estimation.

The data in Figure 129 have a distinctly linear appearance. The axial specimens are stronger than the radial specimens.

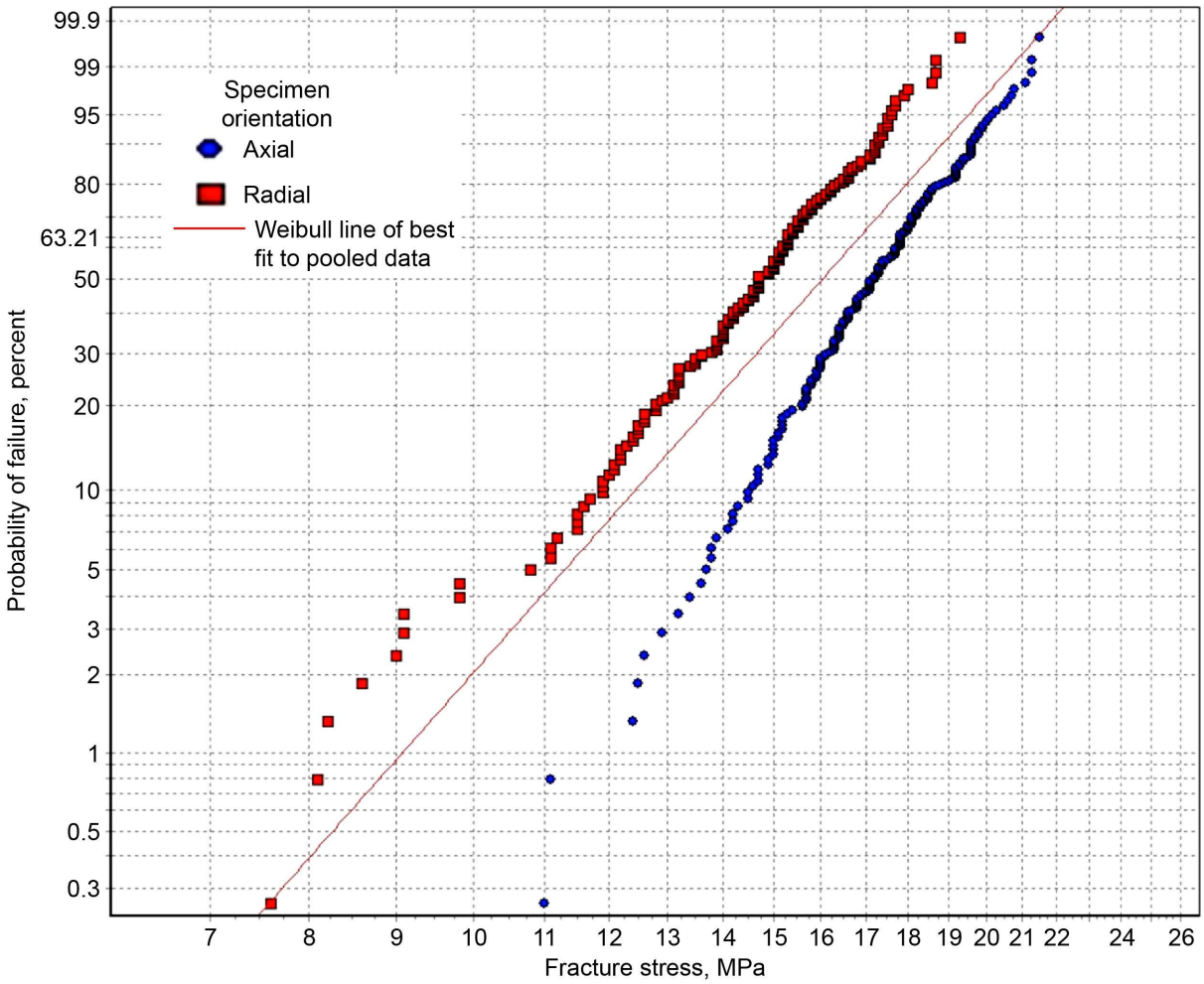

Figure 129.—Weibull plot of fracture stresses of pooled data from slabs 1 to 4 for small tensile specimens from edge of slabs, comparing axial and radial orientations. See Table 45 for a listing of Weibull parameters and 90-percent confidence bounds on parameters.

The difference in Weibull moduli is not large in Figure 130 but is possibly beyond what is expected from statistical uncertainty.

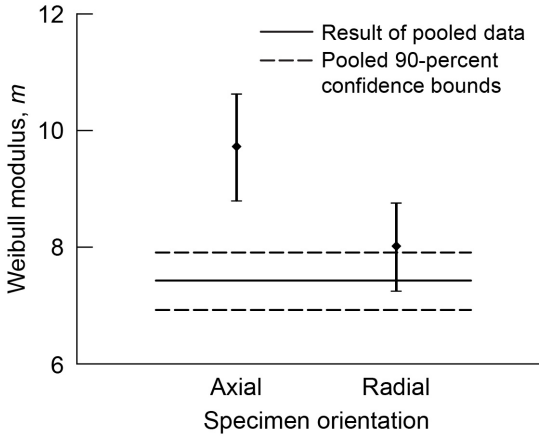

Figure 130.—Weibull modulus and 90-percent confidence bounds on pooled data from slabs 1 to 4 for small tensile specimens from edge of slabs, comparing axial and radial orientations. See Table 45 for a listing of Weibull parameters and 90-percent confidence bounds on parameters.

The difference in characteristic strength is statistically significant in Figure 131—beyond what is expected from statistical uncertainty. See Table 45 for a listing of Weibull parameters and 90-percent confidence bounds on parameters.

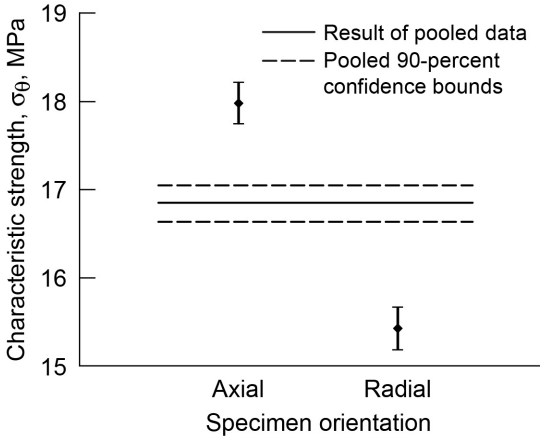

Figure 131.—Characteristic strength and 90-percent confidence bounds on pooled data from slabs 1 to 4 for small tensile specimens from edge of slabs. See Table 45 for a listing of Weibull parameters and 90-percent confidence bounds on parameters.

TABLE 45.—WEIBULL PARAMETERS AND 90-PERCENT CONFIDENCE BOUNDS ON POOLED DATA FROM SLABS 1 TO 4 FOR SMALL TENSILE SPECIMENS FROM EDGE OF SLABS, COMPARING AXIAL AND RADIAL ORIENTATIONS

Specimen type	Number of specimens	Weibull modulus, *m*		Characteristic strength, σ_θ, MPa	
		MLE biased[a]	90-percent confidence	MPa	90-percent confidence
Axial small tensile	190	9.73	8.80/10.62	17.98	17.75/18.22
Radial small tensile	190	8.02	7.25/8.75	15.43	15.19/15.67
Pooled	380	7.43	6.93/7.91	16.85	16.64/17.05

[a]Maximum-likelihood estimation.

In Figure 132, the data for both the axial and radial specimens appear to be reasonably linear, but the slope of the lines appears to be different. The radial specimens are stronger than the axial specimens.

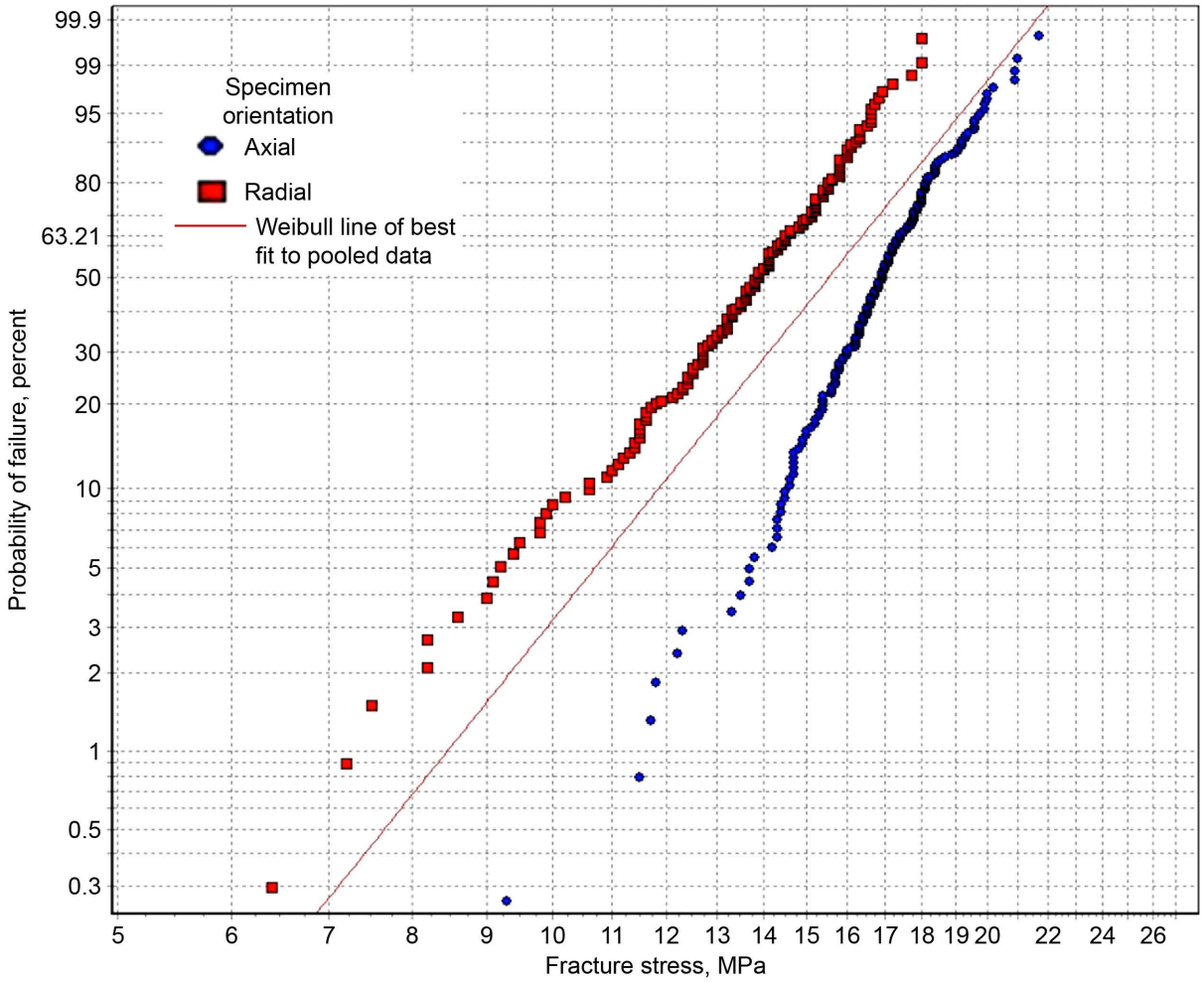

Figure 132.—Weibull plot of fracture stresses of pooled data from slabs 1 to 4 for large tensile specimens from edge of slabs, comparing axial and radial orientations. See Table 46 for a listing of Weibull parameters and 90-percent confidence bounds on parameters.

The difference in Weibull moduli appears to be statistically significant in Figure 133—beyond what is expected from natural statistical variation.

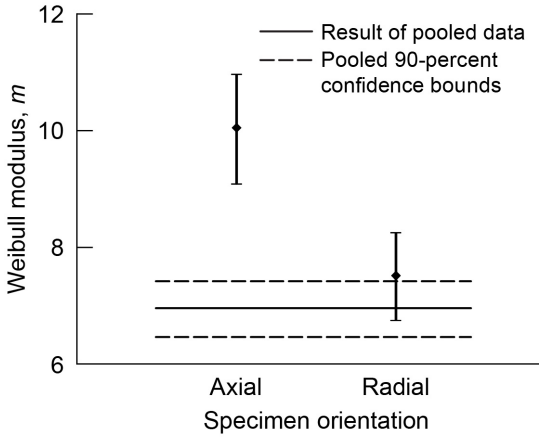

Figure 133.—Weibull modulus and 90-percent confidence bounds on pooled data from slabs 1 to 4 for large tensile specimens from edge of slabs, comparing axial and radial orientations. See Table 46 for a listing of Weibull parameters and 90-percent confidence bounds on parameters.

The difference in characteristic strength is statistically significant in Figure 134—beyond what is expected from natural statistical variation. See Table 46 for a listing of Weibull parameters and 90-percent confidence bounds on parameters.

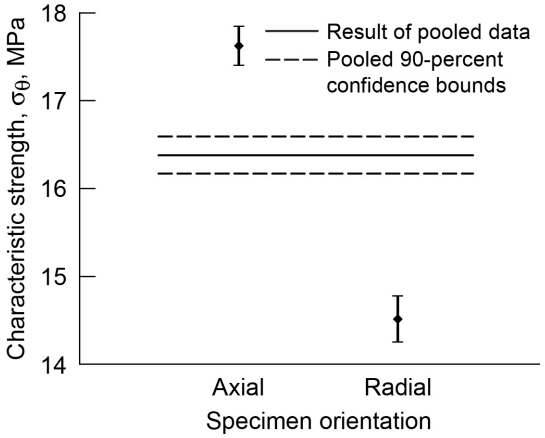

Figure 134.—Characteristic strength and 90-percent confidence bounds on pooled data from slabs 1 to 4 for large tensile specimens from edge of slabs, comparing axial and radial orientations. See Table 46 for a listing of Weibull parameters and 90-percent confidence bounds on parameters.

TABLE 46.—WEIBULL PARAMETERS AND 90-PERCENT CONFIDENCE BOUNDS ON POOLED DATA FROM SLABS 1 TO 4 FOR LARGE TENSILE SPECIMENS FROM EDGE OF SLABS, COMPARING AXIAL AND RADIAL ORIENTATIONS

Specimen type	Number of specimens	Weibull modulus, *m*		Characteristic strength, σ_θ, MPa	
		MLE biased[a]	90-percent confidence	MPa	90-percent confidence
Axial large tensile	191	10.05	9.09/10.96	17.63	17.41/17.85
Radial large tensile	168	7.52	6.75/8.25	14.52	14.26/14.78
Pooled	359	6.96	6.47/7.42	16.38	16.17/16.60

[a]Maximum-likelihood estimation.

In Figure 135, there is a knee in the data for small probability of failure for the radial specimens. The data for the axial specimens have a nonlinear appearance, and the axial specimens are stronger than the radial specimens.

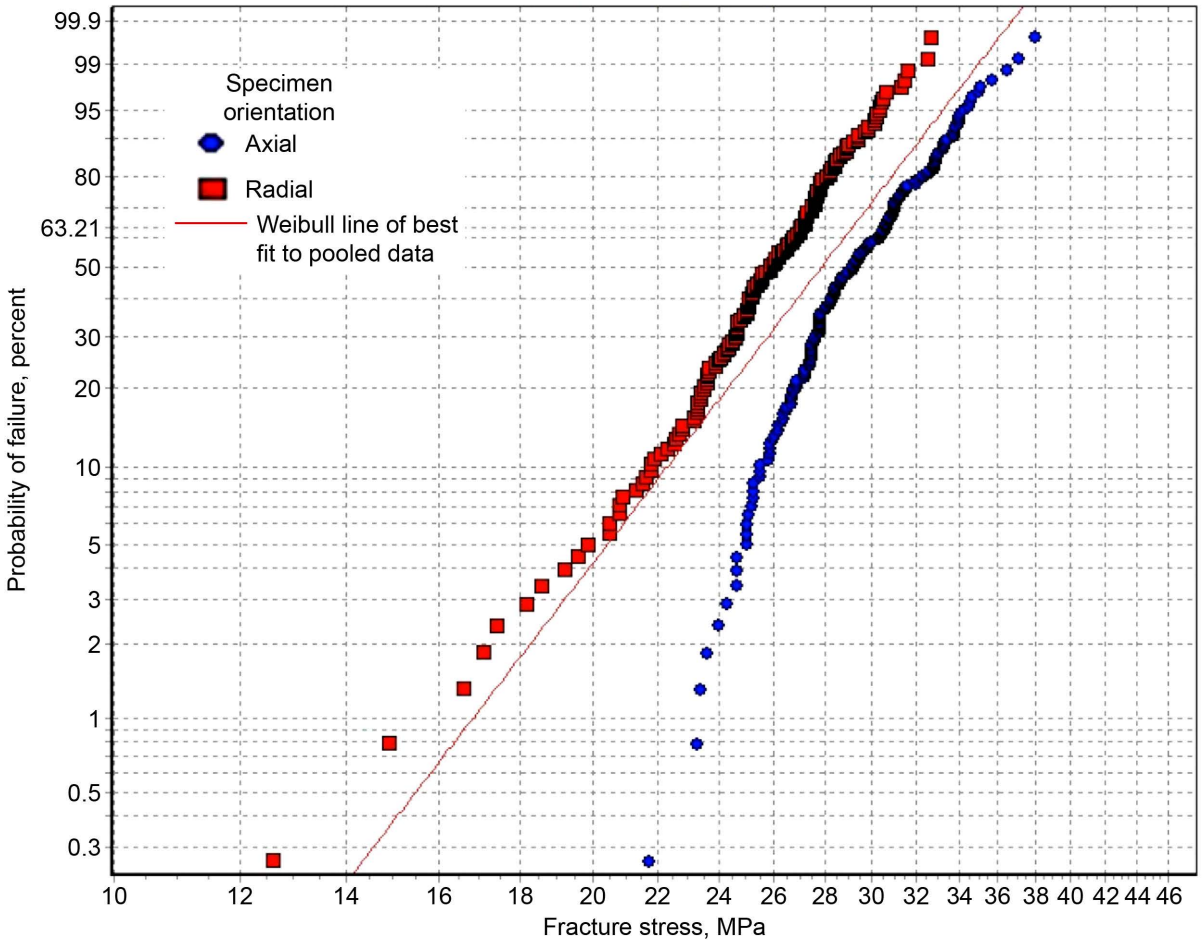

Figure 135.—Weibull plot of fracture stresses of pooled data from slabs 1 to 4 for flexure specimens (with linear-elastic stress response) from edge of slabs, comparing axial and radial orientations. See Table 47 for a listing of Weibull parameters and 90-percent confidence bounds on parameters.

It is unexpected that the difference in Weibull moduli is within statistical uncertainty in Figure 136 considering the different nature of the curves in Figure 135 at low probabilities of failure. The difference in the tails of the distribution does not have a large effect in the overall pooling of the data (assuming that there is a single-flaw population instead of a bimodal distribution of competing failure modes).

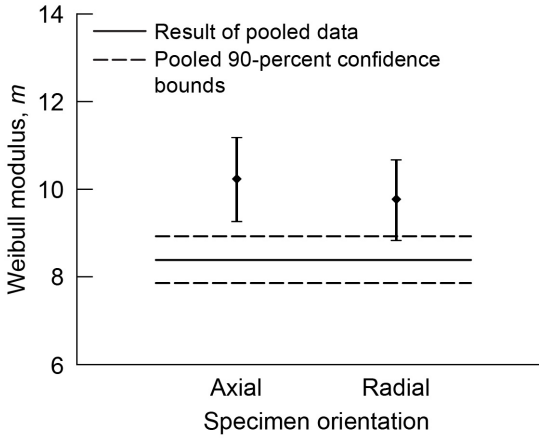

Figure 136.—Weibull modulus and 90-percent confidence bounds on pooled data from slabs 1 to 4 for flexure specimens (with linear-elastic stress response) from edge of slabs, comparing axial and radial orientations. See Table 47 for a listing of Weibull parameters and 90-percent confidence bounds on parameters.

The difference in characteristic strength is statistically significant in Figure 137—beyond what is expected from natural statistical variation. See Table 47 for a listing of Weibull parameters and 90-percent confidence bounds on parameters.

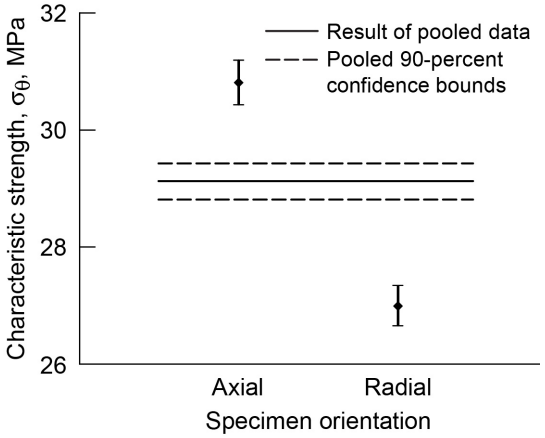

Figure 137.—Characteristic strength and 90-percent confidence bounds on pooled data from slabs 1 to 4 for flexure specimens (with linear-elastic stress response) from edge of slabs, comparing axial and radial orientations. See Table 47 for a listing of Weibull parameters and 90-percent confidence bounds on parameters.

TABLE 47.—WEIBULL PARAMETERS AND 90-PERCENT CONFIDENCE BOUNDS ON POOLED DATA FROM SLABS 1 TO 4 FOR FLEXURE SPECIMENS (WITH LINEAR-ELASTIC STRESS RESPONSE) FROM EDGE OF SLABS, COMPARING AXIAL AND RADIAL ORIENTATIONS

Specimen type	Number of specimens	Weibull modulus, m		Characteristic strength, σ_θ, MPa	
		MLE biased[a]	90-percent confidence	MPa	90-percent confidence
Axial flexure	192	10.24	9.27/11.17	30.82	30.44/31.20
Radial flexure	190	9.78	8.84/10.66	27.00	26.66/27.35
Pooled	382	8.39	7.87/8.92	29.13	28.82/29.44

[a]Maximum-likelihood estimation.

In Figure 138, there is a knee in the data for small probability of failure for the radial specimens. The data for the axial specimens have a nonlinear appearance, and the axial specimens are stronger than the radial specimens.

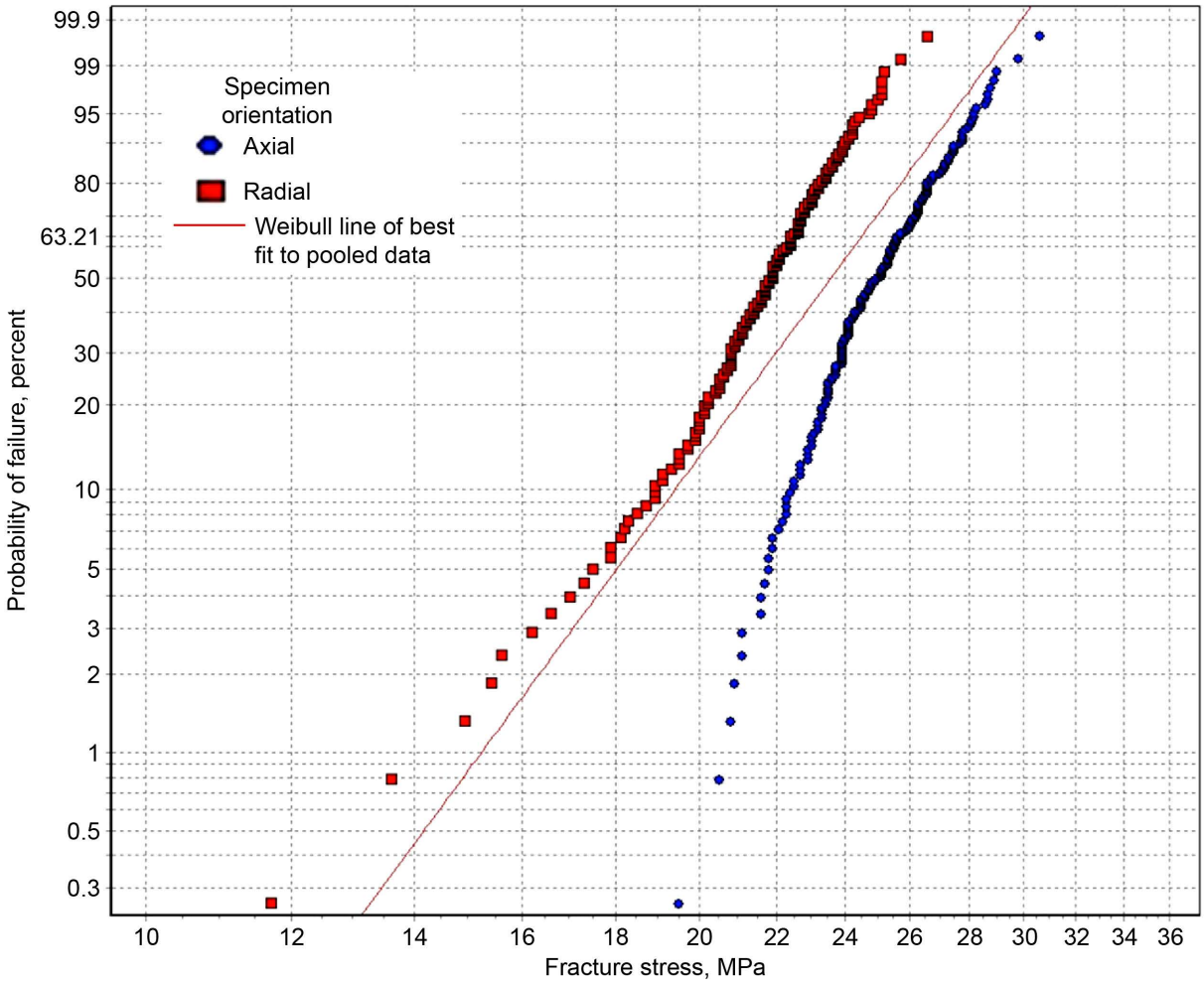

Figure 138.—Weibull plot of fracture stresses of pooled data from slabs 1 to 4 for flexure specimens (with nonlinear-elastic stress response) from edge of slabs, comparing axial and radial orientations. See Table 48 for a listing of Weibull parameters and 90-percent confidence bounds on parameters.

It is unexpected that the difference in Weibull moduli is within statistical uncertainty in Figure 139 considering the different nature of the curves in Figure 138 at low probabilities of failure. The difference in the tails of the distribution does not have a large effect in the overall pooling of the data (assuming that there is a single-flaw population instead of a bimodal distribution of competing failure modes).

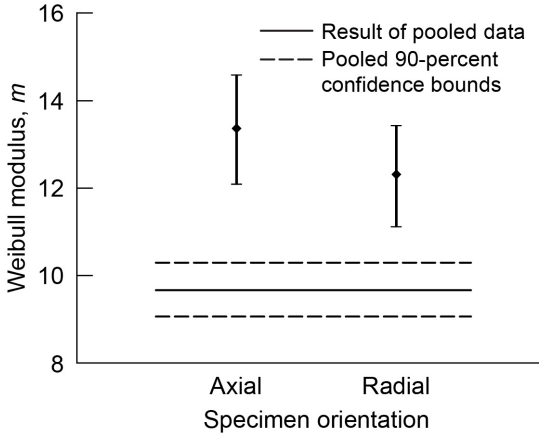

Figure 139.—Weibull modulus and 90-percent confidence bounds on pooled data from slabs 1 to 4 for flexure specimens (with nonlinear-elastic stress response) from edge of slabs, comparing axial and radial orientations. See Table 48 for a listing of Weibull parameters and 90-percent confidence bounds on parameters.

The difference in characteristic strength is statistically significant in Figure 140—beyond what is expected from natural statistical variation. See Table 48 for a listing of Weibull parameters and 90-percent confidence bounds on parameters.

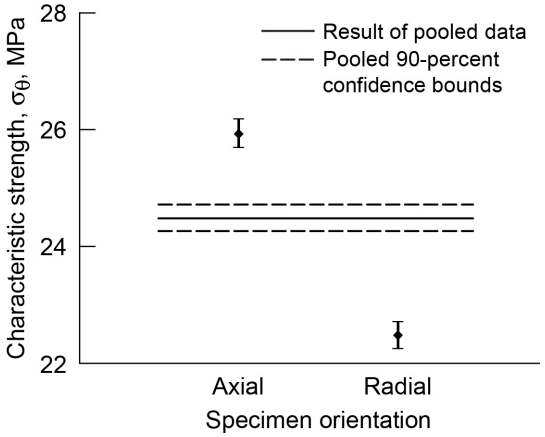

Figure 140.—Characteristic strength and 90-percent confidence bounds on pooled data from slabs 1 to 4 for flexure specimens (with nonlinear-elastic stress response) from edge of slabs, comparing axial and radial orientations. See Table 48 for a listing of Weibull parameters and 90-percent confidence bounds on parameters.

TABLE 48.—WEIBULL PARAMETERS AND 90-PERCENT CONFIDENCE BOUNDS ON POOLED DATA FROM SLABS 1 TO 4 FOR FLEXURE SPECIMENS (WITH NONLINEAR-ELASTIC STRESS RESPONSE) FROM EDGE OF SLABS, COMPARING AXIAL AND RADIAL ORIENTATIONS

Specimen type	Number of specimens	Weibull modulus, m		Characteristic strength, σ_0, MPa	
		MLE biased[a]	90-percent confidence	MPa	90-percent confidence
Axial flexure	192	13.36	12.09/14.57	25.94	25.70/26.19
Radial flexure	190	12.31	11.13/13.43	22.49	22.26/22.72
Pooled	382	9.67	9.07/10.30	24.49	24.27/24.72

[a]Maximum-likelihood estimation.

In Figure 141, the largest difference in strength is seen between axial specimens from the edge of the graphite log and radial specimens from the center of the log. All the data appear to have reasonably linear behavior.

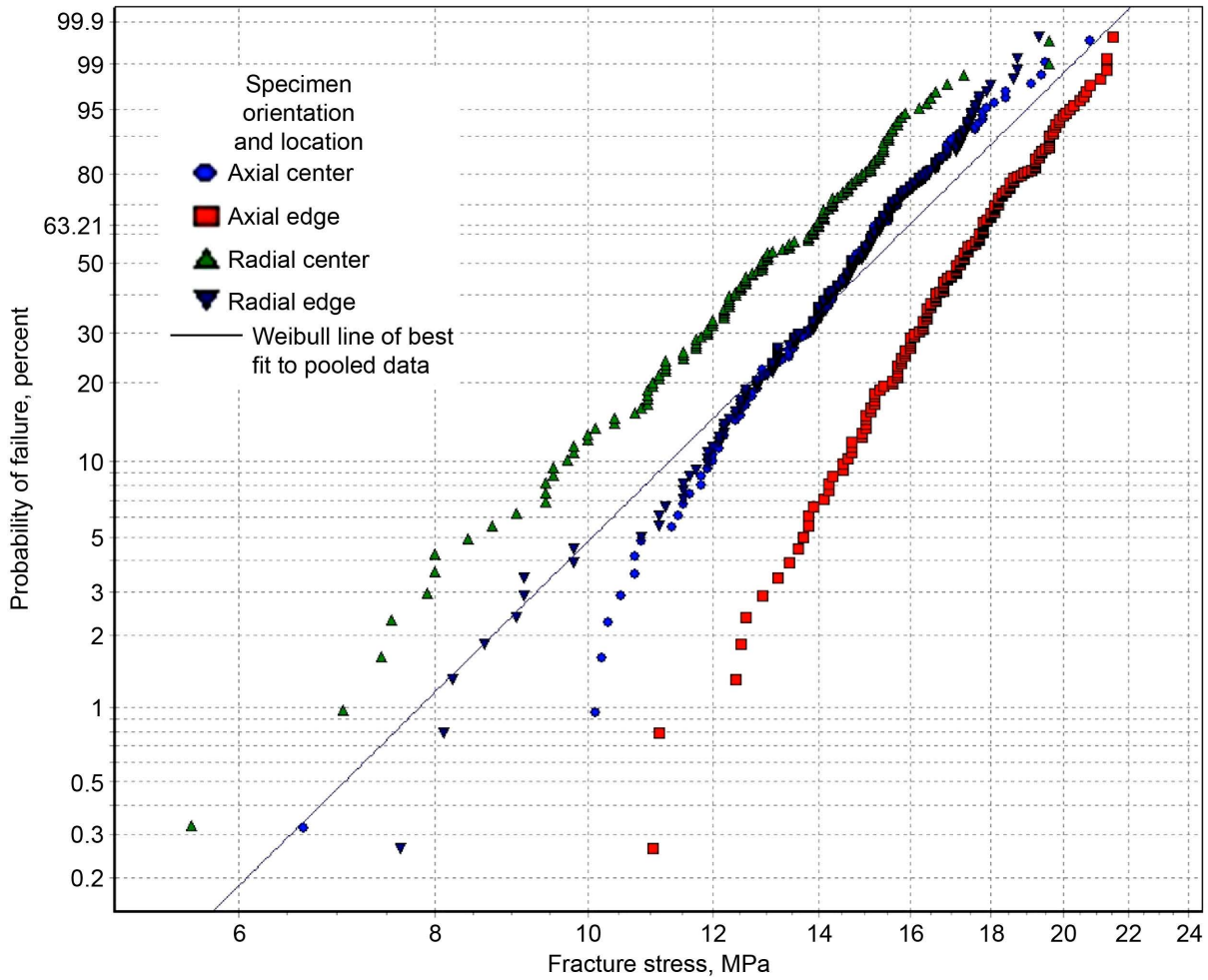

Figure 141.—Weibull plot of fracture stresses of pooled data from slabs 1 to 4 for small tensile specimens, showing effects of orientation and location.

In Figure 142, Weibull moduli for specimens from the center of the graphite log seem to be lower than for specimens from the edge of the log, and Weibull moduli for radial specimens seem to be lower than for axial specimens. The largest difference is between axial specimens from the edge of the log and radial specimens from the center of the log. The Weibull moduli are relatively similar for axial specimens from the center of the log and radial specimens from the edge of the log.

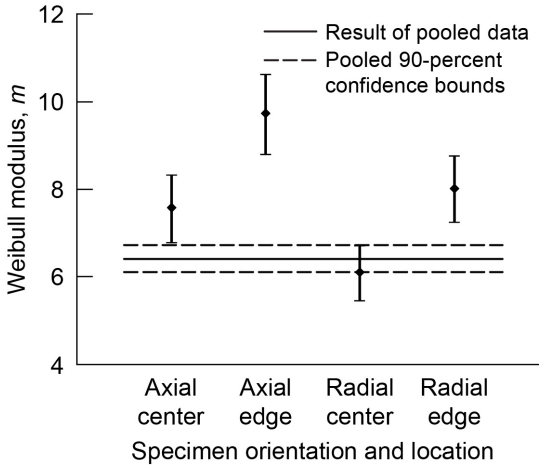

Figure 142.—Weibull modulus and 90-percent confidence bounds on pooled data from slabs 1 to 4 for small tensile specimens, showing effects of orientation and location. See Table 49 for a listing of Weibull parameters and 90-percent confidence bounds on parameters.

In Figure 143, the characteristic strength seems to be lower for specimens from the center of the graphite log than for specimens from the edge of the log, and it seems to be lower for radial specimens than for axial specimens. The largest difference is between axial specimens from the edge of the log and radial specimens from the center of the log. The characteristic strength is similar for axial specimens from the center of the log and radial specimens from the edge of the log.

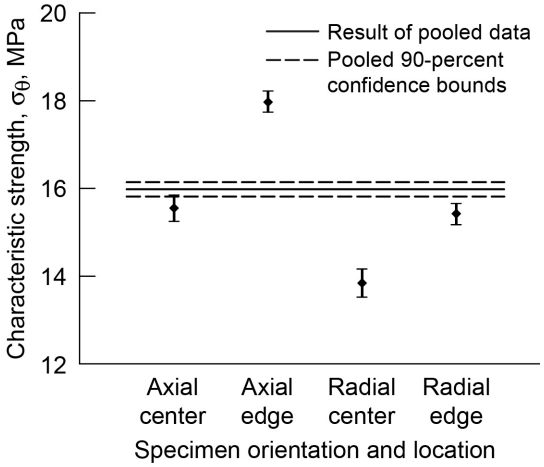

Figure 143.—Characteristic strength and 90-percent confidence bounds on pooled data from slabs 1 to 4 for small tensile specimens, showing effects of orientation and location. See Table 49 for a listing of Weibull parameters and 90-percent confidence bounds on parameters.

Figures 142 and 143 seem to show an interesting correlation between the Weibull modulus and the characteristic strength. When the Weibull modulus is higher, the characteristic strength tends to be higher. This trend would be expected if residual compressive stresses were present. A residual compressive stress would tend to increase the applied stress required for fracture and would also truncate the Weibull distribution with a threshold stress (a stress below which fracture could not occur) such that it would follow a three-parameter Weibull distribution. Fitting a two-parameter Weibull distribution to these data would increase the estimated Weibull modulus (because of the truncated tail of the distribution) in comparison to a situation where no residual stresses were present. It is possible that a similar trend would occur in the presence of a rising *R*-curve. See Table 49 for a listing of Weibull parameters and 90-percent confidence bounds on parameters.

TABLE 49.—WEIBULL PARAMETERS AND 90-PERCENT CONFIDENCE BOUNDS ON POOLED DATA FROM SLABS 1 TO 4 FOR SMALL TENSILE SPECIMENS, SHOWING EFFECTS OF ORIENTATION AND LOCATION

Specimen type	Number of specimens	Weibull modulus, *m*		Characteristic strength, σ_θ, MPa	
		MLE biased[a]	90-percent confidence	MPa	90-percent confidence
Axial center	156	7.58	6.78/8.33	15.56	15.27/15.85
Axial edge	190	9.73	8.80/10.62	17.98	17.75/18.22
Radial center	153	6.11	5.46/6.72	13.85	13.53/14.17
Radial edge	190	8.02	7.25/8.75	15.43	15.19/15.67
Pooled	689	6.42	6.11/6.73	15.99	15.83/16.15

[a]Maximum-likelihood estimation.

In Figure 144, the largest difference in strength is seen between axial specimens from the edge of the graphite log and radial specimens from the center of the log. At lower probabilities of failure, the fracture strength is significantly higher for radial specimens than for axial specimens.

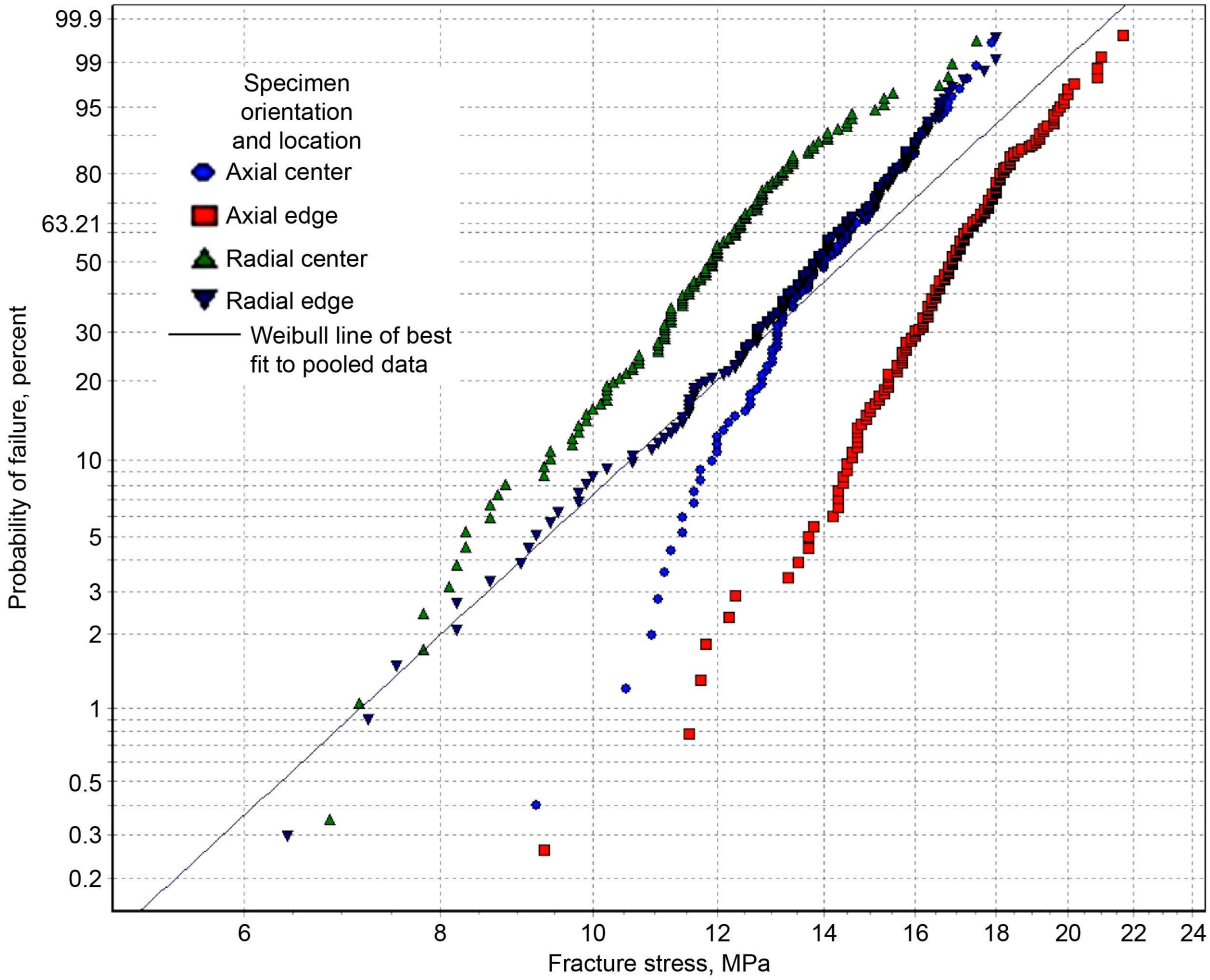

Figure 144.—Weibull plot of fracture stresses of pooled data from slabs 1 to 4 for large tensile specimens, showing effects of orientation and location.

In Figure 145, the Weibull moduli are somewhat lower for specimens from the center of the graphite log than for specimens from the edge of the log, and the Weibull moduli are lower for radial specimens than for axial specimens. The largest difference is between axial specimens from the edge of the log and the radial specimens from the center of the log.

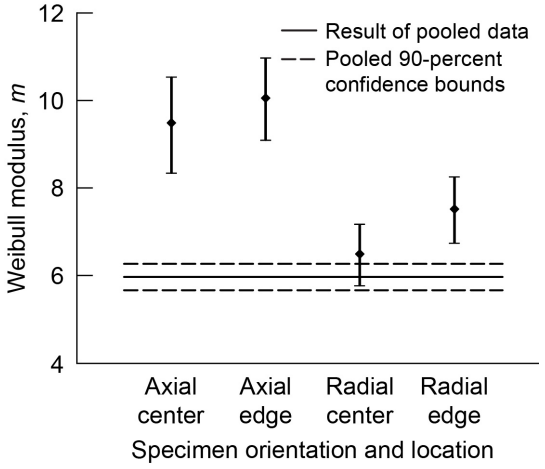

Figure 145.—Weibull modulus and 90-percent confidence bounds on pooled data from slabs 1 to 4 for large tensile specimens, showing effects of orientation and location. See Table 50 for a listing of Weibull parameters and 90-percent confidence bounds on parameters.

In Figure 146, the characteristic strength is lower for specimens from the center of the graphite log than for specimens from the edge of the log, and it seems to be lower for radial specimens than for axial specimens. The largest difference is between axial specimens at the edge of the log and the radial specimens at the center of the log. The characteristic strength is relatively similar for axial specimens from the center of the log and radial specimens from the edge of the log.

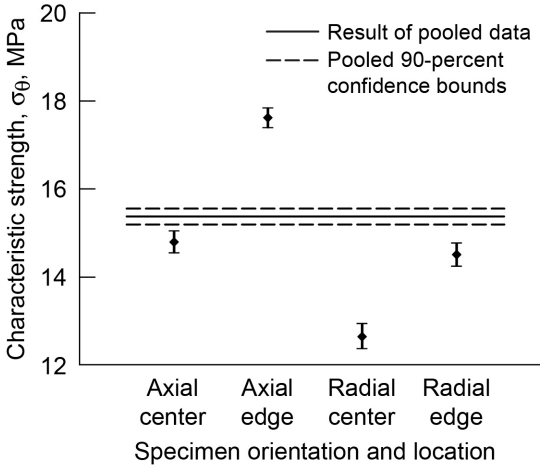

Figure 146.—Characteristic strength and 90-percent confidence bounds on pooled data from slabs 1 to 4 for large tensile specimens, showing effects of orientation and location. See Table 50 for a listing of Weibull parameters and 90-percent confidence bounds on parameters.

Figures 145 and 146 seem to show an interesting correlation between the Weibull modulus and the characteristic strength. When the Weibull modulus is higher, the characteristic strength tends to be higher. This trend would be expected if residual compressive stresses were present. A residual compressive stress would tend to increase the applied stress required for fracture and would also truncate the Weibull distribution with a threshold stress (a stress below which fracture could not occur) such that it would follow a three-parameter Weibull distribution. Fitting a two-parameter Weibull distribution to these data would increase the estimated Weibull modulus (because of the truncated tail of the distribution) in comparison to a situation where no residual stresses were present. It is possible that a similar trend would also occur in the presence of a rising *R*-curve. Note also that at lower probabilities of failure the axial specimens are significantly stronger than the radial specimens. In other words, the tails of the distributions at low probabilities of failure show what appear to be distinctly different behaviors. See Table 50 for a listing of Weibull parameters and 90-percent confidence bounds on parameters.

TABLE 50.—WEIBULL PARAMETERS AND 90-PERCENT CONFIDENCE BOUNDS ON POOLED DATA FROM SLABS 1 TO 4 FOR AXIAL AND RADIAL LARGE TENSILE SPECIMENS, SHOWING EFFECTS OF ORIENTATION AND LOCATION

Specimen type	Number of specimens	Weibull modulus, *m*		Characteristic strength, σ_θ, MPa	
		MLE biased[a]	90-percent confidence	MPa	90-percent confidence
Axial center	126	9.47	8.34/10.52	14.80	14.56/15.05
Axial edge	191	10.05	9.09/10.96	17.63	17.41/17.85
Radial center	143	6.50	5.78/7.17	12.65	12.37/12.94
Radial edge	168	7.52	6.75/8.25	14.52	14.26/14.78
Pooled	628	5.97	5.67/6.27	15.38	15.20/15.56

[a]Maximum-likelihood estimation.

In Figure 147, the largest difference in strength is seen between axial specimens from the edge of the graphite log and radial specimens from the center of the log. At lower probabilities of failure, the axial specimens are stronger than the radial specimens. Note also the nonlinear behavior of the axial specimens.

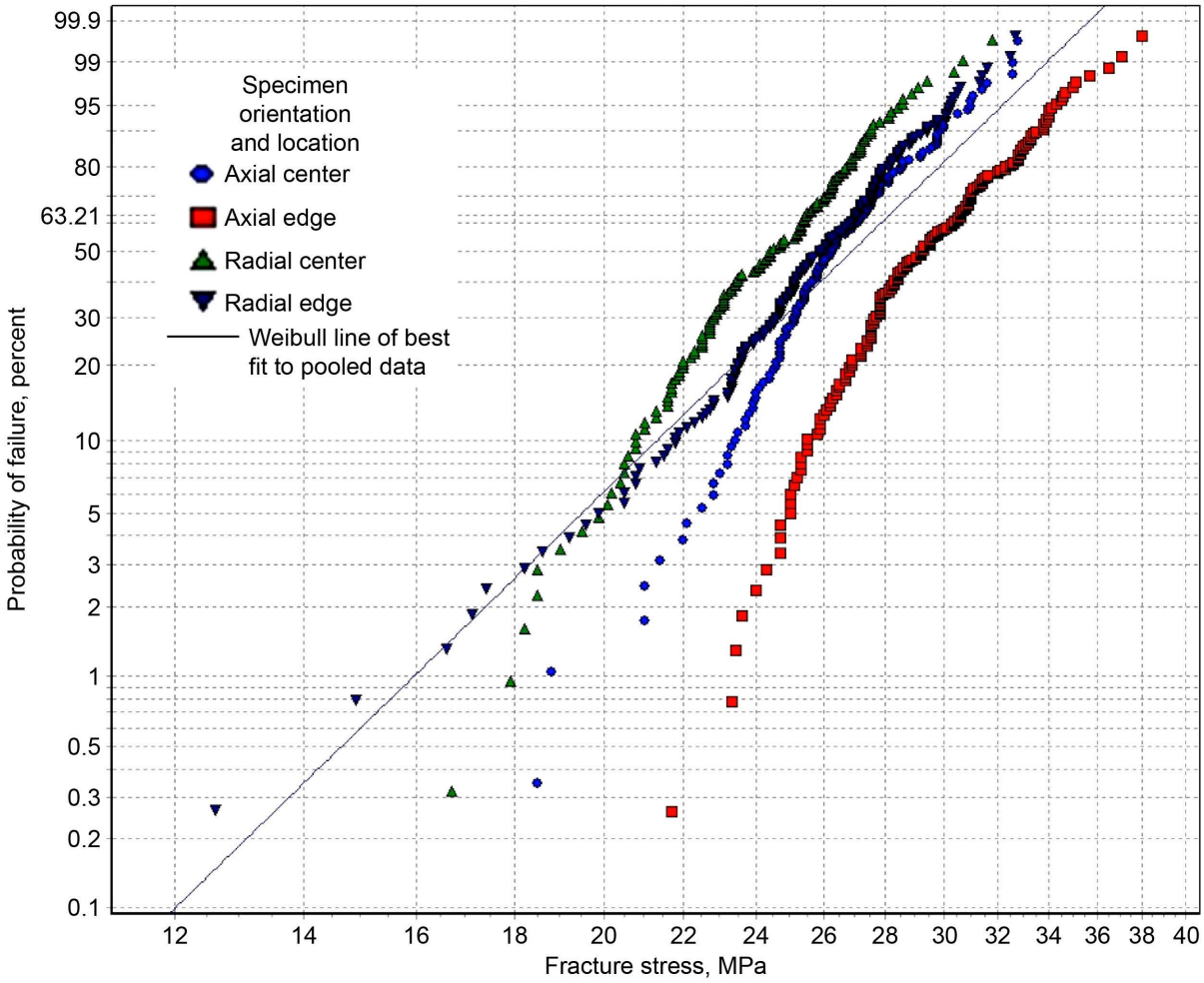

Figure 147.—Weibull plot of fracture stresses of pooled data from slabs 1 to 4 for flexure specimens (with linear-elastic stress response), showing effects of orientation and location.

In Figure 148, Weibull moduli seem to be higher for the axial specimens than for the radial specimens, but otherwise all the Weibull moduli are fairly similar or within expected statistical noise. The trends in the Figure 147 are somewhat similar to the trends seen in Figures 141 and 144; however, in Figure 148 the differences in the Weibull moduli are not as apparent as in Figures 142 and 145. Visual cues from the Weibull plots and the values of the estimated Weibull parameters must both be considered when attempting to interpret the data.

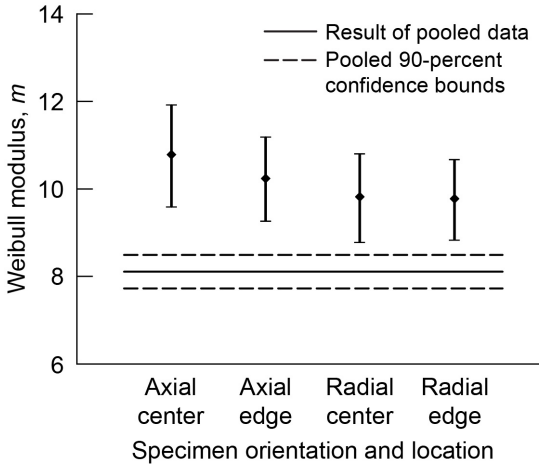

Figure 148.—Weibull modulus and 90-percent confidence bounds on pooled data from slabs 1 to 4 for flexure specimens (with linear-elastic stress response), showing effects of orientation and location. See Table 51 for a listing of Weibull parameters and 90-percent confidence bounds on parameters.

In Figure 149, the characteristic strength seems to be lower for specimens from the center of the graphite log than for specimens from the edge of the log, and it seems to be lower for radial specimens than for axial specimens. The largest difference is between axial specimens from the edge of the log and radial specimens from the center of the log. The characteristic strengths are closer for axial specimens from the center of the log and radial specimens from the edge of the log.

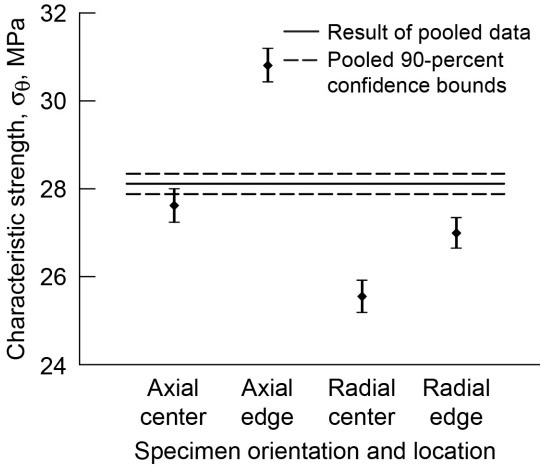

Figure 149.—Characteristic strength and 90-percent confidence bounds on pooled data from slabs 1 to 4 for flexure specimens (with linear-elastic stress response), showing effects of orientation and location. See Table 51 for a listing of Weibull parameters and 90-percent confidence bounds on parameters.

In Figures 148 and 149, the correlation between the Weibull modulus and the characteristic strength is not as strong as in Figures 142 and 143 and in Figures 145 and 146. Weibull moduli and characteristic strengths are higher for the axial specimens than for the radial specimens. However, the difference between the Weibull moduli for the axial and radial specimens does not appear to be statistically different with a high level of confidence because of the overlap of the confidence bounds. Hypothesizing that a correlation between higher Weibull modulus and higher characteristic strength is indicative of residual stresses or rising *R*-curve behavior is more difficult with this set of data. However, the trend in the data for Figure 147 for the axial specimens at lower probabilities of failure is indicative of three-parameter Weibull behavior. Therefore—even though it is not as clear in Figures 148 and 149 as it is in Figures 142 and 143 and in Figures 145 and 146—Figures 148 and 149 do not necessarily invalidate the general observation that, when the Weibull modulus is higher, the characteristic strength tends to be higher. See Table 51 for a listing of Weibull parameters and 90-percent confidence bounds on parameters.

TABLE 51.—WEIBULL PARAMETERS AND 90-PERCENT CONFIDENCE BOUNDS ON POOLED DATA FROM SLABS 1 TO 4 FOR FLEXURE SPECIMENS (WITH LINEAR-ELASTIC STRESS RESPONSE), SHOWING EFFECTS OF ORIENTATION AND LOCATION

Specimen type	Number of specimens	Weibull modulus, *m*		Characteristic strength, σ_θ, MPa	
		MLE biased[a]	90-percent confidence	MPa	90-percent confidence
Axial center	144	10.79	9.60/11.91	27.63	27.25/28.00
Axial edge	192	10.24	9.27/11.17	30.82	30.44/31/20
Radial center	156	9.82	8.78/10.79	25.56	25.20/25.93
Radial edge	190	9.78	8.84/10.66	27.00	26.66/27.35
Pooled	682	8.11	7.74/8.49	28.12	27.89/28.35

[a]Maximum-likelihood estimation.

In Figure 150, the largest difference in strength is between the axial specimens from the edge of the graphite log and the radial specimens from the center of the log. At lower probabilities of failure, the axial specimens are stronger than the radial specimens. Note also the nonlinear behavior of the axial specimens.

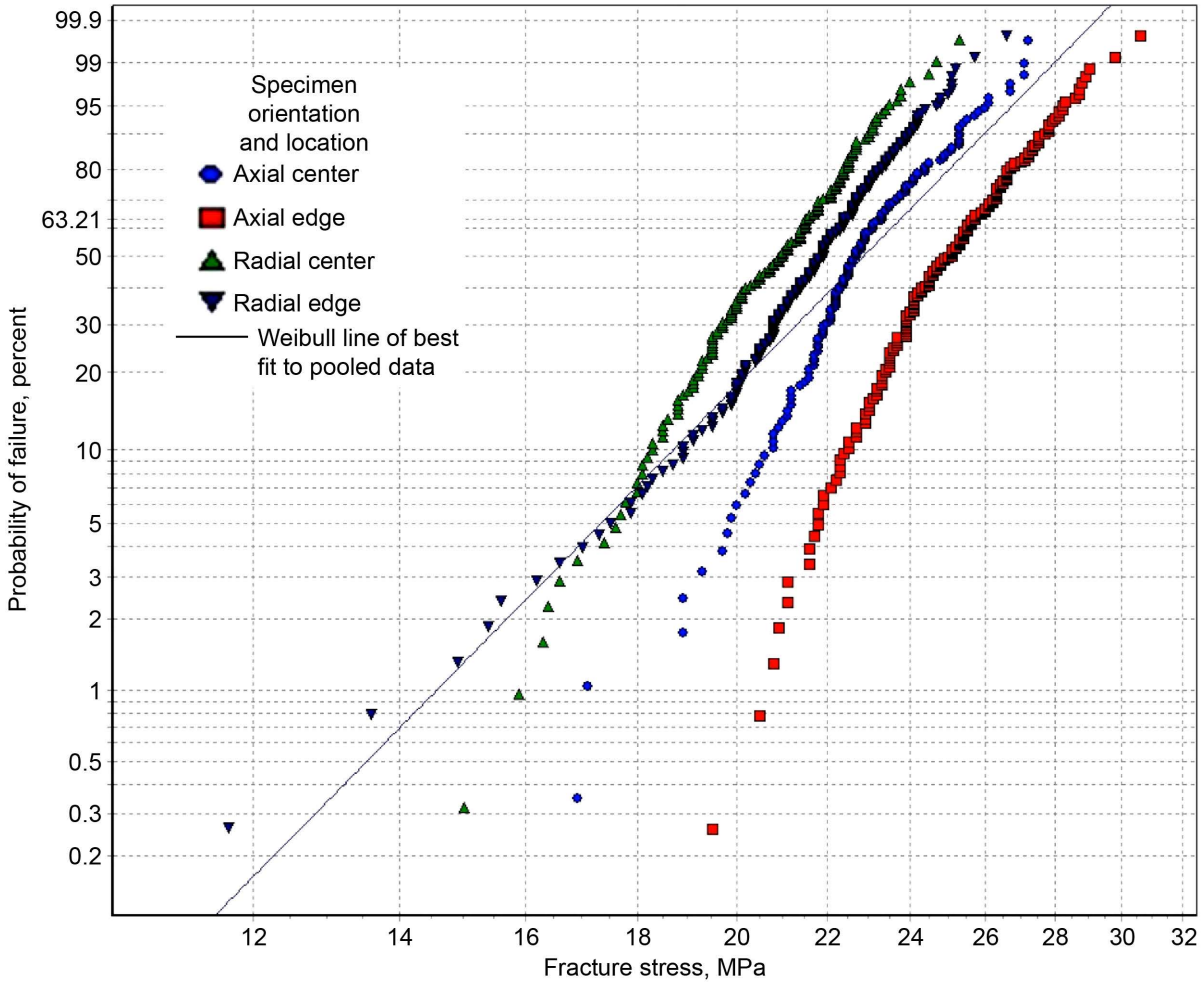

Figure 150.—Weibull plot of fracture stresses of pooled data from slabs 1 to 4 for flexure specimens (with nonlinear-elastic stress response), showing effects of orientation and location.

In Figure 151, the Weibull moduli seem to be slightly higher for the axial specimens than for the radial specimens, but otherwise all the Weibull moduli are fairly similar or within expected statistical noise. The trends in the Figure 150 are somewhat similar to the trends seen in Figures 141 and 144; however, the differences in the Weibull moduli in Figure 151 are not as apparent as in Figures 142 and 145. Visual cues from the Weibull plots and the values of the estimated Weibull parameters must both be considered when attempting to interpret the data.

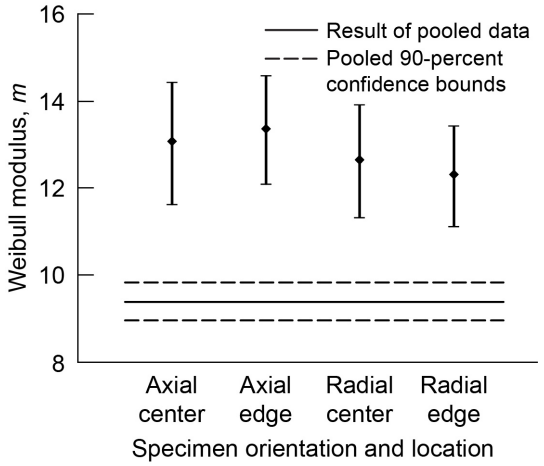

Figure 151.—Weibull modulus and 90-percent confidence bounds on pooled data from slabs 1 to 4 for flexure specimens (with nonlinear-elastic stress response), showing effects of orientation and location. See Table 52 for a listing of Weibull parameters and 90-percent confidence bounds on parameters.

In Figure 152, the characteristic strength seems to be lower for specimens from the center of the graphite log than for specimens from the edge of the log, and it seems to be lower for radial specimens than for axial specimens. The largest difference is between axial specimens from the edge of the log and the radial specimens from the center of the log. The characteristic strengths are closer for axial specimens from the center of the log and radial specimens from the edge of the log.

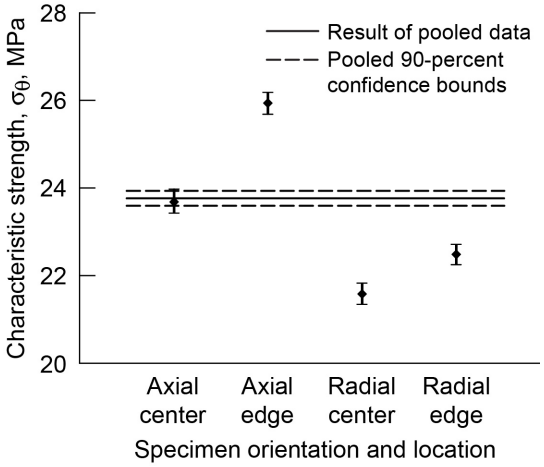

Figure 152.—Characteristic strength and 90-percent confidence bounds on pooled data from slabs 1 to 4 for flexure specimens (with nonlinear-elastic stress response), showing effects of orientation and location. See Table 52 for a listing of Weibull parameters and 90-percent confidence bounds on parameters.

In Figures 151 and 152, the correlation between the Weibull modulus and the characteristic strength is not as strong as in Figures 142 and 143 and in Figures 145 and 146. Weibull moduli and characteristic strength are higher for axial specimens than for radial specimens. However, the difference between the Weibull moduli for the axial and radial specimens does not appear to be statistically different with a high level of confidence because of the overlap of the confidence bounds. Hypothesizing that a correlation between higher Weibull modulus and higher characteristic strength is indicative of residual stresses or rising *R*-curve behavior is more difficult with this set of data. However, in Figure 150, the trend for the axial specimens at lower probabilities of failure is indicative of three-parameter Weibull behavior. Therefore—even though it is not as clear in Figures 151 and 152 as it is in Figures 142 and 143 and in Figures 145 and 146—Figures 151 and 152 do not necessarily invalidate the general observation that, when the Weibull modulus is higher, the characteristic strength tends to be higher. See Table 52 for a listing of Weibull parameters and 90-percent confidence bounds on parameters.

TABLE 52.—WEIBULL PARAMETERS AND 90-PERCENT CONFIDENCE BOUNDS ON POOLED DATA FROM SLABS 1 TO 4 FOR FLEXURE SPECIMENS (WITH NONLINEAR-ELASTIC STRESS RESPONSE), SHOWING EFFECTS OF ORIENTATION AND LOCATION

Specimen type	Number of specimens	Weibull modulus, *m*		Characteristic strength, σ_θ, MPa	
		MLE biased[a]	90-percent confidence	MPa	90-percent confidence
Axial center	144	13.07	11.62/14.42	23.69	23.43/23.96
Axial edge	192	13.36	12.09/14.57	25.94	25.70/26.19
Radial center	156	12.65	11.32/13.91	21.59	21.35/21.83
Radial edge	190	12.31	11.13/13.43	22.49	22.26/22.72
Pooled	682	9.40	8.97/9.84	23.77	23.60/23.94

[a]Maximum-likelihood estimation.

Figure 153 is provided as additional information, but comparing the four sets of pooled data is less clear cut because some of the data are mixed—showing up more than once.

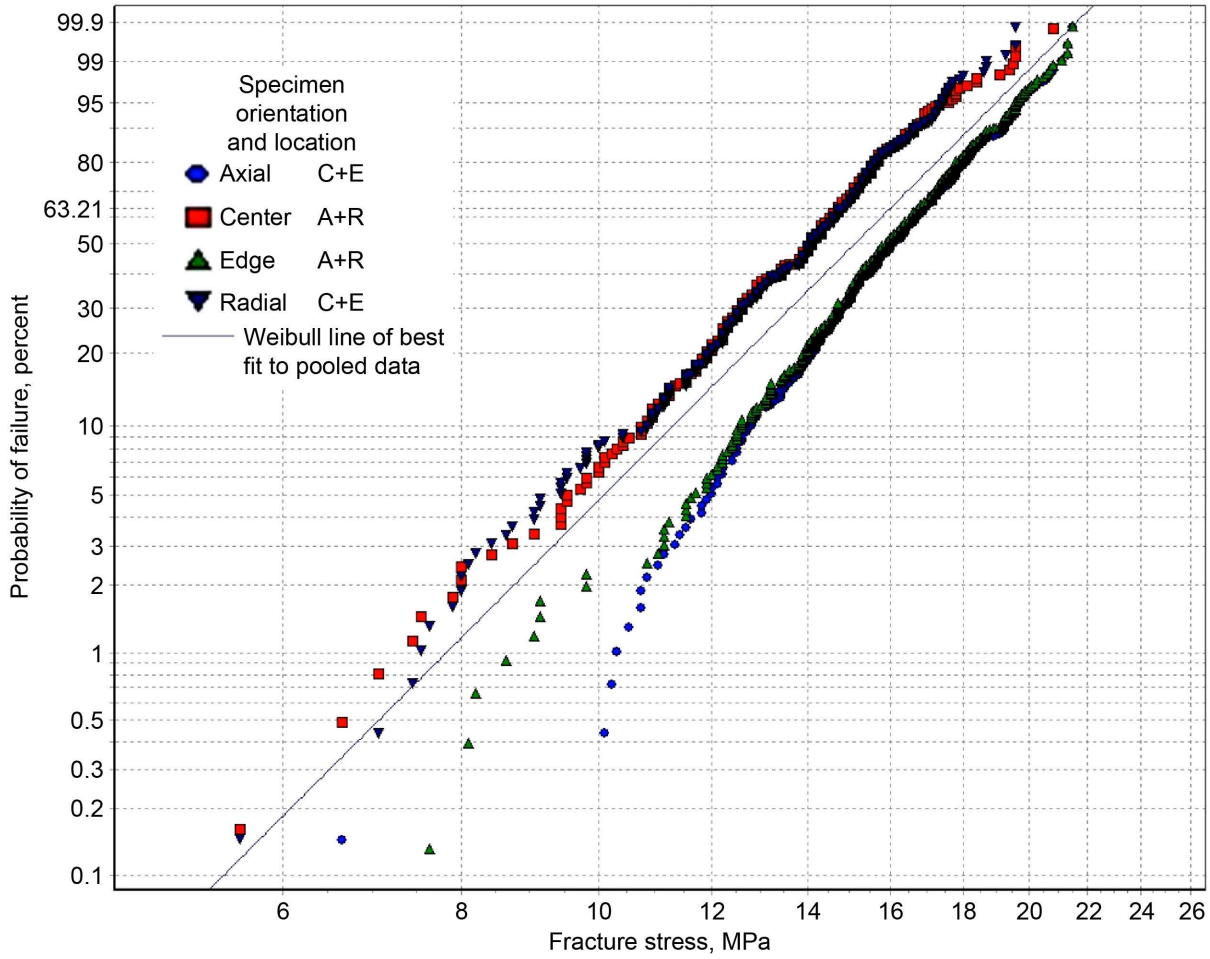

Figure 153.—Weibull plot of fracture stresses of pooled data from slabs 1 to 4 for small tensile specimens, showing effects of orientation and location. Specimens are designated as C+E = pooled data from center and edge of slabs, A+R = pooled data from axial and radial specimens.

Figure 154 is provided as additional information, but comparing the four sets of data is less clear because some of the data are mixed—showing up more than once.

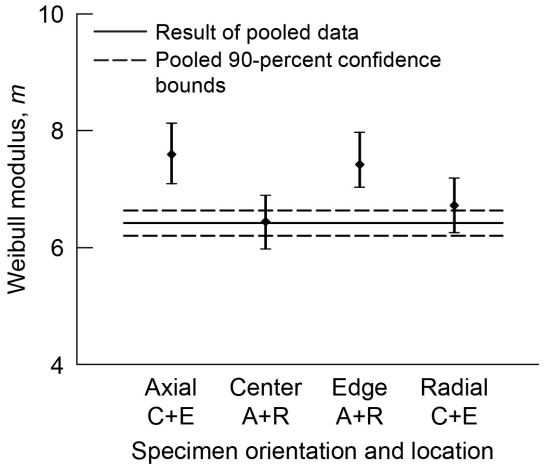

Figure 154.—Weibull modulus and 90-percent confidence bounds on pooled data from slabs 1 to 4 for small tensile specimens, showing effects of orientation and location. Specimens are designated as C+E = pooled data from center and edge of slabs, A+R = pooled data from axial and radial specimens. See Table 53 for a listing of Weibull parameters and 90-percent confidence bounds on parameters.

Figure 155 is provided as additional information, but comparing the four sets of data is less clear because some of the data are mixed—showing up more than once. See Table 53 for a listing of Weibull parameters and 90-percent confidence bounds on parameters.

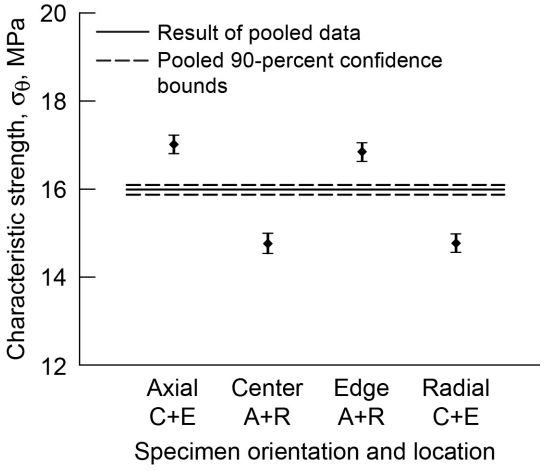

Figure 155.—Characteristic strength and 90-percent confidence bounds on pooled data from slabs 1 to 4 for small tensile specimens, showing effects of orientation and location. Specimens are designated as C+E = pooled data from center and edge of slabs, A+R = pooled data from axial and radial specimens. See Table 53 for a listing of Weibull parameters and 90-percent confidence bounds on parameters.

TABLE 53.—WEIBULL PARAMETERS AND 90-PERCENT CONFIDENCE BOUNDS ON POOLED DATA FROM SLABS 1 TO 4 FOR SMALL TENSILE SPECIMENS, SHOWING EFFECTS OF ORIENTATION AND LOCATION

Specimen type	Number of specimens	Weibull modulus, *m*		Characteristic strength, σ_θ, MPa	
		MLE biased[a]	90-percent confidence	MPa	90-percent confidence
Axial center and edge	346	7.6	7.10/8.13	17.02	16.81/17.23
Axial and radial center	309	6.44	5.98/6.89	14.77	14.54/15.00
Axial and radial edge	380	7.43	6.96/7.92	16.85	16.64/17.05
Radial center and edge	343	6.72	6.26/7.19	14.78	14.57/14.98
Pooled	1378	6.42	6.20/6.64	15.99	15.87/16.11

[a]Maximum-likelihood estimation.

Figure 156 is provided as additional information, but comparing the four sets of data is less clear because some of the data are mixed—showing up more than once.

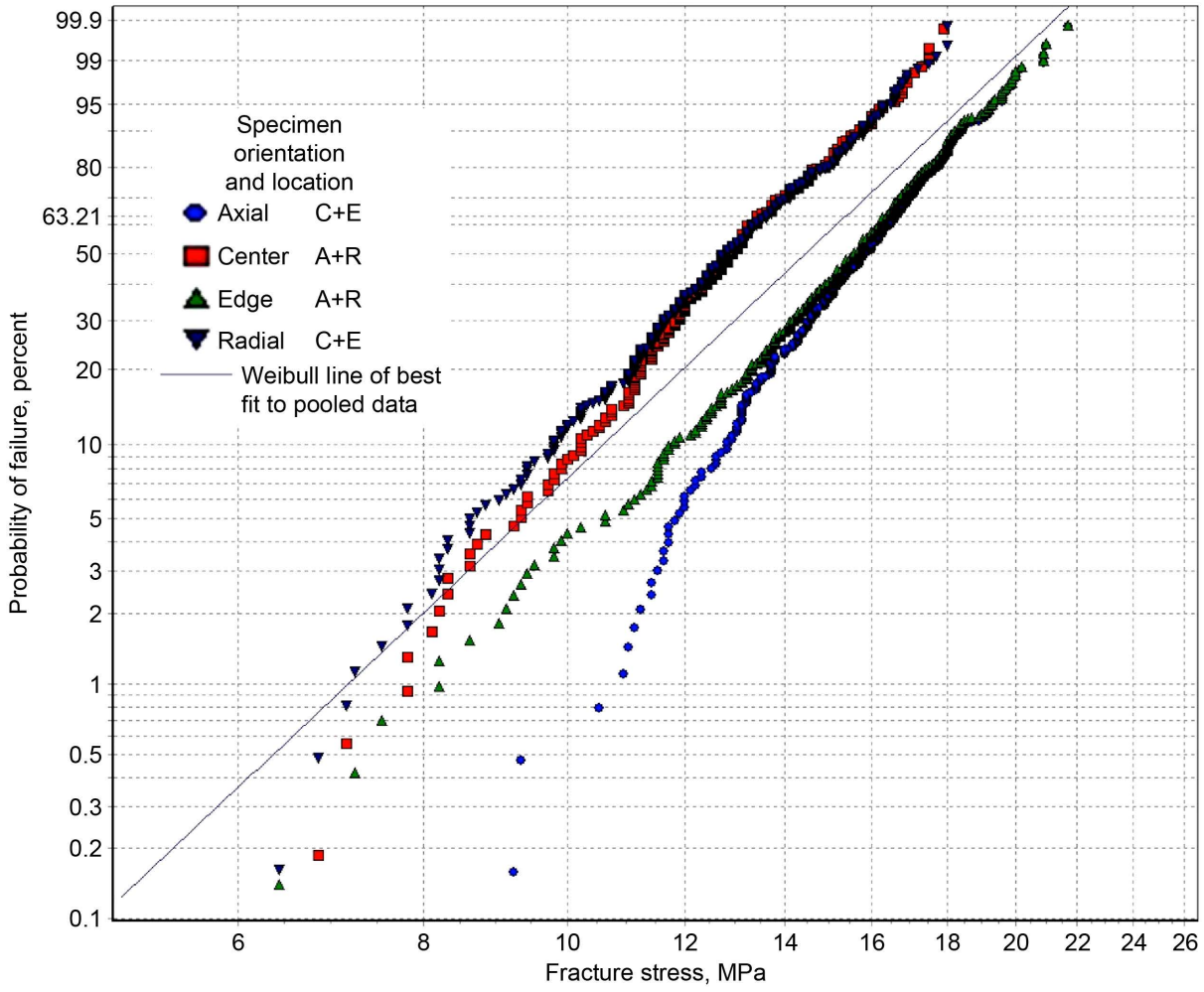

Figure 156.—Weibull plot of fracture stresses of pooled data from slabs 1 to 4 for large tensile specimens, showing effects of orientation and location. Specimens are designated as C+E = pooled data from center and edge of slabs, A+R = pooled data from axial and radial specimens.

Figure 157 is provided as additional information, but comparing the four sets of data is less clear because some of the data are mixed—showing up more than once.

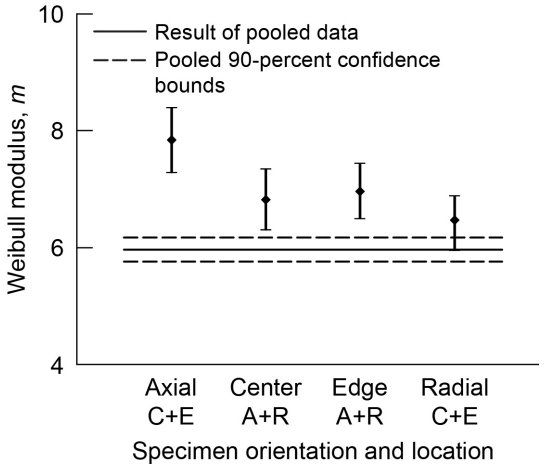

Figure 157.—Weibull modulus and 90-percent confidence bounds on pooled data from slabs 1 to 4 for large tensile specimens, showing effects of orientation and location. Specimens are designated as C+E = pooled data from center and edge of slabs, A+R = pooled data from axial and radial specimens. See Table 54 for a listing of Weibull parameters and 90-percent confidence bounds on parameters.

Figure 158 is provided as additional information, but comparing the four sets of data is less clear because some of the data are mixed—showing up more than once. See Table 54 for a listing of Weibull parameters and 90-percent confidence bounds on parameters.

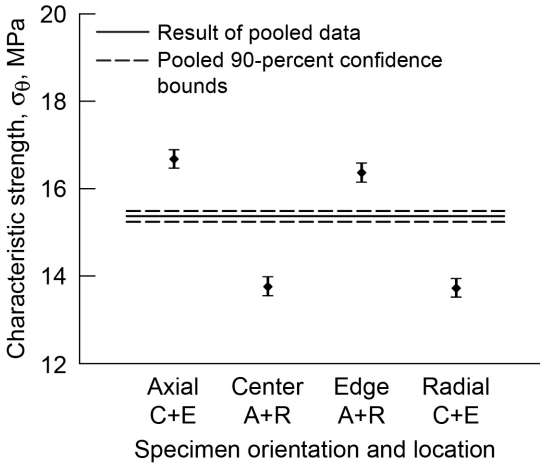

Figure 158.—Characteristic strength and 90-percent confidence bounds on pooled data from slabs 1 to 4 for large tensile specimens, showing effects of orientation and location. Specimens are designated as C+E = pooled data from center and edge of slabs, A+R = pooled data from axial and radial specimens. See Table 54 for a listing of Weibull parameters and 90-percent confidence bounds on parameters.

TABLE 54.—WEIBULL PARAMETERS AND 90-PERCENT CONFIDENCE BOUNDS ON POOLED DATA FROM SLABS 1 TO 4 FOR LARGE TENSILE SPECIMENS, SHOWING EFFECTS OF ORIENTATION AND LOCATION

Specimen type	Number of specimens	Weibull modulus, *m*		Characteristic strength, σ_θ, MPa	
		MLE biased[a]	90-percent confidence	MPa	90-percent confidence
Axial center and edge	317	7.84	7.29/8.39	16.69	16.48/16.89
Axial and radial center	269	6.82	6.31/7.35	13.77	13.56/13.99
Axial and radial edge	359	6.96	6.50/7.44	16.38	16.16/16.59
Radial center and edge	311	6.47	5.96/6.89	13.74	13.53/13.95
Pooled	1256	5.97	5.76/6.18	15.38	15.25/15.50

[a]Maximum-likelihood estimation.

Figure 159 is provided as additional information, but comparing the four sets of data is less clear because some of the data are mixed—showing up more than once.

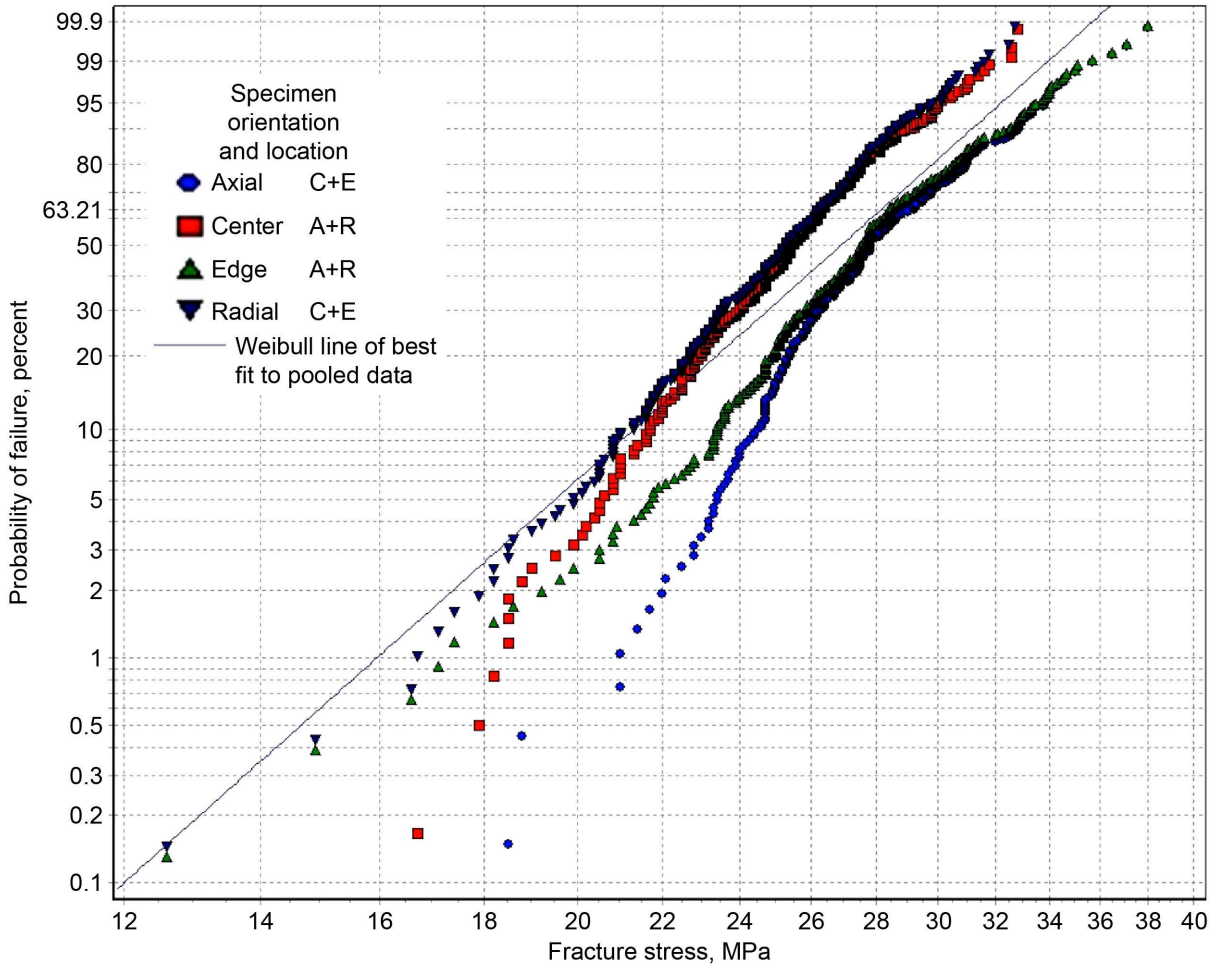

Figure 159.—Weibull plot of fracture stresses of pooled data from slabs 1 to 4 for flexure specimens (with linear-elastic stress response), showing effects of orientation and location. Specimens are designated as C+E = pooled data from center and edge of slabs, A+R = pooled data from axial and radial specimens.

Figure 160 is provided as additional information, but comparing the four sets of data is less clear because some of the data are mixed—showing up more than once.

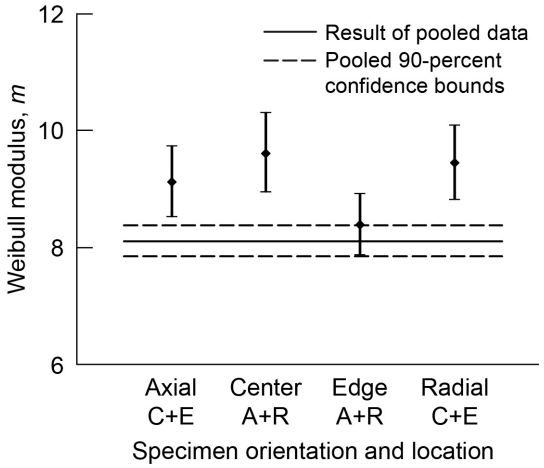

Figure 160.—Weibull modulus and 90-percent confidence bounds on pooled data from slabs 1 to 4 for flexure specimens (with linear-elastic stress response), showing effects of orientation and location. Specimens are designated as C+E = pooled data from center and edge of slabs, A+R = pooled data from axial and radial specimens. See Table 55 for a listing of Weibull parameters and 90-percent confidence bounds on parameters.

Figure 161 is provided as additional information, but comparing the four sets of data is less clear because some of the data are mixed—showing up more than once. See Table 55 for a listing of Weibull parameters and 90-percent confidence bounds on parameters.

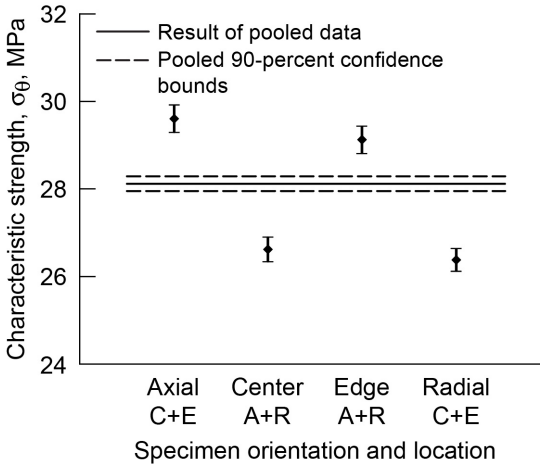

Figure 161.—Characteristic strength and 90-percent confidence bounds on pooled data from slabs 1 to 4 for flexure specimens (with linear-elastic stress response), showing effects of orientation and location. Specimens are designated as C+E = pooled data from center and edge of slabs, A+R = pooled data from axial and radial specimens. See Table 55 for a listing of Weibull parameters and 90-percent confidence bounds on parameters.

TABLE 55.—WEIBULL PARAMETERS AND 90-PERCENT CONFIDENCE BOUNDS ON POOLED DATA FROM SLABS 1 TO 4 FOR FLEXURE SPECIMENS (WITH LINEAR-ELASTIC STRESS RESPONSE), SHOWING EFFECTS OF ORIENTATION AND LOCATION

Specimen type	Number of specimens	Weibull modulus, *m*		Characteristic strength, σ_θ, MPa	
		MLE biased[a]	90-percent confidence	MPa	90-percent confidence
Axial center and edge	336	9.12	8.53/9.73	29.61	29.30/29.92
Axial and radial center	300	9.61	8.95/10.30	26.63	26.35/26.91
Axial and radial edge	382	8.39	7.87/8.92	29.13	28.82/29.44
Radial center and edge	346	9.45	8.83/10.09	26.39	26.13/26.65
Pooled	1346	8.11	7.85/8.38	28.12	27.96/28.28

[a]Maximum-likelihood estimation.

Figure 162 is provided as additional information, but comparing the four sets of data is less clear since some of the data are mixed—showing up more than once.

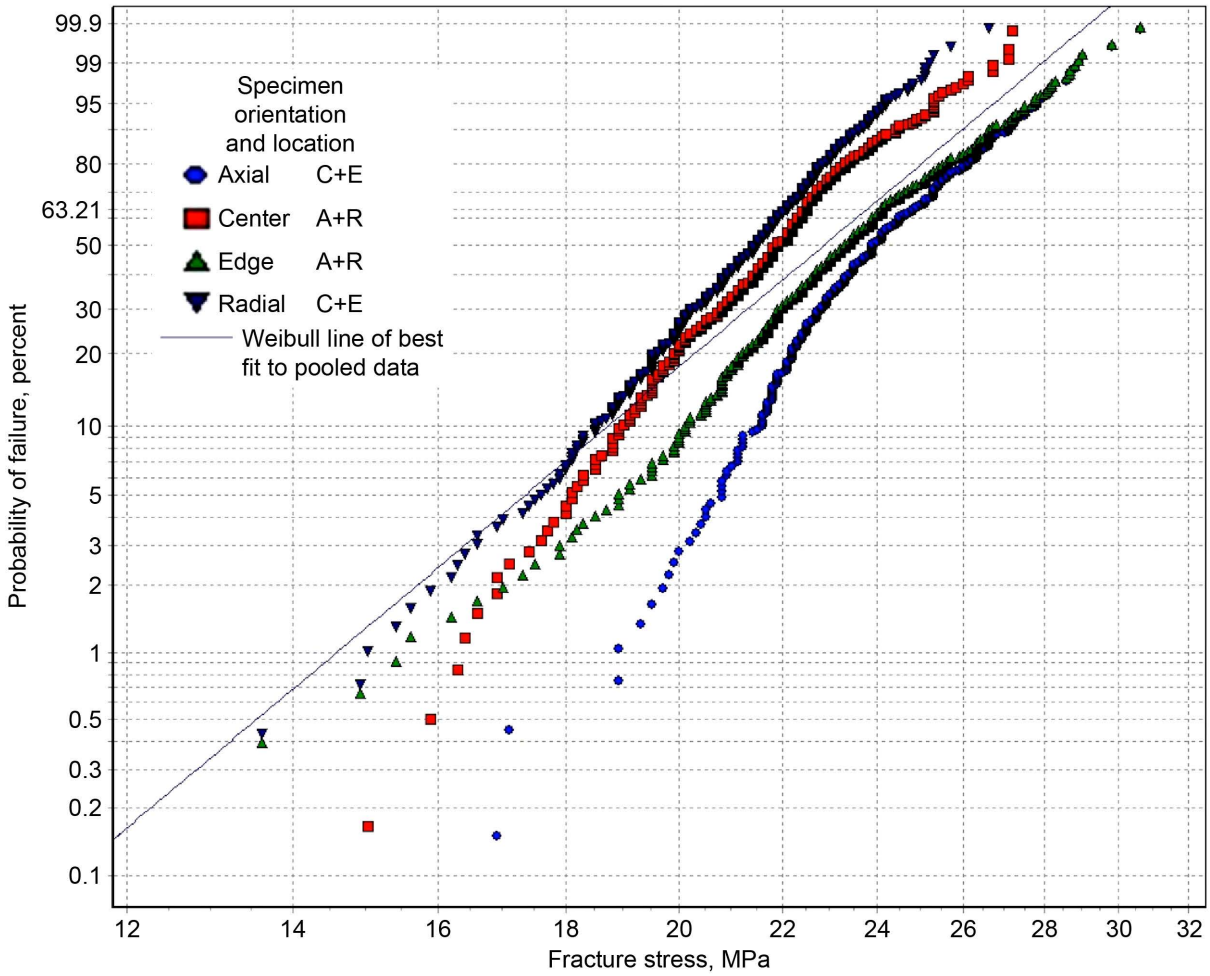

Figure 162.—Weibull plot of fracture stresses of pooled data from slabs 1 to 4 for flexure specimens (with nonlinear-elastic stress response), showing effects of orientation and location. Specimens are designated as C+E = pooled data from center and edge of slabs, A+R = pooled data from axial and radial specimens.

Figure 163 is provided as additional information, but comparing the four sets of data is less clear since some of the data are mixed—showing up more than once.

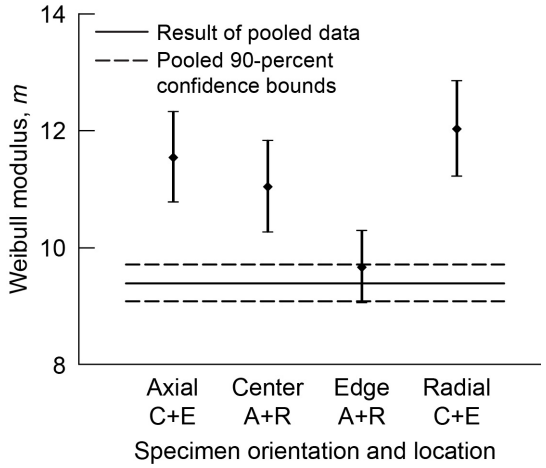

Figure 163.—Weibull modulus and 90-percent confidence bounds on pooled data from slabs 1 to 4 for flexure specimens (with nonlinear-elastic stress response), showing effects of orientation and location. Specimens are designated as C+E = pooled data from center and edge of slabs, A+R = pooled data from axial and radial specimens. See Table 56 for a listing of Weibull parameters and 90-percent confidence bounds on parameters.

Figure 164 is provided as additional information, but comparing the four sets of data is less clear because some of the data are mixed—showing up more than once. See Table 56 for a listing of Weibull parameters and 90-percent confidence bounds on parameters.

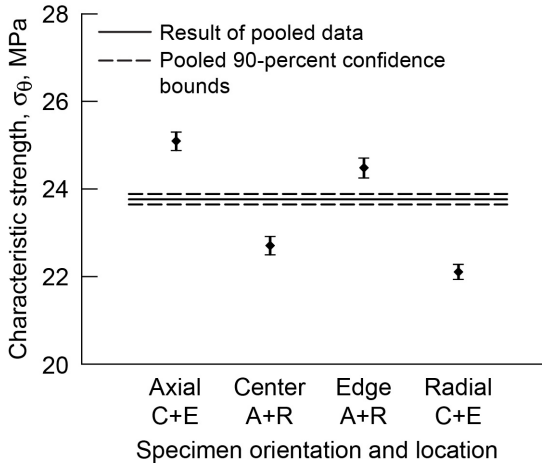

Figure 164.—Characteristic strength and 90-percent confidence bounds on pooled data from slabs 1 to 4 for flexure specimens (with nonlinear-elastic stress response), showing effects of orientation and location. Specimens are designated as C+E = pooled data from center and edge of slabs, A+R = pooled data from axial and radial specimens. See Table 56 for a listing of Weibull parameters and 90-percent confidence bounds on parameters.

TABLE 56.—WEIBULL PARAMETERS AND 90-PERCENT CONFIDENCE BOUNDS ON POOLED DATA FROM SLABS 1 TO 4 FOR FLEXURE SPECIMENS (WITH NONLINEAR-ELASTIC STRESS RESPONSE), SHOWING EFFECTS OF ORIENTATION AND LOCATION

Specimen type	Number of specimens	Weibull modulus, *m*		Characteristic strength, σ_θ, MPa	
		MLE biased[a]	90-percent confidence	MPa	90-percent confidence
Axial center and edge	336	11.54	10.79/12.32	25.10	24.89/25.31
Axial and radial center	300	11.04	10.28/11.83	22.71	22.51/22.92
Axial and radial edge	382	9.67	9.07/10.29	24.49	24.26/24.71
Radial center and edge	346	12.03	11.23/12.85	22.11	21.94/22.28
Pooled	1346	9.39	9.09/9.71	23.77	23.65/23.89

[a]Maximum-likelihood estimation.

Appendix D.—Large (Super) Pooled Data Sets for Slabs 1 to 4 Comparing Small Tensile, Large Tensile, and Flexure Specimen Strength Distribution

In Figure 165, the Weibull best-fit lines assume that all the data have the same value of Weibull modulus and that the Weibull size effect was operating (by accounting for the geometry and loading of the specimens). A linear stress-strain response was assumed in determining the fracture stresses (from Price (1976)), and a linear-elastic finite element model of the four-point cylindrical flexure specimen was used in conjunction with WeibPar to determine the best-fit Weibull modulus and scale parameter (m = 9.65 and σ_o = 33.90 MPa-mm$^{3/m}$).

The WeibPar/CARES analysis shows that the size effect for the experimental data for the two tensile specimen geometries is much smaller than what is expected from the Weibull stress-volume integration, whereas a large size effect exists between the tensile and flexure specimens that is adequately predicted with Weibull stress-volume integration.

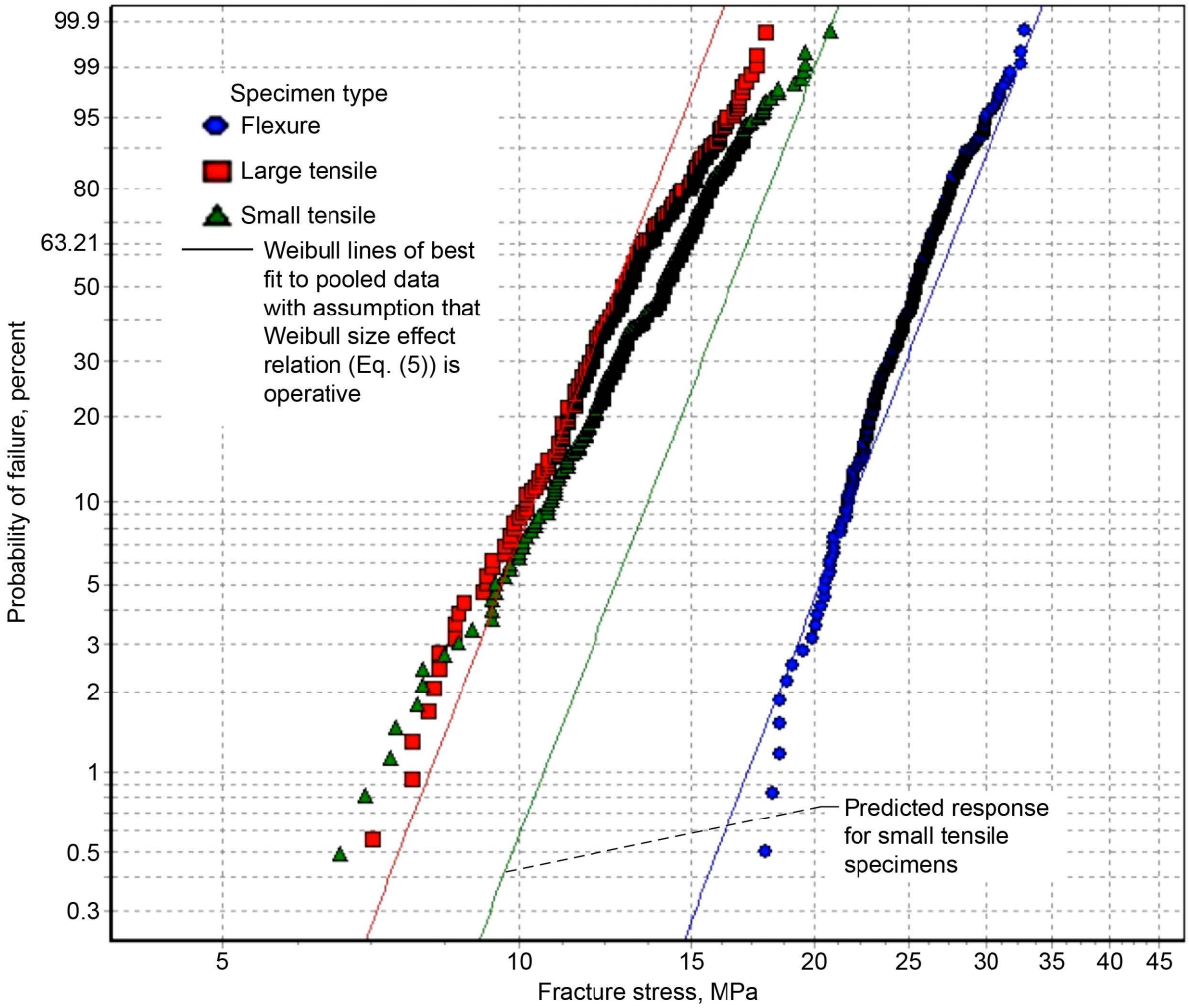

Figure 165.—Weibull plot of fracture stresses of pooled data from slabs 1 to 4 for axial and radial specimens from center of slabs, comparing small tensile, large tensile, and flexure specimens (with linear-elastic stress response). See Table 57 for a listing of Weibull parameters and 90-percent confidence bounds on parameters.

In Figure 166, the Weibull best-fit lines assume that all the data have the same value of Weibull modulus and that the Weibull size effect is operating (by accounting for the geometry and loading of the specimens). A nonlinear stress-strain response was assumed in determining the fracture stresses (from Price (1976)), and a linear-elastic finite element model of the four-point cylindrical flexure specimen was used in conjunction with WeibPar to determine the best-fit Weibull modulus and scale parameter (m = 11.09 and σ_o = 30.15 MPa-mm$^{3/m}$). The predictions for the strength response from the WeibPar/CARES analysis do not account for the changing effective volume with load that is expected from a nonlinear stress-strain response.

The WeibPar/CARES analysis shows that the size effect for the experimental data for the two tensile specimen geometries is much smaller than what is expected from the Weibull stress-volume integration, whereas a large size effect exists between the tensile and flexure specimens that is slightly overpredicted with Weibull stress-volume integration.

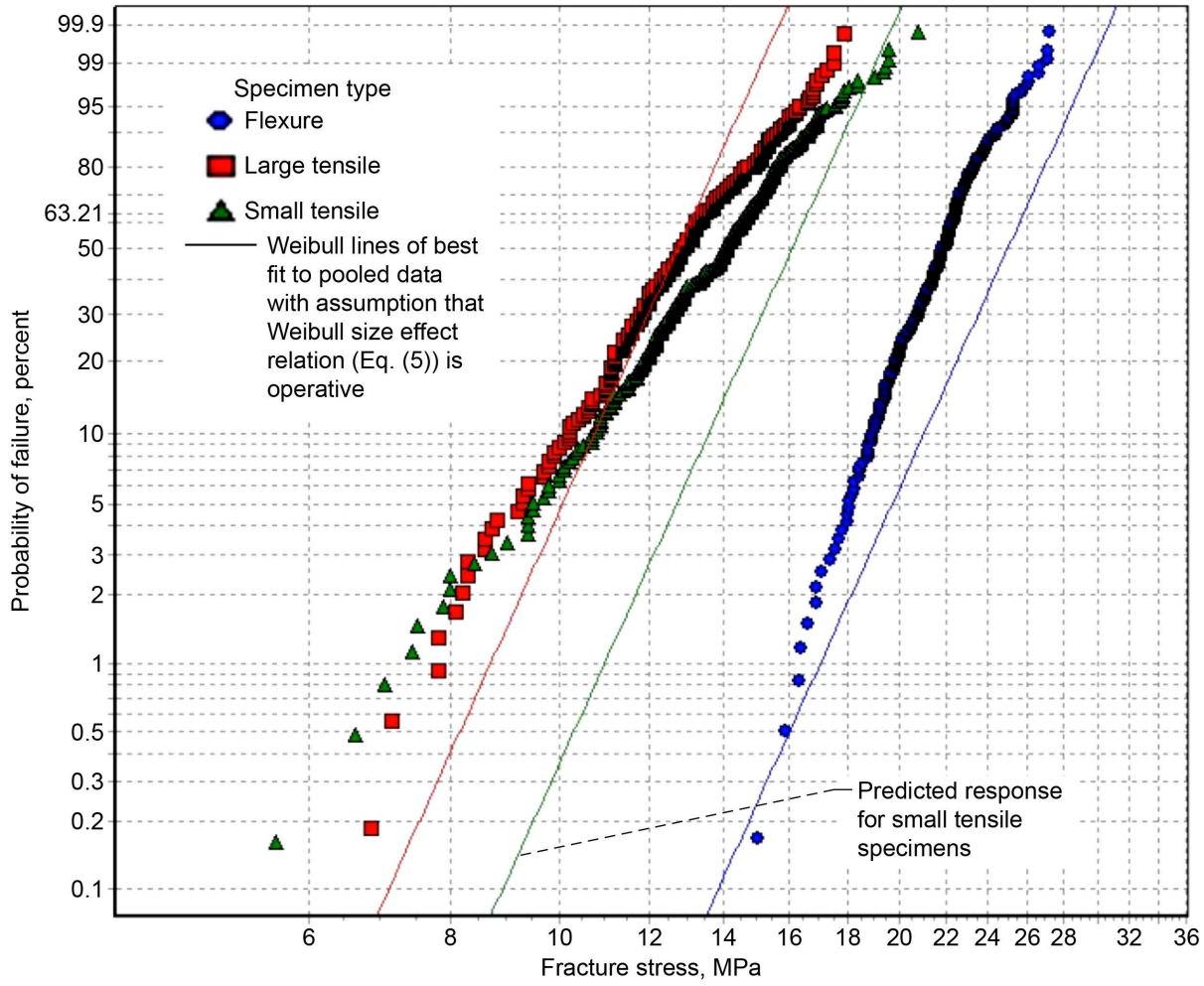

Figure 166.—Weibull plot of fracture stresses of pooled data from slabs 1 to 4 for axial and radial specimens from center of slabs, comparing small tensile, large tensile, and flexure specimens (with nonlinear-elastic stress response). See Table 57 for a listing of Weibull parameters and 90-percent confidence bounds on parameters.

In Figure 167, the Weibull modulus is higher for flexure specimens with nonlinear correction of stresses than for tensile specimens. It has not been established how much of this difference could be attributed to the nonlinear stress-strain response of H–451. An alternative explanation is that a different failure mode with a separate set of Weibull parameters is operating at the surface of the material when it is loaded under flexure.

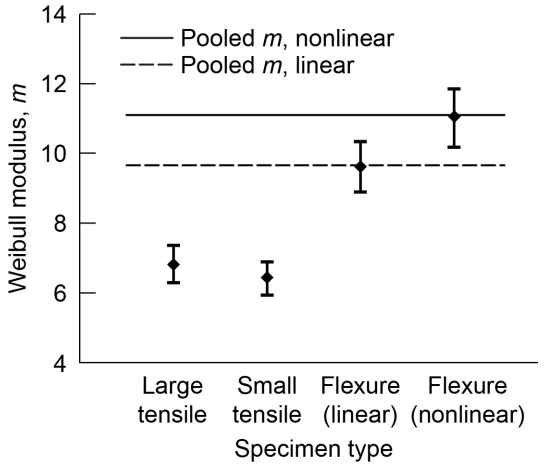

Figure 167.—Weibull modulus and 90-percent confidence bounds on pooled data from slabs 1 to 4 for axial and radial specimens from center of slabs, comparing small tensile, large tensile, and flexure specimens. See Table 57 for a listing of Weibull parameters and 90-percent confidence bounds on parameters.

In Figure 168, the higher characteristic strength of the flexure specimen cannot be explained from natural statistical variation, and the size effect must be explained by other means, such as with Weibull stress-volume integration. On the other hand, the size effect between the small and large tensile specimens is less than what is expected with the Weibull distribution (see Figures 165 and 166). When the fracture stresses were computed from Price (1976), the nonlinear stress-strain response reduced the characteristic strength of the flexure specimen. See Table 57 for a listing of Weibull parameters and 90-percent confidence bounds on parameters.

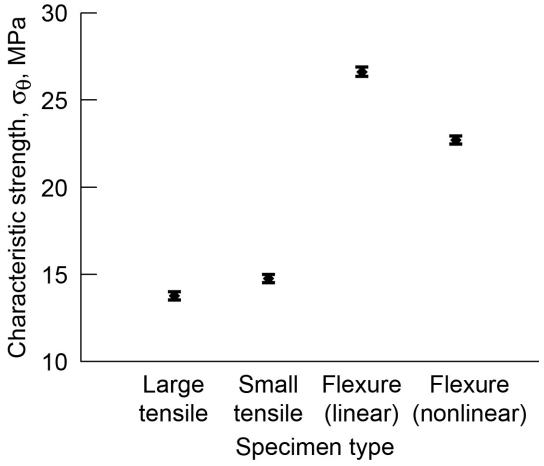

Figure 168.—Characteristic strength and 90-percent confidence bounds on pooled data from slabs 1 to 4 for axial and radial specimens from center of slabs, comparing small tensile, large tensile, and flexure specimens. See Table 57 for a listing of Weibull parameters and 90-percent confidence bounds on parameters.

TABLE 57.—WEIBULL PARAMETERS AND 90-PERCENT CONFIDENCE BOUNDS ON POOLED DATA FROM SLABS 1 TO 4 FOR AXIAL AND RADIAL SPECIMENS FROM CENTER OF SLABS, COMPARING SMALL TENSILE, LARGE TENSILE, AND FLEXURE SPECIMENS

Specimen type	Number of specimens	Weibull modulus, *m*		Characteristic strength, σ_θ, MPa	
		MLE biased[a]	90-percent boot confidence[b]	MPa	90-percent boot confidence[b]
Small tensile	309	6.43	5.94/6.88	14.77	14.55/15.00
Large tensile	269	6.82	6.29/7.36	13.77	13.55/13.98
Flexure, linear[c]	300	9.61	8.95/10.30	26.63	26.35/26.91
Flexure, nonlinear[d]	300	11.04	10.19/11.85	22.71	22.50/22.93
Pooled, linear[c]	878	9.65	----------	------	----------
Pooled, nonlinear[d]	878	11.09	----------	------	----------

[a]Maximum-likelihood estimation.
[b]Calculated from boot confidence bounds for 2000 simulations.
[c]Linear-elastic stress-strain response was assumed.
[d]Nonlinear-elastic stress-strain response was assumed.

In Figure 169, the Weibull best-fit lines assume that all the data have the same value of Weibull modulus and that the Weibull size effect was operating (by accounting for the geometry and loading of the specimens). A linear stress-strain response was assumed in determining the fracture stresses (from Price (1976)), and a linear-elastic finite element model of the four-point cylindrical flexure specimen was used in conjunction with WeibPar to determine the best-fit Weibull modulus and scale parameter (m = 10.35 and σ_o = 37.64 MPa-mm$^{3/m}$).

The WeibPar/CARES analysis shows that the size effect for the experimental data for the two tensile specimen geometries is much smaller than what is expected from the Weibull stress-volume integration, whereas a large size effect exists between the tensile specimen and flexure specimen data that is adequately predicted with Weibull stress-volume integration.

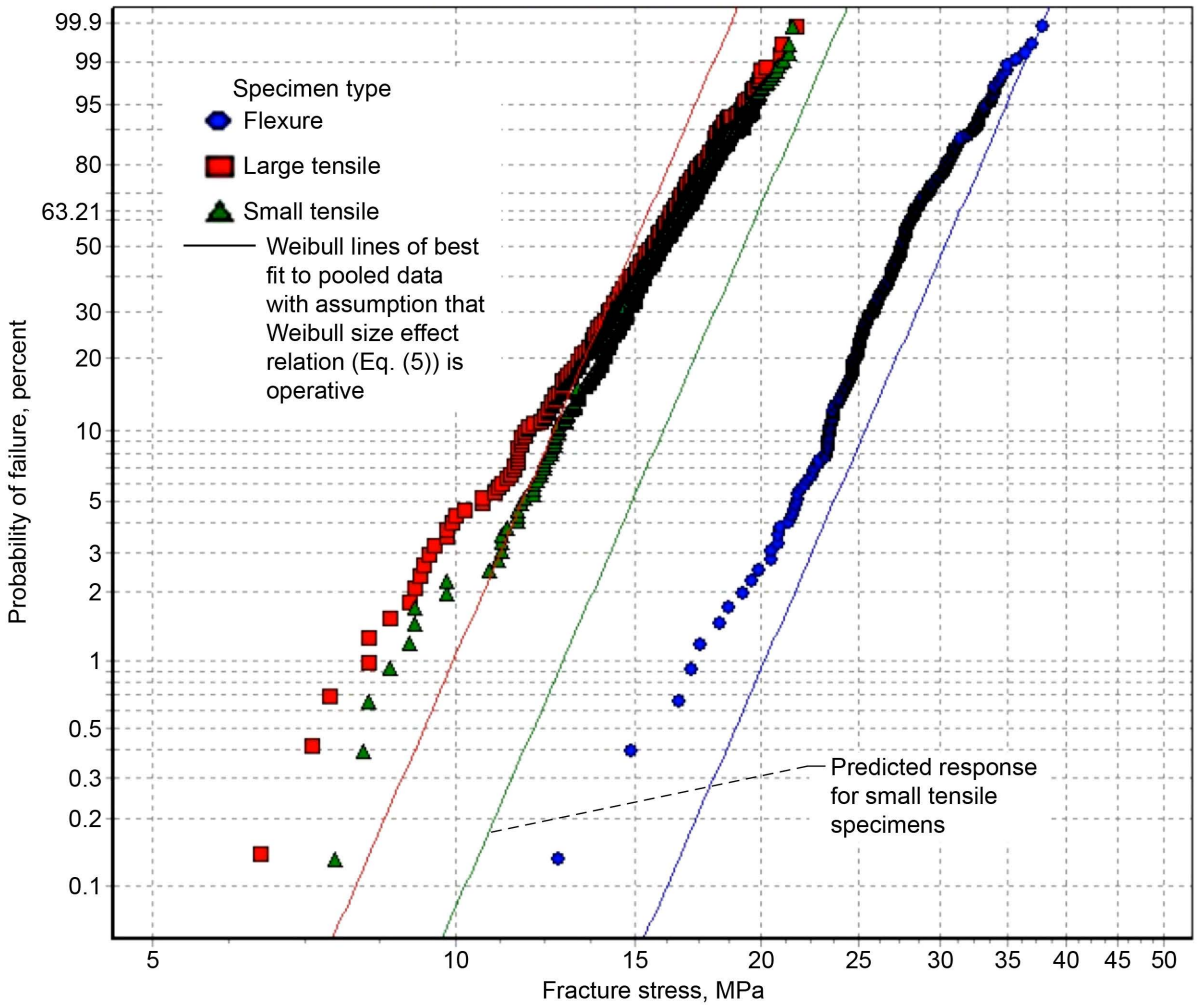

Figure 169.—Weibull plot of fracture stresses of pooled data from slabs 1 to 4 for axial and radial specimens from edge of slabs, comparing small tensile, large tensile, and flexure specimens (with linear-elastic stress response) from edge of slabs. See Table 58 for a listing of Weibull parameters and 90-percent confidence bounds on parameters.

In Figure 170, the Weibull best-fit lines assume that all the data have the same value of Weibull modulus and that the Weibull size effect is operating (by accounting for the geometry and loading of the specimens). A nonlinear stress-strain response was assumed in determining the fracture stresses (from Price (1976)), and a linear-elastic finite element model of the four-point cylindrical flexure specimen was used in conjunction with WeibPar to determine the best-fit Weibull modulus and scale parameter (m = 10.53 and σ_o = 36.61 MPa-mm$^{3/m}$). The predictions for the strength response from the WeibPar/CARES analysis do not account for the changing effective volume with load that is expected from a nonlinear stress-strain response.

The WeibPar/CARES analysis shows that the size effect for the experimental data for the two tensile specimen geometries is much smaller than what is expected from the Weibull stress-volume integration, whereas a large size effect exists between the tensile specimen and flexure specimen data that is overpredicted with Weibull stress-volume integration.

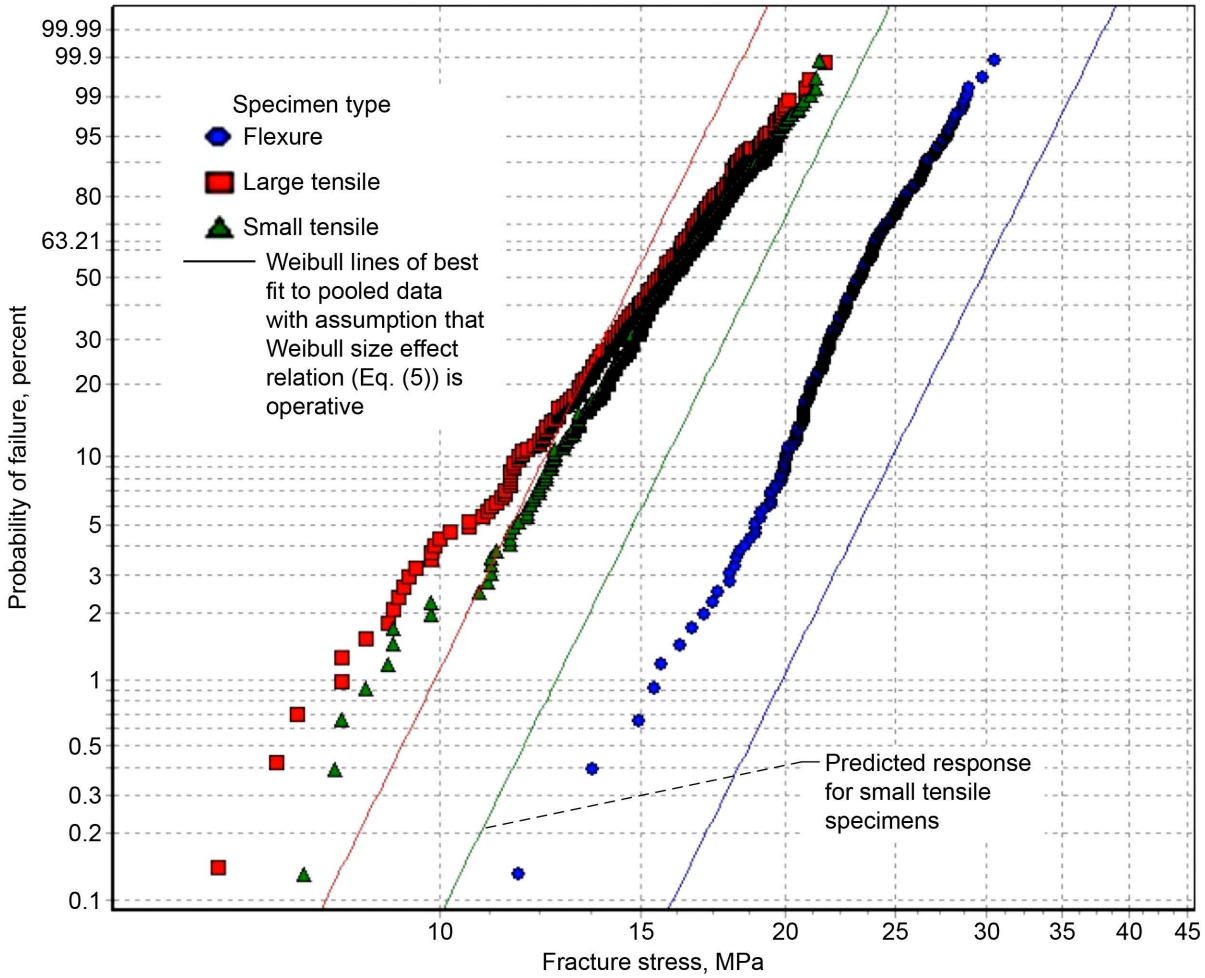

Figure 170.—Weibull plot of fracture stresses of pooled data from slabs 1 to 4 for axial and radial specimens from edge of slabs, comparing small tensile, large tensile, and flexure specimens (with nonlinear-elastic stress response). See Table 58 for a listing of Weibull parameters and 90-percent confidence bounds on parameters.

In Figure 171, the flexure specimen Weibull modulus is higher than that of the tensile specimens. It has not been established how much of this difference could be attributed to the nonlinear stress-strain response of H–451. An alternative explanation is that a different failure mode with a separate set of Weibull parameters is operating at the surface of the material when it is loaded under flexure. The Weibull moduli for the two different sizes of tensile specimens are reasonably similar.

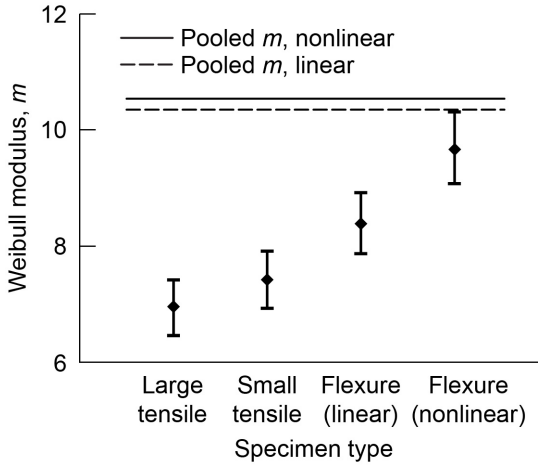

Figure 171.—Weibull modulus and 90-percent confidence bounds on pooled data from slabs 1 to 4 for axial and radial specimens from edge of slabs, comparing small tensile, large tensile, and flexure specimens. See Table 58 for a listing of Weibull parameters and 90-percent confidence bounds on parameters.

In Figure 172, the higher characteristic strength of the flexure specimen cannot be explained from natural statistical variation, and the size effect must be explained by other means, such as with the Weibull distribution. On the other hand, the size effect between the small and large tensile specimens is less than what is expected with the Weibull distribution (see Figures 169 and 170). When the fracture stresses were computed from Price (1976), the nonlinear stress-strain response reduced the characteristic strength of the flexure specimen. See Table 58 for a listing of Weibull parameters and 90-percent confidence bounds on parameters.

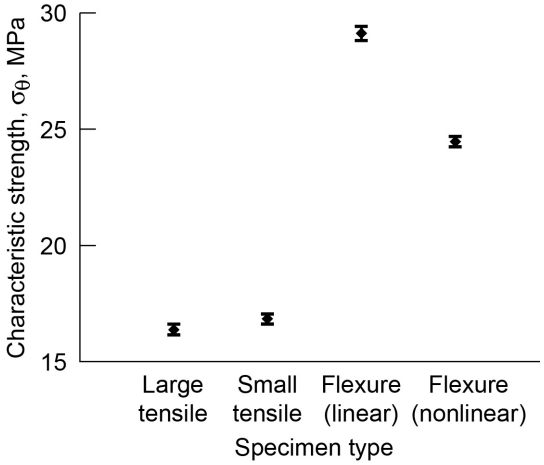

Figure 172.—Characteristic strength and 90-percent confidence bounds on pooled data from slabs 1 to 4 for axial and radial specimens from edge of slabs, comparing small tensile, large tensile, and flexure specimens. See Table 58 for a listing of Weibull parameters and 90-percent confidence bounds on parameters.

TABLE 58.—WEIBULL PARAMETERS AND 90-PERCENT CONFIDENCE BOUNDS ON POOLED DATA FROM SLABS 1 TO 4 FOR AXIAL AND RADIAL SPECIMENS FROM EDGE OF SLABS, COMPARING SMALL TENSILE, LARGE TENSILE, AND FLEXURE SPECIMENS

Specimen type	Number of specimens	Weibull modulus, m		Characteristic strength, σ_θ, MPa	
		MLE biased[a]	90-percent boot confidence[b]	MPa	90-percent boot confidence[b]
Small tensile	380	7.43	6.93/7.91	16.85	16.64/17.05
Large tensile	359	6.96	6.47/7.42	16.38	16.17/16.60
Flexure, linear[c]	382	8.39	7.87/8.92	29.13	28.82/29.44
Flexure, nonlinear[d]	382	9.67	9.07/10.30	24.49	24.27/24.72
Pooled, linear[c]	1121	10.35	----------	------	----------
Pooled, nonlinear[d]	1121	10.53	----------	------	----------

[a]Maximum-likelihood estimation.
[b]Calculated from boot confidence bounds for 2000 simulations.
[c]Linear-elastic stress-strain response was assumed.
[d]Nonlinear-elastic stress-strain response was assumed.

In Figure 173, the Weibull best-fit lines assume that all the data have the same value of Weibull modulus and that the Weibull size effect was operating (by accounting for the geometry and loading of the specimens). A linear stress-strain response was assumed in determining the fracture stresses (from Price (1976)), and a linear-elastic finite element model of the four-point cylindrical flexure specimen was used in conjunction with WeibPar to determine the best-fit Weibull modulus and scale parameter (m = 10.78 and σ_o = 37.00 MPa-mm$^{3/m}$).

The WeibPar/CARES analysis shows that the size effect for the experimental data for the two tensile specimen geometries is much smaller than what is expected from the Weibull stress-volume integration, whereas a large size effect exists between the tensile specimen and flexure specimen data that is adequately predicted with Weibull stress-volume integration.

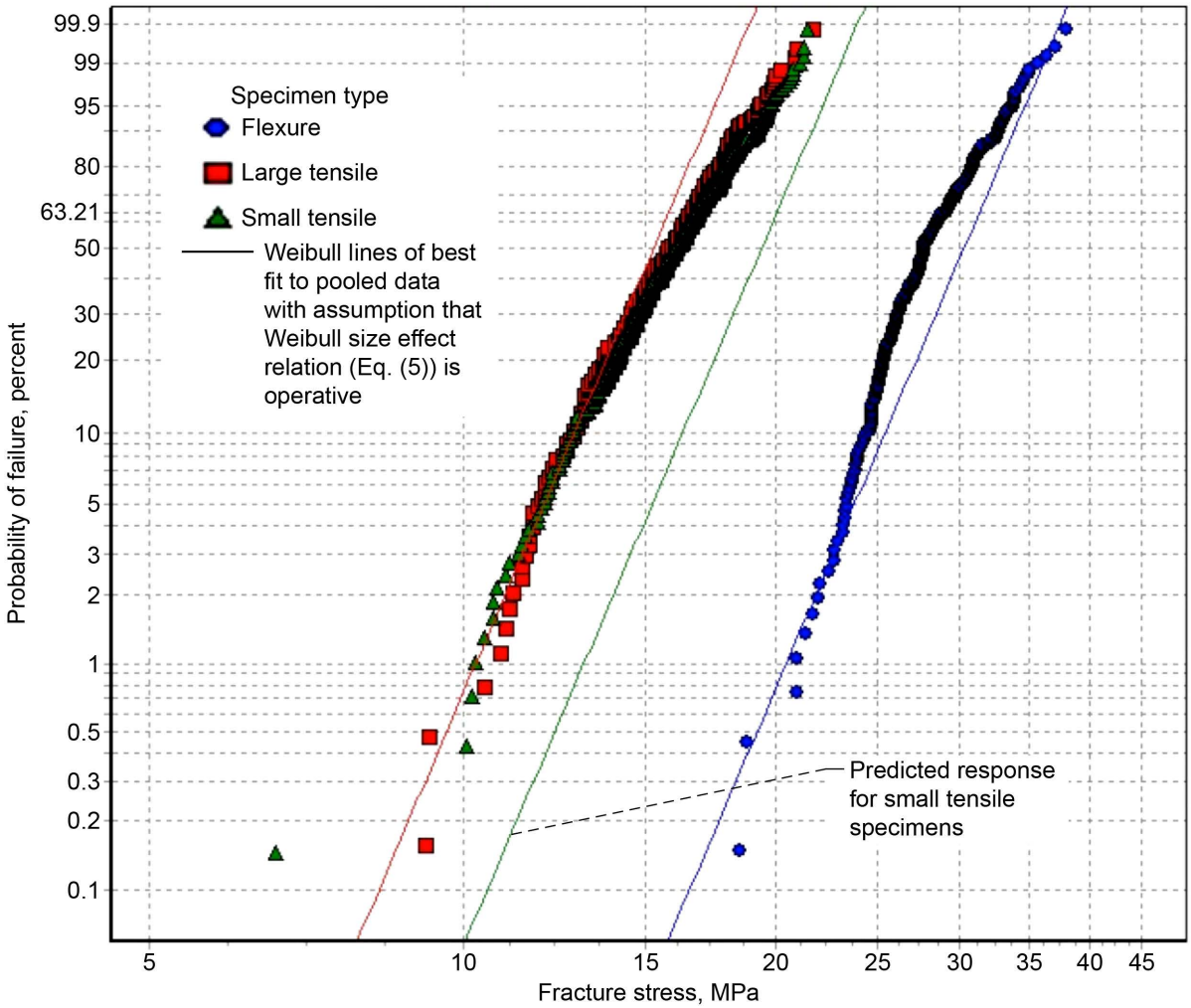

Figure 173.—Weibull plot of fracture stresses of pooled data from slabs 1 to 4 for axial specimens from pooled center and edge of slabs, comparing small tensile, large tensile, and flexure specimens (with linear-elastic stress response). See Table 59 for a listing of Weibull parameters and 90-percent confidence bounds on parameters.

In Figure 174, the Weibull best-fit lines assume that all the data have the same value of Weibull modulus and that the Weibull size effect is operating (by accounting for the geometry and loading of the specimens). A nonlinear stress-strain response was assumed in determining the fracture stresses (from Price (1976)), and a linear-elastic finite element model of the four-point cylindrical flexure specimen was used in conjunction with WeibPar to determine the best-fit Weibull modulus and scale parameter (m = 11.92 and σ_o = 34.10 MPa-mm$^{3/m}$). The predictions for the strength response from the WeibPar/CARES analysis do not account for the changing effective volume with load that is expected from a nonlinear stress-strain response.

The WeibPar/CARES analysis shows that the size effect for the experimental data for the two tensile specimen geometries is much smaller than what is expected from the Weibull stress-volume integration, whereas a large size effect exists between the tensile specimen and flexure specimen data that is overpredicted with Weibull stress-volume integration.

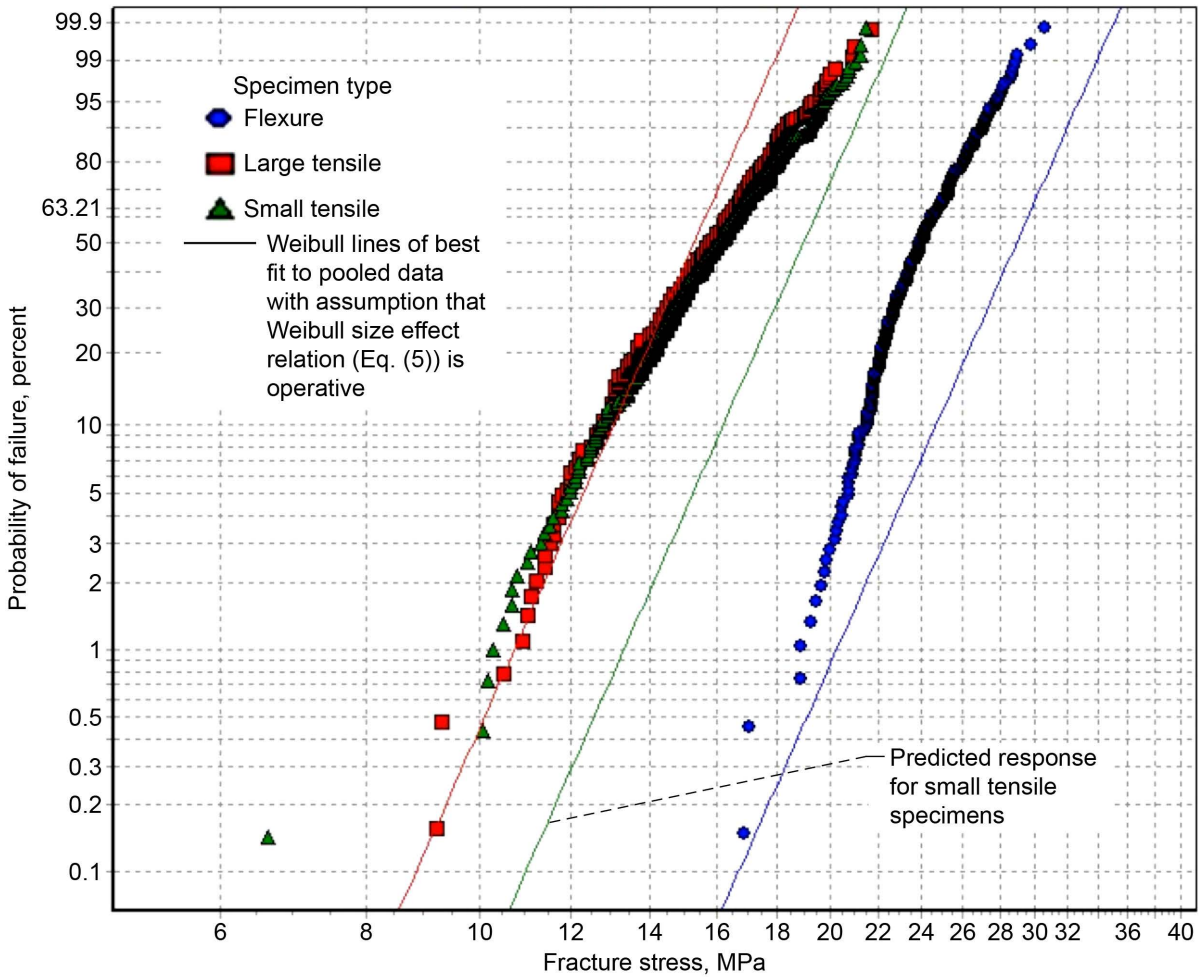

Figure 174.—Weibull plot of fracture stresses of pooled data from slabs 1 to 4 for axial specimens from pooled center and edge of slabs, comparing small tensile, large tensile, and flexure specimens (with nonlinear-elastic stress response). See Table 59 for a listing of Weibull parameters and 90-percent confidence bounds on parameters.

In Figure 175, the Weibull modulus is significantly higher for the flexure specimens than for the tensile specimens—beyond what is expected from natural statistical variation. It has not been established how much of this difference could be attributed to the nonlinear stress-strain response of H–451. An alternative explanation is that a different failure mode with a separate set of Weibull parameters is operating at the surface of the material when it is loaded under flexure. The Weibull moduli for the two different sizes of tensile specimens are quite similar.

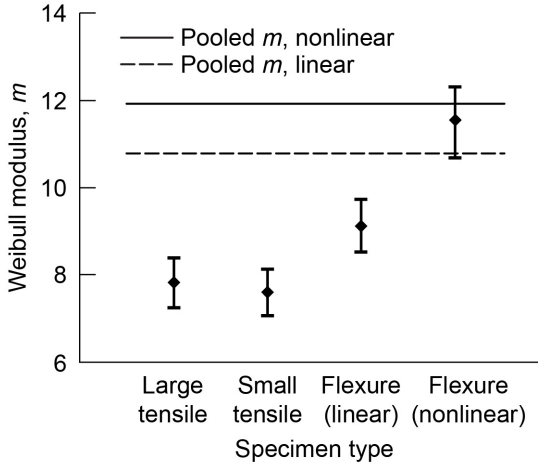

Figure 175.—Weibull modulus and 90-percent confidence bounds on pooled data from slabs 1 to 4 for axial specimens from pooled center and edge of slabs, comparing small tensile, large tensile, and flexure specimens. See Table 59 for a listing of Weibull parameters and 90-percent confidence bounds on parameters.

In Figure 176, the higher characteristic strength of the flexure specimen cannot be explained from natural statistical variation, and the size effect must be explained by other means, such as with the Weibull distribution. On the other hand, the size effect between the small and large tensile specimens is less than what is expected with the Weibull distribution (see Figs. 173 and 174). When the fracture stresses were computed from Price (1976), the nonlinear stress-strain response reduced the characteristic strength of the flexure specimen. See Table 59 for a listing of Weibull parameters and 90-percent confidence bounds on parameters.

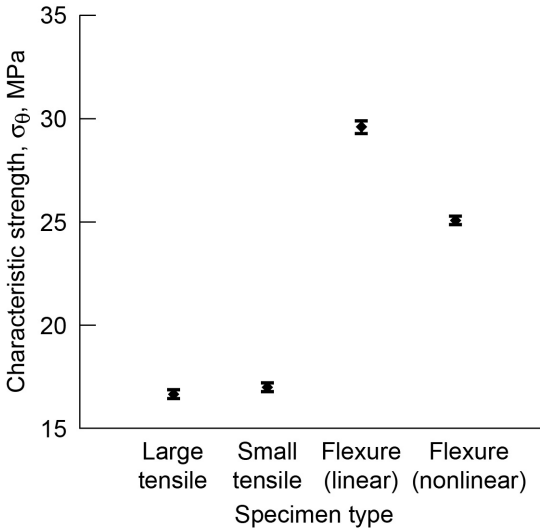

Figure 176.—Characteristic strength and 90-percent confidence bounds on pooled data from slabs 1 to 4 for axial specimens from pooled center and edge of slabs, comparing small tensile, large tensile, and flexure specimens. Note that pooled data results are not shown because different specimen geometries are being compared. Characteristic strength can only be compared for data sets involving similar geometries. See Table 59 for a listing of Weibull parameters and 90-percent confidence bounds on parameters.

TABLE 59.—WEIBULL PARAMETERS AND 90-PERCENT CONFIDENCE BOUNDS ON POOLED DATA FROM SLABS 1 TO 4 FOR AXIAL SPECIMENS FROM POOLED CENTER AND EDGE OF SLABS, COMPARING SMALL TENSILE, LARGE TENSILE, AND FLEXURE SPECIMENS

Specimen type	Number of specimens	Weibull modulus, *m*		Characteristic strength, σ_θ, MPa	
		MLE biased[a]	90-percent boot confidence[b]	MPa	90-percent boot confidence[b]
Small tensile	346	7.60	7.07/8.14	17.02	16.81/17.23
Large tensile	317	7.83	7.25/8.39	16.69	16.47/16.89
Flexure, linear[c]	336	9.12	8.53/9.73	29.61	29.30/29.92
Flexure, nonlinear[d]	336	11.54	10.69/12.30	25.10	24.89/25.30
Pooled, linear[c]	999	10.78	----------	------	----------
Pooled, nonlinear[d]	999	11.92	----------	------	----------

[a]Maximum-likelihood estimation.
[b]Calculated from boot confidence bounds for 2000 simulations.
[c]Linear-elastic stress-strain response was assumed.
[d]Nonlinear-elastic stress-strain response was assumed.

In Figure 177, the Weibull best-fit lines assume that all the data have the same value of Weibull modulus and that the Weibull size effect was operating (by accounting for the geometry and loading of the specimens). A linear stress-strain response was assumed in determining the fracture stresses (from Price (1976)), and a linear-elastic finite element model of the four-point cylindrical flexure specimen was used in conjunction with WeibPar to determine the best-fit Weibull modulus and scale parameter (m = 9.71 and σ_o = 33.77 MPa-mm$^{3/m}$).

The WeibPar/CARES analysis shows that the size effect for the experimental data for the two tensile specimen geometries is much smaller than what is expected from the Weibull stress-volume integration, whereas a large size effect exists between the tensile specimen and flexure specimen data that is adequately predicted with Weibull stress-volume integration.

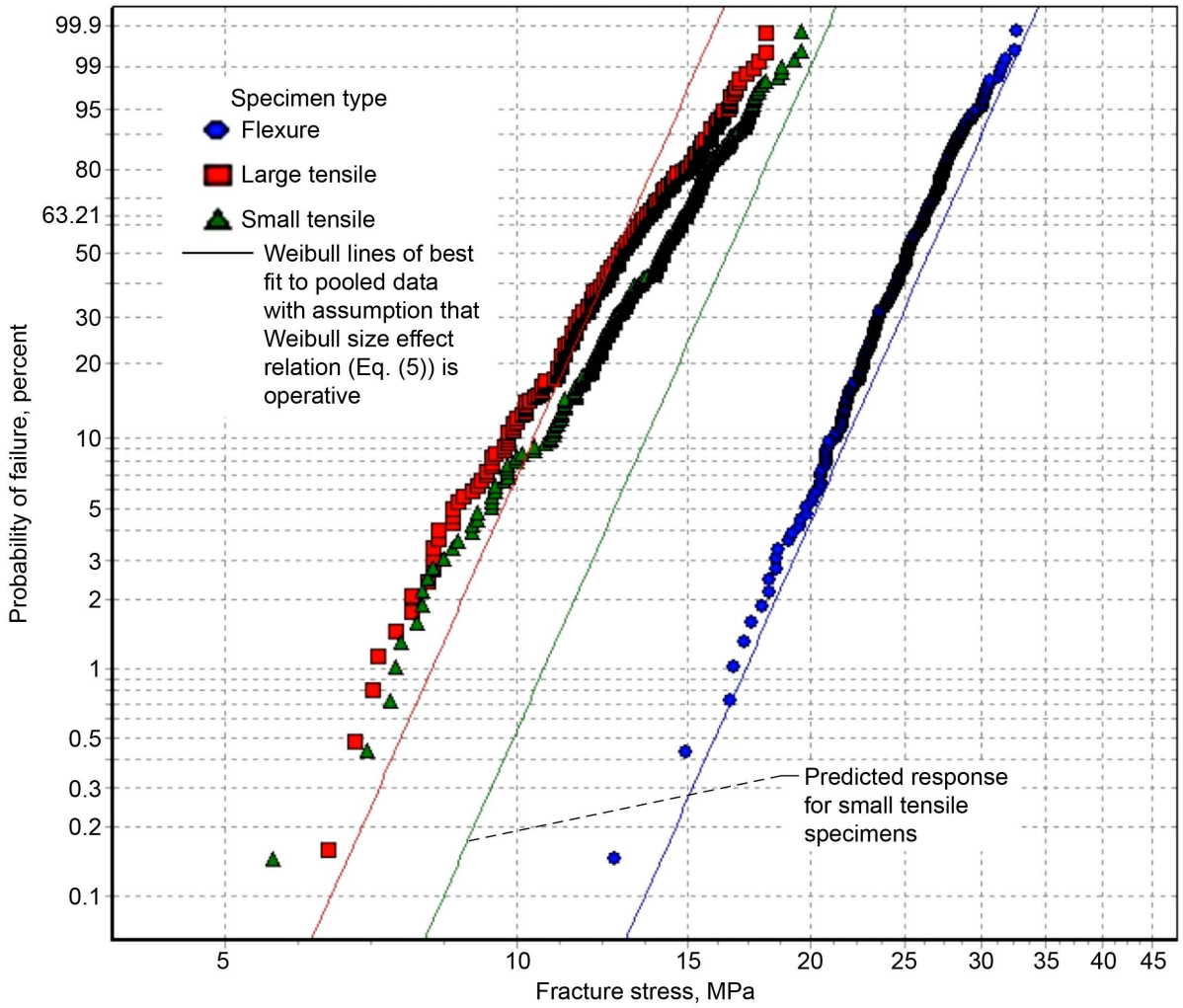

Figure 177.—Weibull plot of fracture stresses of pooled data from slabs 1 to 4 for radial specimens from pooled center and edge of slabs, comparing small tensile, large tensile, and flexure specimens (with linear-elastic stress response). See Table 60 for a listing of Weibull parameters and 90-percent confidence bounds on parameters.

In Figure 178, the Weibull best-fit lines assume that all the data have the same value of Weibull modulus and that the Weibull size effect is operating (by accounting for the geometry and loading of the specimens). A nonlinear stress-strain response was assumed in determining the fracture stresses (from Price (1976)), and a linear-elastic finite element model of the four-point cylindrical flexure specimen was used in conjunction with WeibPar to determine the best-fit Weibull modulus and scale parameter (m = 11.00 and σ_o = 30.30 MPa-mm$^{3/m}$). The predictions for the strength response from the WeibPar/CARES analysis do not account for changing effective volume with load that is expected from a nonlinear stress-strain response.

The WeibPar/CARES analysis shows that the size effect for the experimental data for the two tensile specimen geometries is much smaller than what is expected from the Weibull stress-volume integration, whereas a large size effect exists between the tensile specimen and flexure specimen data that is overpredicted with Weibull stress-volume integration.

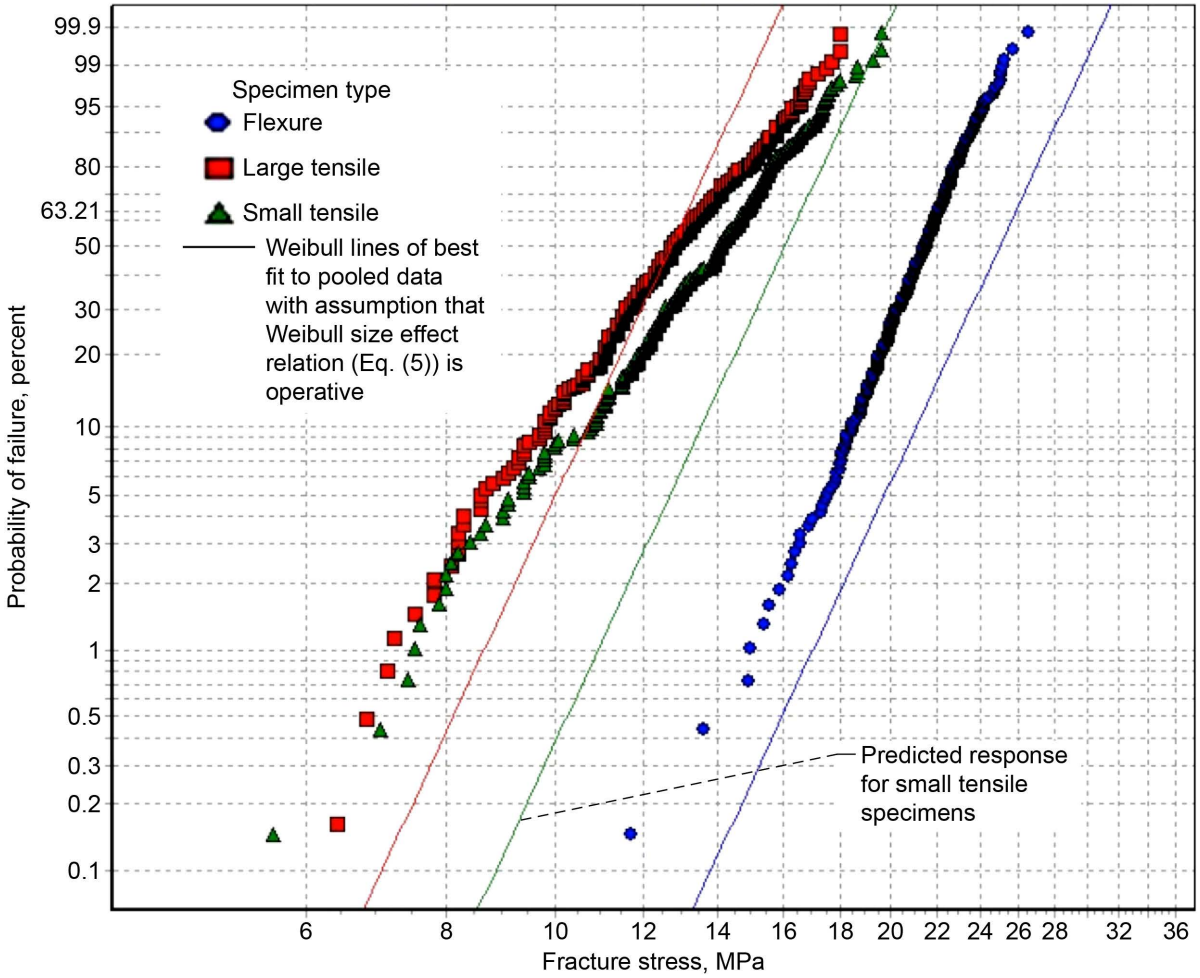

Figure 178.—Weibull plot of fracture stresses of pooled data from slabs 1 to 4 for radial specimens from pooled center and edge of slabs, comparing small tensile, large tensile, and flexure specimens (with nonlinear-elastic stress response). See Table 60 for a listing of Weibull parameters and 90-percent confidence bounds on parameters.

In Figure 179, the Weibull modulus is significantly higher for flexure specimens than for tensile specimens—beyond what is expected from natural statistical variation. It has not been established how much of this difference could be attributed to the nonlinear stress-strain response of H–451. An alternative explanation is that a different failure mode with a separate set of Weibull parameters is operating at the surface of the material when it is loaded under flexure. The Weibull moduli for the two different sizes of tensile specimens are quite similar.

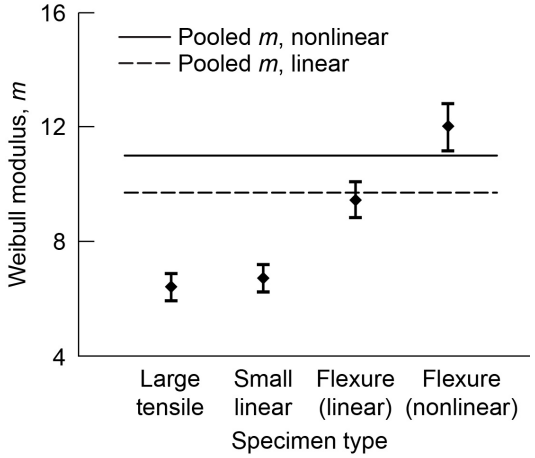

Figure 179.—Weibull modulus and 90-percent confidence bounds on pooled data from slabs 1 to 4 for radial specimens from pooled center and edge of slabs, comparing small tensile, large tensile, and flexure specimens. See Table 60 for a listing of Weibull parameters and 90-percent confidence bounds on parameters.

In Figure 180, the higher characteristic strength of the flexure specimen cannot be explained from natural statistical variation, and the size effect must be explained by other means such as with the Weibull distribution. On the other hand, the size effect between the small and large tensile specimens is less than what is expected with the Weibull distribution (see Figs. 177 and 178). When the fracture stresses were computed from Price (1976), the nonlinear stress-strain response reduced the characteristic strength of the flexure specimen. See Table 60 for a listing of Weibull parameters and 90-percent confidence bounds on parameters.

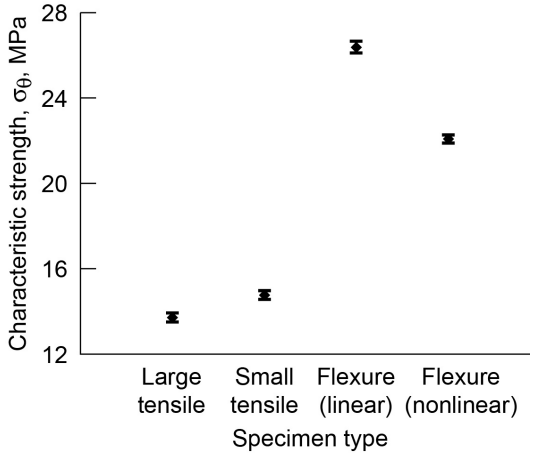

Figure 180.—Characteristic strength and 90-percent confidence bounds on pooled data from slabs 1 to 4 for radial specimens from pooled center and edge of slabs, comparing small tensile, large tensile, and flexure specimens. See Table 60 for a listing of Weibull parameters and 90-percent confidence bounds on parameters.

TABLE 60.—WEIBULL PARAMETERS AND 90-PERCENT CONFIDENCE BOUNDS ON POOLED DATA FROM SLABS 1 TO 4 FOR RADIAL SPECIMENS FROM POOLED CENTER AND EDGE OF SLABS, COMPARING SMALL TENSILE, LARGE TENSILE, AND FLEXURE SPECIMENS

Specimen type	Number of specimens	Weibull modulus, m		Characteristic strength, σ_θ, MPa	
		MLE biased[a]	90-percent boot confidence[b]	MPa	90-percent boot confidence[b]
Small tensile	343	6.72	6.23/7.18	14.78	14.57/14.99
Large tensile	311	6.42	5.94/6.88	13.74	13.54/13.95
Flexure, linear[c]	346	9.45	8.83/10.09	26.39	26.13/26.65
Flexure, nonlinear[d]	346	12.03	11.17/12.81	22.11	21.94/22.28
Pooled, linear[c]	1000	9.71	----------	------	----------
Pooled, nonlinear[d]	1000	11.01	----------	------	----------

[a]Maximum-likelihood estimation.
[b]Calculated from boot confidence bounds for 2000 simulations.
[c]Linear-elastic stress-strain response was assumed.
[d]Nonlinear-elastic stress-strain response was assumed.

In Figure 181 the Weibull best-fit lines assume that all the data have the same value of Weibull modulus and that the Weibull size effect was operating (by accounting for the geometry and loading of the specimens). A linear stress-strain response was assumed in determining the fracture stresses (from Price (1976)), and a linear-elastic finite element model of the four-point cylindrical flexure specimen was used in conjunction with WeibPar to determine the best-fit Weibull modulus and scale parameter (m = 9.24 and σ_o = 39.10 MPa-mm$^{3/m}$).

The WeibPar/CARES analysis shows that the size effect for the experimental data for the two tensile specimen geometries is much smaller than is expected from the Weibull stress-volume integration, whereas a large size effect exists between the tensile specimen and flexure specimen data that is adequately predicted with Weibull stress-volume integration.

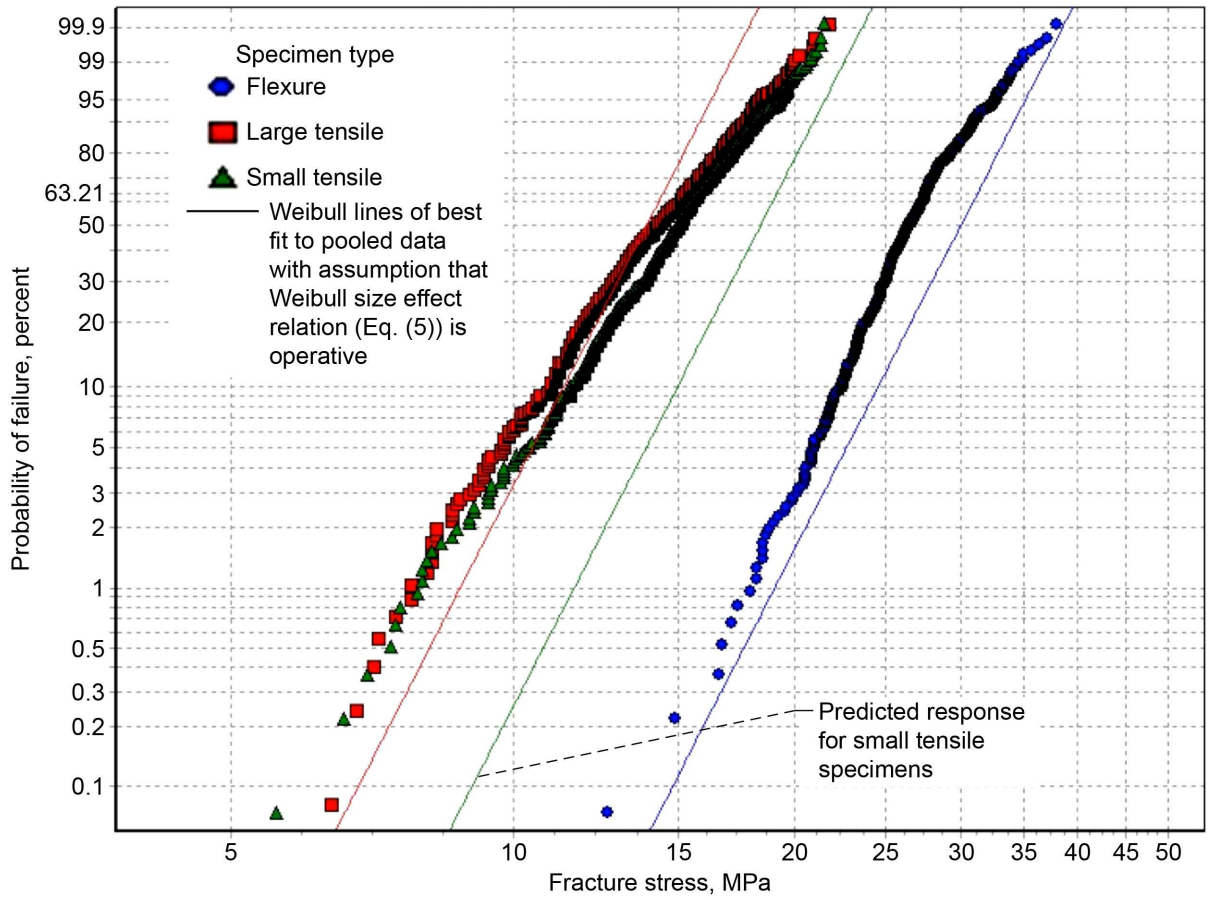

Figure 181.—Weibull plot of fracture stresses of pooled data from slabs 1 to 4 for axial and radial specimens from center and edge of slabs, comparing small tensile, large tensile, and flexure specimens (with linear-elastic stress response). See Table 61 for a listing of Weibull parameters and 90-percent confidence bounds on parameters.

In Figure 182 the Weibull best-fit lines assume that all the data have the same value of Weibull modulus and that the Weibull size effect is operating (by accounting for the geometry and loading of the specimens). A nonlinear stress-strain response was assumed in determining the fracture stresses (from Price (1976)), and a linear-elastic finite element model of the four-point cylindrical flexure specimen was used in conjunction with WeibPar to determine the best-fit Weibull modulus and scale parameter (m = 8.75 and σ_o = 40.34 MPa-mm$^{3/m}$). The predictions for the strength response from the WeibPar/CARES analysis do not account for changing effective volume with load that would be expected from a nonlinear stress-strain response.

The WeibPar/CARES analysis shows that the size effect for the experimental data for the two tensile specimen geometries is much smaller than what is expected from the Weibull stress-volume integration, whereas a large size effect exists between the tensile specimen and flexure specimen data that is overpredicted with Weibull stress-volume integration.

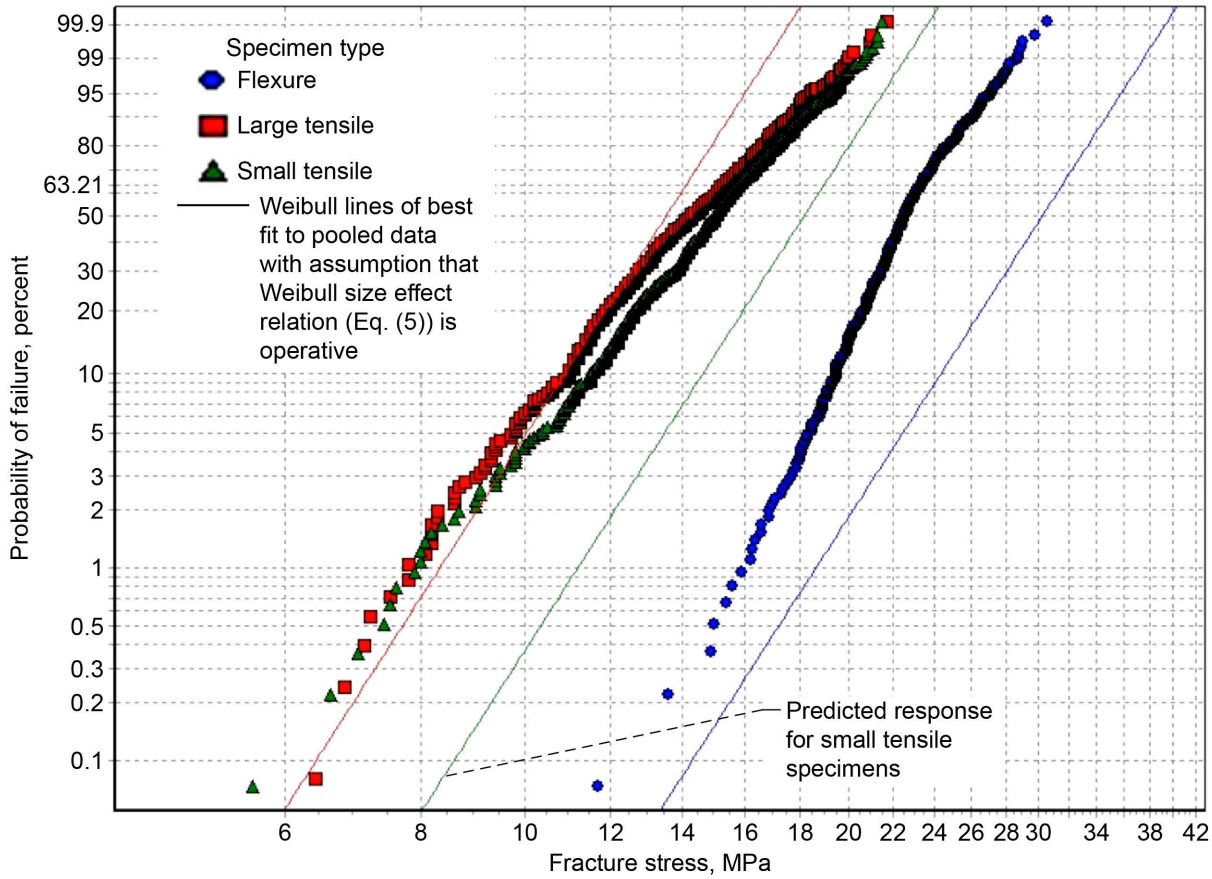

Figure 182.—Weibull plot of fracture stresses of pooled data from slabs 1 to 4 for axial and radial specimens from center and edge of slabs, comparing small tensile, large tensile, and flexure specimens (with nonlinear-elastic stress response). See Table 61 for a listing of Weibull parameters and 90-percent confidence bounds on parameters.

In Figure 183, the Weibull modulus is significantly higher for the flexure specimens than for the tensile specimens—beyond what is expected from natural statistical variation. It has not been established how much of this difference could be attributed to the nonlinear stress-strain response of H–451. An alternative explanation is that a different failure mode with a separate set of Weibull parameters is operating at the surface of the material when it is loaded under flexure. The Weibull moduli for the two different sizes of tensile specimens are reasonably similar.

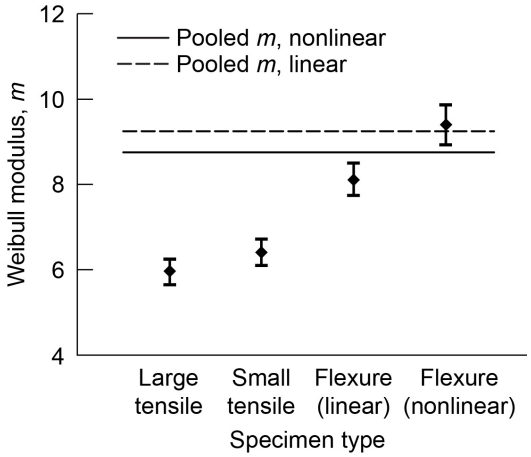

Figure 183.—Weibull modulus and 90-percent confidence bounds on pooled data from slabs 1 to 4 for axial and radial specimens from center and edge of slabs, comparing small tensile, large tensile, and flexure specimens See Table 61 for a listing of Weibull parameters and 90-percent confidence bounds on parameters.

In Figure 184, the higher characteristic strength of the flexure specimen cannot be explained from natural statistical variation, and the size effect must be explained by other means such as with the Weibull distribution. On the other hand, the size effect between the small and large tensile specimens is less than what is expected with the Weibull distribution (see Figures 181 and 182). When fracture stresses were computed from Price (1976), the nonlinear stress-strain response reduced the characteristic strength of the flexure specimen. See Table 61 for a listing of Weibull parameters and 90-percent confidence bounds on parameters.

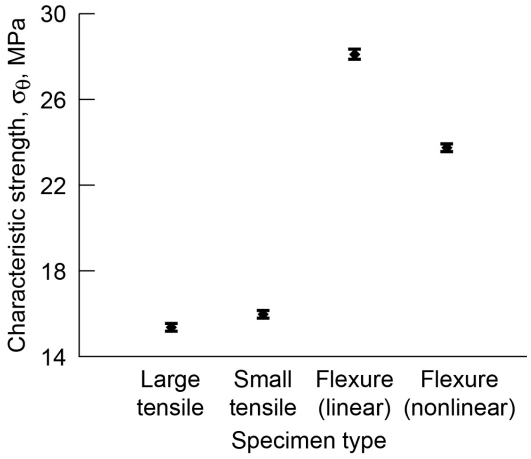

Figure 184.—Characteristic strength and 90-percent confidence bounds on pooled data from slabs 1 to 4 for axial and radial specimens from center and edge of slabs, comparing small tensile, large tensile, and flexure specimens. See Table 61 for a listing of Weibull parameters and 90-percent confidence bounds on parameters.

TABLE 61.—WEIBULL PARAMETERS AND 90-PERCENT CONFIDENCE BOUNDS ON POOLED DATA FROM AXIAL AND RADIAL SPECIMENS FROM CENTER AND EDGE OF SLABS, COMPARING SMALL TENSILE, LARGE TENSILE, AND FLEXURE SPECIMENS

Specimen type	Number of specimens	Weibull modulus, m		Characteristic strength, σ_θ, MPa	
		MLE biased[a]	90-percent boot confidence[b]	MPa	90-percent boot confidence[b]
Small tensile	689	6.42	6.10/6.72	15.99	15.83/16.16
Large tensile	628	5.97	5.66/6.26	15.38	15.20/15.56
Flexure, linear[c]	682	8.11	7.74/8.49	28.12	27.89/28.35
Flexure, nonlinear[d]	682	9.40	8.92/9.85	23.77	23.60/23.94
Pooled, linear[c]	1999	9.24	----------	------	----------
Pooled, nonlinear[d]	1999	8.75	----------	------	----------

[a]Maximum-likelihood estimation.
[b]Calculated from boot confidence bounds for 2000 simulations.
[c]Linear-elastic stress-strain response was assumed.
[d]Nonlinear-elastic stress-strain response was assumed.

Appendix E.—Large (Super) Pooled Data Sets for Small |and Large Tensile Specimens

The two groups in Figure 185—axial specimens from the edge of the slabs and radial specimens from the center of the slabs—show the largest difference in characteristic strength of the four total groups of large tensile specimens (axial center, axial edge, radial center, and radial edge). The figure shows a fairly distinct grouping of the data for the two groups.

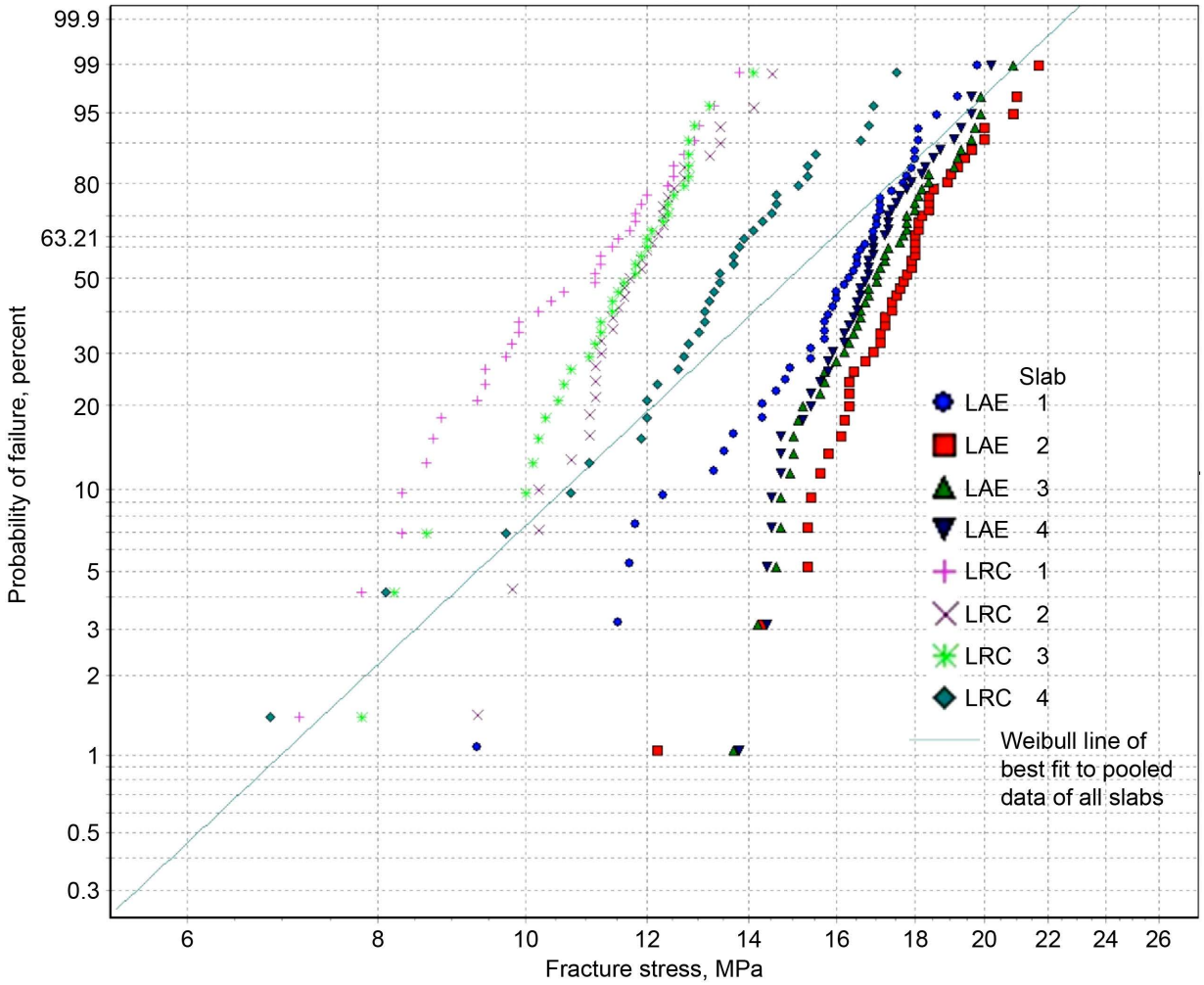

Figure 185.—Weibull plot of fracture stresses on individual slabs 1 to 4 for large tensile specimens, comparing axial specimens from edge of slabs with radial specimens from center of slabs. Specimens are designated as L = large tensile, A = axial, E = edge of slabs, R = radial, and C = center of slabs.

Figure 186 has a more consistent grouping of the Weibull moduli, and slabs 1 and 4 have lower Weibull moduli for the radial specimens from the center of the slabs.

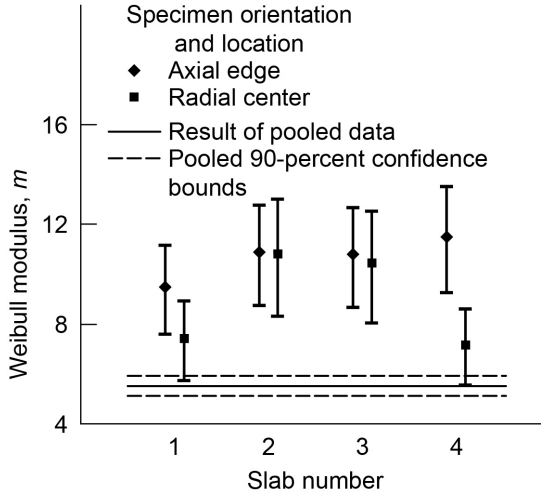

Figure 186.—Weibull modulus and 90-percent confidence bands on individual slabs 1 to 4 for large tensile specimens, comparing axial specimens from edge of slabs with radial specimens from center of slabs. See Table 62 for a listing of Weibull parameters and 90-percent confidence bounds on parameters.

The two groups in Figure 187—axial specimens from the edge of the slabs and radial specimens from the center of the slabs—show the largest difference in characteristic strength of the four total groups of large tensile specimens (axial center, axial edge, radial center, and radial edge). See Table 62 for a listing of Weibull parameters and 90-percent confidence bounds on parameters.

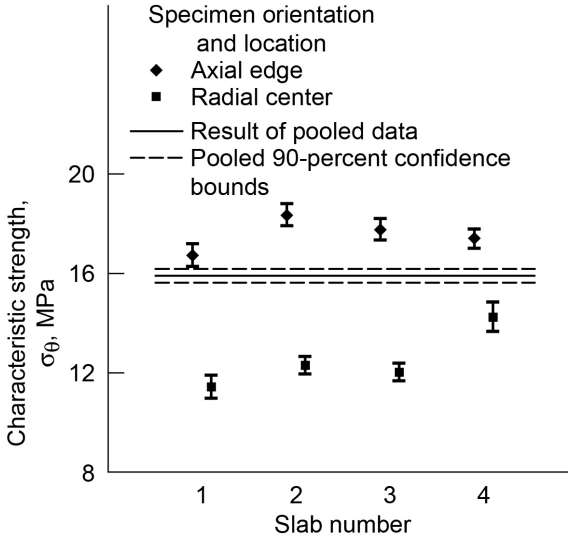

Figure 187.—Characteristic strength and 90-percent confidence bounds on individual slabs 1 to 4 for large tensile specimens, comparing axial specimens from edge of slabs with radial tensile specimens from center of slabs.

TABLE 62.—WEIBULL PARAMETERS AND 90-PERCENT CONFIDENCE BOUNDS ON INDIVIDUAL DATA FROM SLABS 1 TO 4 FOR LARGE TENSILE SPECIMENS, COMPARING INDIVIDUAL AXIAL SPECIMENS FROM EDGE OF SLABS AND RADIAL SPECIMENS FROM CENTER OF SLABS

Specimen orientation and location	Number of specimens	Weibull modulus, *m*		Characteristic strength, σ_θ, MPa	
		MLE biased[a]	90-percent confidence	MPa	90-percent confidence
Axial edge	47	9.48	7.60/11.14	16.75	16.3/17.22
Axial edge	48	10.89	8.76/12.78	18.37	17.94/18.82
Axial edge	48	10.79	8.68/12.66	17.79	17.37/18.23
Axial edge	48	11.5	9.25/15.50	17.43	17.04/17.82
Radial center	36	7.44	5.75/8.92	11.44	10.98/11.91
Radial center	35	10.81	8.31/13.00	12.32	11.97/12.67
Radial center	36	10.45	8.07/12.53	12.04	11.69/12.39
Radial center	36	7.18	5.54/8.61	14.26	13.68/14.88
Pooled	334	5.51	5.13/5.92	15.93	15.65/16.20

[a]Maximum-likelihood estimation.

In Figure 188, the typical slope of the data for the axial specimens from the edge of the slabs appears to be higher than that of the data for the radial specimens from the center of the slabs. These two groups of small tensile specimens (axial edge and radial center) show the largest difference in characteristic strength of the four total groups (axial center, axial edge, radial center, and radial edge), and Figure 188 shows a distinct grouping of the data for the two groups.

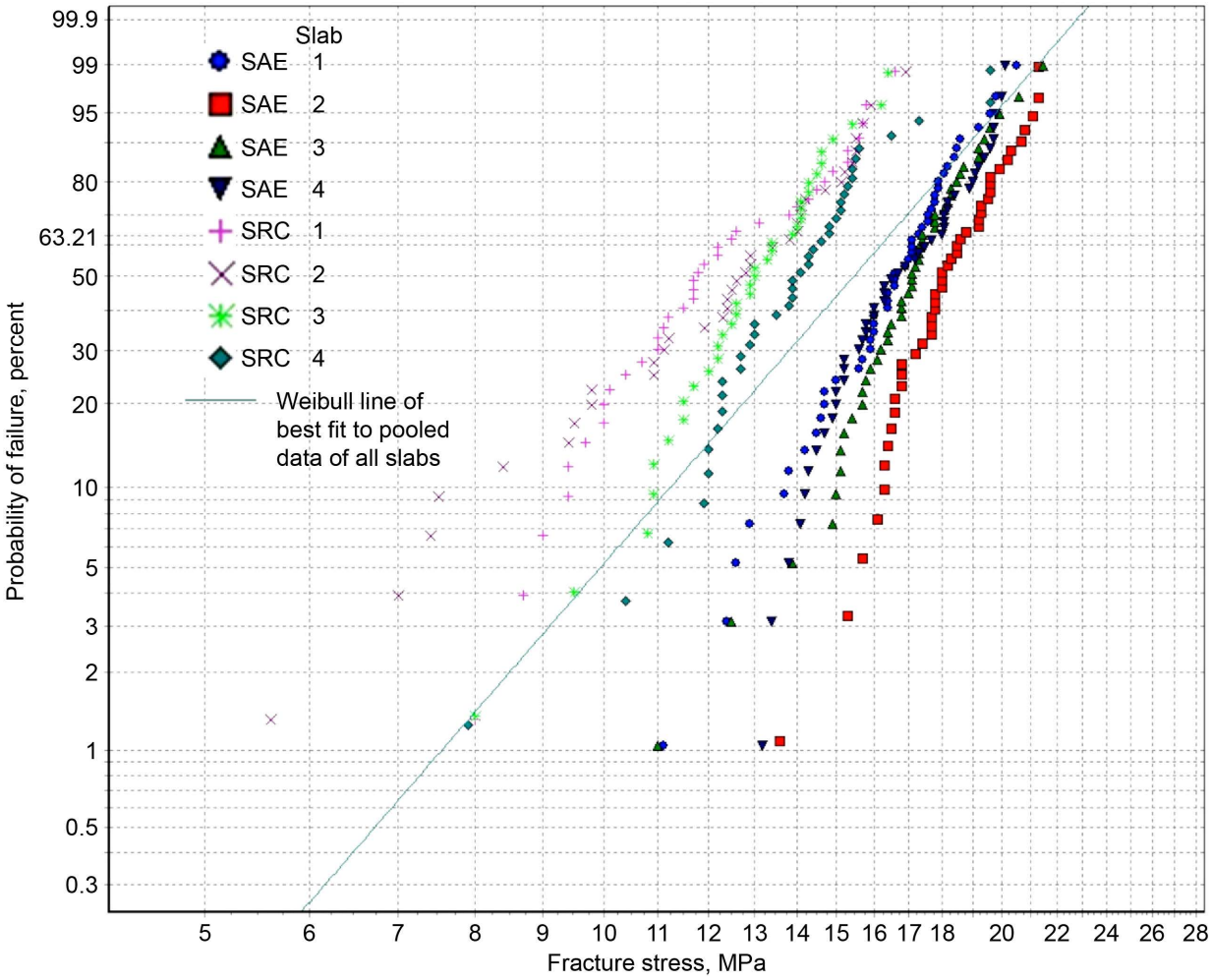

Figure 188.—Weibull plot of fracture stresses on individual slabs 1 to 4 for small tensile specimens, comparing axial specimens from edge of slabs and radial specimens from center of slabs. See Table 63 for a listing of Weibull parameters and 90-percent confidence bounds on parameters. Specimens are designated as S = small tensile, A = axial, E = edge of slabs, R = radial, and C = center of slabs.

In Figure 189, the Weibull moduli for the axial small tensile specimens from the edge of the slabs appear to be higher than those for the radial small tensile specimens from the center of the slabs.

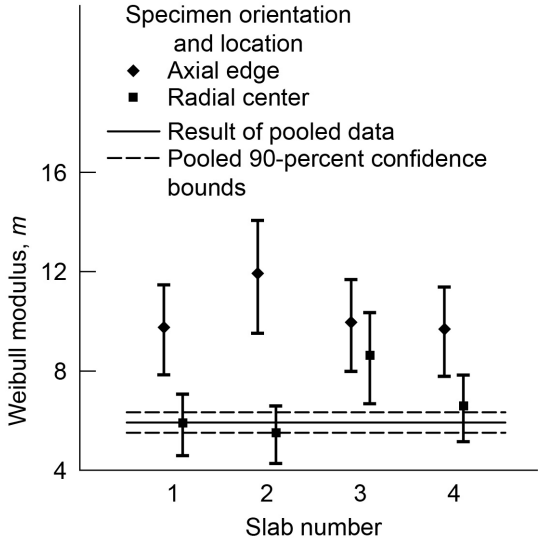

Figure 189.—Weibull modulus and 90-percent confidence bands on individual slabs 1 to 4 for small tensile specimens, comparing axial specimens from edge of slabs with radial specimens from center of slabs. See Table 63 for a listing of Weibull parameters and 90-percent confidence bounds on parameters.

The two groups of small tensile specimens in Figure 190 (axial edge and radial center) show the largest difference in characteristic strength of the four total groups (axial center, axial edge, radial center, and radial edge). See Table 63 for a listing of Weibull parameters and 90-percent confidence bounds on parameters.

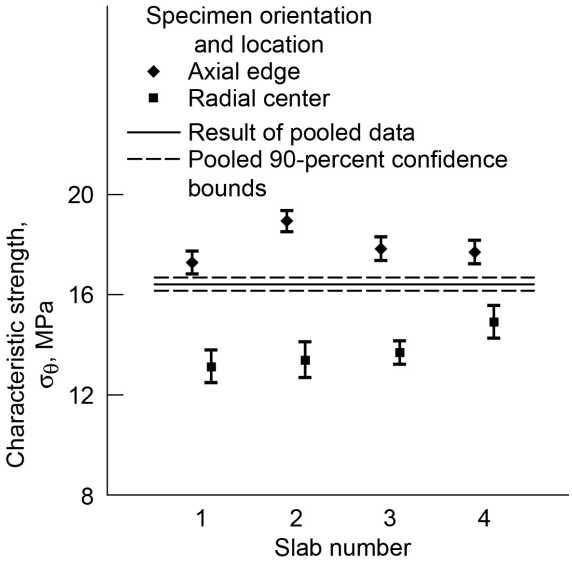

Figure 190.—Characteristic strength and 90-percent confidence bounds on individual slabs 1 to 4 for small tensile specimens, comparing axial specimens from edge of slabs with radial specimens from center of slabs.

TABLE 63.—WEIBULL PARAMETERS AND 90-PERCENT CONFIDENCE BOUNDS ON INDIVIDUAL DATA FROM SLABS 1 TO 4 FOR SMALL TENSILE SPECIMENS

Specimen orientation and location	Number of specimens	Weibull modulus, m		Characteristic strength, σ_θ, MPa	
		MLE biased[a]	90-percent confidence	MPa	90-percent confidence
Axial edge	48	9.77	7.86/11.47	17.30	16.85/17.76
Axial edge	46	11.93	9.54/14.05	18.96	18.54/19.38
Axial edge	48	9.95	8.00/11.67	17.85	17.39/18.32
Axial edge	48	9.69	7.80/11.38	17.71	17.25/18.19
Radial center	38	5.93	4.61/7.08	13.14	12.51/13.81
Radial center	38	5.52	4.29/6.59	13.40	12.71/14.13
Radial center	37	8.63	6.69/10.34	13.71	13.24/14.18
Radial center	40	6.58	5.16/7.84	14.92	14.29/15.58
Pooled	343	5.92	5.51/6.34	16.44	16.18/16.70

[a]Maximum-likelihood estimation.

In Figure 191, the Weibull moduli are reasonably comparable for the large and small tensile specimens with respect to the individual slabs.

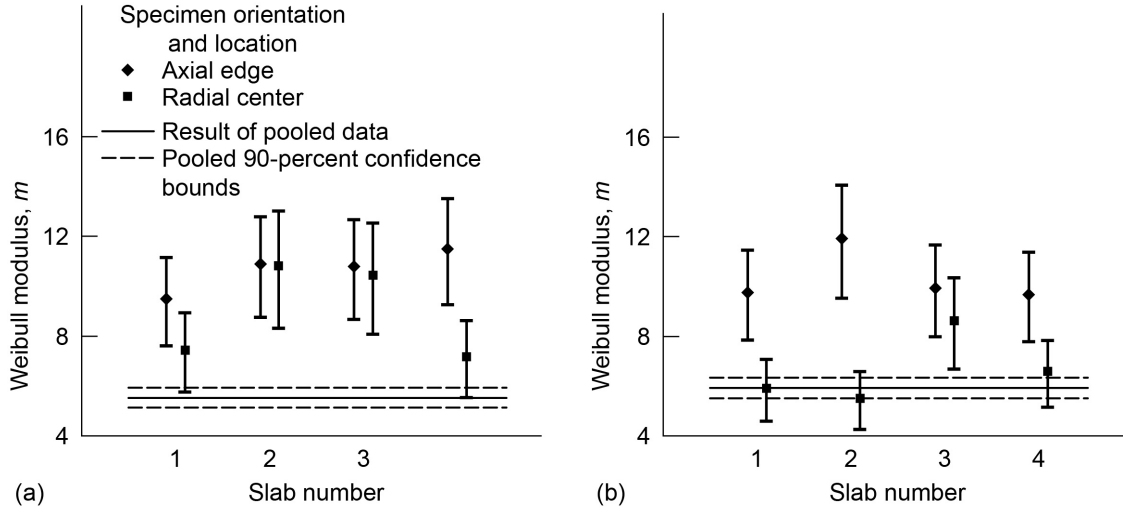

Figure 191.—Weibull modulus and 90-percent confidence bands on individual slabs 1 to 4, showing a side-by-side comparison of Figures 186 and 189, comparing axial specimens from edge of slabs and radial specimens from center of slabs. (a) Large tensile specimens. (b) Small tensile specimens.

In Figure 192, the characteristic strengths are similar for the large and small tensile specimens. This difference for the individual slabs appears to be equal to or smaller than variations from slab to slab. From this sampling, it seems reasonable to pool data from the large and small tensile specimens without regard to size effect corrections.

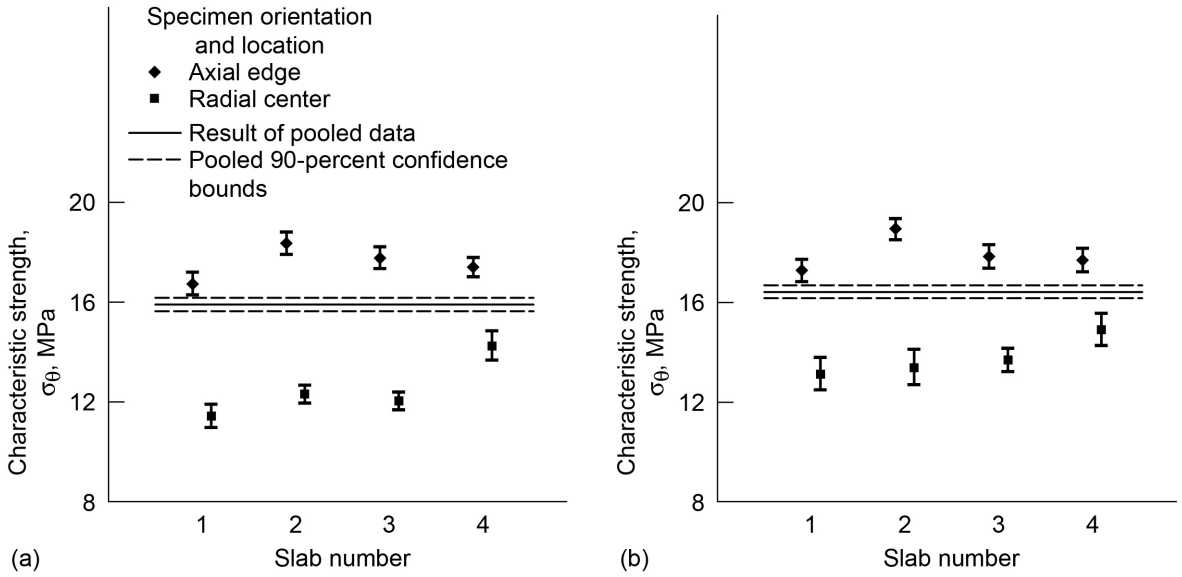

Figure 192.—Characteristic strength and 90-percent confidence bounds on individual slabs 1 to 4, showing a side-by-side comparison of Figures 187 and 190, comparing axial specimens from edge of slabs and radial specimens from center of slabs. (a) Large tensile specimens. (b) Small tensile specimens.

The intent of Figure 193 is to show that the size effect between the large and small tensile specimens is so minor that the data can be pooled (without accounting for size effect) into a larger data set comprising all tensile specimens. Note that, for the most part, the strength varies more for the different orientations and locations than between the large and small tensile specimens.

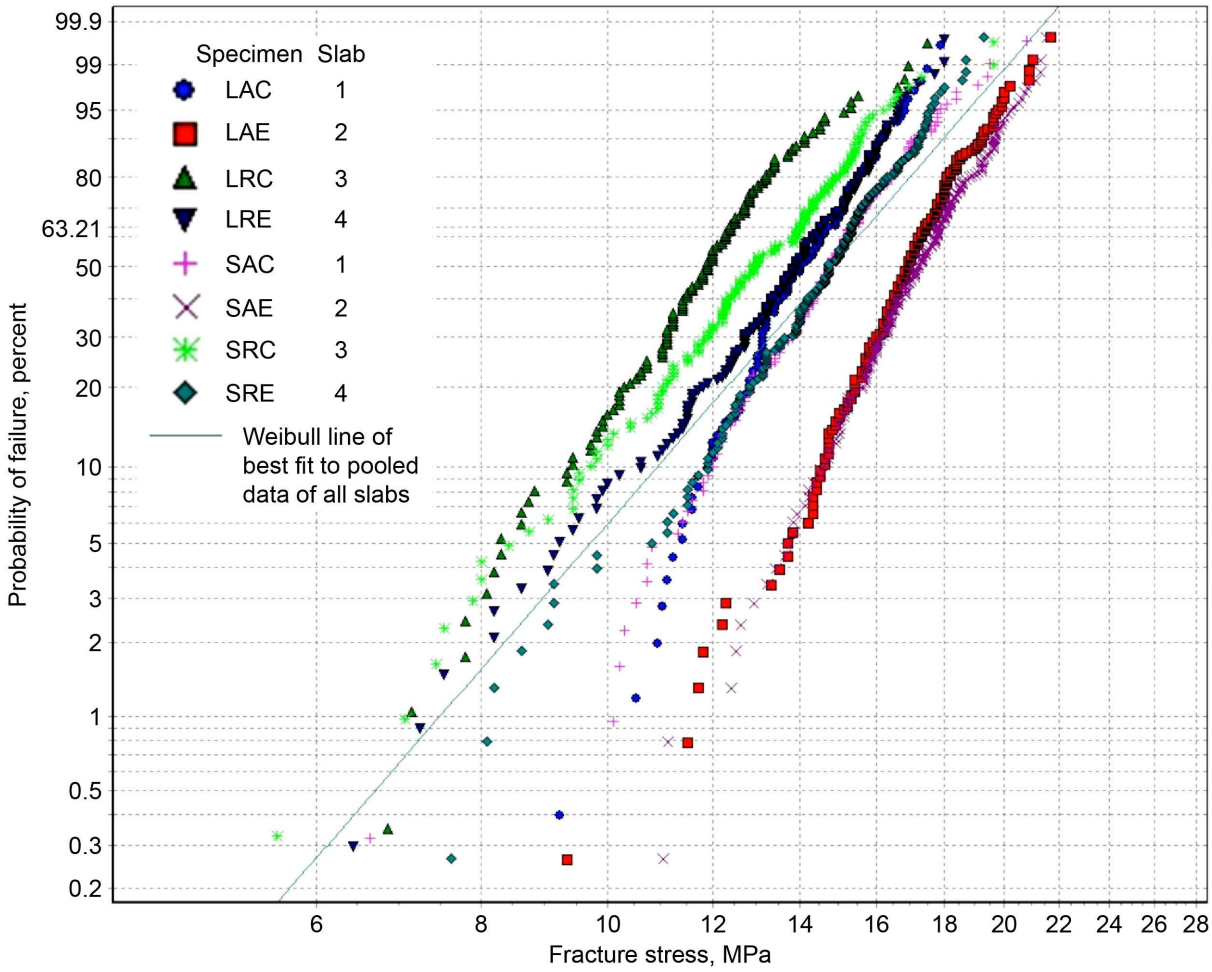

Figure 193.—Weibull plot of fracture stresses on individual slabs 1 to 4 for pooled large and small tensile specimens, showing effects of orientation and location. Specimens are designated as L = large tensile, A = axial, C = center of slabs, E = edge of slabs, R = radial, and S = small tensile.

Figure 194 shows relatively good correlation between the Weibull moduli of the large and small tensile specimens.

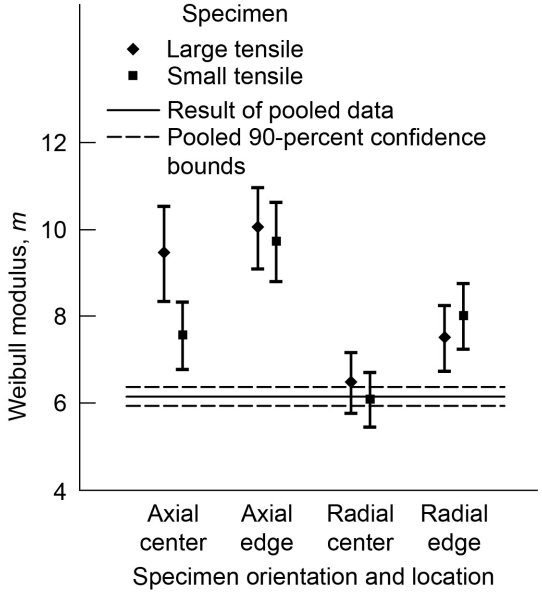

Figure 194.—Weibull modulus and 90-percent confidence bands on pooled data from slabs 1 to 4 for large and small tensile specimens, showing effects of specimen orientation and location. See Table 64 for a listing of Weibull parameters and 90-percent confidence bounds on parameters.

Figure 195 shows relatively good correlation between the characteristic strengths of the large and small tensile specimens, indicating that differences for different orientations and locations are as large or larger than the size effect between the large and small tensile specimens. See Table 64 for a listing of Weibull parameters and 90-percent confidence bounds on parameters.

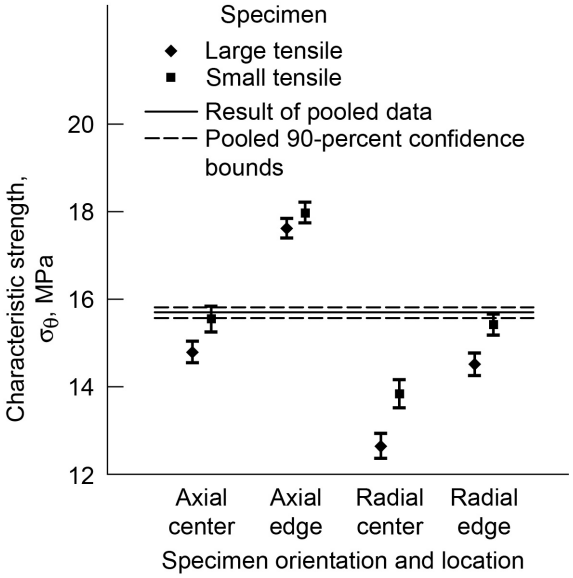

Figure 195.—Characteristic strength and 90-percent confidence bounds on pooled data from slabs 1 to 4 for large and small tensile specimens, showing effects of specimen orientation and location. See Table 64 for a listing of Weibull parameters and 90-percent confidence bounds on parameters.

TABLE 64.—WEIBULL PARAMETERS AND 90-PERCENT CONFIDENCE BOUNDS ON POOLED DATA FROM SLABS 1 TO 4 FOR LARGE AND SMALL TENSILE SPECIMENS

Specimen orientation and location	Number of specimens	Weibull modulus, *m*		Characteristic strength, σ_θ, MPa	
		MLE biased[a]	90-percent confidence	MPa	90-percent confidence
Large tensile specimens					
Axial center	126	9.47	8.34/10.52	14.80	14.56/15.05
Axial edge	191	10.05	9.09/10.96	17.63	17.41/17.85
Radial center	143	6.50	5.78/7.17	12.65	12.37/12.94
Radial edge	168	7.52	6.75/8.25	14.52	14.26/14.78
Small tensile specimens					
Axial center	156	7.58	6.78/8.33	15.56	15.27/15.85
Axial edge	190	9.73	8.80/10.62	17.98	17.75/18.22
Radial center	153	6.11	5.46/6.72	13.85	13.53/14.17
Radial edge	190	8.02	7.25/8.75	15.43	15.19/15.67
Pooled	1317	6.16	5.95/6.38[b]	15.70	15.58/15.83[b]

[a]Maximum-likelihood estimation.
[b]Calculated from boot confidence bounds for 2000 simulations.

In Figure 196, the effects of specimen orientation seem to be more dominant than the effects of location, indicating that the next logical grouping of data is for orientation only.

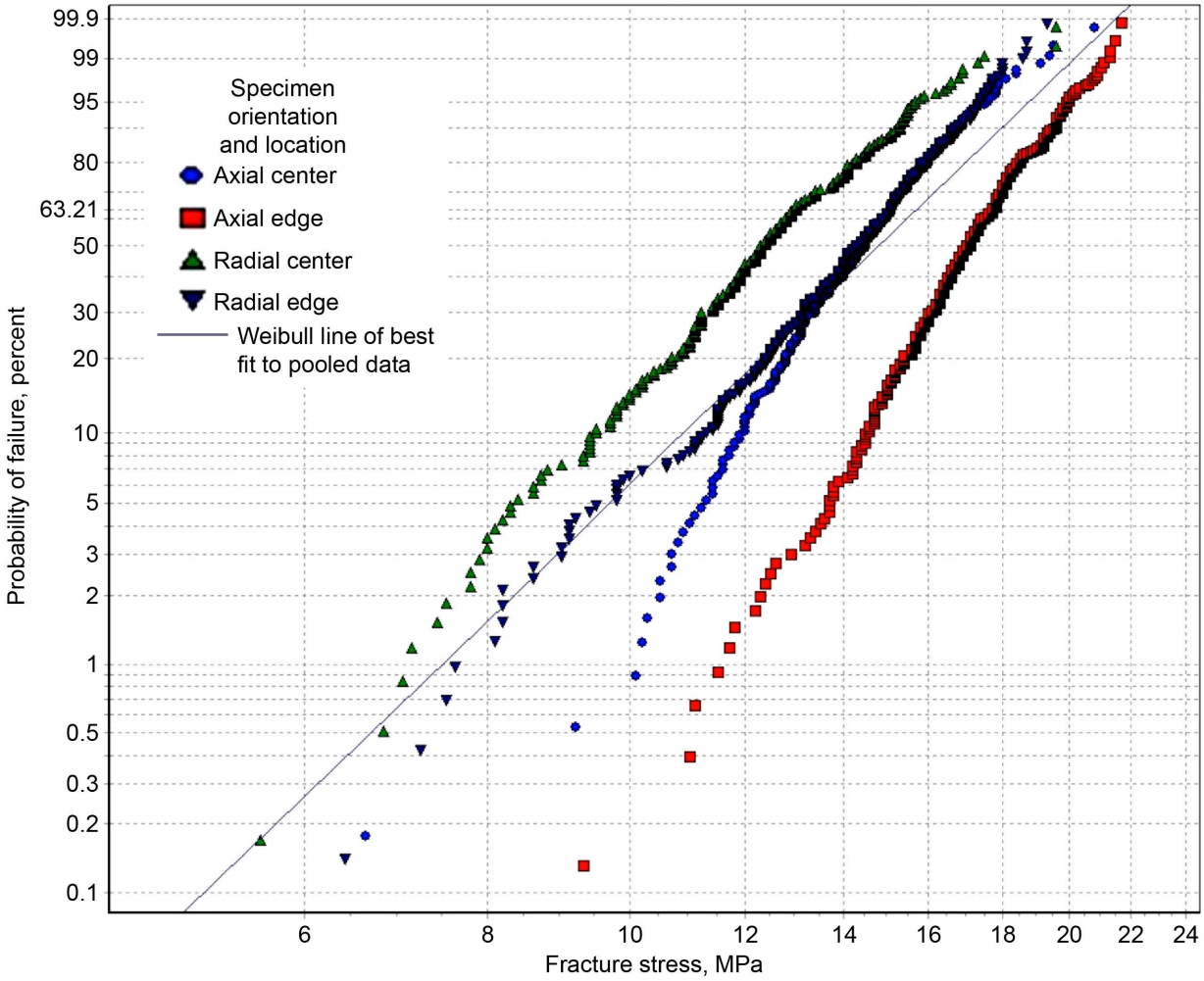

Figure 196.—Weibull plot of fracture stresses on pooled data from slabs 1 to 4 for large and small tensile specimens, showing effects of specimen orientation and location without considering size effect.

In Figure 197, the largest difference, which is statistically significant, is between the axial specimens at the edge of the slab and the radial specimens at the center of the slab.

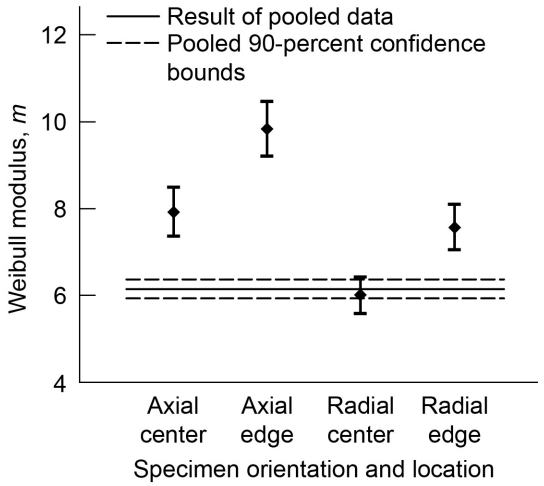

Figure 197.—Weibull modulus and 90-percent confidence bands on pooled data from slabs 1 to 4 for large and small tensile specimens, showing effects of specimen orientation and location. See Table 65 for a listing of Weibull parameters and 90-percent confidence bounds on parameters.

In Figure 198, characteristic strengths for specimens from the center of the slabs seem to be lower than for specimens from the edge of the slabs, and characteristic strengths for radial specimens seem to be lower than for axial specimens. The largest difference is between axial specimens from the edge of the slabs and radial specimens from the center of the slabs. The characteristic strengths are relatively similar for axial specimens from the center of the slabs and radial specimens from the edge of the slabs.

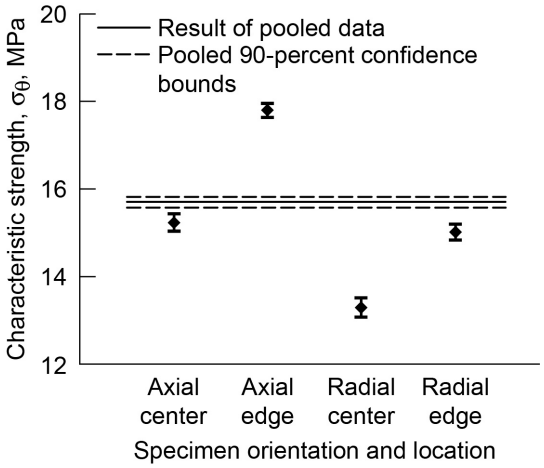

Figure 198.—Characteristic strength and 90-percent confidence bounds on pooled data from slabs 1 to 4 for large and small tensile specimens, showing effects of specimen orientation and location. See Table 65 for a listing of Weibull parameters and 90-percent confidence bounds on parameters.

Figures 197 and 198 seem to show an interesting correlation between the Weibull modulus and the characteristic strength. When the Weibull modulus is higher, the characteristic strength tends to be higher. This trend would be expected if residual compressive stresses were present. A residual compressive stress would tend to increase the applied stress required for fracture and would also truncate the Weibull distribution with a threshold stress (a stress below which fracture could not occur) such that it would follow a three-parameter Weibull distribution. Fitting a two-parameter Weibull distribution to these data would increase the estimated Weibull modulus (because of the truncated tail of the distribution) in comparison to a situation where no residual stresses were present. It is possible that a similar trend would occur in the presence of a rising R-curve. See Table 65 for a listing of Weibull parameters and 90-percent confidence bounds on parameters.

TABLE 65.—WEIBULL PARAMETERS AND 90-PERCENT CONFIDENCE BOUNDS ON POOLED DATA FROM SLABS 1 TO 4 FOR POOLED LARGE AND SMALL TENSILE SPECIMENS

Specimen orientation and location	Number of specimens	Weibull modulus, m		Characteristic strength, σ_θ, MPa	
		MLE biased[a]	90-percent confidence[b]	MPa	90-percent confidence
Axial center	282	7.92	7.37/8.50	15.24	15.04/15.44
Axial edge	381	9.83	9.21/10.46[b]	17.81	17.65/17.97[b]
Radial center	296	6.02	5.60/6.44	13.30	13.08/13.52
Radial edge	358	7.57	7.06/8.10[b]	15.02	14.84/15.20[b]
Pooled	1317	6.16	5.95/6.38[b]	15.70	15.58/15.83[b]

[a]Maximum-likelihood estimation.
[b]Calculated from boot confidence bounds for 2000 simulations.

In Figure 199, the effects of specimen orientation seem to be more dominant than the size effect between the large and small tensile specimens.

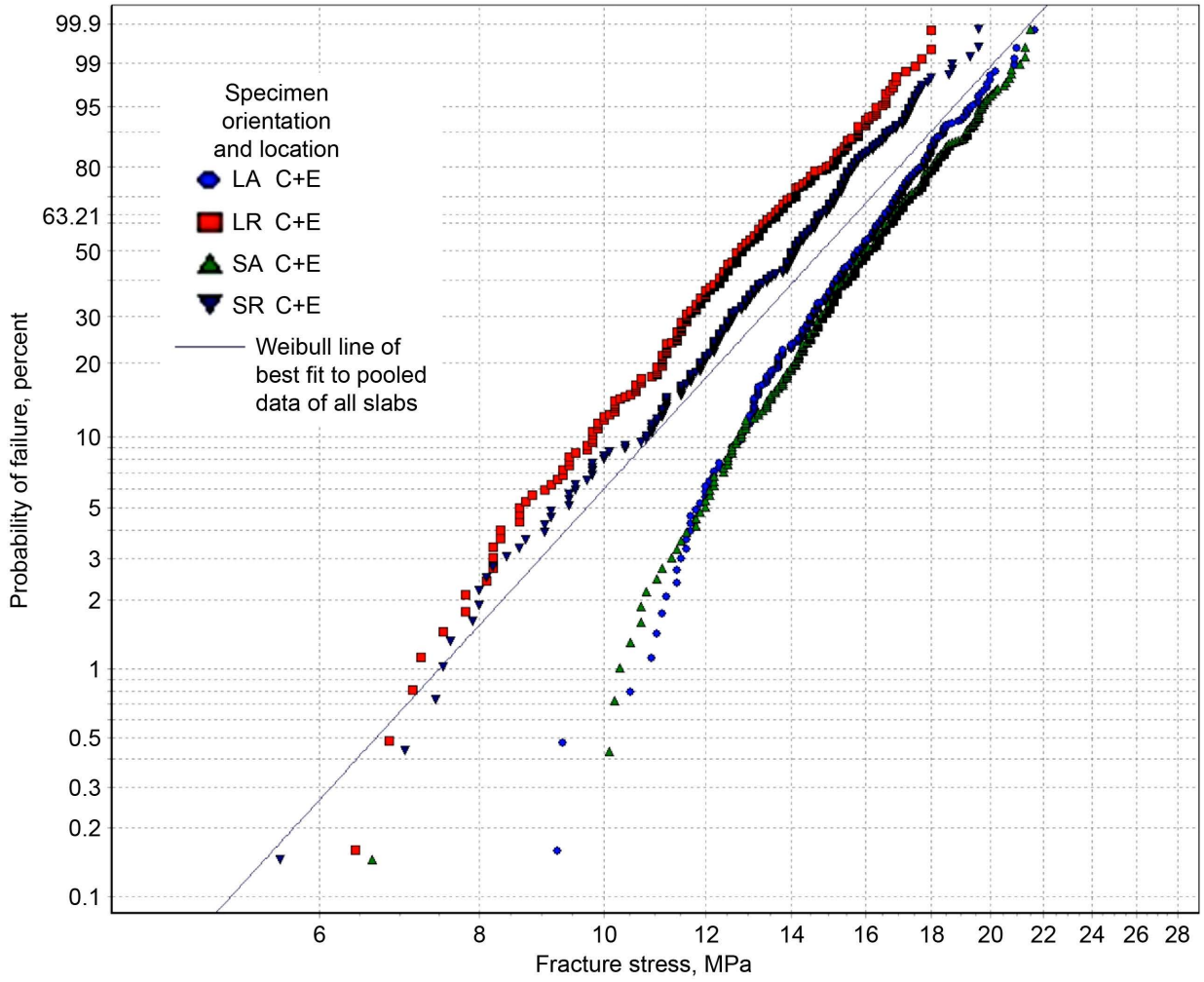

Figure 199.—Weibull plot of fracture stresses of pooled data from slabs 1 to 4 for pooled center and edge specimens, showing effects of specimen orientation. Specimens are designated as L = large tensile, A = axial, R = radial, C+E = pooled data from center and edge of slabs, and S = small tensile.

In Figure 200, the largest difference, which is statistically significant, is between the axial and radial specimens. The difference between Weibull moduli for large and small tensile specimens with a given orientation is not statistically significant; that is, it is within expected natural statistical variation.

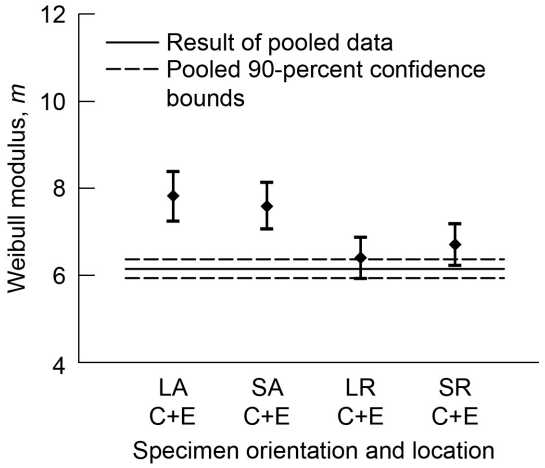

Figure 200.—Weibull modulus and 90-percent confidence bands on pooled data from slabs 1 to 4 for pooled center and edge specimens, showing effects of specimen orientation and size effect. See Table 66 for a listing of Weibull parameters and 90-percent confidence bounds on parameters.

Figure 201 shows that characteristic strengths for the small tensile specimens are higher than for the large tensile specimens. However, the difference is small for axial specimens and may not be statistically significant. The difference is larger for radial specimens and is statistically significant—beyond what is expected from natural statistical variation.

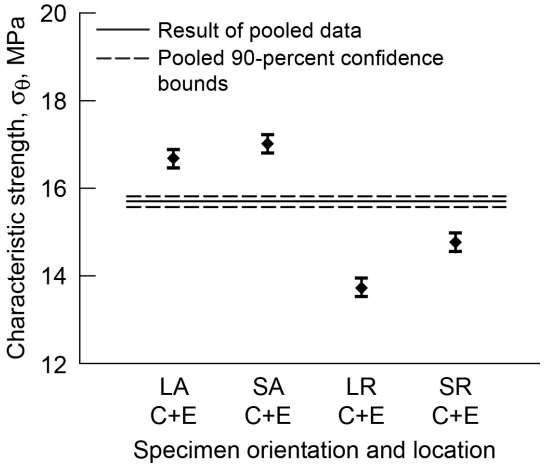

Figure 201.—Characteristic strength and 90-percent confidence bounds on pooled data from slabs 1 to 4 for pooled center and edge specimens, showing effects of specimen orientation and size effect. Specimens are designated as L = large tensile, A = axial, C+E = pooled data from center and edge of slabs, S = small tensile, and R = radial. See Table 66 for a listing of Weibull parameters and 90-percent confidence bounds on parameters.

Figure 202 clearly shows that the size effect is considerably smaller than what would be expected with Weibull stress-volume integration.

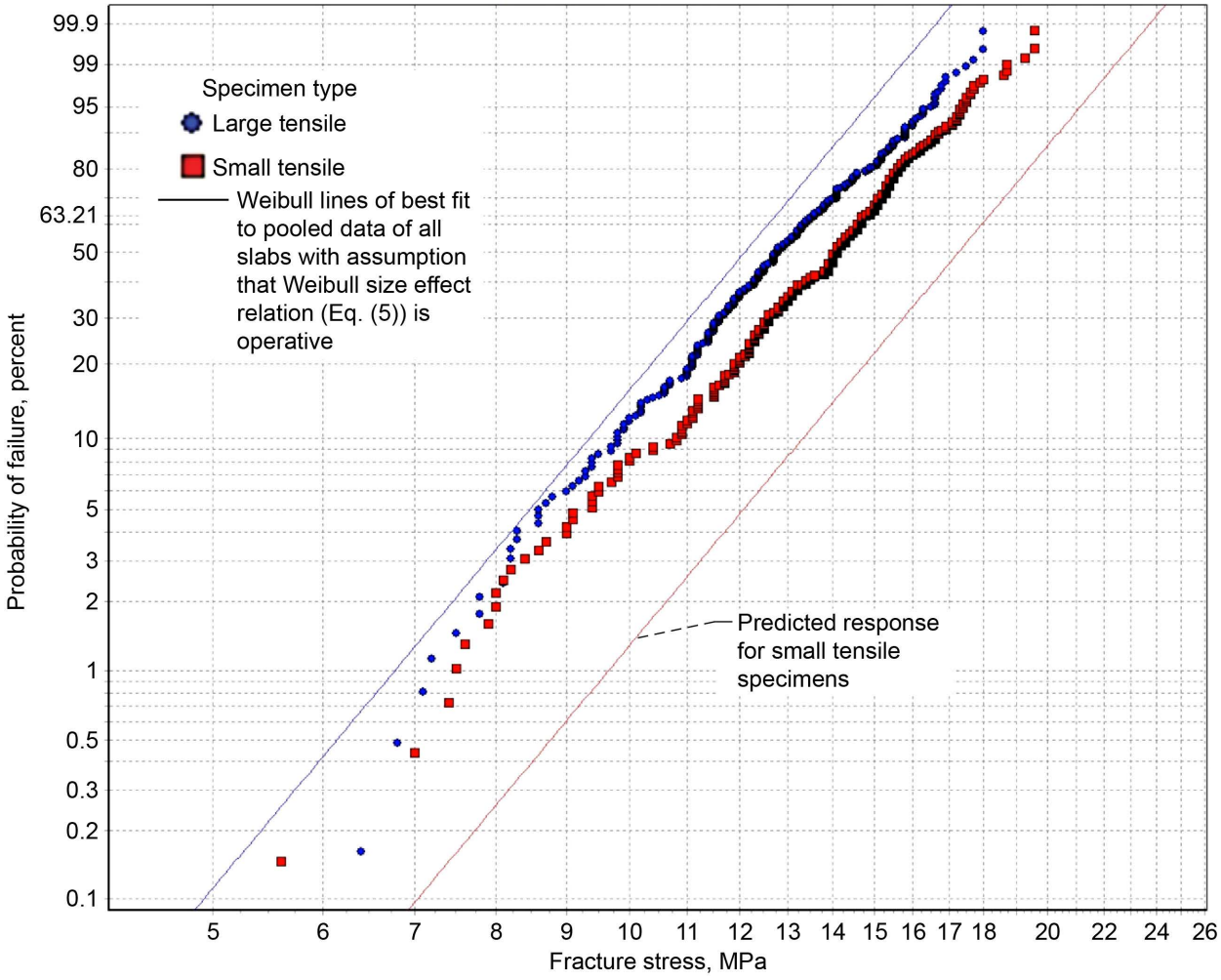

Figure 202.—Weibull plot of fracture stresses on pooled data from slabs 1 to 4 for radial specimens pooled for center and edge of slabs, showing size effect. Shown are the lines of best fit to the data for the predicted volume-based size effect from the Weibull distribution for m = 7.27.

Figure 203 clearly shows that the size effect is significantly smaller than what would be expected with Weibull stress-surface-area integration.

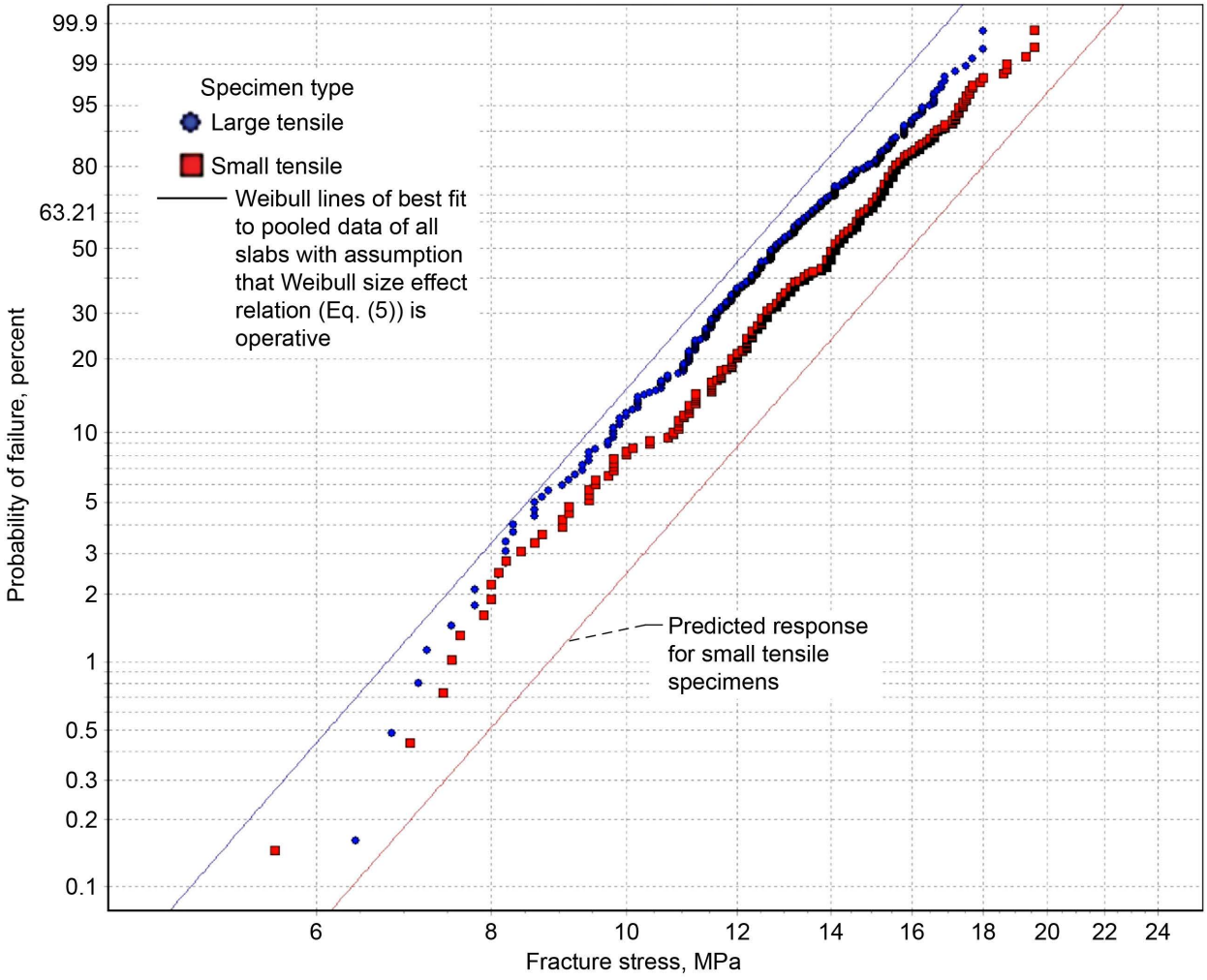

Figure 203.—Weibull plot of fracture stresses on pooled data from slabs 1 to 4 for radial specimens pooled for center and edge of slabs, showing size effect. Shown are the lines of best fit to the data for the predicted surface-area-based size effect from the Weibull distribution for m = 7.1.

Figures 202 and 203 show that the size effect from the experimental data is considerably smaller than what is expected with the Weibull distribution, based either on the specimen volume or on the specimen surface area. See Table 66 for a listing of Weibull parameters and 90-percent confidence bounds on parameters.

TABLE 66.—WEIBULL PARAMETERS AND 90-PERCENT CONFIDENCE BOUNDS ON POOLED DATA FROM SLABS 1 TO 4 FOR CENTER AND EDGE OF SLABS

Specimen orientation	Number of specimens	Weibull modulus, *m*		Characteristic strength, σ_θ, MPa	
		MLE biased[a]	90-percent boot confidence[b]	MPa	90-percent boot confidence[b]
Large tensile specimens					
Axial	317	7.83	7.25/8.39	16.69	16.47/16.89
Radial	311	6.42	5.94/6.88	13.74	13.54/13.95
Small tensile specimens					
Axial	346	7.60	7.07/8.14	17.02	16.81/17.23
Radial	343	6.72	6.23/7.18	14.78	14.57/14.99
Pooled	1317	6.16	5.95/6.38	15.70	15.58/15.83

[a]Maximum-likelihood estimation.
[b]Calculated from boot confidence bands for 2000 simulations.

In Figure 204, note the fairly linear appearance of the data for the radial specimens versus the somewhat curved appearance of the data for the axial specimens. Also note that the lowest strength axial specimen seems to depart from the trend in the data. This highlights the care needed in fitting to data when a three-parameter Weibull distribution is used. Had that lowest strength point not been present in the data set, a three-parameter fit to the remaining data might have indicated a threshold strength higher than the lowest strength—which is clearly a false scenario in this case.

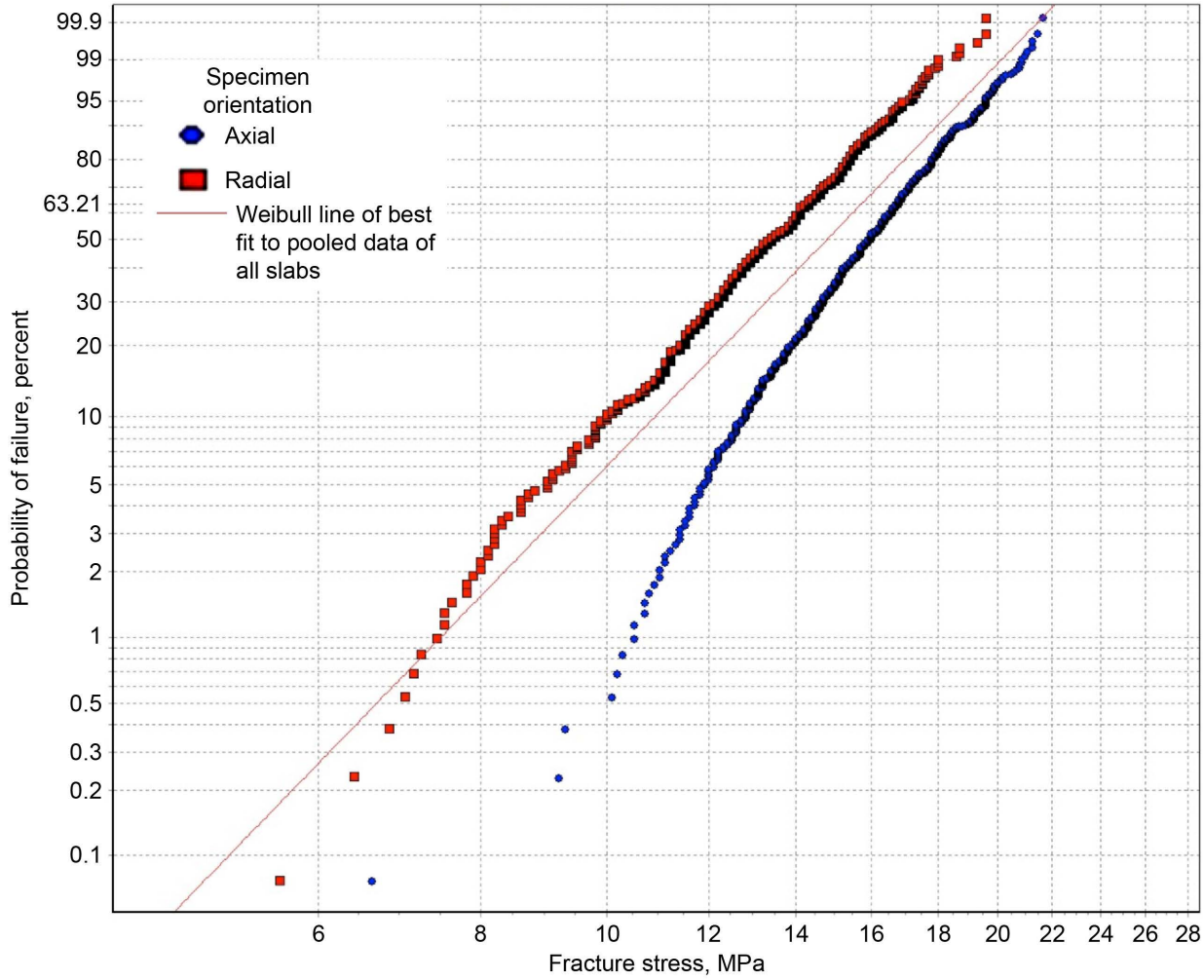

Figure 204.—Weibull plot of fracture stresses on pooled data from slabs 1 to 4 for large and small tensile specimens, showing effects of specimen orientation for data pooled without considering size effect.

In Figure 205, the difference in Weibull moduli appears to be statistically significant—beyond what is expected from natural statistical variation. See Table 67 for a listing of Weibull parameters and 90-percent confidence bounds on parameters.

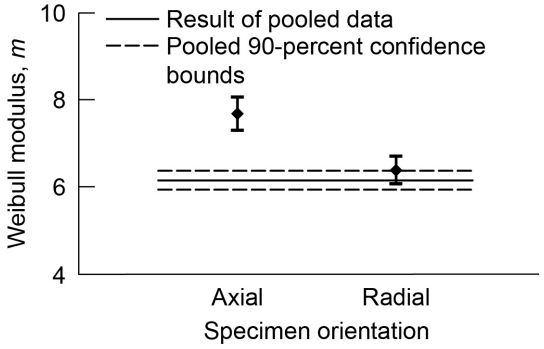

Figure 205.—Weibull modulus and 90-percent confidence bands on pooled data from slabs 1 to 4 for large and small tensile specimens, showing effects of specimen orientation.

In Figure 206, the difference between the characteristic strengths of the axial and radial specimens is statistically significant—beyond what is expected for natural statistical variation. See Table 67 for a listing of Weibull parameters and 90-percent confidence bounds on parameters.

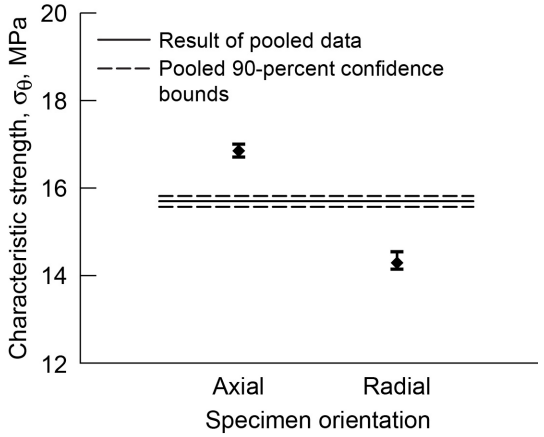

Figure 206.—Characteristic strength and 90-percent confidence bounds on pooled data from slabs 1 to 4 for large and small tensile specimens, showing effects of specimen orientation.

Figures 205 and 206 seem to show an interesting correlation between the Weibull modulus and the characteristic strength. When the Weibull modulus is higher, the characteristic strength tends to be higher. This trend would be expected if residual compressive stresses were present. A residual compressive stress would tend to increase the applied stress required for fracture and would also truncate the Weibull distribution with a threshold stress (a stress below which fracture could not occur) such that it would follow a three-parameter Weibull distribution. Fitting a two-parameter Weibull distribution to these data would increase the estimated Weibull modulus (because of the truncated tail of the distribution) in comparison to a situation where no residual stresses were present. It is possible that a similar trend would occur in the presence of a rising R-curve. However, as Figure 204 shows, caution should be exercised when fitting a three-parameter Weibull distribution to the data for the axial specimens. See Table 67 for a listing of Weibull parameters and 90-percent confidence bounds on parameters.

TABLE 67.—WEIBULL PARAMETERS AND 90-PERCENT CONFIDENCE BOUNDS ON POOLED DATA FROM SLABS 1 TO 4 FOR LARGE AND SMALL TENSILE SPECIMENS

Specimen orientation	Number of specimens	Weibull modulus, m		Characteristic strength, σ_θ, MPa	
		MLE biased[a]	90-percent boot confidence[b]	MPa	90-percent boot confidence[b]
Axial	663	7.68	7.31/8.06	16.86	16.71/17.01
Radial	654	6.39	6.08/6.62	14.3	14.15/14.55
Pooled	1317	6.16	5.95/6.38	15.70	15.58/15.83

[a]Maximum-likelihood estimation.
[b]Calculated from boot confidence bands for 2000 simulations.

In Figure 207 the Weibull best-fit lines assume that all the data have the same value of Weibull modulus and that the Weibull size effect, as a function of specimen volume, is operating (by accounting for the geometry and loading of the specimens). Note that the predicted size effect is appreciably larger than that observed from the experimental data. The same situation would be true if the size effect were computed as a function of the specimen surface area (this case is not shown).

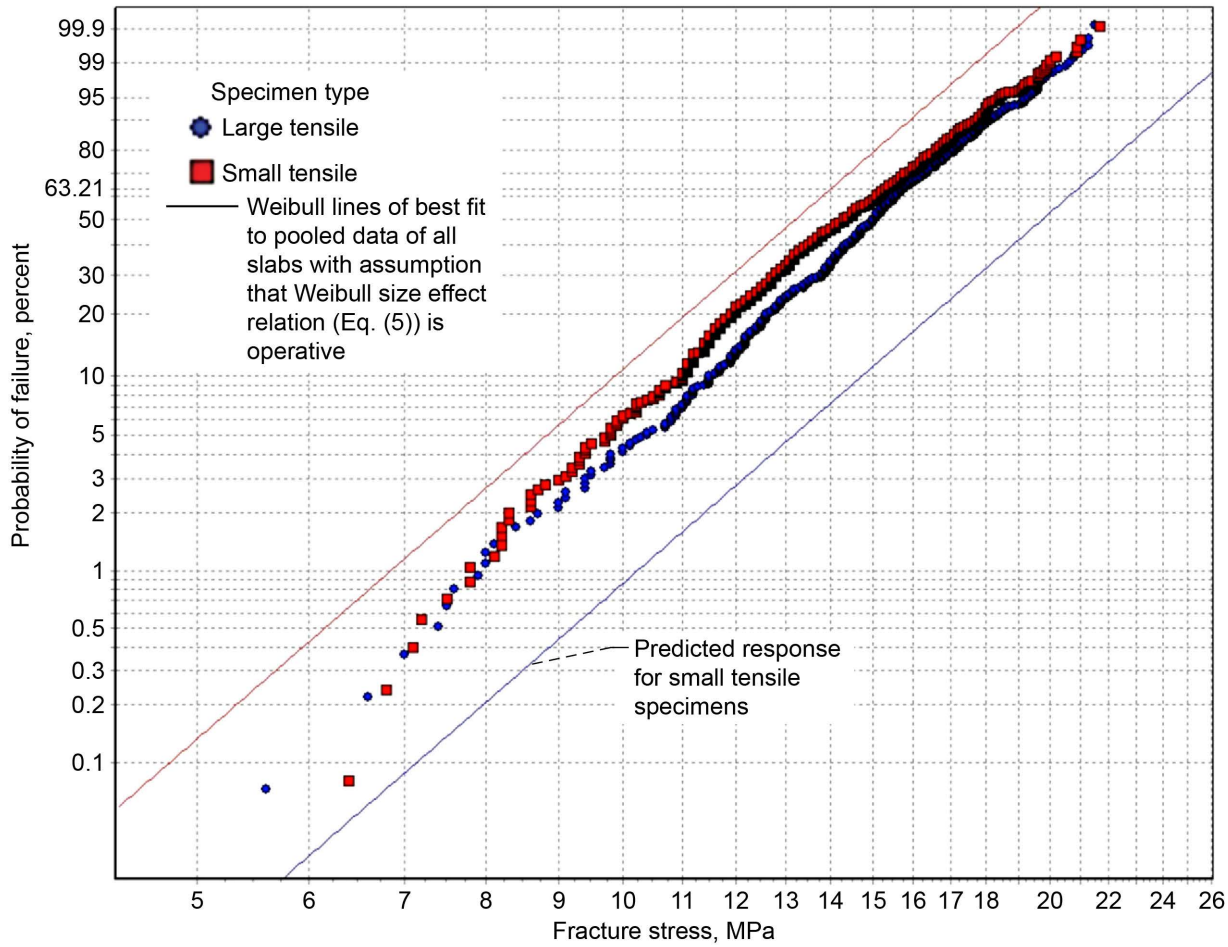

Figure 207.—Weibull plot of fracture stresses for pooled data from slabs 1 to 4 for axial and radial specimens from center and edge of slabs, comparing large and small tensile specimens.

Note that the Weibull line shown in Figure 208 was for data pooling without considering size effect and, therefore, represents a line of best fit to all the data.

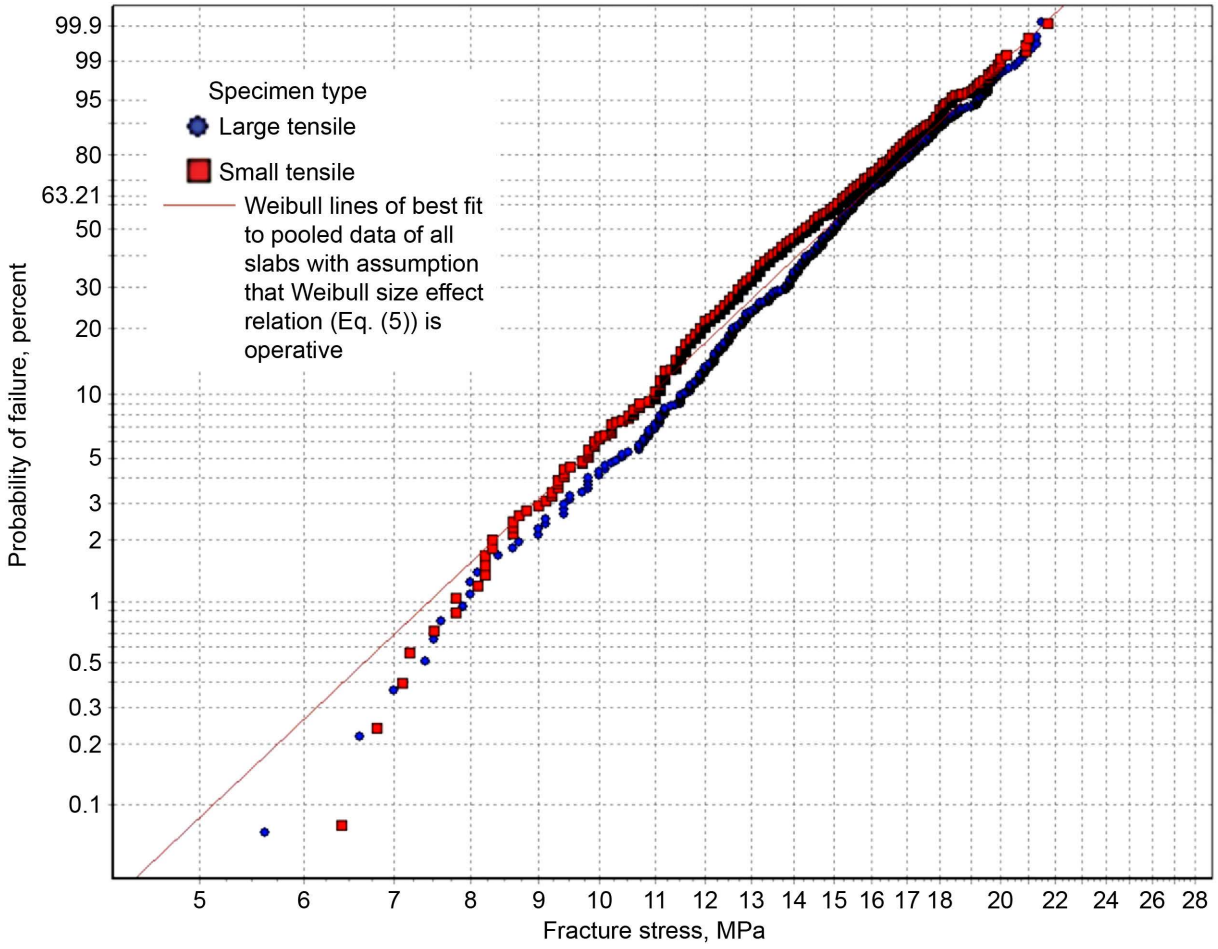

Figure 208.—Weibull plot of fracture stresses for data pooled from slabs 1 to 4 for axial and radial specimens from center and edge of slabs, comparing large and small tensile specimens without considering size effect.

In Figure 209, the Weibull moduli for the large and small tensile specimens are quite similar and within a reasonable margin that could be expected from natural statistical variation.

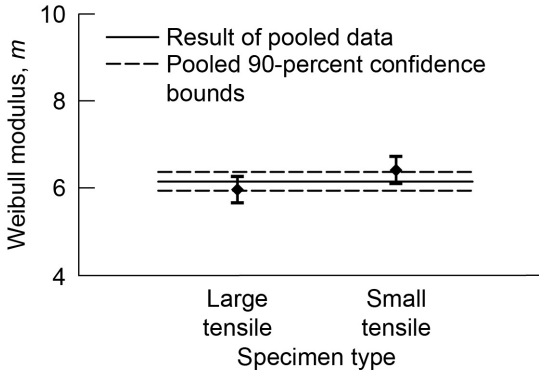

Figure 209.—Weibull modulus and 90-percent confidence bands on pooled data from slabs 1 to 4 for axial and radial specimens from center and edge of slabs, comparing large and small tensile specimens. See Table 68 for a listing of Weibull parameters and 90-percent confidence bounds on parameters.

In Figure 210, the difference in characteristic strength is small—on the order of 4 percent. However, the difference is still large enough to be statistically significant. See Table 68 for a listing of Weibull parameters and 90-percent confidence bounds on parameters.

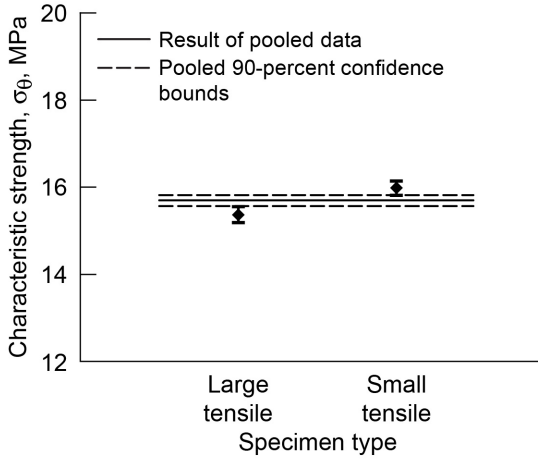

Figure 210.—Characteristic strength and 90-percent confidence bounds on pooled data from slabs 1 to 4 for axial and radial specimens from center and edge of slabs, comparing large and small tensile specimens.

TABLE 68.—WEIBULL PARAMETERS AND 90-PERCENT CONFIDENCE BOUNDS ON POOLED DATA FROM SLABS 1 TO 4 FOR AXIAL AND RADIAL SPECIMENS FROM CENTER AND EDGE OF SLABS

Specimen type	Number of specimens	Weibull modulus, *m*		Characteristic strength, σ_θ, MPa	
		MLE biased[a]	90-percent boot confidence[b]	MPa	90-percent boot confidence[b]
Large tensile	628	5.97	5.67/6.27	15.38	15.2/15.56
Small tensile	689	6.42	6.11/6.73	15.99	15.83/16.15
Pooled	1317	6.16	5.95/6.38	15.70	15.58/15.83

[a]Maximum-likelihood estimation.
[b]Calculated from boot confidence bands for 2000 simulations.

Figure 211 pools all the large and small tensile specimen data into one set. See Table 69 for the Weibull parameters.

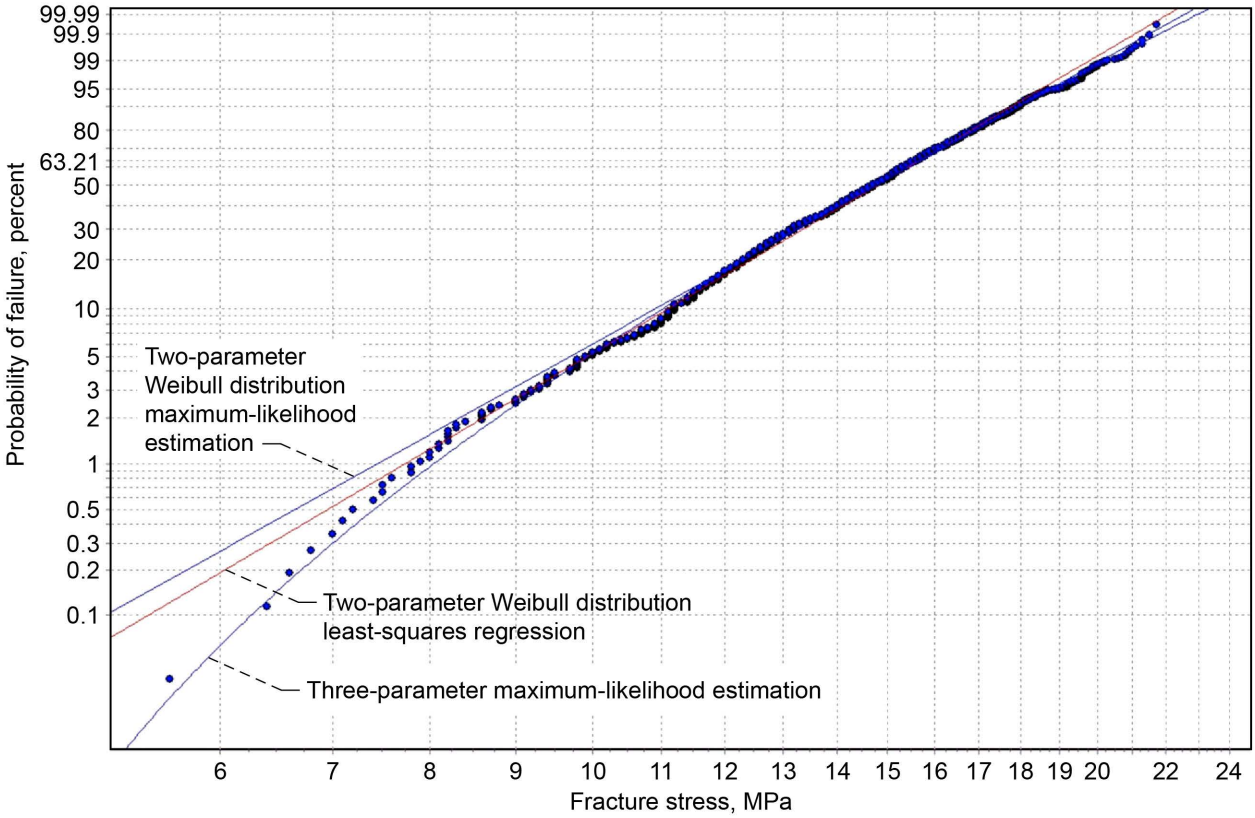

Figure 211.—Weibull plot of fracture stresses for data from all large and small tensile specimens pooled into one set without considering size effect—pooled slabs 1 to 4, large and small tensile specimens, axial and radial orientations, and center and edge of slabs. Weibull lines of best fit to pooled data of all slabs are shown.

TABLE 69.—WEIBULL PARAMETERS CALCULATED BY VARIOUS METHODS
[For data pooled for all small and large tensile specimens (1317 total) without considering size effect.]

Specimen type	Calculation method	Weibull modulus, m		Characteristic strength, σ_θ, MPa	
		Estimated	90-percent boot confidence[a]	Estimated	90-percent boot confidence[a]
Small and large tensile	Maximum-likelihood-estimated, two-parameter (MLE) biased.	6.16	5.95/6.38	15.70	15.58/15.82
Small and large tensile	Least-squares-estimated (LIN2) two-parameter Weibull parameters.	6.52	----------	15.67	----------
Small and large tensile	Maximum-likelihood-estimated, three parameter (MLE3) biased.	4.73	----------	12.22[b]	----------

[a]Calculated from boot confidence bounds based on 2000 simulations.
[b]Threshold or location parameter, σ_l, 3.41 MPa.

Pooling the data with the flexure specimens seems to significantly skew the plot in Figure 212, but to an unknown degree. The distortion of the curve from that of Figure 211 is due to the size-effect scaling, which in this case does not appear to be satisfactory. The best-fit line from WeibPar has a slope of $m = 6.44$ for 1317 specimens.

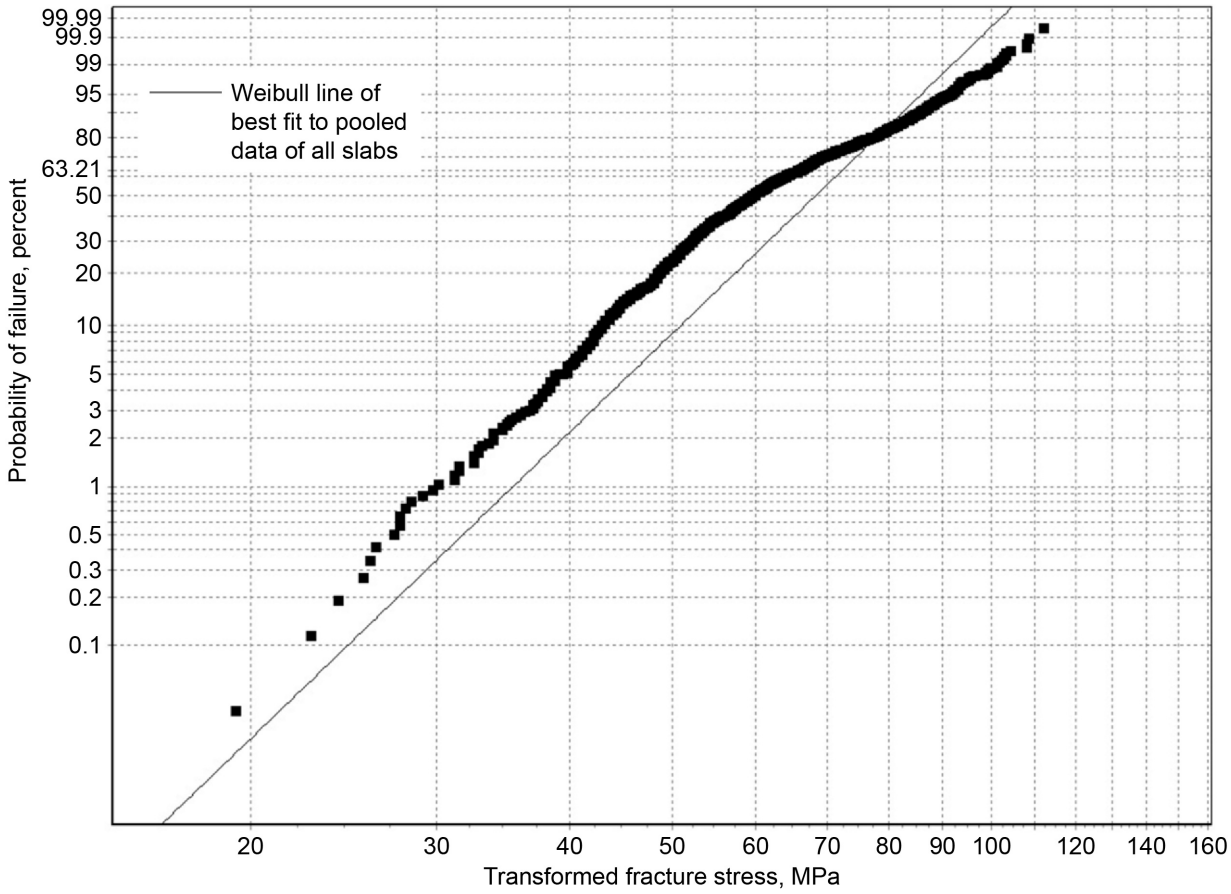

Figure 212.—Weibull plot of fracture stresses for data from all large and small tensile specimens pooled into one set and adjusted for size scale per WeibPar methodology—pooled slabs 1 to 4, large and small tensile specimens, axial and radial orientations, and center and edge of slabs. Data were transformed to a unit volume strength.

Pooling the data with the flexure specimens seems to significantly skew the plot in Figure 213—but to an unknown degree. Pooling of the flexure and tensile specimens does not appear to be satisfactory. The best-fit line from WeibPar has a slope of $m = 9.53$ for 1999 specimens.

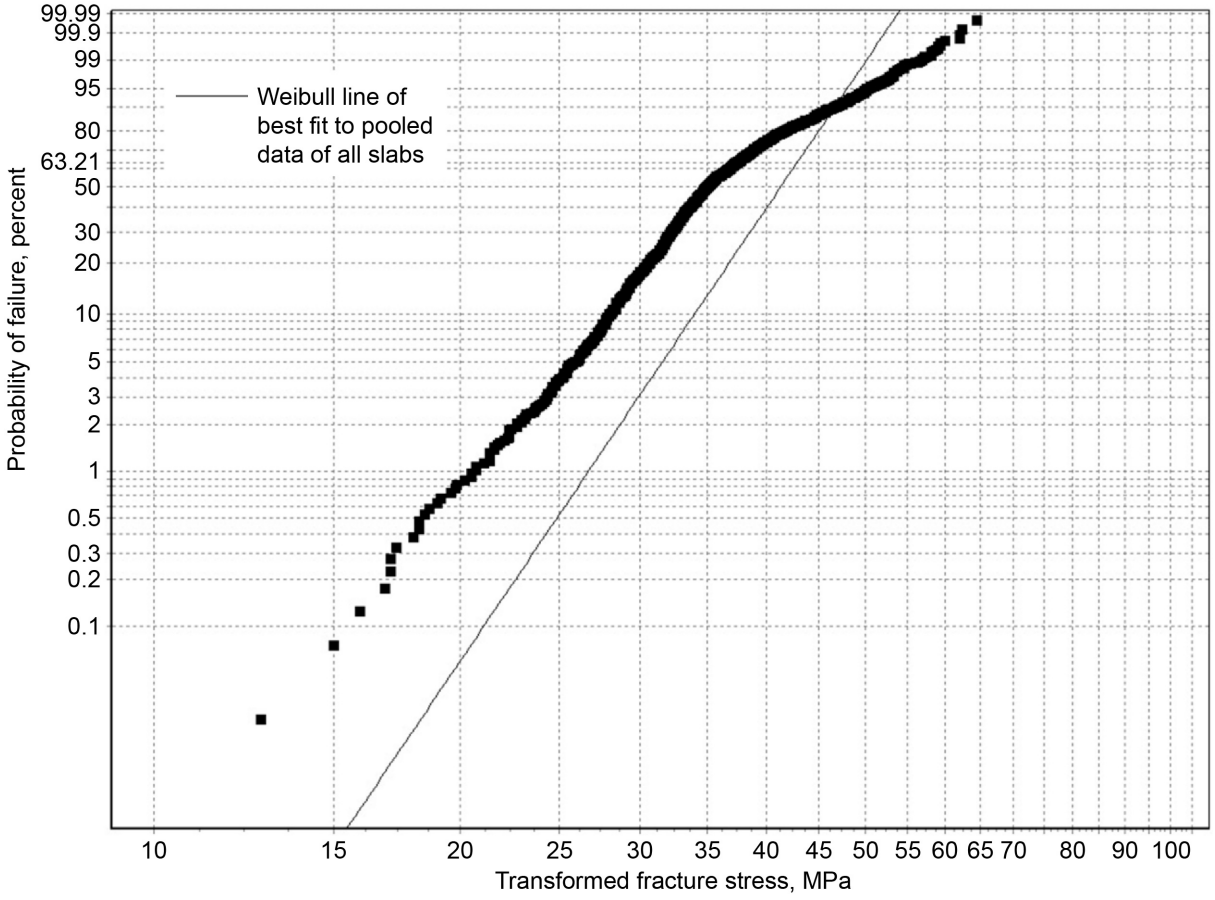

Figure 213.—Weibull plot of fracture stresses for data from all large tensile, small tensile, and flexure specimens pooled into one set and adjusted for size scale per WeibPar methodology—pooled slabs 1 to 4, large and small tensile specimens, axial and radial orientations, and center and edge of slabs. Data were transformed to a unit volume strength of 1 mm^3.

Figure 214 is provided as additional information.

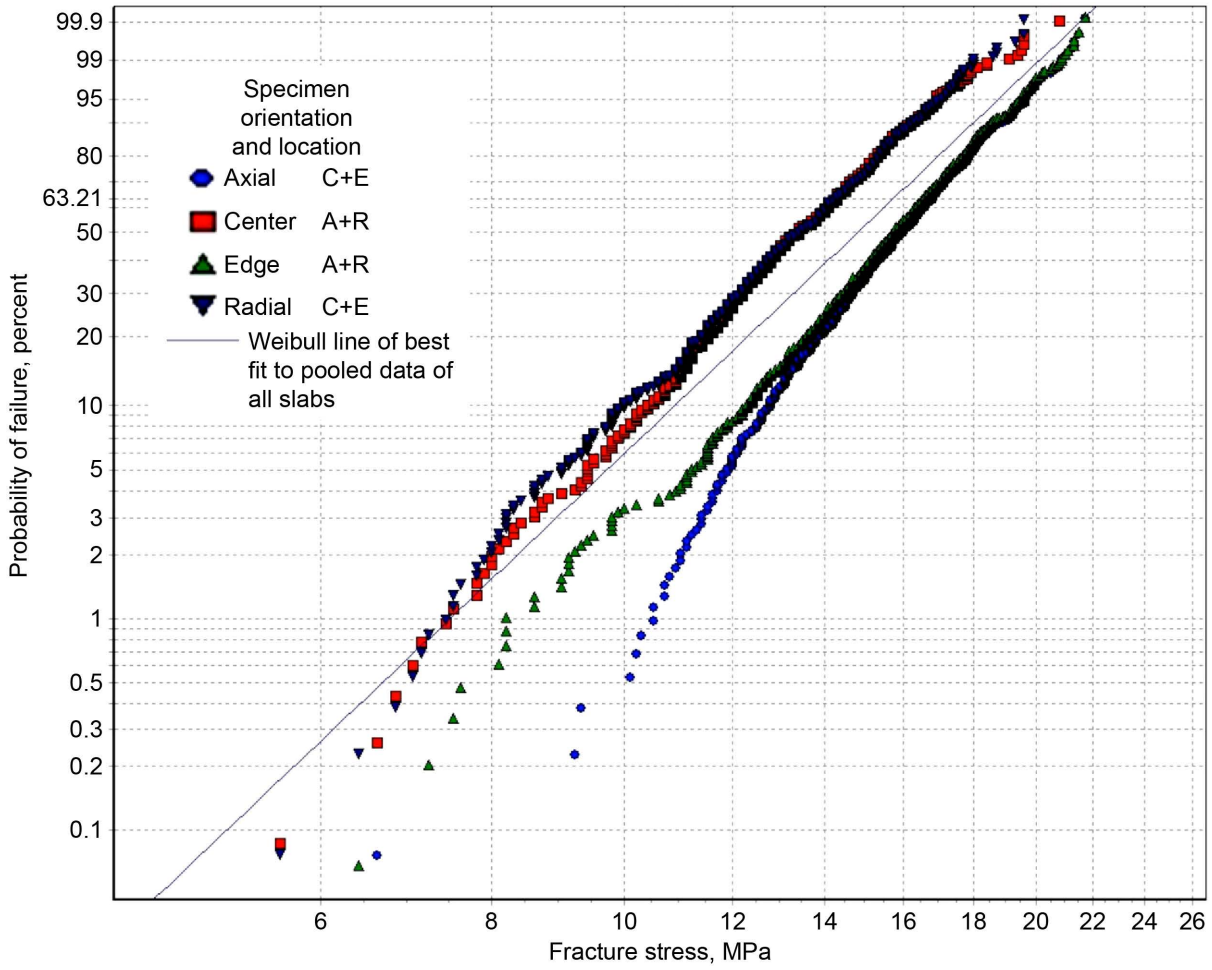

Figure 214.—Weibull plot of fracture stresses of data pooled from slabs 1 to 4 for large and small specimens without considering size effect, showing effects of orientation and location. Specimens are designated as C+E = pooled data from center and edge of slabs and A+R = pooled data from axial and radial specimens.

Figure 215 is provided as additional information.

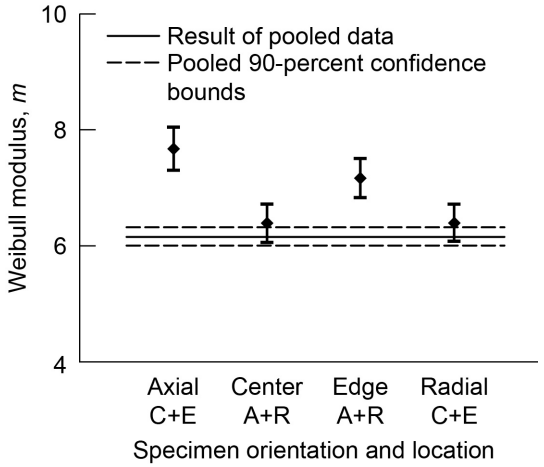

Figure 215.—Weibull modulus and 90-percent confidence bands of data pooled from slabs 1 to 4 for large and small specimens without considering size effect, showing effects of orientation and location. Specimens are designated as C+E = pooled data from center and edge of slabs and A+R = pooled data from axial and radial specimens.

Figure 216 is provided as additional information. See Table 70 for a listing of Weibull parameters and 90-percent confidence bounds on parameters.

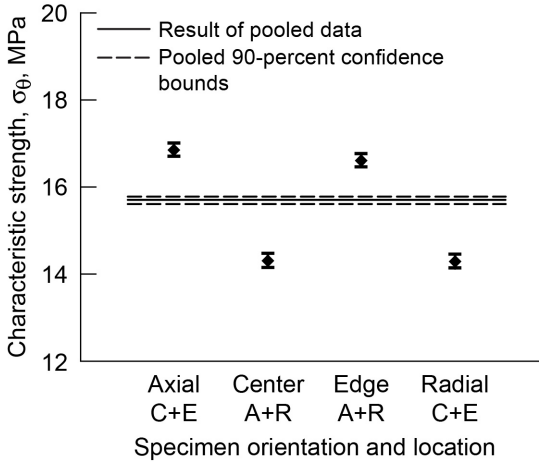

Figure 216.—Characteristic strength and 90-percent confidence bounds of data pooled from slabs 1 to 4 for large and small specimens without considering size effect, showing effects of orientation and location. Specimens are designated as C+E = pooled data from center and edge of slabs and A+R = pooled data from axial and radial specimens.

TABLE 70.—WEIBULL PARAMETERS AND 90-PERCENT CONFIDENCE BOUNDS ON POOLED DATA FROM SLABS 1 TO 4 FOR LARGE AND SMALL TENSILE SPECIMENS

Specimen orientation and location	Number of specimens	Weibull modulus, *m*		Characteristic strength, σ_θ, MPa	
		MLE biased[a]	90-percent boot confidence[b]	MPa	90-percent boot confidence[b]
Axial center and edge	663	7.68	7.31/8.05	16.86	16.71/17.01
Center axial and radial	578	6.39	6.06/6.72	14.32	14.16/14.49
Edge axial and radial	739	7.17	6.84/7.51	16.62	16.47/16.77
Radial center and edge	654	6.39	6.08/6.72	14.30	14.15/14.46
Pooled	2634	6.16	6.01/6.32	15.70	15.62/15.79

[a]Maximum-likelihood estimation.
[b]Calculated from boot confidence bands for 2000 simulations.

Appendix F.—Comparison of WeibPar and Price Results

Table 71 compares WeibPar results with those from the Price (1976) report. The mean and standard deviation results compare very well, adding confidence that the table values from the Price report were properly transcribed. Differences in Weibull moduli are noted. Price used least squares linear regression, but comparison with the WeibPar least squares linear regression results shows significant differences. The nature of these differences is unknown, but WeibPar has been tested extensively, and the WeibPar results are expected to be correct.

TABLE 71.—WEIBPAR AND PRICE RESULTS FOR MEAN, STANDARD DEVIATION, AND WEIBULL MODULUS

Slab number (linear or nonlinear)[a]	WeibPar results				Price (1976) results		
	Mean	Standard deviation	Weibull modulus, m, LS/MLE[b]	Characteristic strength, σ_θ, LS/MLE[b], MPa	Mean, MPa	Standard deviation	Weibull modulus, m
Axial small tensile specimens from center of slabs							
1	15.85	2.43	7.99/ 7.64	16.82/ 16.87	15.9	2.4	7.5
2	15.01	1.30	14.43/ 12.99	15.56/ 15.59	15.0	1.3	13.4
3	13.66	1.97	7.75/ 9.39	14.52/ 14.41	13.7	2.0	6.8
4	14.08	1.98	8.90/ 8.36	14.86/ 14.92	14.1	2.0	8.2
Axial small tensile specimens from edge of slabs							
1	16.45	2.01	9.88/ 9.77	17.29/ 17.30	16.4	2.0	9.4
2	18.19	1.71	13.39/ 11.93	18.90/ 18.96	18.2	1.7	12.6
3	17.02	1.93	10.68/ 9.95	17.83/ 17.85	17.0	1.9	10.0
4	16.83	1.98	11.02/ 9.69	17.61/ 17.71	16.8	2.0	10.0
Axial large tensile specimens from center of slabs							
1	15.27	1.78	10.06/ 11.48	16.04/ 15.98	15.3	1.8	8.9
2	14.68	1.08	16.55/ 18.14	15.15/ 15.12	14.7	1.1	15.2
3	13.24	1.06	16.84/ 12.17	13.65/ 13.74	13.3	1.1	14.4
4	13.11	1.52	11.30/ 9.26	13.69/ 13.79	13.1	1.5	10.0
Axial large tensile specimens from edge of slabs							
1	15.88	2.15	8.58/ 9.48	16.80/ 16.75	15.9	2.2	8.1
2	17.60	1.75	12.52/ 10.89	18.34/ 18.37	17.6	1.7	11.8
3	17.03	1.69	13.07/ 10.79	17.70/ 17.79	17.0	1.7	11.9
4	16.72	1.53	14.34/ 11.50	17.33/ 17.43	16.7	1.5	12.9
Axial flexure specimens from center of slabs							
1 (nonlinear)	23.55	2.42	11.63/ 12.68	24.59/ 24.55	23.6	2.4	11.1
1 (linear)	27.38	3.37	9.63/ 10.22	28.81/ 28.77	27.4	3.4	-----
2 (nonlinear)	22.58	1.15	24.80/ 21.15	23.08/ 23.11	22.6	1.2	22.9
2 (linear)	26.62	1.73	19.55/ 16.12	27.35/ 27.42	26.6	1.7	-----
3 (nonlinear)	22.76	1.55	19.67/ 13.98	23.37/ 23.50	22.8	1.6	17.1
3 (linear)	25.92	2.12	16.6/ 11.51	26.74/ 26.93	25.9	2.1	-----
4 (nonlinear)	22.73	2.26	12.74/ 11.41	23.66/ 23.74	22.7	2.3	11.7
4 (linear)	26.21	3.15	10.59/ 9.27	27.46/ 27.60	26.2	3.2	----
Axial flexure specimens from edge of slabs							
1 (nonlinear)	24.65	1.54	21.67/ 16.07	25.26/ 25.39	24.7	1.5	19.7
1 (linear)	28.59	2.24	17.53/ 12.68	29.45/ 29.65	28.6	2.2	-----
2 (nonlinear)	24.79	2.05	15.22/ 14.30	25.65/ 25.70	24.8	2.1	14.5
2 (linear)	29.96	3.31	11.47/ 10.34	31.29/ 31.41	30.0	3.3	-----
3 (nonlinear)	25.83	2.18	14.99/ 13.21	26.74/ 26.81	25.8	2.2	14.1
3 (linear)	30.35	3.22	11.96/ 10.20	31.66/ 31.79	30.4	3.2	-----
4 (nonlinear)	24.81	1.98	16.07/ 13.85	25.63/ 25.72	24.8	2.0	14.9
4 (linear)	28.89	2.91	12.88/ 10.82	30.05/ 30.20	28.9	2.9	-----
Radial small tensile specimens from center of slabs							
1	12.19	2.29	6.86/ 5.93	13.01/ 13.14	12.2	2.3	6.2
2	12.33	2.79	4.92/ 5.52	13.45/ 13.40	12.3	2.8	4.6
3	12.96	1.76	8.80/ 8.63	13.70/ 13.70	13.0	1.8	8.3
4	13.99	2.19	8.04/ 6.58	14.84/ 14.92	14.0	2.2	7.2

TABLE 71.—WEIBPAR AND PRICE RESULTS FOR MEAN, STANDARD DEVIATION, AND WEIBULL MODULUS

Slab number (linear or nonlinear)[a]	WeibPar results				Price (1976) results		
	Mean	Standard deviation	Weibull modulus, m, LS/MLE[b]	Characteristic strength, σ_θ, LS/MLE[b], MPa	Mean, MPa	Standard deviation	Weibull modulus, m
Radial small tensile specimens from edge of slabs							
1	13.04	1.93	7.79/ 8.82	13.86/ 13.81	13.0	1.9	7.2
2	15.24	1.80	10.41/ 9.71	15.99/ 16.02	15.2	1.8	9.7
3	14.08	2.14	7.54/ 8.97	14.99/ 14.92	14.1	2.1	6.8
4	15.71	1.84	10.45/ 10.53	16.48/ 16.50	15.7	1.8	9.9
Radial large tensile specimens from center of slabs							
1	10.72	1.71	7.69/ 7.44	11.40/ 11.44	10.7	1.7	7.2
2	11.80	1.13	13.36/ 10.81	12.26/ 12.32	11.8	1.1	12.4
3	11.46	1.39	9.78/ 10.45	12.06/ 12.04	11.5	1.4	9.1
4	13.37	2.26	6.73/ 7.18	14.31/ 14.26	13.4	2.3	6.2
Radial large tensile specimens from edge of slabs							
1	12.14	2.47	5.69/ 6.26	13.11/ 13.10	12.1	2.5	5.3
2	13.89	2.01	8.66/ 8.23	14.68/ 14.75	13.9	2.0	8.0
3	14.03	1.33	13.06/ 13.09	14.59/ 14.61	14.0	1.3	12.1
4	14.62	1.84	9.66/ 9.42	15.38/ 15.40	14.6	1.9	9.2
Radial flexure specimens from center of slabs							
1 (nonlinear)	20.28	1.89	13.41/ 12.65	21.07/ 21.11	20.3	1.9	13.1
1 (linear)	23.67	2.74	10.84/ 9.93	24.78/ 24.87	23.7	2.7	-----
2 (nonlinear)	19.90	1.90	12.84/ 12.57	20.71/ 20.73	19.9	1.9	12.3
2 (linear)	23.40	2.78	10.35/ 9.77	24.54/ 24.60	23.4	2.8	-----
3 (nonlinear)	21.10	1.59	16.65/ 16.76	21.77/ 21.81	21.1	1.6	15.7
3 (linear)	24.54	2.27	13.60/ 12.55	25.48/ 25.55	24.5	2.3	-----
4 (nonlinear)	21.67	1.69	16.34/ 14.14	22.37/ 22.44	21.7	1.7	15.0
4 (linear)	25.73	2.61	12.73/ 10.50	26.78/ 26.91	25.7	2.6	-----
Radial flexure specimens from edge of slabs							
1 (nonlinear)	20.32	2.68	8.72/ 11.01	21.48/ 21.36	20.3	2.7	8.0
1 (linear)	24.13	3.83	7.11/ 8.68	25.77/ 25.62	24.1	3.8	-----
2 (nonlinear)	21.29	1.77	14.97/ 13.59	22.04/ 22.07	21.3	1.8	14.9
2 (linear)	25.32	2.70	11.72/ 10.24	26.43/ 26.51	25.3	2.7	-----
3 (nonlinear)	22.78	1.58	18.70/ 15.21	23.43/ 23.52	22.8	1.6	17.0
3 (linear)	26.71	2.37	14.78/ 11.74	27.66/ 27.81	26.7	2.4	----
4 (nonlinear)	21.88	1.93	13.67/ 14.57	22.72/ 22.69	21.9	1.9	12.9
4 (linear)	26.49	3.06	10.36/ 10.44	27.80/ 27.79	26.5	3.1	-----

[a]Applies only to flexure specimens; indicates that linear-elastic stress-strain response or nonlinear-elastic stress-strain response was assumed.
[b]Least-squares maximum-likelihood estimation (MLE).

Appendix G.—Symbols

d	diameter of the specimen
E	slope of the stress-strain curve at zero strain; Young's modulus
h_o	characteristic grain size
i	number of the ranked value
m	Weibull modulus
m_S	area-based Weibull modulus
m_V	volume-based Weibull modulus
n	number of rupture specimens in a particular sample
P_f	probability of failure
P_{fV}	probability of failure as a function of volume
r	random number
R_2	coefficient of determination
V	volume
V_e	effective volume
ε	strain
ε_f	true outer fiber strain at fracture
ε_o	constant for a given type of graphite which characterizes the curvature of the stress-strain curve
σ	stress
σ_f	maximum stress (or extreme fiber stress) for tensile or flexural loading at the instant of failure
σ_l	threshold or location parameter
σ_o	Weibull scale parameter
σ_θ	volume- or area-based characteristic strength

Superscript

m	volume- or area-based fast fracture Weibull modulus

References

Arai, T.; and Oku, T.; 1979: The Effect of Nonlinear Stress-Strain Relationship on the Bend Strength of Isotropic Graphite. J. Nuclear Materials, vol. 79, issue 1, pp. 227–234.

Barnett, Ralph L., et al.; 1967: Fracture of Brittle Materials Under Transient Mechanical and Thermal Loading. AFFDL–TR–66–220.

Batdorf, S.B.; and Crose, J.G.; 1974: A Statistical Theory for the Fracture of Brittle Structures Subjected to Nonuniform Polyaxial Stresses. J. Appl. Mech. Trans. ASME, vol. 41, no. 2, pp. 459–464.

Batdorf, S.B.; and Heinisch, H.L., Jr.; 1978: Weakest Link Theory Reformulated for Arbitrary Fracture Criterion. J. Am. Ceram. Soc., vol. 61, no. 7, pp. 355–358.

Bazant, Zdenek P.; and Li, Z.; 1995: Modulus of Rupture: Size Effect Due to Fracture Initiation in Boundary Layer. J. Structural Engrg., vol. 121, no. 4, pp. 739–746.

Bramblett, G.C.; Fisher, C.R.; and Swart, F.E.; 1981: Operational Experience at Fort St. Vrain. International Atomic Energy Agency, HTGR Knowledge Base, pp. 6–10. http://www.iaea.org/inisnkm/nkm/aws/htgr/abstracts/abst_iwggcr1_01.html Accessed Dec. 13, 2011.

Chinnathambi, Karthik.; 2011: Microstructural Characterization of Nuclear Graphites. Presented at the 12th International Nuclear Graphite Specialist Meeting (INGSM–12), Jeju, Korea. http://www.ingsm-12.org/users/ingsm12/download/Karthik_Microstructure-Pore.pdf/ Accessed Dec. 12, 2011.

Connecticut Reserve Technologies, Inc.; 2009: WeibPar 4.1 User Guide. Version 4.1. http://www.weibpar.com Accessed Sept. 2009.

Danzer, Robert, et al.; 2008: Fracture of Ceramics. Adv. Eng. Mat., vol. 10, no. 4, pp. 275–298.

Department of Defense; 2002: Composite Materials Handbook. Volume 1. Polymer Matrix Composites Guidelines for Characterization of Structural Materials. MIL–HDBK–17–1F.

Freudenthal, Alfred M.; 1968: Statistical Approach to Brittle Fracture. Fracture: An Advanced Treatise, H. Liebowitz, ed., Vol. II, pp. 592–619.

Generation IV International Forum; 2010: Preparing Today for Tomorrow's Energy Needs. http://www.gen-4.org/ Accessed Oct. 22, 2010.

Ho, F.; 1979: A Modified Weibull Theory for the Strength of Granular Brittle Material. General Atomic Company Series GA–A 15228.

Idaho National Laboratory, Oak Ridge National Laboratory, and Argonne National Laboratory; 2005: Next Generation Nuclear Plant Research and Development Program Plan. Idaho National Engineering and Environmental Laboratory, Idaho Falls, ID, INEEL/EXT–05–02581. http://www.inl.gov/technicalpublications/Documents/3028298.pdf Accessed June 18, 2008.

Johnson, C.A.; 1983: Fracture Statistics of Multiple Flaw Distributions. Fracture Mechanics of Ceramics, Vol. 5—Surface Flaws, Statistics, and Microcracking, R.C. Bradt, et al., eds., Plenum Press, New York, NY, pp. 365–386.

Li, Haiyan; and Fok, Alex Siu-Lun; 2009: An Analytical Study on the Effects of Strain Gradient on the Fracture Statistics of Quasi-Brittle Materials. J. Nucl. Mater., vol. 394, nos. 2–3, pp. 136–143.

Liu, Chi-Chao; 1997: A Comparison Between the Weibull and Lognormal Models Used to Analyse Reliability Data. Ph.D. Thesis, University of Nottingham.

Nemeth, Noel N.; and Bratton, Robert L.; 2010: Overview of Statistical Models of Fracture for Nonirradiated Nuclear-Graphite Components. Nucl. Eng. Des., vol. 240, no. 1, pp. 1–29.

Nemeth, Noel N., and Bratton, Robert L., 2011: Statistical Models of Fracture Relevant to Nuclear-Grade Graphite: Review and Recommendations. NASA/TM—2011-215805.

Nemeth, Noel N., et al.; 2007: Fabrication and Probabilistic Fracture Strength Prediction of High-Aspect-Ratio Single Crystal Silicon Carbide Microspecimens With Stress Concentration. Thin Sol. Fi. (NASA/TM—2005-213986), vol. 515, no. 6, pp. 3283–3290.

Nemeth, Noel N., et al.; 2003: CARES/Life Ceramics Analysis and Reliability Evaluation of Structures Life Prediction Program. NASA/TM—2003-106316.

Pai, Shantaram S.; and Gyekenyesi, John P.; 1988: Calculation of Weibull Strength Parameters and Batdorf Flaw-Density Constants for Volume- and Surface-Flaw-Induced Fracture in Ceramics. NASA TM–100890.

Pinner, Joe; 2010: Fort St. Vrain Power Station History, Overview. http://www.fsvfolks.org/FSVHistory_2.html Accessed July 26, 2012

Price, R.J.; 1976: Statistical Study of the Strength of Near-Isotropic Graphite. General Atomic Project 3224 (GA–A13955 and UC–77).

Sookdeo, Steven; Nemeth, Noel N.; and Bratton, Robert L.; 2008: Reliability Assessment of Graphite Specimens Under Multiaxial Stresses. NASA/TM—2008-215204.

Strizak, J.P.; 1991: The Effect of Volume on the Tensile Strength of Several Nuclear-Grade Graphites. The Status of Graphite Development for Gas Cooled Reactors, IAEA–TECDOC–690, pp. 233–241.

Thoman, D.R.; Bain, L.J.; and Antle, C.E.; 1969: Inferences on the Parameters of the Weibull Distribution. Technomet., vol. 11, no. 3, pp. 445–460.

Tucker, M.O.; Rose, A.P.G.; and Burchell, T.D.; 1986: The Fracture of Polygranular Graphites. Carbon, vol. 24, no. 5, pp. 581–602.

U.S. Department of Energy; 2008: Energy Efficiency & Renewable Energy, Advanced Manufacturing Office, Process Heating Systems. http://www1.eere.energy.gov/industry/bestpractices/process_heat.html Last updated Apr. 16, 2008, Accessed Oct. 22, 2010.

U.S. DOE Nuclear Energy Research Advisory Committee and the Generation IV International Forum; 2002: A Technology Roadmap for Generation IV Nuclear Energy Systems, Ten Nations Preparing Today for Tomorrow's Energy Needs. GIF–002–00. http://www.gen-4.org/PDFs/GenIVRoadmap.pdf Accessed April 4, 2012.

Woolley, R.L.; 1965: The Yield Curve and the Compressive Strength of Polycrystalline Graphite. Philos. Mag., vol. 11, no. 112, pp. 799–807.

REPORT DOCUMENTATION PAGE		Form Approved OMB No. 0704-0188

1. REPORT DATE *(DD-MM-YYYY)*	2. REPORT TYPE	3. DATES COVERED *(From - To)*
01-10-2012	Technical Memorandum	

4. TITLE AND SUBTITLE
Large-Scale Weibull Analysis of H-451 Nuclear-Grade Graphite Specimen Rupture Data

5a. CONTRACT NUMBER
SAA3-824-1

5b. GRANT NUMBER

5c. PROGRAM ELEMENT NUMBER

6. AUTHOR(S)
Nemeth, Noel, N.; Walker, Andrew; Baker, Eric, H.; Murthy, Pappu, L.; Bratton, Robert, L.

5d. PROJECT NUMBER

5e. TASK NUMBER

5f. WORK UNIT NUMBER
WBS 392259.02.03.0683.12

7. PERFORMING ORGANIZATION NAME(S) AND ADDRESS(ES)
National Aeronautics and Space Administration
John H. Glenn Research Center at Lewis Field
Cleveland, Ohio 44135-3191

8. PERFORMING ORGANIZATION REPORT NUMBER
E-18080

9. SPONSORING/MONITORING AGENCY NAME(S) AND ADDRESS(ES)
National Aeronautics and Space Administration
Washington, DC 20546-0001

10. SPONSORING/MONITOR'S ACRONYM(S)
NASA

11. SPONSORING/MONITORING REPORT NUMBER
NASA/TM-2012-217409

12. DISTRIBUTION/AVAILABILITY STATEMENT
Unclassified-Unlimited
Subject Category: 37
Available electronically at http://www.sti.nasa.gov
This publication is available from the NASA Center for AeroSpace Information, 443-757-5802

13. SUPPLEMENTARY NOTES

14. ABSTRACT
A Weibull analysis was performed of the strength distribution and size effects for 2000 specimens of H-451 nuclear-grade graphite. The data, generated elsewhere, measured the tensile and four-point-flexure room-temperature rupture strength of specimens excised from a single extruded graphite log. Strength variation was compared with specimen location, size, and orientation relative to the parent body. In our study, data were progressively and extensively pooled into larger data sets to discriminate overall trends from local variations and to investigate the strength distribution. The CARES/Life and WeibPar codes were used to investigate issues regarding the size effect, Weibull parameter consistency, and nonlinear stress-strain response. Overall, the Weibull distribution described the behavior of the pooled data very well. However, the issue regarding the smaller-than- expected size effect remained. This exercise illustrated that a conservative approach using a two-parameter Weibull distribution is best for designing graphite components with low probability of failure for the in-core structures in the proposed Generation IV (Gen IV) high-temperature gas-cooled nuclear reactors. This exercise also demonstrated the continuing need to better understand the mechanisms driving stochastic strength response. Extensive appendixes are provided with this report to show all aspects of the rupture data and analytical results.

15. SUBJECT TERMS
Graphite; Weibull; Size effect; CARES/Life; WeibPar; Nuclear; Gen-IV; Quasi-brittle; Monte-Carlo; Strength distribution; Tensile; Flexure; Bend; Four-point; Nonlinear

16. SECURITY CLASSIFICATION OF:			17. LIMITATION OF ABSTRACT	18. NUMBER OF PAGES	19a. NAME OF RESPONSIBLE PERSON
a. REPORT	b. ABSTRACT	c. THIS PAGE			STI Help Desk (email:help@sti.nasa.gov)
U	U	U	UU	212	19b. TELEPHONE NUMBER *(include area code)* 443-757-5802